

KIT SCIENTIFIC REPORTS 7617

Annual Report 2011

Institute for Nuclear Waste Disposal

H. Geckeis, T. Stumpf (Eds.)

H. Geckeis, T. Stumpf (Eds.)

Annual Report 2011

Institute for Nuclear Waste Disposal

Image Source

Cover Pictures © H. Geckeis

Electrospray generated from an aqueous solution for time-of-flight mass measurements

AFM picture of dried gibbsite particles on mica

Luminescence of curium(III) in aqueous solution

Karlsruhe Institute of Technology
KIT SCIENTIFIC REPORTS 7617

Annual Report 2011

Institute for Nuclear Waste Disposal

by
H. Geckeis, T. Stumpf (Eds.)

The Institute for Nuclear Waste Disposal, INE, (Institut für Nukleare Entsorgung) belongs to the KIT Energy Center. The KIT Energy Center with its 1100 employees is one of the largest energy research centers in Europe. It bundles the energy research activities of the KIT, the merger of the former Forschungszentrum Karlsruhe and Universität Karlsruhe and reknown cooperation partners. By this, it crosses the lines between disciplines and combines fundamental and applied research in all relevant energies for industry, household, service and mobility.

The involved institutes and research groups conduct the research work on their own authority. The joining of subjects, the interdisciplinary collaboration of scientists, and the common use of high-end devices and installations, develops a new quality of research and teaching. The KIT Energy Center develops solutions in energy technology from a single source and acts as a highly valuable consultancy institution for politics, business, and society in all questions of energy.

(<http://www.energy.kit.edu/>)

Impressum

Karlsruher Institut für Technologie (KIT)
KIT Scientific Publishing
Straße am Forum 2
D-76131 Karlsruhe
www.ksp.kit.edu

KIT – Universität des Landes Baden-Württemberg und
nationales Forschungszentrum in der Helmholtz-Gemeinschaft



Diese Veröffentlichung ist im Internet unter folgender Creative Commons-Lizenz
publiziert: <http://creativecommons.org/licenses/by-nc-nd/3.0/de/>

KIT Scientific Publishing 2012
Print on Demand

ISSN 1869-9669

H. Geckeis, T. Stumpf (Eds.)

Annual Report 2011

Institute for Nuclear Waste Disposal

Image Source

Cover Pictures © H. Geckeis

Electrospray generated from an aqueous solution for time-of-flight mass measurements

AFM picture of dried gibbsite particles on mica

Luminescence of curium(III) in aqueous solution

Karlsruhe Institute of Technology
KIT SCIENTIFIC REPORTS 7617

Annual Report 2011

Institute for Nuclear Waste Disposal

by
H. Geckeis, T. Stumpf (Eds.)

The Institute for Nuclear Waste Disposal, INE, (Institut für Nukleare Entsorgung) belongs to the KIT Energy Center. The KIT Energy Center with its 1100 employees is one of the largest energy research centers in Europe. It bundles the energy research activities of the KIT, the merger of the former Forschungszentrum Karlsruhe and Universität Karlsruhe and reknown cooperation partners. By this, it crosses the lines between disciplines and combines fundamental and applied research in all relevant energies for industry, household, service and mobility.

The involved institutes and research groups conduct the research work on their own authority. The joining of subjects, the interdisciplinary collaboration of scientists, and the common use of high-end devices and installations, develops a new quality of research and teaching. The KIT Energy Center develops solutions in energy technology from a single source and acts as a highly valuable consultancy institution for politics, business, and society in all questions of energy.

(<http://www.energy.kit.edu/>)

Impressum

Karlsruher Institut für Technologie (KIT)
KIT Scientific Publishing
Straße am Forum 2
D-76131 Karlsruhe
www.ksp.kit.edu

KIT – Universität des Landes Baden-Württemberg und
nationales Forschungszentrum in der Helmholtz-Gemeinschaft



Diese Veröffentlichung ist im Internet unter folgender Creative Commons-Lizenz
publiziert: <http://creativecommons.org/licenses/by-nc-nd/3.0/de/>

KIT Scientific Publishing 2012
Print on Demand

ISSN 1869-9669

Table of contents

1	Introduction to the Institute for Nuclear waste Disposal (INE)	1
2	Highlights	5
3	Education and training	7
4	National and international cooperation	9
5	Fundamental studies: Process understanding on a molecular scale	13
5.1	Chemistry and thermodynamic of actinides in aqueous solution	13
5.2	Metal ion sorption onto mineral surfaces	19
5.3	Retention of radionuclides by secondary phase formation.....	25
6	Applied studies: Radionuclide retention in the multi-barrier system	33
6.1	Key processes affecting corrosion of nuclear waste forms	33
6.2	Safety analysis on the basis of waste form performance, kinetics, thermodynamics and sorption	39
6.3	Colloid impact on radionuclide (RN) migration.....	42
6.4	Numerical simulation and database	48
7	Separation of long-lived minor actinides	51
8	Vitrification of high-level radioactive liquid waste	57
9	Development of actinide speciation methods	61
9.1	R&D projects conducted at the INE-Beamline for Actinide Research at ANKA and at external SR sources.....	61
9.2	Laser spectroscopy.....	65
9.3	Mass spectrometry methods.....	69
9.4	NMR spectroscopy – first results of actinide-N-donor complexes.....	72
9.5	Computational chemistry	76
10	Radiation protection research	81
11	Publications	87

1 Introduction to the Institute for Nuclear Waste Disposal (INE)

The R&D at the Institute for Nuclear Waste Disposal, INE, (Institut für Nukleare Entsorgung) of the Karlsruhe Institute of Technology (KIT) focuses on (i) long term safety research for nuclear waste disposal, (ii) immobilization of high level radioactive waste (HLW), (iii) separation of minor actinides from HLW and (iv) radiation protection.

All R&D activities are integrated into the program Nuclear Safety Research within the KIT-Energy Center. INE contributes to German prudent research for the safety of nuclear waste disposal, which is the responsibility of the Federal Government.

Projections based on scheduled operation times for nuclear power plants (Amendment to German Atomic Energy Act, August 2011) in Germany, indicate about a total of 17,770 tons of spent nuclear fuel will be generated. About 6,670 tons have been shipped to France and the UK up until 2005 for reprocessing, to recover plutonium and uranium. Therefore two types of high level, heat producing radioactive waste have to be disposed of safely: spent fuel and vitrified high level waste from reprocessing (HLW glass).

There is an international consensus that storage in deep geological formations is the safest way to dispose of high level, heat producing radioactive waste. It ensures the effective protection of the population and the biosphere against radiation exposure over very long periods of time. The isolation and immobilization of nuclear waste in a repository is ensured by the appropriate combination of redundant barriers (multi-barrier system).

Long term safety research for nuclear waste disposal at KIT-INE deals mainly with the geochemical contribution to the safety case, involving aquatic chemistry of radionuclides in the geochemical environment of a repository. Work concentrates on the disposal of spent fuel and HLW-glass in rock salt, as well as in clay and crystalline rock formations. The actinides and long-lived fission products play the central role, as they dominate HLW radiotoxicity over long periods of time.

Relevant long term scenarios for nuclear repositories in deep geological formations have to take into account possible radionuclide transport via the groundwater pathway. Thermomechanical studies are performed at INE, in order to describe the evolution of the repository after closure. Possible groundwater intrusion into emplacement caverns is assumed to cause waste form corrosion and eventually radionuclide release. Radionuclide mobility is

then determined by the various geochemical reactions in complex aquatic systems: i.e. dissolution of the nuclear waste form (HLW glass, spent fuel), radiolysis phenomena, redox reactions, complexation with inorganic and organic ligands, colloid formation, surface reactions at mineral surfaces, precipitation of solid phases and solid solutions. Prediction and quantification of all these processes require thermodynamic data and a comprehensive understanding of these processes at a molecular scale.

Relevant radionuclide concentrations in natural groundwater lie in the nano-molar range, which is exceedingly small in relation to the main groundwater components. Quantification of chemical reactions occurring in these systems calls for the application and development of new sophisticated methods and experimental approaches, which provide insight into the chemical speciation of radionuclides at very low concentrations. To this end, innovative laser and X-ray spectroscopic techniques are continuously developed and applied. A theoretical group performs quantum chemical calculations on actinide complexes as an additional tool to support both interpretation of experimental results and experiment design.

Long term safety of a nuclear waste repository must be demonstrated by application of modelling tools on real natural systems over geological time scales. The experimental research programme at INE aims to acquire fundamental knowledge on such model subsystems and to derive the required model parameters. Geochemical models and thermodynamic databases are developed as a basis for the description of radionuclide geochemical behaviour in complex natural aquatic systems. The prediction of radionuclide migration in the geosphere necessitates coupled modelling of geochemistry and transport. Transferability and applicability of model predictions are examined by designing dedicated laboratory experiments, field studies in underground laboratories and by studying natural analogue systems. This strategy allows to identify and to analyse key uncertainties related to the accuracy and the relevance of the developed models.

Within the R&D topic **immobilization of high level radioactive waste**, INE contributes to the decommissioning of nuclear facilities. The core process technology for the Vitrification Plant (VEK) on the site of the former Karlsruhe Reprocessing Plant (WAK; located at KIT Campus North) has been developed by INE. INE was involved in functional testing of major

process systems, as well as in the performance of the cold test operation and played a leading role in hot operation of the VEK plant. The project has been finalized in February 2011 by transportation of the produced 140 glass canisters to the Zwischenlager Nord (ZLN) near Lubmin for interim storage.

The Partitioning & Transmutation (P&T) strategy is pursued in many international research programmes. The objective is to reduce significantly the long term radiotoxicity, as well as the long term heat production of spent fuel by reduction of the actinide inventory. INE research activities in P&T are focused on the partitioning step, i.e. **separation of minor actinides from HLW**. The R&D aims to develop efficient separation processes for minor actinide for subsequent transmutation into short-lived or stable fission products. INE develops highly selective extracting agents and performs experiments to derive kinetic and thermodynamic data for extraction reactions. R&D spans experimental, analytical and theoretical work, dedicated to understanding extraction ligand selectivity on a molecular scale, in order to develop and optimise extraction processes.

The new R&D topic at INE, **radiation protection**, focuses on the assessment of radiation exposures on man by estimating doses either from external radiation fields or from incorporation of radionuclides. The vision behind this work is to provide techniques and models for an individualized dosimetry, which goes beyond the current approach of applying reference models in dose assessments. The exposed individual with his or her anatomical and physiological properties, as well as the (properly characterized) radiation fields, are taken into account in an individualized dosimetry. The researchers closely cooperate with the KIT safety management KSM.

In 2011 the **Institute for Nuclear Waste Disposal** had **108 employees** working in the seven departments, which reflect the R & D and organizational tasks of the institute (Fig. 1): (i) safety of nuclear waste disposal, (ii) geochemistry, (iii) radiochemistry, (iv) actinide speciation, (v) vitrification of high level waste, (vi) radiation protection research and (vii) scientific/technical coordination and analytical chemistry. INE laboratories are equipped with all necessary infrastructures to perform radionuclide/actinide research, including hot cells, alpha glove boxes, inert gas alpha glove boxes and radionuclide laboratories. State-of-the-art analytical instruments and methods are applied for analysis and speciation of radionuclides and radioactive materials.

α -, β -, γ -spectroscopy instruments exist for the sensitive detection and analysis of radionuclides. Trace element and isotope analysis is made by instrumental analytical techniques such as X-ray fluorescence spectroscopy (XRF), atomic absorption spectroscopy (AAS), ICP-atomic emission spectroscopy (ICP-AES) and ICP-mass spectrometry (Quadrupole-ICP-MS and high resolution ICP-MS). Methods available for surface sensitive analysis and characterisation of solid samples include X-ray diffraction (XRD), atomic force microscopy (AFM) and laser-ablation coupled with ICP-MS. Two new instruments have been recently installed: an X-ray photoelectron spectrometer (XPS) and an environmental scanning electron microscope (ESEM). INE scientists also have direct access to a TEM instrument at a nearby institute (Institut für Angewandte Materialien) on the KIT Campus North site. Laser spectroscopic techniques are developed and applied for sensitive actinide and fission product speciation such as time-resolved laser fluorescence spectroscopy (TRLFS), laser photo acoustic spectroscopy (LPAS), laser-induced breakdown detection (LIBD) and Raman spectroscopy. A tuneable optical parametric oscillator (OPO) laser system with TRLFS-detection is used for high resolution spectroscopy at liquid helium temperature. Speciation of actinide-ion complexation and polymerization products in solution is facilitated by nano electrospray time-of-flight mass-spectrometry (ESI TOF MS). Structural insight into actinide species is obtained by extended X-ray fine structure (EXAFS) spectroscopy at the INE-Beamline at the Karlsruhe synchrotron source ANKA. The INE-Beamline, in the direct vicinity of INE hot laboratories and in combination with the other analytic methods, represents a world-wide unique experimental and analytic infrastructure, which both profits from and contributes to INE's expertise in the field of chemistry and spectroscopy of the actinides. Quantum chemical calculations are performed on INE's computing cluster which is equipped with 17 nodes and 76 processors. A 400 MHz-NMR spectrometer adapted to measuring radioactive liquid samples rounds off the analytical and speciation portfolio of INE.

Additional facilities at INE include a non-radioactive vitrification test facility (PVA) used to investigate and to simulate vitrification processes for hot plants. The INE CAD workstations enable construction and planning of hardware components, process layout and flow sheets. The institute workshop is equipped with modern machine tools to manufacture components for specific experimental and analytical devices in hot laboratories

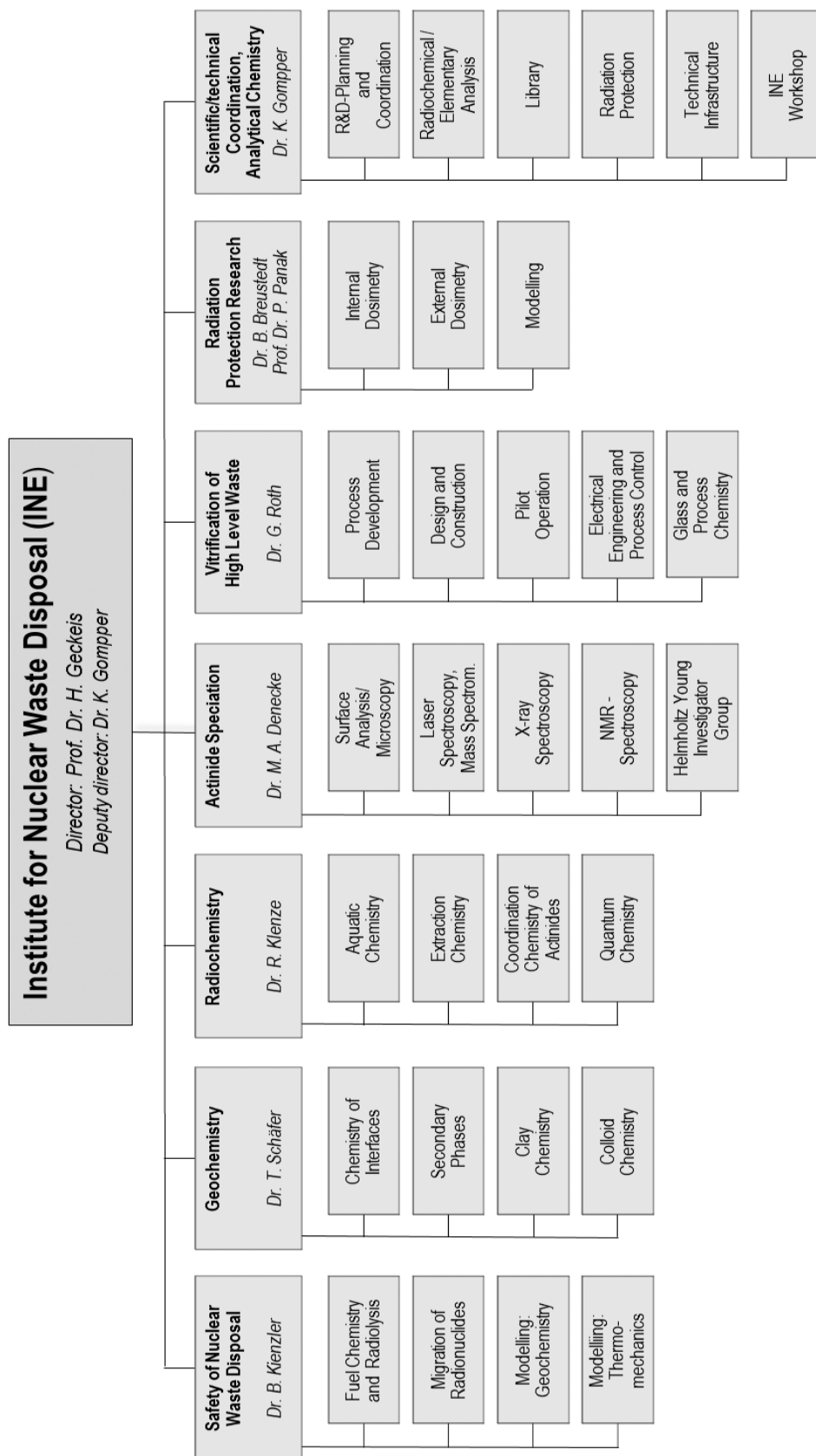


Fig. 1: Organization Chart of INE

2 Highlights

Contributions collected in this report provide a representative overview of the scientific outcome of INE R&D activities in 2011. Some highlights of the research activities are listed below:

As part of the on-going investigations of **secondary phase formation and chemical speciation of trivalent actinides** during precipitation of the studies in 2011 focused on incorporation of trivalent f-elements into the isostructural minerals strontianite (SrCO_3) and celestite (SrSO_4). The strategy here was to decouple the effect of structure from that due to the anion. These activities expanded previous work with aragonite and gypsum, where it was found that aragonite incorporates Eu^{3+} and Cm^{3+} , whereas only surface sorption was observed in gypsum. The new results demonstrate that both Eu^{3+} and Cm^{3+} are incorporated into the (orthorhombic) sulfate mineral celestite, isostructural to aragonite. The substitution mechanism is most likely dictated by the symmetry of the substitution site and the electronic structure of the dopant atom (see chapter 5.3 and 9.2).

The “Preliminary Safety Analysis Gorleben (vSG)” project is focused on long-term safety to demonstrate in a transparent way whether the Gorleben site is suited for safe final disposal at all and, if so, under what conditions. INE contributed to this project by formulating **source terms for radionuclide release from high-level waste glass, from spent nuclear fuel** and from compacted hulls and end pieces of fuel elements (CSD-C waste). The source term is based on kinetically and thermodynamically controlled mobilization / retention processes and on the influence of disposal concept and on temperature. Maximum expected concentrations of the radionuclides Am, Th, U, Np, Pu, Tc, Zr, Se and rare earth elements have been derived for a simplified evolution scenario of the disposal. INE elaborated on features, events and processes (FEP) relevant for application of the source terms in safety analysis.

Americium(III) complexes are thought to be nearly diamagnetic and therefore are expected to exhibit small NMR Knight shifts. In general all measured ^1H and ^{13}C resonances for the Am(III)-BTP system studied this year exhibit only minor shifts from resonances of the pure ligand.

The spectra show exceptionally small line widths and 2D spectra are accessible without further adaptation. Only **^{15}N NMR-resonances of coordinated nitrogen atoms in close proximity to the metal cation show exceptionally high chemical shifts** compared to isostructural lanthanide complexes, indicating very high electron density in this position. This electron density is not propagated onto the aromatic ring system, as no effect is observed on the resonances of adjacent ^{13}C nuclei in the pyridine ring. This is the first observation of a major spectral difference between actinide and lanthanide complexes of N-donor-ligands so far (Chapter 9.5).

The first international application of **KIT-INE's vitrification technology** for high level liquid waste (HLLW) is the VPC Project, which started in November 2009. Based on the basic design created in 2010, the main project activities in 2011 were dedicated to embellishment of the Detailed Design (DD) of the vitrification plant and the intermediate storage building for waste glass canisters. The scope of the DD carried out by INE covers the core process (HLLW reception, HLLW and glass frit feeding, glass melting, electric power supply for the melter including melter instrumentation and control, and wet off-gas treatment system). The DD provides the basis for procurement of the process equipment to be delivered to China by the German consortium in 2013. Special R&D work has been carried out for an improved melter off-gas pipe design with respect to a technique for periodic cleaning to overcome problems associated with the previous cleaning technique using air blasters (Chapter 8.2).

The **new whole body counter** developed at INE was used for the first real person measurements within the context of the Fukushima incident. More than 20 Persons returning post-Fukushima from Japan have been measured at KIT. Incorporation of slight amounts of fission products (e.g., I-131, Cs-137) were only detected in two persons. A first calibration of the counter was generated by Monte Carlo simulations and later confirmed by measurements with a brick phantom (Chapter 10).

3 Education and training

Teaching of students and promotion of young scientists is of fundamental importance to ensure high level competence and to maintain a leading international position in the fields of nuclear and radiochemistry. INE scientists are strongly involved in teaching at KIT-Campus South and the Universities of Heidelberg, Berlin, Jena and Mainz.

Prof. Dr. Horst Geckeis, director of INE, holds a professorship for radiochemistry at KIT Campus South, Department Chemistry and Biosciences. He teaches fundamental and applied radiochemistry for chemistry students in bachelor, master and diploma courses. A radiochemistry module consisting of basic and advanced lectures on nuclear chemistry topics and laboratory courses has been set up for diploma and master students in Karlsruhe.

Prof. Dr. Petra Panak, heading a working group on actinide speciation at INE, holds a professorship of radiochemistry at the University of Heidelberg. A basic course in radiochemistry is offered for bachelor and/or master students. An advanced course comprised of chemistry of f-elements and medical applications of radionuclides is also offered. The advanced radiochemistry lectures are supplemented by scientific internships at the INE radioactive laboratories.

Nearly 35 students from Karlsruhe and Heidelberg participated in two 3-week radiochemistry laboratory courses in 2011 held at KIT-CN in the FTU radiochemistry and hot laboratories at INE. Some students are intensifying their knowledge in nuclear/radiochemistry topics during scientific internships at INE. Obviously students became interested in nuclear chemistry topics and appreciate the various semester courses.

Dr. Andreas Bauer is lecturing Clay Mineralogy at the University of Jena. His lecture deals with mineralogical characterization of these fine materials and the importance of quantifying surface reactions. In the second part of the lectures sound, practical advice on powder X-ray diffraction in general is provided, as well as a useful set of step-by step instructions for the novice.

Lectures and practical units taught by Dr. Thorsten Schäfer at the Freie Universität Berlin, Institute of Geological Sciences, Department of Earth Sciences, focused in 2011 on a master degree course on laboratory and field methods in hydrogeology, including performance and analysis of tracer tests using conservative, weakly sorbing tracers and colloids, pumping

tests and determination of hydraulic parameters (Applied Hydrogeology III)

Dr. Thorsten Stumpf gave lectures at the KIT Campus South, Department Chemistry and Biosciences, in the field of chemistry of f-elements and inorganic chemistry. The seminar portion of the inorganic course was assisted by Dr. Tonya Vitova.

The lecture of Dr. Clemens Walther at the University of Mainz dealt with electric power generation. All currently applied major techniques for electricity generation were presented in the course, with a focus on nuclear energy and the scientific basics of nuclear fission. Advantages and drawbacks of each technique were compared and present resources, sustainability and technical development discussed.

Dr. Bastian Breustedt gave a lecture on biokinetics of radionuclides at KIT Campus South, Department Electrical Engineering and Information Technology. He also lectured in and co-organized a three week European Training course on Radiological Protection held at KIT-Campus North. This course was organized in the EC FP7 project ENETRAP2 and implemented pilot modules for a unified European Radiation Protection Training Scheme developed within ENETRAP.

Dr. Frank Becker gave lectures at the Baden-Wuerttemberg Cooperative State University (DHBW). The lectures comprised principles of statistics and measurements, atomic physics and nuclear physics.

Through this close cooperation with universities, students are educated in the field of nuclear and actinide chemistry, which most universities can no longer offer. Hence, INE makes a vital contribution to the intermediate and long-perspective of maintaining nuclear science competence.

PhD-students

In 2011 twenty students worked at INE on their doctoral dissertations; seven of them were awarded their doctorate. Topics of the theses are:

- Structural study on Cm(III) and Eu(III) complexes with ligands relevant to partitioning
- Interaction of trivalent lanthanides and actinides on various aluminium oxides/hydroxides minerals at the water interface
- Molecular dynamics and quantum-chemical calculations on aquatic actinide complexes

- Investigation of solubility and redox chemistry of Neptunium and Plutonium.
- Study on the complexation behaviour of actinides by ESI-MS
- Impact of kinetics and flow path heterogeneity on the migration of nanoparticle/radionuclide
- Incorporation of elements with low solubility in alkaline borosilicate glasses for the immobilisation of high-radioactive liquid waste
- Influence of pore clogging on the diffusion properties of porous media during geochemical perturbation: experiments and modelling
- Interaction of human serum transferrin with actinides and lanthanides
- Complexation of partitioning relevant N-donor ligands – water soluble BTP ligands for the i-SANEX process
- Comparative NMR-Studies of extraction agents for the separation of trivalent actinides
- Characterisation of bonding differences by high-resolution X-Ray emission and inelastic X-Ray scattering techniques.
- Technetium mobility in natural systems, influence of ferrous iron speciation.
- Technetium redox processes and Technetium (IV) solubility in dilute to highly saline systems.
- Sorption of trivalent actinides on magnetite.
- Stochastic aspects of internal dosimetry
- Design and setup of a new HP Ge detector based body counter capable of detecting also low energy photon emitters.
- Development of anthropomorphic models for in vivo measurements in radiation protection.
- Monte Carlo simulation of mixed neutron-gamma radiation fields and dosimetry devices.
- Simulation of the partial body dose during handling scenarios in inhomogeneous, time variant beta-/photon radiation fields.

4 National and international cooperation, conferences and workshops

INE R&D involves numerous national and international cooperation and projects. These are described in the following.

National

INE is involved in various bi- and multilateral cooperations with national research centers, universities and industrial partners on different topics. The projects are partly supported by the German Federal Ministry for Economics and Technology (BMW), the Federal Ministry for Education and Research (BMBF), the Federal Ministry for the Environment, Nature Conservation and Nuclear Safety (BMU), the German Research Foundation (DFG) and the Helmholtz Association (HGF).

Primary goal within the collaborative project **VESPA** with partners GRS, FZD-IRC and FZJ-IEF is to reduce the conservatism in the assumptions currently made in performance assessment calculations concerning the radionuclides ^{14}C , ^{79}Se , ^{129}I and ^{99}Tc . There is reasonable evidence that sorption values for radionuclides on organics, clay surfaces, layered double hydroxides or steel corrosion products are significantly higher than currently used in modeling approaches. This could, in "what if" scenarios, lead to significantly lower radionuclide release rates than currently predicted. The project VESPA focuses on the reduction of these uncertainties.

Within the **THEREDA** project, INE generates a centrally managed and administered database of evaluated thermodynamic parameters in cooperation with the Gesellschaft für Anlagen- und Reaktorsicherheit (GRS) mbH, Braunschweig, Helmholtzzentrum Dresden-Rossendorf, Institut für Ressourcenökologie (HZDR-IRE), Technische Universität Bergakademie Freiberg, Institut für Anorganische Chemie (TU-BAF) and AF-Colenco AG, Baden (Schweiz). Thermodynamic data are required for environmental applications in general and radiochemical issues in particular. This database is to be developed to a national (reference) standard and will be the basis for performance assessment calculations for a national nuclear waste repository.

The **HATT** project focus is on the migration of radionuclides in natural clay formations and in bentonite, considered as technical barrier. Within this project not only the mechanism of radionuclide sorption onto clay is studied, but also the influence of organic matter naturally occurring in the clay stone on the radionuclide migration. Parallel to the characterization of

clay organic compounds, the interaction of actinides with humic substances, kerogen-like compounds and small organic molecules are examined. Besides INE, the members of this collaborative project are GRS, FZD-IRC, University of Mainz, University of Potsdam, University of Munich and University of Saarland.

The bilateral GRS-INE project **KOLLORADO-2** started mid-2009 as successor of the KOLLORADO project, focusing on the erosion stability of compacted bentonite barrier as a function of the contact water chemistry/hydraulics and the formation of near-field colloids/nanoparticles as potential carriers for actinides/radionuclides. Both a detailed experimental program investigating the influence of surface roughness/charge heterogeneity on nanoparticle mobility and actinide bentonite nanoparticle sorption reversibility, as well as approaches to implement the acquired process understanding in reactive transport modeling codes comprise the project activities.

In the BMBF/DFG funded joint research project **RECAWA** with partners from KIT (Institute of Reinforced Concrete Structure and Building Materials; KIT-IfMB, Institute of Mineralogy and Geochemistry; KIT-IMG), the University Frankfurt (Institute of Geoscience, UniFaM-IfG) and industrial partners (Rheinkalk Akdolit, Lafarge Cement and Schäfer Kalk), basic understanding of processes with regard to the reactivity and dynamics of calcite mineral surfaces during crystal growth in aquatic systems are being developed. INE focuses on the immobilization of environmentally relevant anionic trace elements (e.g., Se) on calcite surfaces using an integrated approach on the basis of batch sorption and co-precipitation experiments with molecular calculations and spectro-microscopic information.

The BMBF project funded in the framework of the funding concept 'Basic research Energy 2020+' entitled "**Grundlegende Untersuchungen zur Entwicklung und Optimierung von Prozessen zur Abtrennung langlebiger Radionuklide** (Partitioning)" continued in 2010. This is a cooperative project between KIT (both Campus North and South), Forschungszentrum Jülich and the Universities of Erlangen and Heidelberg and aims at understanding the differing reactivity between 4f and 5f elements with the ultimate goal of using this information to optimize their separation in partitioning.

The general aim of the BMWi Joint Project on the **Comparison of Constitutive Models III** is to check the ability of numerical models to describe correctly relevant deformation phenomena in rock salt under various influences, and thus increase confidence in numerical simulations and thereby enhance acceptance of results. Another aim is to identify possibilities for further model development and improvement.

Within the BMBF-project **Radiation and environment I** INE is responsible for the work package “Sources of uncertainty in internal dosimetry – analysis of biokinetic models”, in which biokinetic models for actinides have been analyzed for variations in their predictions as a function of parameter variability. The resulting uncertainties of the dose estimations have been assessed. In collaboration with HMGU Munich, the methods developed at INE have been applied in an uncertainty analysis for the new biokinetic model of zirconium developed at HMGU. In the succeeding BMBF-project **Radiation and Environment II**, INE is responsible for the work package “Efficiency calibration of in-vivo counters with anthropomorphic models adapted to individuals”. In this work package, the influence of different anatomies on the calibration of in-vivo counters and subsequent dosimetry measurements are studied and quantified. By modifying the models, a better agreement between the geometries of measurement and calibration shall be reached. Different biometric parameters of the individual are measured and used in the adaption of the models.

The Virtual Institute (VI) “**Advanced Solid-Aqueous Radio-Geochemistry**”, supported by the HGF and coordinated by INE, began in March 2008. The work is focused on the elucidation of reaction mechanisms, which are responsible for the migration and/or retardation of radionuclides. The investigations cover over a broad scale of complexity, from thorough study of model systems for solid solution formation (calcite, powellite), up to monitoring the complex interaction of cations and anions with cementitious material under repository conditions. Experimental work, modern spectroscopy and Monte Carlo simulations, as well as quantum mechanical calculations are performed to achieve a process understanding on a molecular level. Members of the VI are KIT, the Universities of Frankfurt (Germany) and Oviedo (Spain), the Research Center Jülich and the Paul Scherrer Institute (PSI) in Switzerland.

The Helmholtz young investigator group (HYIG) “**Advanced synchrotron-based systematic investigations of actinide (An)**

and lanthanide (Ln) systems to understand and predict their reactivity” started July 2011 and will systematically investigate in-situ the electronic and coordination structure of actinides and chemical homologue lanthanide systems with novel synchrotron-based high resolution X-ray emission/inelastic scattering techniques. The experimental results are supported by theoretical calculations and simulations with quantum chemical codes. These investigations will improve our understanding of actinide/lanthanide reactivity in repository systems and waste matrices on a molecular scale and thereby support the reliability of evaluation of repository long term safety. The elucidation of electronic and coordination structures of, e.g., actinide/lanthanide extraction ligand complexes will find application in optimization of separation technologies of lanthanide cations from minor actinides (partitioning), while at the same time provide basic insight into structure-reactivity relationships of actinide elements, which is a present scientific frontier.

International

Two international projects focus on the stability of the conducting features of bentonite buffer/backfill in contact with water and the influence of colloids on radionuclide migration in crystalline host rock: the Colloid Formation and Migration (**CFM**) experiment, coordinated by NAGRA (National Cooperative for the Disposal of Radioactive Waste, Switzerland), and the Colloid Project, initiated by SKB (Swedish Nuclear Fuel and Waste Management Co., Sweden). Both projects are currently jointly working together using the experimental set-up at the Grimsel Test Site (Switzerland). Additional partners involved are from Japan (JAEA, AIST, CRIEPI), South Korea (KAERI), Finland (POSIVA Oy), Switzerland (NAGRA, PSI-LES), and Spain (CIEMAT). INE plays a decisive role in the laboratory program of both projects and is also mainly carrying out the field activities.

EURATOM 7th Framework Program

The Collaborative Project (CP) “Redox Controlling Systems” (**ReCosy**) started in April 2008. Main objectives of ReCosy are the sound understanding of redox phenomena controlling the long-term release/retention of radionuclides in nuclear waste disposal and providing tools to apply the results to performance assessment/safety case. The project is coordinated by INE, with Amphos 21 as the coordination secretariat and 32 institutions from 13 European countries contributing over the four-year duration of this CP. The international interest in ReCosy is large and organizations from the Finland,

Japan, Korea, UK and USA have signed associated group agreements.

An additional Collaborative Project (CP) continued this year, namely "Cation diffusion in clayrocks" (**CatClay**), which began in June 2010. The aim of CatClay is to improve understanding of the phenomena governing migration of radionuclides in clayrocks as potential host rocks for the deep geological disposal of nuclear waste. The project focuses on the diffusion-driven transport of cationic species, Sr^{2+} , Zn^{2+} and Eu^{3+} , which are more or less strongly sorbed on clay mineral surfaces. CatClay, coordinated by CEA, combines model and experimental developments from the partners, ANDRA, BRGM, CEA, SCK-CEN, PSI-LES, Appelo Hydrochemical Consultant and KIT-INE.

The CP "Actinide Recycling by Separation and Transmutation" (**ACSEPT**) is dedicated to the development of actinide separation processes. It is a four year project (2008-2012) coordinated by CEA. KIT-INE leads the "hydrometallurgy" domain. The consortium consists of 34 members from Europe, Japan and Australia. ACSEPT is a continuation of previous FP4, FP5 and FP6 partitioning projects in which KIT-INE also participated.

INE continues to be a core member in **ACTINET-I3**, the follow-up project to the European "Network of Excellence for Actinide Sciences" (ACTINET-6, with EC FP6 and ended in 2008). ACTINET-I3 is an Integrated Infrastructure Initiative and commenced in January 2010. In contrast to the former ACTINET, the present consortium has only eight members. These are the leading European actinide laboratories: CEA, JRC-ITU and KIT-INE, as well as FZD, PSI, CNRS, KTH and UNIMAN. The objectives of ACTINET-I3 are: (i) to establish and strengthen a network of actinide facilities across the EU and to foster their joint development in terms of capacity and performance; (ii) to support and manage jointly a program of access to appropriate infrastructures for training and associated research projects making use of the proposed facilities; (iii) to conduct on a limited scale a set of Joint Research Activities (JRA) involving consortium member organisations, with an objective to improve the performance of infrastructures by developing new relevant instrumentations and/or data of common interest; (iv) to provide open access to the actinide laboratories and the integrated beamlines for outside scientists to perform experimental work within well-defined joint research projects. Further, these activities are complemented by a virtual infrastructure, the Theoretical User Lab, providing support in

theoretical and computational chemistry and modeling, with a focus on the complementarities between theory and experiment.

The **EURACT-NMR** project is a new 32 month coordination and support action starting February 2011 and is established to provide transnational access to the Karlsruhe Actinide NMR Centre of Excellence with state-of-the-art nuclear magnetic resonance facilities at the KIT-INE and JRC Institute for Transuranium Elements (ITU). These institutes have two 400 MHz NMR spectrometers, which have been adapted to allow advanced nuclear magnetic resonance experiments on radioactive solid and liquid materials. The aim of EURACT-NMR is to open up unique and newly available actinide nuclear magnetic resonance facilities to nuclear researchers across Europe and EC associated countries. Additionally it will help to nurture nuclear magnetic resonance expertise and awareness amongst the European nuclear research community, in order to develop new experimental validation methods for complex models of the behaviour in nuclear materials and processes.

Activities of the collaborative project **SKIN** (Slow processes in close-to-equilibrium conditions for radionuclides in water/solid systems of relevance to nuclear waste management) began upon its establishment in February 2011. Solid/liquid chemical equilibrium hypotheses (sorption, solubility, solid-solution formation) are key concepts in the assessment of nuclear waste safety. The project intends to assess the effect of surface properties on apparent solubility, as well as the kinetics of incorporation of radionuclides in the structure of a solid phase, and the associated reaction mechanisms for various solids in a systematic manner, using isotope exchange under close-to-equilibrium conditions.

The collaborative project **CROCK** (crystalline rock retention processes) aims at improving the safety case for crystalline rock far-field as a radionuclide migration barrier. Uncertainty and associated conservatism are the key problems in including radionuclide retention for improving safety prognoses. The overall CROCK objective is to develop a methodology for decreasing the uncertainty in the long-term prediction of the radionuclide migration in the crystalline rock far-field. Key aspects of radionuclide retention in this case are regarded, i.e. chemical processes and enhanced residence time in stagnant flow-system regions (matrix diffusion). The project started on January 1, 2011 and will last 30 months.

The **BOOSTER** project (BiO-dOSimetric Tools for triagE to Responders) addresses the requirement of effective management of an incident involving exposure of large numbers of people to radioactive material. BOOSTER is a capability project designed to research and develop new bio-dosimetric tools, in order to quickly evaluate the level of potential casualties, determine by appropriate sensors their consequences, allow an efficient triage of exposed people, integrate a useful and usable toolbox, train civil protection operators and define commercial exploitation potentialities.

Conferences and workshops

INE has organized a series of workshops and conferences or has contributed significantly to the organization:

- **Goldschmidt 2011** Conference, August 14-19, 2011 in Prague, **Session 8e: “Current Challenges in Predicting Trace Metals Mobility in the Environment”**
- **Goldschmidt 2011** Conference, August 14-19, 2011 in Prague, **Session 8j: “Nanoparticles, interfacial processes and nuclear waste management”**
- International symposium on **“Clays under Micro- to Nanoscopic Resolution”**, September 6-8, 2011 in Karlsruhe
- **MIGRATION 2011**, 13th International Conference on the **Chemistry and Migration Behaviour of Actinides and Fission Products in the Geosphere**, September 18-23, 2011 in Beijing, China
- Basic Training Course **“Monte Carlo Simulations for Micro- and Nanodosimetry”** funded by the Karlsruhe House of Young Scientists (KHYS), October 25-26, 2011, KIT-Campus North
- **Actinide Brine Chemistry in a Salt-Based Repository (ABC-Salt II)**, November 7- 8, 2011 in Karlsruhe
- International Workshop on **High Temperature Aqueous Chemistry (HiTAC)**, November 9, 2011, KIT-Campus North

5 Fundamental studies: Process understanding on a molecular scale

The subsequent chapter on fundamental studies focuses on a bottom-up approach of recent achievements on an atomistic scale on basic actinide chemistry in aqueous solution, actinide interaction with mineral/water interfaces and the formation of actinide/long-lived fission product containing solid solution phases. These in detail mechanistic understandings will allow describing exactly the relevant processes to reliably predict migration of actinides and long-lived fission products in the near- and far-field of a nuclear repository in deep geological formations. In order to ensure trustworthy predictions of retention/retardation mechanisms and their thermodynamic quantification provision of reliable thermodynamic data and models but also fundamental understanding of molecular scale processes is needed, especially under higher ionic strengths.

The reported studies deal with the chemistry of actinides in aqueous solution to derive realistic actinide solubility data, spectroscopic studies on the interaction of actinides with aluminium /hydr(oxides) and ferric iron phases to implement realistic surface complexes in modeling approaches and the structural entrapment of actinides and long-lived fission product in neo-formations of mineral phases due to the geochemical gradient induced by the multi-barrier concept. These fundamental studies detailed here provide the basis for the applied studies on natural systems relevant for safety assessment.

5.1 Chemistry and thermodynamics of actinides in aqueous solution

M. Altmaier, D. Bach, D. Fellhauer^{a,b}, X. Gaona, K. Hinz, T. Kobayashi^d, P.J. Panak, J. Rothe, A. Skerencak, E. Yalcintas

In co-operation with:

Th. Fanghänel^{a,b}, H. Moriyama^c, M.-L. Morkos^c, T. Sasaki^d

^a JRC-ITU, European Commission, Karlsruhe, Germany; ^b Heidelberg University, Heidelberg, Germany; ^c Research Reactor Institute, Kyoto University, Osaka, Japan; ^d Department of Nuclear Engineering, Kyoto University, Kyoto, Japan

Introduction

The aqueous chemistry of actinides and long-lived fission products plays an important role in activities related to nuclear waste disposal. Based upon a fundamental understanding of the main processes controlling the chemical behaviour of radionuclides in aqueous systems, it becomes possible to predict how the radionuclide solubility in a repository will evolve as function of different geochemical boundary conditions and to derive radionuclide source terms for possible scenarios. The work performed on the aqueous chemistry of actinide and long-lived fission products is therefore directly bridging basic scientific investigations (presented here) with questions related to an applied context (e.g. Gorleben, Asse).

The solubility and chemical speciation of radionuclides in aqueous solution has been a focus of research activities at INE for two decades. Aim of the mostly experimentally oriented investigations is a comprehensive thermodynamic description of actinide solubility and speciation based upon correct and robust chemical and thermodynamic models. Advanced spectroscopic techniques, giving chemical information on a molecular scale, are frequently used to complement the thermodynamic data evaluation performed on a macroscopic level. Consistent sets of thermodynamic

data are published in peer reviewed journals and contributed to thermodynamic databases, e.g. THEREDA or NEA-TDB.

Among several other research activities at KIT-INE related to actinide redox chemistry, much effort has recently been focussed on neptunium chemistry under redox neutral or oxidising conditions. The investigations are covering a broad range of chemical boundary conditions and include detailed analysis of both solid and aqueous Np(V) and Np(VI) phases. Reflecting the continuing strong commitment of KIT-INE to actinide brine chemistry, the studies range from dilute to concentrated salt brines, relevant for waste disposal in salt rock formations.

Over the last years, increasing research efforts have been focussed on the aqueous chemistry and thermodynamics of actinides at elevated temperature conditions. At present, the influence of elevated temperatures on aqueous actinide chemistry is not properly understood and the available thermodynamic database insufficient. As two examples from our ongoing successful studies, work on temperature effects affecting Zr-oxyhydroxide solid phase stability and Zr(IV) solubility and studies on Cm(III)-propionate complexation are presented.

Solubility and speciation of Np(V) in alkaline CaCl₂ Solutions

The solubility and speciation of Np(V) under highly saline conditions is an interesting aspect of actinide chemistry and relevant in the context of nuclear waste disposal in rock salt formations. In order to investigate the hitherto unknown solution chemistry of Np(V) in concentrated alkaline CaCl₂ solutions and to derive a comprehensive thermodynamic model, a series of solubility experiments have been performed and complemented by advanced spectroscopy techniques.

Solubility batch experiments with Np(V) in 0.25, 1.0, 2.0, 3.5 and 4.5 M CaCl₂ at pH_c = 8 - 12 were prepared under inert gas atmosphere. The supernatant aqueous solutions were analysed for pH_c, E_h, Np concentration (LSC) and Np speciation (UV-VIS-NIR, EXAFS) over several months. Solid phases were characterized by XRD, quantitative chemical analysis, DTA, XANES, EXAFS and SEM-EDS. Based upon the solubility data, solid phase characterization and spectroscopic evidence, a comprehensive thermodynamic model is evaluated using both the specific ion interaction theory (SIT) [1] and Pitzer approach [2].

Freshly precipitated greenish NpO₂OH(s) was equilibrated in 2.0 M CaCl₂ at pH_m = 11.5 and transformed into a gray secondary solid phase CaNpO₂(OH)_{2.6}Cl_{0.4}·2H₂O(s). Aliquots of this solid were then distributed to 0.25 – 4.5 M CaCl₂ matrix solutions at defined pH conditions. Further transformation of this solid phase into a more stable and hence less soluble reddish Ca_{0.5}NpO₂(OH)₂·1.3H₂O(s) was observed over time. The solubility curves of this solubility limiting phase are divided into three regions:

(a) Between pH_c = 8 and 10, a systematic decrease of the Np(V) concentration with a slope of -2 (log [Np(V)] vs. pH_c) is observed as expected for the equilibrium Ca_{0.5}NpO₂(OH)₂(s) + 2 H⁺ ⇌ NpO₂⁺ + 2 H₂O + 0.5 Ca²⁺. The predominance of the NpO₂⁺ ion in this pH_c range was confirmed by UV-VIS-NIR spectroscopy.

(b) A constant equilibrium concentration independent of pH but increasing with CaCl₂ concentration from log [Np] = -8.5 (0.25 M CaCl₂) to -6.0 (4.5 M CaCl₂) is found at pH_c = 10.8 – 11.2. This can be explained by the formation of a second Np(V) hydrolysis complex.

(c) In the most alkaline pH_c range 11.2 – 12.0 investigated and CaCl₂ ≥ 1.0 M, the solubility increases systematically with pH_c with a defined slope of +3 (log Np vs. pH_c). Considering Ca_{0.5}NpO₂(OH)₂·1.3H₂O(s) as the solubility controlling solid phase, the enhanced Np(V) concentration indicates the formation of Np(V)-hydrolysis species with more than 2 OH⁻ li-

gands, unknown in analogue Na salt systems at [OH⁻] < 1 M.

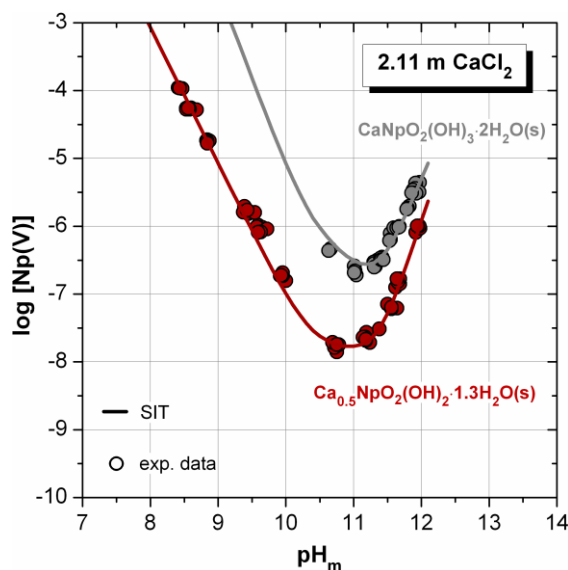


Fig. 1: Solubility of Np(V) in 2.0 M CaCl₂ solution. Lines represent calculations based upon Pitzer model.

In order to analyze the aqueous Np speciation under the most alkaline conditions, EXAFS studies have been performed at the INE beamline for actinide research at ANKA, Karlsruhe. Np(V) is surrounded by oxygen atoms in the first coordination sphere reflecting a distorted neptunyl structure. Strong Ca backscattering observed in the second coordination sphere evidences the formation of a ternary Ca-Np(V)-OH complex not described before. Consequently, two new aqueous Np(V) complexes have been proposed to describe the solubility and speciation of Np(V) in alkaline CaCl₂ media, Ca[NpO₂(OH)₂]⁺ and Ca₃[NpO₂(OH)₅]²⁺. This interesting new finding is relevant for assessing Np solubility and proves that ternary Ca-An-OH complex formation is not limited to the tri- and tetravalent actinides [3-6] but constitutes a general phenomenon in alkaline CaCl₂ solutions.

Solubility and speciation of Np(VI) in dilute to concentrated alkaline NaCl solutions

The solution chemistry of Np(VI) under alkaline conditions so far is largely unknown. In the aqueous phase, the formation of hexavalent anionic species (e.g. NpO₂(OH)₃⁻ and NpO₂(OH)₄²⁻) has been proposed, although no thermodynamic data are currently selected in the NEA reviews. In analogy to U(VI), the pre-

precipitation of Na- and Ca-neptunates(VI) may also be expected. The formation and relevance of these aqueous neptunium(VI) species and solids in oxidising alkaline solution has recently been proven in spectroscopic studies by X. Gaona et al. [7], but accurate thermodynamic data is lacking so far.

Solubility experiments with $^{237}\text{Np(VI)}$ were conducted in dilute to concentrated carbonate free NaCl solutions ($0.1 \text{ M} \leq I \leq 5.0 \text{ M}$) under inert gas atmosphere to assess the thermodynamic properties of the aqueous species and solid compounds forming under alkaline conditions. In all cases, solubility curves were characterized by three well-defined regions (Fig. 2a): (i) $\sim 7 \leq \text{pH}_m \leq \sim 9.5$, showing a steep decrease in the solubility with a slope of approximately -3 ; (ii) $\sim 9.5 \leq \text{pH}_m \leq \sim 11$, with a nearly pH-independent $[\text{Np}]$ and (iii) $\sim 11 \leq \text{pH}_m \leq \sim 13.5$, showing an increase in the solubility with a well-defined slope of $+1$.

The characterization of the solid phases controlling the solubility was done by XRD (Fig. 2b), quantitative chemical analysis and SEM-EDS, indicating the prevalence of a solid phase with a Na:Np ratio of 1:1, likely $\text{NaNpO}_2\text{O(OH)(cr)}$ (or $\text{Na}_2\text{Np}_2\text{O}_7 \cdot \text{H}_2\text{O}$). EXAFS (Fig 2c) further indicated the predominance of a neptunate-like structure with significantly short Np-O_{ax} and Np-O_{eq} distances ($1.76 \pm 0.02 \text{ \AA}$ and $2.12 \pm 0.03 \text{ \AA}$, respectively).

The slope analyses of these solubility data, together with the stoichiometries determined for the solid phases as well as direct chemical analogies with U(VI), led to the definition of the equilibrium reactions $\text{NaNpO}_2\text{O(OH)(cr)} + \text{H}_2\text{O} \rightleftharpoons \text{Na}^+ + \text{NpO}_2(\text{OH})_3^-$ and $\text{NaNpO}_2\text{O(OH)(cr)} + 2\text{H}_2\text{O} \rightleftharpoons \text{Na}^+ + \text{NpO}_2(\text{OH})_4^{2-} + \text{H}^+$ to prevail in the regions "ii" and "iii" of the solubility curves. The equilibrium reaction controlling Np(VI) solubility in region "i" remains unclear, although it is suspected that reduction to Np(V) may have occurred under the pH_m and E_h conditions of the study. The work is ongoing and will be completed with the thermodynamic modelling considering both SIT and Pitzer approaches.

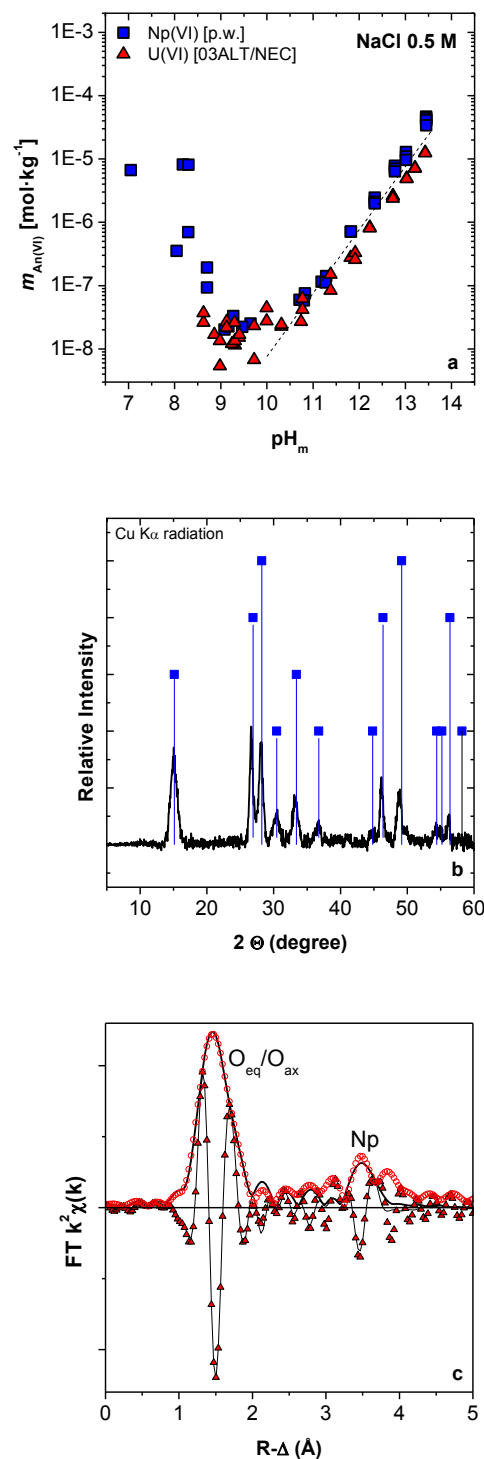


Fig. 2: (a) Solubility curve of Np(VI) [p.w.] and U(VI) [8] in NaCl 0.5 M; (b) XRD spectra of a selected solid phase from solubility experiment at $I = 1.0 \text{ M}$ NaCl. Squares mark peak positions and relative intensities reported in [9] for $\text{Na}_2\text{Np}_2\text{O}_7$; (c) Experimental and theoretical k^2 -weighted Fourier transforms for a Np(VI) solid equilibrated in 2.5 M NaCl.

Effect of temperature on the solubility and solid phase of Zirconium hydroxide

For room temperature conditions it is known that the strong hydrolysis of Zr(IV) leads to mononuclear, polynuclear, and colloidal hydrolysis species in aqueous systems. The total solubility of amorphous Zr(IV) hydroxide can be derived as the sum of these solution species and correlated to the characteristics of the solubility limiting amorphous Zr(IV) hydroxide solid phase [10]. The description of radionuclide solubility at elevated temperatures, needs to address systematic effects on the thermodynamic stability of the solid phases in addition to changes in solution chemistry. At elevated temperature, a transformation of the amorphous solid phase precipitated initially from oversaturation into a more crystalline solid phase with lower Gibbs energy can be expected [11,12]. As a case study exploring systematic trends expected also for other actinide solid phases, temperature effects on solid Zr(IV) hydroxide phase stability and total Zr(IV) solubility in 0.5 M NaClO₄ and 0.5 M NaCl were investigated.

The sample solutions investigated in this study were prepared from oversaturation approach leading to precipitation of nanocrystalline "amorphous" phases at 0.01 M total initial Zr concentration. The hydrogen ion concentration (pH_c) was adjusted at pH_c 0 – 6. The sample solutions were kept in an oven controlled at 50°C, 70°C and 90°C. After given periods, samples were taken out from the oven and slowly cooled down to room temperature. The pH_c and [Zr] was then measured after ultrafiltration (3 - 100 kD, Millipore) at RT. The solid samples were treated in a similar manner in 0.5 M NaCl. The precipitates were separated by centrifugation and prepared at room temperature. XRD and TEM were used to investigate the crystallinity and particle size of the solid phase.

Fig. 3 shows the solubility (2-3 nm ultrafiltration) after heating intervals at 90°C compared to the reference solubility data of Zr(OH)₄(am) and ZrO₂(cr) at RT [13,14]. The solubility after heating at 90°C significantly decreased within several days. The values after 18 d are close to the solubility of ZrO₂(cr) measured from undersaturation, suggesting the transformation of the initial nanocrystalline solid into a more crystalline phase.

The XRD spectra of the solid phase after heating at 90°C for 34 days showed several sharp peaks corresponding to ZrO₂(cr) in contrast to the very broad peaks found for the initial solid. The result of TEM analysis shows agglomeration of solid particles and growth in average

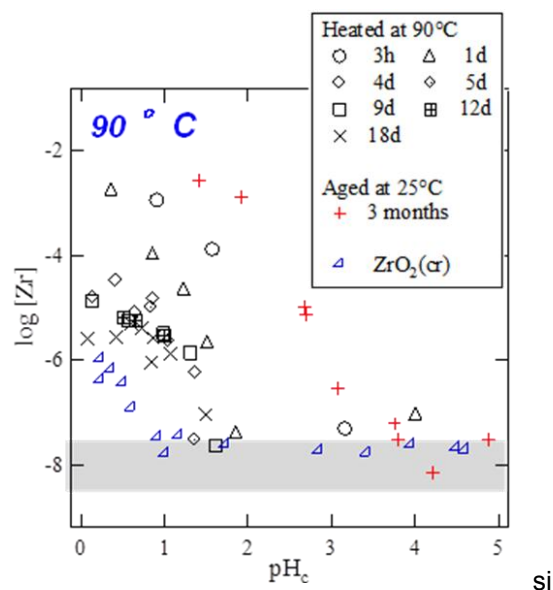


Fig. 3: Zr(IV) solubility after heating at 90°C compared with Zr(OH)₄(am) and ZrO₂(cr) solubility at room temperature.

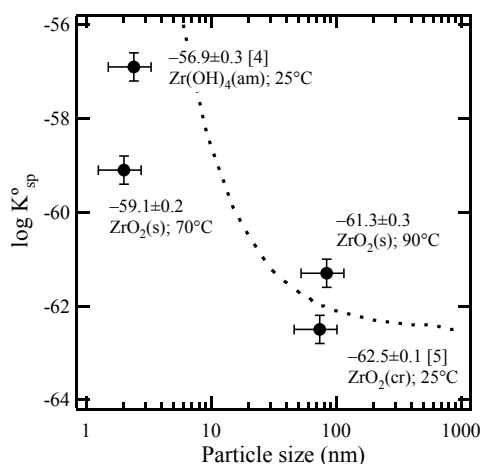


Fig. 4: Effect of particle size on solubility product of Zr oxides. The broken line represents the calculated line reflecting the particle size effect.

size after heating. The average size of the agglomerated solid particles is about 80 nm, while the particle size of initial nanocrystalline "amorphous" solid is about 2 nm. In the TEM image of the solid phase stored at 90°C, each agglomerate exhibits the same crystal orientation. From XRD and TEM analysis, it is obvious that the initial "amorphous" solid phase was transformed into larger Zr oxide crystallites after ageing at elevated temperatures.

The results can also be systematized by applying a relationship between solubility product values (or Gibbs energy) and the particle size of the solid metal oxide phases as shown in Fig. 4. Because of the larger molar surface area of smaller particles, the contributions from surface energy to the total Gibbs energy of

formation are higher, and hence the total solubility of smaller particles is expected to be systematically higher than of larger particles having the same stoichiometry and crystal structure [15]. As shown in Fig. 4, the thermodynamic stability of the Zr solid phases observed in the present study agrees with the theoretical curve based on the Schindler effect. This work clearly supports the predicted thermodynamic trend to more crystalline and hence less soluble solid phases controlling solubility under elevated temperature conditions.

Complexation of Cm(III) with propionate in aqueous NaCl at increased temperatures.

The thermodynamics of the formation of $[Cm(Prop)_n]^{3-n}$ ($n = 1, 2$) complexes in aqueous NaCl solution was studied by TRLFS at $T = 25 - 90^\circ\text{C}$. Systematic experimental series were performed at different ionic strengths and varying ligand concentrations. The thermodynamic $\log K_n^0(T)$ equilibrium constants were derived from the conditional stability constants using the SIT approach. The integrated van't Hoff equation was used to determine the thermodynamic constants ($\Delta_r H_m^0$) from the temperature dependent $\log K_n^0(T)$ values. Furthermore, $\Delta \epsilon_n(T)$ values ($n = 1, 2$) were obtained by using linear SIT regression analysis. The results of the present work are compared to literature values determined in NaClO_4 medium [16].

The species distribution was determined as a function of the ligand concentration by peak deconvolution of the Cm emission spectra at every studied temperature. The results show a distinct increase of the molar fractions of the $[Cm(Prop)_n]^{3-n}$ species with increasing propionate concentration and/or temperature. The chemical equilibrium is shifted towards the complexed species at $T > 25^\circ\text{C}$. These results are in excellent agreement with literature [16].

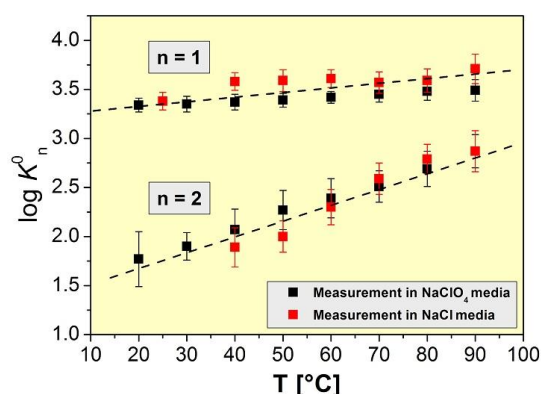


Fig. 5: $\log K_n^0(T)$ values for the $[Cm(Prop)_n]^{3-n}$ complexes ($n = 1, 2$), determined in aqueous NaCl (red, p.w.) and NaClO_4 (black, [16]).

The formation of the 1:1- and 1:2 complexes is confirmed by slope analysis at every studied temperature. For this, the free ligand concentration $[Prop]_{eq}(T)$ is calculated as a function of the temperature using the temperature dependent $\log K_s^0(T)$ of propionic acid [16].

The conditional stepwise stability constants ($\log K_n^0(T)$) were determined as a function of the ionic strength and extrapolated to $I_m = 0$ with the SIT approach [1]. The $\log K_n^0(T)$ values are displayed in Fig. 5 together with the literature data for aqueous NaClO_4 medium. The $\log K_1^0(25^\circ\text{C}) = 3.38 \pm 0.09$ increases moderately by 0.33 orders of magnitude over the studied temperature range. By comparison, $\log K_2^0$ shows a distinctively stronger temperature dependency, the values increasing by almost one order of magnitude. These results are again in excellent agreement with NaClO_4 data (see Fig. 5).

The $\log K_n^0(T)$ values are linearly correlated with the reciprocal temperature. Thus, the integrated van't Hoff equation is used to model the temperature dependency of the stability constants, assuming constant $\Delta_r H_m^0$ and $\Delta_r C_{p,m}^0 = 0$. The thermodynamic constants in NaCl and NaClO_4 media are shown in Table 1.

Tab. 1: Thermodynamic data of the stepwise formation of $[Cm(Prop)_n]^{3-n}$ ($n = 1, 2$) in NaCl (p.w.) and NaClO_4 medium [16]

NaCl medium	n = 1	n = 2
$\Delta_r H_m^0$ [kJ/mol]	6.0 ± 1.6	49.2 ± 4.1
$\Delta_r S_m^0$ [J/mol·K]	86.7 ± 3.1	191.8 ± 12.1
NaClO ₄ medium	n = 1	n = 2
$\Delta_r H_m^0$ [kJ/mol]	5.8 ± 1.1	30.4 ± 2.3
$\Delta_r S_m^0$ [J/mol·K]	83.2 ± 3.6	138.3 ± 7.8

The results show positive $\Delta_r H_m^0$ and $\Delta_r S_m^0$ values indicating that the formation of the $[Cm(Prop)_n]^{3-n}$ complexes is entropy driven. The results for the first Cm-propionate complex are in very good agreement with the data determined in NaClO_4 . For the second complex, $\Delta_r H_m^0$ is by 19 kJ/mol and $\Delta_r S_m^0$ by 53 J/mol·K higher than the value for the NaClO_4 medium.

Using linear SIT regression analysis of the $\log K_n^0 - \Delta z^2 D$ data, the $\Delta \epsilon_n(T)$ values for the respective complexation reactions were determined. The results are displayed in Fig. 6 together with the literature data for the NaClO_4 electrolyte system. The $\Delta \epsilon_n$ values show no clear temperature dependency which is in good agreement with literature [16,17]. Thus,

constant values of $\Delta\epsilon_1 = -0.11 \pm 0.04$ and $\Delta\epsilon_2 = -0.14 \pm 0.10$ are determined, respectively. The $\Delta\epsilon_n$ values for the NaCl- and NaClO₄ medium are in good agreement, which is expected for complexation reactions with the same charge of the ligands and the metal.

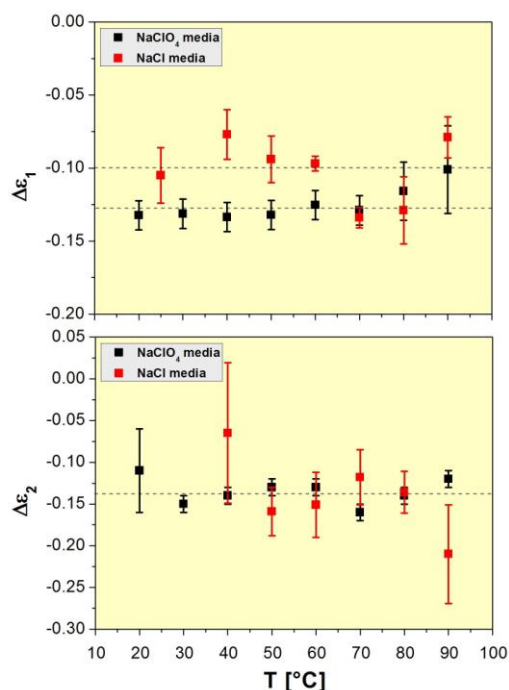


Fig. 6: $\Delta\epsilon_n(T)$ values for the stepwise formation of the $[Cm(Prop)_n]^{3-n}$ complexes in NaCl (red, p.w.) and NaClO₄ (black, [16]) media.

Using the parameters of $\epsilon(\text{Am}^{3+}, \text{Cl}^-) = 0.23 \pm 0.02$ and $\epsilon(\text{Ac}^-, \text{Na}^+) = 0.08 \pm 0.01$, given by the NEA-TDB, the ion-ion-interaction coefficients for the $[Cm(Prop)_n]^{3-n}$ complexes ($n = 1, 2$) in aqueous NaCl solution are calculated [17]. The results are displayed in Tab. 2, together with the data for the NaClO₄ medium.

Tab. 2: Ion-ion-interaction coefficients for the stepwise formation of $[Cm(Prop)_n]^{3-n}$ ($n = 1, 2$).

	$n = 1$	$n = 2$
$\epsilon(\text{CmProp}_n^{3-n}, \text{Cl}^-)$	0.21 ± 0.09	0.15 ± 0.11
$\epsilon(\text{CmProp}_n^{3-n}, \text{ClO}_4^-)$	0.45 ± 0.09	0.44 ± 0.11

The ion-ion interaction coefficients of the Cm(III) propionate complexes with Cl⁻ determined in this work are of particular interest for

the description of the migration behavior of trivalent actinides in natural clay formations at elevated ionic strength conditions. Furthermore, this study contributes to establishing a comprehensive thermodynamic database applicable for elevated temperature conditions.

References

- [1] L. Ciavatta, *Annali di Chimica (Rome)* 70 551-567 (1980).
- [2] K. S. Pitzer, CRC Press, Boca Raton, Florida (1991).
- [3] M. Altmaier et al., *Radiochim. Acta* 96, 541-550 (2008).
- [4] Th. Rabung et al., *Radiochim. Acta* 96, 551-559 (2008).
- [5] D. Fellhauer et al., *Radiochim. Acta* 98, 541-548 (2010).
- [6] B. Brendebach et al., *Inorg. Chem.* 46, 6804-6810 (2007).
- [7] X. Gaona, et al., *Radiochimica Acta* DOI: 10.1524/ract.2012.1948 (2012).
- [8] M. Altmaier, et al., *Proceedings of the Migration 2003 Conference*, Gyeongju (Korea).
- [9] C. Keller, et al., *Journal of Inorganic Nuclear Chemistry*, 27, 1205-1223.
- [10] P. Brown et al., *Chemical Thermodynamics of Zirconium*, Elsevier, Amsterdam (2005).
- [11] V. Keramidis and W. White, *J. Am. Ceram. Soc.*, 57, 22-24 (1974).
- [12] G. Štefanič et al., *Thermochim. Acta*, 303, 31-39 (1997).
- [13] T. Sasaki et al., *Radiochim. Acta*, 94, 489-494 (2006).
- [14] T. Kobayashi et al., *J. Nucl. Sci. Technol.*, 44, 90-94 (2007).
- [15] P. Schindler, *Adv. Chem. Ser.*, 67, 196-221 (1967).
- [16] A. Skerencak, et al., *J. of Sol. Chem.*, 2011, submitted.
- [17] R. Guillaumont, et al., *Chemical Thermodynamics Vol. 5.*, Elsevier, Amsterdam (2003).

5.2 Metal ion sorption onto mineral surfaces

T. Kupcik, A. Schnurr, J. Lützenkirchen, Th. Rabung, F. Heberling, D. Garcia¹, V. Petrov², K. Dardenne, Th. Fanghänel³, H. Geckeis

¹Amphos21, Passeig de Garcia i Faria, 49-51, 1-1 08019 Barcelona, Spain

²Chemistry Department, Lomonosov Moscow State University, 119991 Leninskie gory, 1/3, MSU, Moscow, Russia

³Universität Heidelberg, Physikalisch-Chemisches Institut, Im Neunheimer Feld 253, D-69120 Heidelberg

Introduction

Mechanistic insight into the complex phenomenon of radionuclide interactions with mineral surfaces is of utmost importance for performance assessment of nuclear waste repositories. Part of the complexity is due to the fact that apart from retardation processes as sorption, precipitation or incorporation reactions at mineral surfaces enhanced radionuclide transport via attachment to mobile colloidal phases needs to be considered. Colloid transport and retention is among other effects affected by the surface charge of the mobile and immobile phases. For a fundamental understanding of sorption/incorporation processes and transport phenomena reliable thermodynamic descriptions are required which ideally include a maximum of the relevant mechanistic insight. The present contribution addresses the study of adsorption reactions using EXAFS (extended X-ray absorption fine structure), presents thermodynamic model calculations that describe adsorption phenomena up to very high salt contents and finally highlights that mineral surface structure may affect charging behaviour of mineral surfaces as would be relevant to colloid retention but also to radionuclide adsorption reactions.

EXAFS investigations on the sorption of Gd(III) onto aluminium (hydr)oxides

Extensive metal-ion sorption studies on different aluminium (hydr)oxides have been performed over the last years [1-4]. Pure aluminium (hydr)oxides are of minor importance in the context of nuclear waste disposal but similar reactive surface groups occur on aluminosilicates (e.g. clays) and are highly efficient in metal ion retention. In addition, aluminium (hydr)oxides are considered as isomorphous model phases for ferric iron (hydr)oxides which are abundant in nature and serve as strong sorbents for contaminants [5].

Our previous work investigated sorption and speciation of trivalent metal ions (Gd and Cm) on aluminium minerals (γ -Al₂O₃ [1,3], α -Al(OH)₃ [4]) by TRLFS (time resolved laser fluorescence spectroscopy) and EXAFS. Several Cm surface species could be identified in the pH range between 3 and 13 by TRLFS. In the case of γ -Al₂O₃, complementary EXAFS

investigations revealed metal ion coordination to four oxygen atoms of the alumina surface. Unfortunately, no definite sorption sites could be identified due to the presence of only one oxygen coordination shell [3]. In the present report we present our EXAFS results on the interaction of Gd(III) with gibbsite (α -Al(OH)₃) and bayerite (β -Al(OH)₃) at pH 8.

Experimental

The synthesis and characterization of gibbsite is reported elsewhere [3]. The gibbsite stock suspension has a pH value of around 4, which causes relatively high dissolved Al concentration. To avoid Al(OH)₃ precipitation in a subsequent adsorption experiment the gibbsite suspension was equilibrated at the solubility minimum (pH ~ 6.2) for four months prior to the sorption study. Bayerite was synthesized by titration of an aluminate solution with HCl to pH 9 at elevated temperatures [6, 7].

For the sorption study, suspensions containing $6.4 \cdot 10^{-5}$ M Gd were prepared. To ensure similar sorption densities Γ a solid content of 1.9 g/L is used for gibbsite compared to 6 g/L for bayerite taking into account the higher specific surface area of gibbsite. The pH was raised slowly over three days to pH 8. ICP-MS of the supernatants obtained after ultracentrifugation. ICP-MS showed an almost quantitative uptake of the added Gd.

X-ray absorption spectroscopy was performed at the INE-Beamline for actinide research at the ANKA 2.5 GeV synchrotron radiation facility, KIT, Karlsruhe.

Results and discussion

Fig. 1 shows exemplarily the k^2 weighted EXAFS function (A) and the corresponding FT transformed spectra (B) for the system Gd/gibbsite together with theoretical fit curves. Table 1 summarizes the metric parameters obtained in the fit for gibbsite and bayerite. The experimental data are reproduced well with r -factors ranging from 0.1% for bayerite to 0.3% for gibbsite. The FT spectra exhibit an intense peak at 1.9 Å ($R-\Delta$) (not phase corrected) representing oxygen atoms in the first coordination sphere. After phase correction similar metal-O distances and coordination numbers are obtained (Table 1). No splitting of the oxygen peak is discernible but high Debye-Waller factors are obtained. For both systems

two aluminium shells could be fitted to the EXAFS data. Modelling the data with only one Al shell leads to a significant deviation compared to the measured spectra.

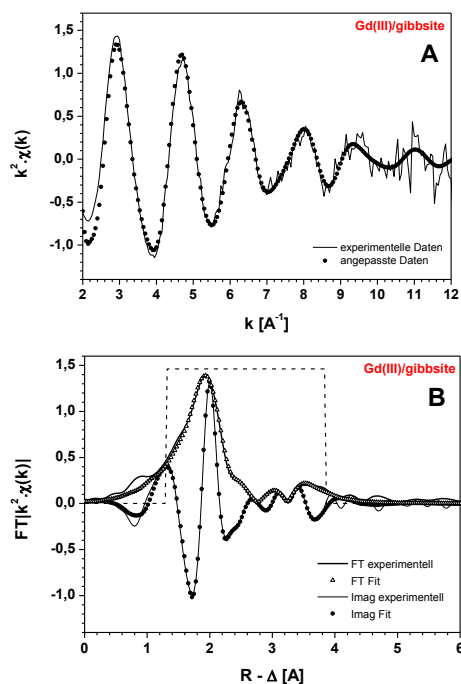


Fig. 1: k^2 weighted EXAFS function (A) and the corresponding FT transformed spectra (B) for Gd sorbed onto gibbsite at pH 8.

Table 1: EXAFS parameter for the interaction of Gd with bayerite and gibbsite at pH 8.

	shell	R (Å) (±0.01)	N (±20%)	$\sigma^2 \cdot 10^3$ (Å ²)
Bayerite	O	2.39	7.4	8.8
	Al	3.54	3.2	12.1
	Al	3.80	2.2	9.0
Gibbsite	O	2.40	7.6	8.6
	Al	3.44	1.8	7.4
	Al	3.76	7.4	25.8

R = interatomic distance, N = coordination number, σ^2 = Debye-Waller factor. $S_0^2 = 1$.

We note an increase in the Gd-Al distance from gibbsite to bayerite for both aluminium shells but stronger for the first shell. A large Debye-Waller (σ^2) (e.g. first Al-shell for bayerite and second Al-shell for gibbsite) indicates Al backscatter atoms in different distances. In general, coordination numbers tend to be higher when σ^2 increase. These parameters are correlated as acting both on the amplitude of the signal (N linear dependency and σ^2 exponential decrease). As the Debye-

Waller factor differs for bayerite and gibbsite it is not obvious to get direct comparison of the associated coordination numbers when the σ^2 are too different as observed for the second Al-shell in the case of gibbsite ($\sigma^2 = 0.0258 \text{Å}^2$; $N = 7.4 \pm 1.5$). In this case, the absolute value of N is most likely not reliable.

Gd(III) sorption onto gibbsite

The Gd-O distance and coordination number are in accordance with the values for the Gd aquo ion ($R_{\text{Gd-O}} = 2.42 \pm 0.02 \text{Å}$; $N = 8 - 9$) [8]. Based on earlier TRLFS results on the interaction of curium with gibbsite [9] a ternary complex with different oxygen ligands (H_2O , OH^- , surface aluminol groups) in the first coordination sphere of the central metal ion is plausible. Therefore, slightly different Gd-O distances are likely. In this case, the EXAFS spectra are dominated by the backscattering of the nearest oxygen atom [10], while oxygens at larger distance (including an additional oxygen shell) cannot be resolved [11]. Potential sorption sites on both the basal (001) and the edge faces are highlighted in Fig. 2. On the basal surface the metal ion can in principle be bound either by two (B1 and B2) or three (B3-B5) doubly coordinated aluminol groups. A monodentate coordination can be ruled out, due to the fact that a monodentate bonding with both a flexible Gd-O bond and a flexible binding angle (Al-O-Gd) would lead to variable Gd-Al distances and therefore very likely to destructive interferences [12]. For the edge sites, both bi- and tridentate coordination geometries are possible (tridentate: E2, bidentate: E1 and E3-E6). In contrast to sorption onto the basal surface, sorption at edge faces takes place via singly coordinated aluminol groups (Al-OH) or, in case of E6, singly and doubly coordinated aluminol groups, respectively. In order to determine the relevant sorption sites the measured Gd-Al parameters are compared with Gd-Al distances (with $R \leq 4 \text{Å}$) and coordination numbers for all possible sites. Binding sites at the edge faces between the $\text{Al}(\text{OH})_6$ layers are not considered because the Gd-Al distance for these sites is $> 4 \text{Å}$ and therefore significantly longer than the EXAFS Gd-Al distances. Based on this interpretation, for the first Al shell the sorption sites B1, B3, B4 and B5 on the basal surface can be ruled out due to longer (B5) or shorter (B1, B3 and B4) Gd-Al distances than indicated by EXAFS. This leaves **B2** as the only possible Gd sorption site on the basal surface. In addition, a value of $N = 2$ in this coordination geometry is in good agreement with the EXAFS value of $N = 1.8 \pm 0.4$ (Table 1). An analogous interpretation for the edge sites points to a metal ion coordination at **E1**, as the other

sorption sites exhibit longer (E2-E5) or shorter (E6) Gd-Al distances.

However, the expected coordination number of $N = 1$ for E1 is lower than the N value determined by EXAFS analysis. Apart from the first Al shell, an additional second shell is determined by EXAFS. For the sites B2 and E1 (already been selected for the first Al shell) the second Al neighbours are expected at distances $R_{\text{Gd-Al}} \geq 4.0 \text{ \AA}$. Therefore it can be deduced, that Gd is attached to an additional sorption site. The experimental Gd-Al distance fits to a coordination to **E4** and **E5** at the edge sites, and to **B5** at the basal surface. The high Debye-Waller factor ($\sigma^2 = 0.0258 \text{ \AA}^2$) for this aluminium shell can be due to the slightly different Gd-Al distances in these coordination geometries. Furthermore, the sorption sites B2, E4 and E5 can also be considered as tetradentate sites with binding to two oxygens in the first coordination sphere ($R_{\text{Gd-O}} \sim 2.40 \text{ \AA}$) and two oxygens at $R_{\text{Gd-O}} \gg 2.40 \text{ \AA}$.

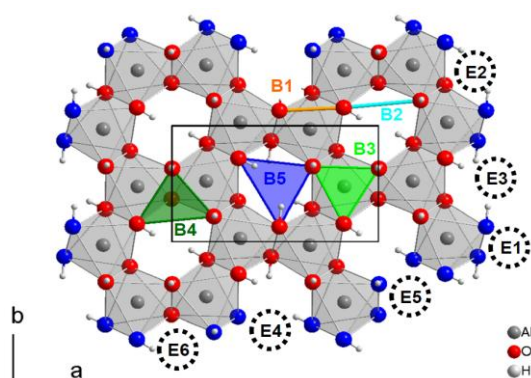


Fig. 2: Plan view onto the gibbsite (001) surface showing the surface unit cell and possible sorption sites. Doubly coordinated aluminol groups are depicted in red, singly coordinated aluminol groups in blue.

Gd(III) sorption onto bayerite

As in the case of gibbsite, three backscattering shells can be fitted to the EXAFS data for the interaction of Gd with bayerite. The Gd-O distance and coordination number N are comparable to the values determined for gibbsite (Table 1). All possible sorption sites on the bayerite surface [18] are depicted in Fig. 3.

Due to the structural analogy of the gibbsite and bayerite surfaces, similar sorption sites with similar Gd-O/Al distances and coordination numbers N are determined. For the first Al shell, the sorption sites B1 and B3-B5 on the basal plane can be ruled out due to too long or short Gd-Al distances, leaving **B2** as the only plausible binding site. On the edge surface, metal ion coordination can only take place via **E1** and **E3**. However, the expected Al coordi-

nation numbers of $N = 1 - 2$ for E1 and E3 are lower than the value derived by EXAFS ($N = 3.2 \pm 0.6$). For the second Al shell, no adequate Gd-Al distances can be found for the sorption sites B2, E1 and E3. This finding points to the existence of Gd in an additional sorption geometry. **B5** (basal surface) coordination leads to a reasonable Gd-Al distance but the theoretical N value of 6 is significantly higher than the experimental value ($N = 2.2 \pm 0.4$). On the edge surface, the Gd-Al distance as well as the coordination number for the sorption sites **E4** and **E5** is in good agreement with the experimental EXAFS data.

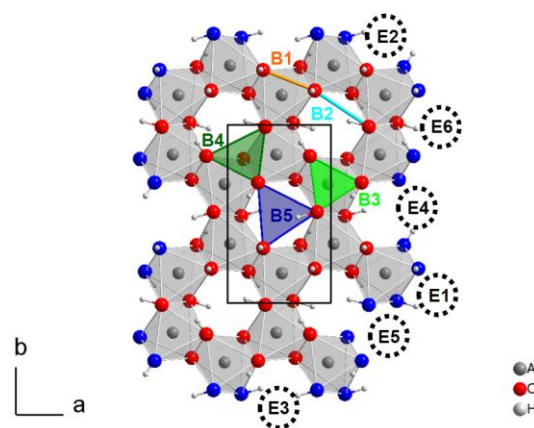


Fig. 3: Plan view onto the bayerite (001) surface with the surface unit cell and possible sorption sites.

Conclusions

Our EXAFS results show suitable coordination sites for Gd on both the basal and the edge surfaces of gibbsite and bayerite. In these coordination environments Gd is bonded in a bi- or tridentate form by doubly or singly coordinated Al-OH groups. In addition, a tetradentate coordination is also likely, when oxygen atoms in a second shell are considered to participate in bonding. Together with a constant Gd coordination number of $N = 8$, 5 – 6 $\text{H}_2\text{O}/\text{OH}^-$ ligands remain in the first Gd coordination sphere. This result is in good agreement with former TRLS results [9]. Furthermore, our EXAFS results point to the fact that the existence of one single sorption site is unlikely and that the metal ion is bound to several sites simultaneously, leading to the presence of several Gd(III) sorption species on the mineral surfaces.

Trivalent Metal Ion Sorption under Saline Conditions

In the past, many experimental studies were performed to quantify and to understand sorption processes and to describe them with surface complexation models. However, almost all experimental data are restricted to low ionic strength conditions and a large gap exists for experimental data at ionic strength > 1 M. Saline conditions are not restricted to solutions relevant to rock salt formations as e.g. in the Waste Isolation Pilot Plant (WIPP) in the USA and the Gorleben, Morsleben and Asse sites in Germany. Elevated salt concentrations up to 6.5 M are also found in sedimentary rocks which are currently under investigation within nuclear waste disposal programs [13, 14]. At present it is completely unclear, whether existing sorption data and sorption model approaches can be applied to saline conditions.

In the present work, experiments have been performed with illite (illite de Puy) and Na-montmorillonite (Na-SWy-2) as representative clay minerals. In all cases sorption of Eu(III) radiolabelled with ^{152}Eu was studied in batch experiments, where ionic strength was varied up to 4 M NaCl. Solid/liquid ratios were 2 g/L. Metal ion concentrations were at 2×10^{-7} M. Experiments with Cm(III) and the time resolved laser fluorescence spectroscopy (TRLFS) are designed to obtain detailed information on the metal ion speciation at the mineral surfaces as a function of ionic strength. In both systems we observed a clear shift of the sorption edges to higher pHc ($-\log[\text{H}^+]$) and decreasing sorption with increasing ionic strength (Fig. 4). Competition of Na(I) with Eu(III) for the cation exchange sites is responsible for the strong decrease in uptake at low pH and higher ionic strength.

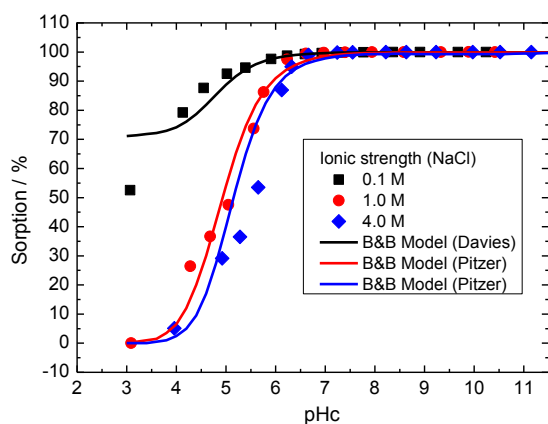


Fig. 4: Eu sorption onto illite at different ionic strength. Comparison between experiment and modelling using the model of Bradbury and Bayens [15].

Eu(III) sorption to clay minerals under variable ionic strength conditions was predicted by a well established non-electrostatic sorption model, calibrated at lower ionic strength (2SPNE/CE, Bradbury and Baeyens [15]). The Pitzer formalism was used to calculate activity coefficients for aqueous species. We assumed in our calculations that the nature of the Eu(III) surface species does not vary at different ionic strength conditions. Furthermore, the applied model does not consider the formation of Na^+ inner-sphere surface complexes. Model calculations for different ionic strengths yield fair agreement with the experimental data and reproduce the observed trend. This finding suggests that the shift in sorption edges with increasing ionic strength is basically due to a variation of ion activities and a concomitant change in aqueous metal ion speciation.

TRLFS experiments with Cm(III) indicate no significant differences for sorbed inner-sphere Cm(III) complexes at low and high ionic strength conditions. Emission peak positions and lifetimes are quite comparable. This spectroscopic finding confirms model assumptions mentioned above. Our preliminary study indicates that the non-electrostatic 2SPNE/CE model can be applied to predict sorption of trivalent actinide ions also for elevated ionic strength conditions at least in NaCl dominated solutions. More detailed TRLFS measurements are planned and experiments will be extended to MgCl_2 and CaCl_2 rich brines.

While the previous example uses a non-electrostatic surface complexation model and blind predictions, a similar approach was tested on the quartz-Eu(III) system. Titrations of the quartz sample showed that it is necessary to involve two surface sites, similar to observations made by Ong et al. [16]. With activity coefficients for aqueous species calculated separately and a Basic Stern model (i.e. a common electrostatic model), it was possible to fit a simple model to the titration and the experimental adsorption data (Fig. 5). At present we refrain from involving the expected surface speciation (i.e. hydrolysed species) on the two sites because this would increase the number of adjustable parameters, and the model would be over-parameterised. Since the current (simple) model is sufficient to describe the data, spectroscopic information are required to refine that model.

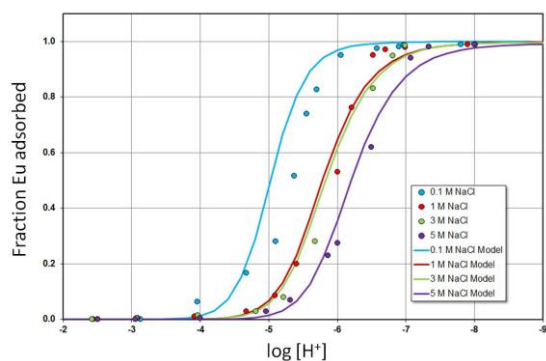


Fig. 5: Eu sorption onto quartz at different ionic strength. The model is a 2-site Basic Stern model involving two Eu-surface species (Si_i-O-Eu^{2+} , with $l = 1, 2$).

Conclusions

Both examples show that it is possible to extend the surface complexation formalism to highly saline solutions of monovalent ions based on the appropriate treatment of aqueous speciation and therefore without introducing more complex surface complexation models.

Surface structural constraints on charging properties of oxide surfaces

It is expected that surface structure of a mineral surface in contact with electrolyte solutions is responsible for its charging and adsorption properties, and that the structure finally determines the isoelectric point (IEP) of that surface. Consequently changes in surface structure due to ageing should cause changes in the observed IEP. Furthermore, it has been shown that the hematite 001 plane is surprisingly reactive when other planes are exposed [17]. Usually the solubility of ferric ion oxides is rather low, however for hematite single crystals it has been observed that dissolved iron is transferred from the edges where it dissolves to the basal plane, where it is adsorbed. In the present study this knowledge was used to create situations favourable for the above reactions [17]. This was done by exposing part of the edge surfaces of one of the crystals to the flow path in a streaming potential device. The isoelectric point of the original hematite 001 samples obtained by streaming potential was about 5.5, which is rather low for iron oxides, but not untypical for oxide single crystals. Subsequent streaming potential measurements caused a shift of the IEP to nearly 9, which is close to that of hematite particles, and did not change in subsequent runs (see Figure 6).

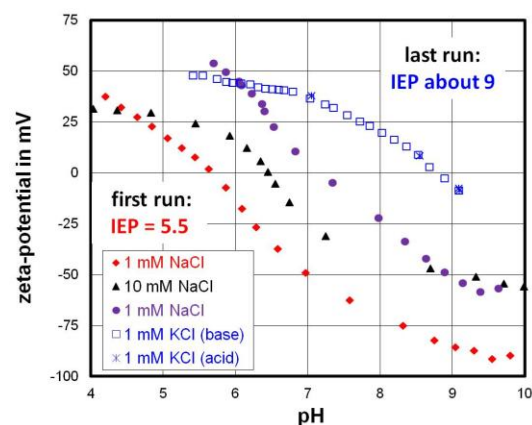


Fig. 6: Zeta-potential of hematite 001 as a function of pH at various times of exposures to electrolyte solutions.

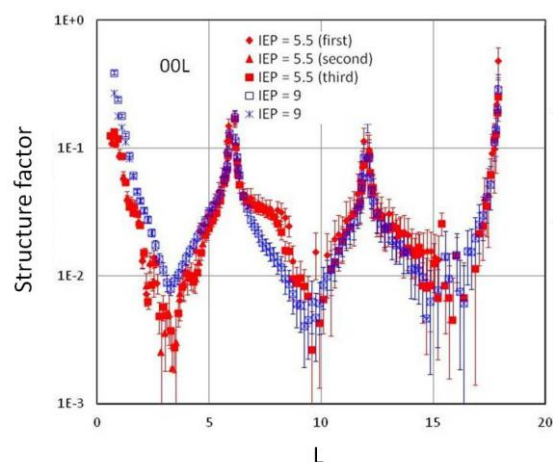


Fig. 7: Surface diffraction data for the two hematite samples (00L rod) with IEP 5.5 and 9, respectively.

To verify whether the initial and final samples differed in surface structure, surface diffraction studies were carried out with the respective samples. The results are shown in Figure 7. There is a pronounced shoulder in the original sample with IEP 5.5, which has clearly disappeared in the aged sample with IEP 9. As a next step it will be attempted to determine models for the two surface structures and to obtain the corresponding IEPs based on the MUSIC model [6].

Conclusions

The experimental study has shown that the surface charge behaviour of hematite 001 is easily modified by simple aging processes, when edge surface of hematite is available. These changes were retrieved in surface structural studies, where the initial and final samples clearly differ. This should allow the use of the surface structure to retrieve the measured IEPs using available theoretical approaches.

References

- [1] T. Rabung, T. Stumpf, H. Geckeis, R. Klenze, J.I. Kim, *Radiochim. Acta* 88, 711-716 (2000).
- [2] Th. Rabung, D. Schild, H. Geckeis, R. Klenze, Th. Fanghänel, *J. Phys. Chem. B* 108, 17160-17165 (2004).
- [3] Th. Rabung, H. Geckeis, X.K. Wang, J. Rothe, M.A. Denecke, R. Klenze, Th. Fanghänel, *Radiochim. Acta* 94, 609-618 (2006).
- [4] N. Huittinen, T. Rabung, J. Lützenkirchen,, S.C. Mitchell, B.R. Bickmore, J. Letho, H. Geckeis, *J. Colloid Interface Sci.* 332, 158-164 (2009).
- [5] R.M. Cornell, U. Schwertmann, *The iron oxides – structure, properties, reactions, occurrences and uses* 2nd edition, Wiley-VCH, GmbH&Co. KGaA.
- [6] T. Hiemstra, H. Yong, W.H. van Riemsdijk, *Langmuir* 15, 5942-5955 (1999).
- [7] G. Lefèvre, M. Fédoroff, *Mater. Lett.* 56, 978-983 (2002).
- [8] S. Ishiguro, Y. Umebayashi, M. Komiya, *Coord. Chem. Rev.* 226, 103-111 (2003).
- [9] T. Kupcik, N. Huittinen, T. Rabung, J. Lützenkirchen, H. Geckeis, T. Fanghänel, *KIT Scientific Reports* 7600, 22-27 (2010).
- [10] J.R. Bargar, G.E. Brown, Jr., G.A. Parks, *Geochim. Cosmochim. Acta* 61, 2617-2637 (1997).
- [11] J.R. Bargar, S.N. Towle, G.E. Brown, Jr., G.A. Parks, *J. Colloid Interface Sci.* 185, 473-492 (1997).
- [12] K. Dardenne, T. Schäfer, M.A. Denecke, J. Rothe, J.I. Kim, *Radiochim. Acta*, 89, 469-479 (2001).
- [13] Laboratory for Waste Management, Nuclear Energy and Safety Research Department, Paul Scherrer Institute (PSI), Progress Report 2010.
- [14] P. Vilks, Technical Report NWMO TR-2009-18 (2009).
- [15] M.H. Bradbury, B. Baeyens, *Geochim. Cosmochim. Acta* 73, 990-1003 (2009).
- [16] S. Ong, X. Zhao, K.B. Eisenthal, *Chem. Phys. Letters* 191, 327-335 (1992).
- [17] S.V. Yanina, K.M. Rosso, *Science* 320, 218-222 (2008).

5.3 Retention of radionuclide by secondary phases formation

N. Finck, A. Chagneau, F. Heberling, K. Holliday, K. Dardenne, S. Heck, T. Stumpf, M. Böttle, V. Metz, T. Schäfer

Secondary phases may form over geological time scales upon contact of the High Level nuclear Waste (HLW) matrix with groundwater. The neo-formation of such alteration phases represents a significant retention potential for radiotoxic and long-lived radionuclides (RN) in aqueous systems. Beside reactions at the surface, RN binding may occur by incorporation in the bulk structure (co-precipitation), resulting in long-term immobilization, especially if a (meta)stable solid solution forms. Currently, the mechanism of RN incorporation in selected mineral phases relevant in the disposal of HLW in deep repositories is investigated at INE. Molecular-scale information is obtained by combining various complementary spectroscopic techniques. Most of the activities in this field are related to the retention of actinides, but also the binding of long-lived fission products.

An(III)/Ln(III) – strontianite/celestite

The leading role of ligand strength in uptake mechanisms of Eu(III) and Cm(III) by secondary phases of the carbonate/sulfate system was previously outlined by the work of Schmidt et al., 2009 [1]. These authors observed that Eu(III) and Cm(III) are incorporated into aragonite structure (CaCO_3) and only form inner-sphere surface complexes with gypsum ($\text{CaSO}_4 \cdot 2\text{H}_2\text{O}$). To determine the role of the lattice parameters, a continuative study was performed on two minerals isostructural with aragonite and belonging to the carbonate/sulfate system as well: celestite (SrSO_4) and strontianite (SrCO_3).

Experimental

Celestite and strontianite were precipitated in the presence of Eu(III) and Cm(III) in mixed flow reactors. A surface growth controlled precipitation was assured by adding seeding crystal to the suspension (pure SrSO_4 or SrCO_3). The saturation indexes were fixed at 3.5 for the carbonate system and at 0.8 for the sulfate system. The solutions were analyzed by ICP-MS along the precipitation experiments to quantify the uptake of the dopants. The X-ray diffractograms of the precipitated phases were characteristic of pure celestite and strontianite. The minerals were then analyzed by Time Resolved Laser Fluorescence Spectroscopy (TRLFS).

Results and discussion

Uptake quantification – In the case of celestite (SrSO_4), the quantification of the uptake was not possible, as the difference in Eu(III) and Cm(III) concentrations between the initial and final solution was within the experimental and analytical uncertainty (less than 5%). In the case of strontianite (SrCO_3), about 100% of the dopants in solution were trapped by the mineral phase. Such differences in behaviors highlight the important role of the ligand strength, here CO_3 ligands being stronger than SO_4 . However, further studies will investigate the systems under the same saturation index to quantify this ligand strength effect.

Uptake mechanisms – The uptake mechanisms were characterized by TRLFS. For both Eu: SrSO_4 and Eu: SrCO_3 , the single peak observed for the excitation spectra indicates the presence of one single species of Eu(III) (Fig. 1). The difference in the two peaks intensity confirm the quantification results: the uptake of the dopants is much lower in the sulfate system than it is in the carbonate system. The same observations were made for the Cm(III). The excitation spectra of Cm: SrSO_4 resulted also in a single peak, indicated the presence of a single species of Cm(III). However, it was a little different for Cm: SrCO_3 . The excitation spectra revealed a quadruple peak, reproducible for each fluorescence maximum. It is therefore a 4-fold splitting of the $^8\text{S}_{7/2}$ ground state in a single Cm(III) species, characteristic of a strong interaction between the dopant and the carbonate ligand.

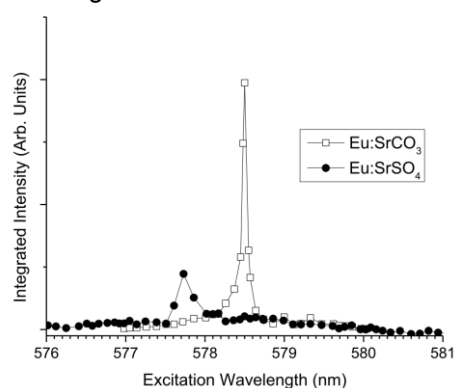


Fig. 1: Excitation spectra of Eu(III) doped celestite and strontianite over the $^5\text{D}_0 \rightarrow ^7\text{F}_{0,1,2}$ transitions at low temperature (16 K).

The fluorescence lifetimes of Eu(III) and Cm(III) for both carbonate and sulfate systems presented a mono-exponential decay,

reinforcing the conclusion of a single species (Fig. 2). The long lifetimes (e.g. 1.6 ms and 0.47 ms for Eu:SrCO₃ and Cm:SrCO₃, respectively) correspond to a total loss of the hydration sphere of the dopants, therefore clearly indicating an incorporation of the Eu(III) and Cm(III) into celestite and strontianite structure. This conclusion shows the importance of the lattice parameters in the uptake mechanisms of trivalent lanthanides and actinides by secondary phases.

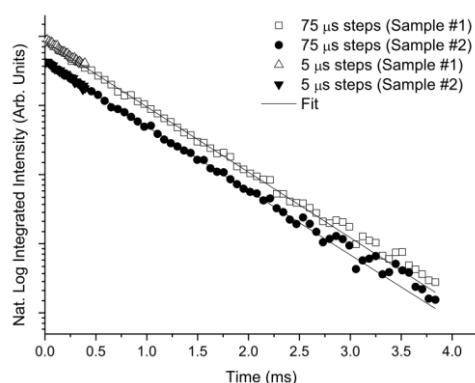


Fig. 2: Lifetime measurements of two celestite samples performed with time steps of 5 and 75 μ s at low temperature (16 K). Lines represent fit from the standard mono-exponential decay equation.

An(III) – clay minerals

Clay minerals may form as secondary phases upon alteration of the HLW waste matrix in the presence of groundwater. These minerals have a high affinity for trivalent *f*-elements. Various distinct molecular-scale binding mechanisms have been identified, but information on the retention by incorporation in the bulk structure is limited. Hectorite, a magnesian smectite frequently observed in HLW glass corrosion experiments [2], was precipitated in the presence of Am(III).

Experimental

Hectorite was synthesized in the presence of Am(III) (AmCopHec) following a multi-step synthesis protocol [3]. A freshly precipitated Am(III)-containing brucite precursor was aged at 90°C for one week in the presence of LiF and a silica sol. The resulting hectorite was washed to remove any remaining precursor phase. Separately, an Am(III)-containing brucite (AmCopBru) was freshly precipitated under identical experimental conditions, and Am(III) aquo ions were contacted with hectorite in suspension ($m/V = 2$ g/L; TotAm = 105 μ M; pH = 6.4(1); $I = 0.5$ M NaClO₄; sample AmAdsHec). The solid phases were characterized by XRD and SEM. Americium L_{III}-edge EXAFS data were collected for all

samples at the INE-Beamline for actinide research at ANKA.

Results and discussion

XRD – The X-ray powder diffractogram of AmCopBru was identical to that of pure brucite (Fig. 3). No additional phase was detected meaning that the actinide had no effect on the precipitation. However, the diffraction peak assigned to the (001) plane had higher relative intensity in AmCopBru as in brucite. This may suggest that Am is structurally associated with this plane because heavy elements have higher scattering properties as lighter ones. No difference in the diffractogram of AmCopHec compared to that of hectorite can be seen. Consequently, hectorite crystallized from the precursor phase.

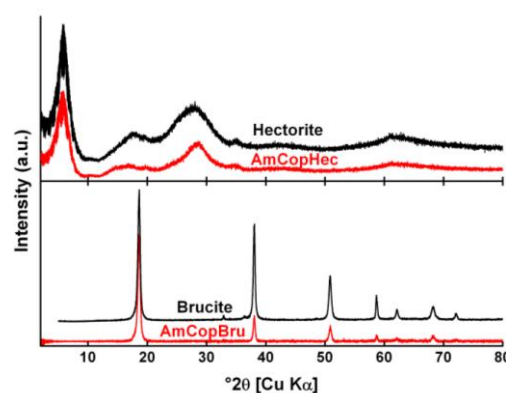


Fig. 3: X-ray diffractograms of hectorite, AmCopHec, brucite and AmCopBru.

SEM – The SEM micrograph of AmCopBru shows a layered structure, as expected for brucite (Fig. 4). The morphologies of AmCopHec and hectorite (here in AmAdsHec) are very similar. Both solid phases display a “corn flake-like morphology” typical for minerals formed at high precipitation rate. No significant influence of Am could be detected.

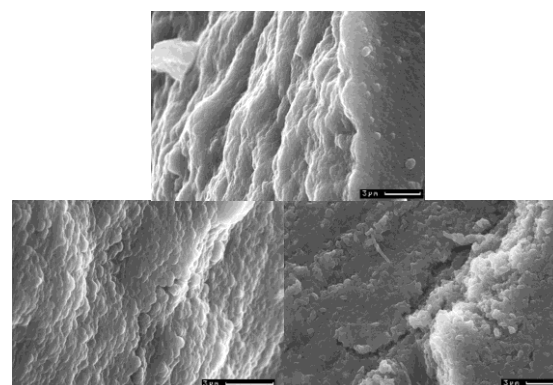


Fig. 4: SEM micrographs of AmCopBru (top), AmCopHec (lower left) and AmAdsHec (lower right).

EXAFS Spectroscopy – EXAFS data provided information on the Am local chemical environment. The aquo ions are 9-fold coordinated to O atoms from hydration water

molecules. In AmCopBru, the first coordination sphere consists in 7 oxygen backscatterers located at $d(\text{Am-O}) = 2.43(2) \text{ \AA}$. Two Mg subshells were detected at 3.22(2) and 3.44(2) \AA : these distances are slightly larger and shorter as the sum of $d(\text{Mg-Mg})$ in brucite (3.14 \AA [4]) and the increase in atomic radii [5] from Mg ($r^{\text{VI}}\text{Mg(II)} = 0.72 \text{ \AA}$) to Am ($r^{\text{VI}}\text{Am(III)} = 0.98 \text{ \AA}$). Consequently, this result can be interpreted as a structural substitution of Mg for Am. After crystallization of AmCopHec from AmCopBru, the interatomic distances shortened to $d(\text{Am-O}) = 2.40(2) \text{ \AA}$ and $d(\text{Am-Mg}) = 3.17(2) \text{ \AA}$. This trend agrees with the decrease observed from brucite ($d(\text{Mg-O}) = 2.10 \text{ \AA}$; $d(\text{Mg-Mg}) = 3.14 \text{ \AA}$ [4]) to hectorite ($d(\text{Mg-O}) = 2.08 \text{ \AA}$; $d(\text{Mg-Mg}) = 3.04 \text{ \AA}$ [6]). The octahedral environment is further supported by the O shell containing 6.1(1.2) atoms. Additionally, Si backscatterers were detected at 3.47(5) \AA . The O and Mg shells are located at slightly larger distances in AmAdsHec ($d(\text{Am-O}) = 2.42(1) \text{ \AA}$; $d(\text{Am-Mg}) = 3.22(1) \text{ \AA}$) and the next nearest Si shell is located at significantly larger distance ($d(\text{Am-Si}) = 3.81(5)$). Consequently, the Am local environments upon adsorption and upon co-precipitation are significantly different. The most effective retention is very likely the structural incorporation.

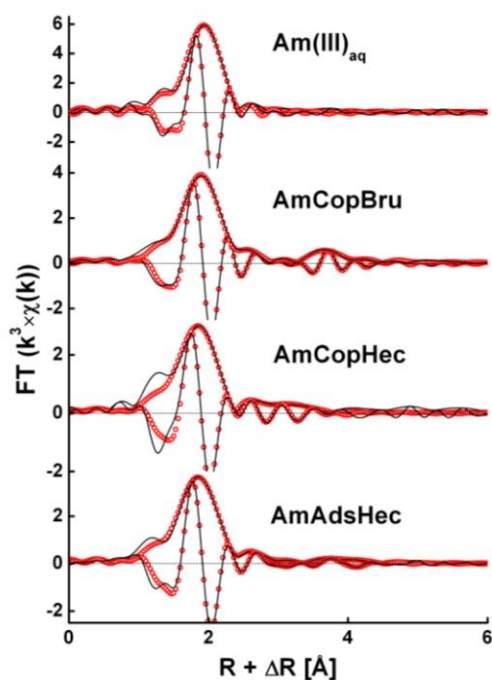


Fig. 5: Fourier transforms (FTs) of EXAFS data collected for the Am-containing samples together with that of the aquo ions.

Selenium(IV) incorporation into calcite

Selenium-79 is a long lived fission product with a half live of 1.1 Ma [7]. It is formed e.g. by nuclear fission of Uranium-235. At environmental conditions Selenium may be

present in several oxidation states: Se(-II), Se(-I), Se(0) in reducing environments, Se(IV) and Se(VI) at oxidizing conditions. While the reduced Se species and elemental Selenium form stable hardly soluble phases, mineral phases formed by the oxidized species are more soluble [8]. Besides this the oxidized Se species show only weak interactions with most common mineral surfaces. Therefore Selenium-79 is usually expected to migrate unretarded through aquifer systems. For these reasons Selenium-79 has often been considered a critical RN for the safe disposal of nuclear waste.

Calcite is a common mineral in many formations considered as potential host rocks for a nuclear waste disposal e.g. as component of clay stones (up to 20 %) or as fracture filling material in granitic rocks. It is a corrosion product of concrete based materials which are part of the technical barrier. Numerous studies have shown that especially Se(IV), in aqueous solution present as selenite anion (Se(IV)O_3^{2-}), which is chemically and structurally similar to carbonate, interacts with calcite and may adsorb at the calcite surface or be incorporated into the calcite structure [9-13].

In the study presented here the focus is set on the co-precipitation of Se(IV) with calcite at room temperature and low calcite supersaturation.

Experimental details

Coprecipitation experiments at $0.3 < \text{SI}(\text{Calcite}) < 1$ are performed in mixed flow reactors (MFR). The MFR is fed with three input solutions containing CO_3^{2-} , Ca^{2+} , and SeO_3^{2-} , respectively composed to achieve an initial $\text{SI}(\text{calcite})$ of ~ 1 at pH 7.8. NaCl is added to all solutions to fix the ionic strength at 0.01 mol/L. The solution in the MFR is stirred permanently and contains 300 mg calcite seed crystals with a specific surface area of 0.5 m^2/g . To be able to cover a large Se(IV) concentration range ($10^{-13} \text{ mol/L} - 10^{-4} \text{ mol/L}$), spikes of ^{75}Se were added to the Se(IV) input solution, and Se concentration was measured by gamma-spectroscopy. Calcite precipitation and Se(IV) coprecipitation was monitored by measuring SeO_3^{2-} and Ca^{2+} concentrations before and after the MFR, respectively.

The Se(IV) incorporation species in a Se(IV) doped calcite powder from a MFR experiment has been characterized by Se K-edge EXAFS measurements. An additional Se-doped calcite single-crystal sample has been prepared by growing a thin calcite layer onto a (104) terminated calcite single crystal in a batch type co-precipitation experiment. Starting from 20 mL of calcite and air equilibrated solution

Se(IV) was added to reach an initial concentration of 2 mmol/L. pH was increased by adding NaOH to reach an initial pH of ~10 and correspondingly an SI_{Calcite} of ~1.2. During the reaction period of 6 days the pH decreased from 10 to 9.75. This corresponds, according to PhreeqC [14] model calculations, to 0.6 mmol/L calcite precipitation, what results in a 50 to 100 μm thick layer of precipitated Se(IV) doped calcite.

The Se(IV) doped calcite single crystal was used for polarization dependent grazing incidence EXAFS measurements, to gain information about the selenite orientation relative to the calcite crystal structure. Three Se-K-edge EXAFS spectra were recorded at an incidence angle of the x-ray beam relative to the calcite(104) surface close to the calcite critical angle ($\sim 0.15^\circ$ at 12.660 keV). Three different orientations were investigated: beam parallel to the short diagonal of the calcite rhomb ($\epsilon \parallel [010]$; "bpa"), beam at $\sim 10^\circ$ to the long diagonal of the calcite rhomb ($\epsilon \parallel$ to [43-1], "bpb"), and beam parallel to the edge of the calcite crystal ($\epsilon \parallel [46-1]$, "bpk").

Results

Results of the powder EXAFS measurements are shown in Table 1. Bond distances (R) and coordination numbers (CN) both fit perfectly with a selenite anion incorporated into calcite, substituting a carbonate ion in the crystal structure.

Tab. 1: Selenium environment in calcite as obtained from the analysis of the EXAFS spectrum measured on the sample powder.

	CN	R [Å]	$\sigma^2[\text{Å}^2]$
Se-O1	3.0±0.3	1.68±0.01	0.001
Se-O2	2.3±1.5	2.83±0.08	0.010
Se-Ca1	2.7±1.8	3.27±0.06	0.012
Se-Ca2	2.5±1.9	3.53±0.06	0.010

K- and R-space spectra obtained in the polarization dependent measurements are shown in Figure 6.

Already qualitatively the different amplitudes of the EXAFS oscillations obtained at different orientations clearly indicate that the selenite ions must have a preferential orientation relative to the calcite crystal structure.

For a quantitative analysis different effective coordination numbers (CN_{eff}) were fit to the spectra measured at different orientations, while bond distances and Debye-Waller parameters were kept the same for all orientations. Modeled bond distances are within uncertainty the same as measured for the powder sample.

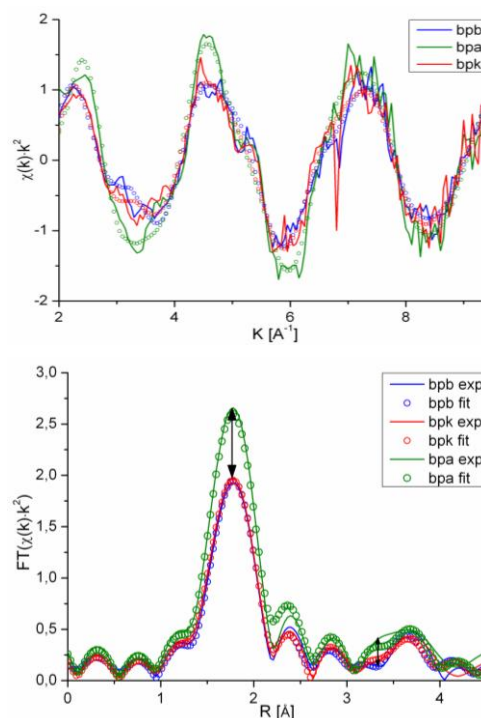


Fig. 6: Measured (lines) and modeled (circles) EXAFS spectra in k- (upper graph) and R-space (lower graph) measured on a Se(IV) doped calcite single crystal at three different orientations: „bpa“, „bpb“, and „bpk“.

Equation 1 (modified after [15]):

$$CN_{\text{eff}} = 3 \sum_i \left(\frac{\bar{R}_i G \bar{\epsilon}}{|\bar{R}_i| |\bar{\epsilon}|} \right)^2 \quad (\text{eq. 1}),$$

links the orientation of the sample in the beam (defined by the polarization vector ϵ (in crystal coordinates)) and the position of the i atoms surrounding Selenium in one shell (defined by the linking vectors R_i) to the effective coordination number of this particular shell (G is the metric tensor of calcite). Using this equation it was possible to find an environment of SeO_3^{2-} within the calcite structure that matches the effective coordination numbers as well as the measured bond distances. A ball and stick representation of the resulting structure is shown in Figure 7.

Both EXAFS experiments indicate that selenite can be structurally incorporated into calcite, where it substitutes one carbonate ion in the structure. The incorporation of the larger and slightly pyramidal selenite ion into the calcite structure causes slight strain in the calcite structure. The formula of calcite containing a mole fraction X of selenite is:

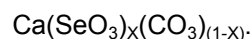


Figure 8 shows the selenite to carbonate ratio in the solid phase plotted against the selenite to carbonate activity ratio in the corresponding

aqueous solution as observed in MFR experiments. A partition coefficient D can be derived from the slope of the straight line through the data points. The fact that D seems to be constant over the whole concentration investigated, suggests that calcium selenite forms an ideal solid solution with calcite. However, the incorporation is higher than thermodynamically expected, because the solubility of the hypothetical calcium selenite endmember ($\log K_{SP} = -6.7 \pm 0.4$) would according to solid solution thermodynamics be lower than that of a known calcium selenite phase ($\text{CaSeO}_3 \cdot \text{H}_2\text{O}$, $\log K_{SP} = -6.40 \pm 0.25$).

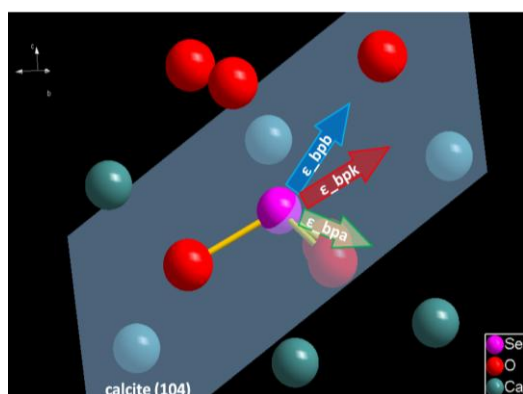


Fig. 7: Structural environment of Se(IV) incorporated into the calcite structure. Indicated in the picture are the orientation of the calcite(104) face and the orientations of polarization vector during the polarization dependent measurements.

Within uncertainty the solubility products of $\text{CaSeO}_3 \cdot \text{H}_2\text{O}$ and the hypothetical calcium selenite end member are the same, nevertheless it will be subject of further studies if selenite incorporation into calcite can be described as formation of an ideal solid solution or if kinetic effects play an central role in the incorporation process.

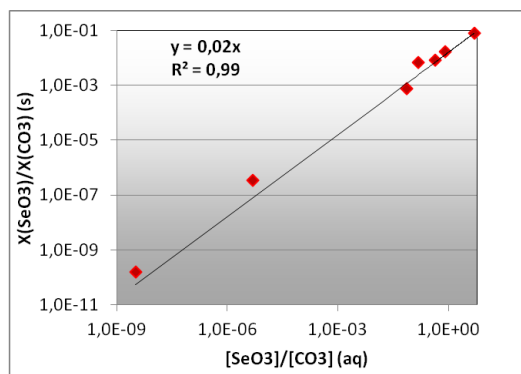


Fig. 8: MFR experiments indicate a constant partition coefficient, $D = 0.02 \pm 0.01$, for selenite incorporation into calcite over the whole concentration range investigated.

Retention of $^{226}\text{Ra}^{2+}$ by barite

^{226}Ra is a critical radionuclide with respect to the long-term safety of various types of nuclear waste repositories. Hence, the fate of radium has been deserved special attention in safety case studies and performance assessment (PA) studies for planned high level waste disposal in crystalline host rocks (e.g., in Japan, Sweden, Switzerland – see [16,17] and references therein) and low-level waste disposal in rock salt (e.g., in Germany). The knowledge about the solubility behavior of Ra is quite uncertain depending on the process considered. Thus, most PA calculations performed for ^{226}Ra assume that its solubility is limited by precipitation of $\text{RaSO}_4(\text{s})$ in the range of $10^{-7} \text{ mol} \cdot (\text{kg H}_2\text{O})^{-1}$. Abundant information from early radiochemical experimental studies and recent studies on natural systems as well as anthropogenic systems indicate that radium readily forms solid solutions with barite. It is expected that the formation of $(\text{Ba,Ra})\text{SO}_4$ solid solutions reduces the maximal radium concentration by several orders of magnitude in comparison to the solubility with respect to a pure $\text{RaSO}_4(\text{s})$ end member. Retention of radium by (radio)barite may occur via co-precipitation or via (re)precipitation processes.

In the present study retention of $^{226}\text{Ra}^{2+}$ by barite in aqueous solution is studied in a barite (re)precipitation experiment with a $^{226}\text{Ra}^{2+}$ doped barite suspension at $I = 0.1 \text{ mol} \cdot (\text{kg H}_2\text{O})^{-1}$ at ambient temperature. This experiment is an extension of our previous study on $^{226}\text{Ra}^{2+}$ retention by barite [18]; it has been extended in order to demonstrate unambiguously that steady state conditions were achieved.

Experimental details

Uptake of $^{226}\text{Ra}^{2+}$ by barite was determined in a static batch type experiments at room temperature (20°C). The experiment was conducted with synthetic barium sulfate "ReagentPlus®" (purity = 99 %; Sigma Aldrich®) suspended in $0.1 \text{ mol} \cdot (\text{kg H}_2\text{O})^{-1}$ NaCl solution. 10 mg of the barite powder was pre-equilibrated for one week in 10 mL NaCl solution (barite surface / solution volume ratio of $0.001 \text{ m}^2/\text{mL}$). After the pre-equilibration 9 mL of a $^{226}\text{Ra}(\text{NO}_3)_2$ stock solution to the suspension to have a radium doping of $2.95 \cdot 10^{-7} \text{ mol} \cdot (\text{kg H}_2\text{O})^{-1}$. Concentrations of dissolved $^{226}\text{Ra}^{2+}$ were monitored for 678 days by means of α -spectrometry using a Canberra 74/01 analysis chamber with a PIPS detector and a S100 multi-channel analyser.

Results and discussion

The temporal evolution of the apparent $^{226}\text{Ra}^{2+}$ radioactivity concentration in solution while in contact with barite is presented in Fig. 9. A significant decrease in aqueous $^{226}\text{Ra}^{2+}$ concentration by at least one order of magnitude within the first 50 days can be observed. According to the α -spectrometry data the ^{226}Ra concentration in solution decreased from 155 Bq/mL after 92 days to 87 ± 9 Bq/mL after 678 days. Within error, a constant steady state $^{226}\text{Ra}^{2+}$ concentration was achieved between 140 and 678 days (Fig. 9).

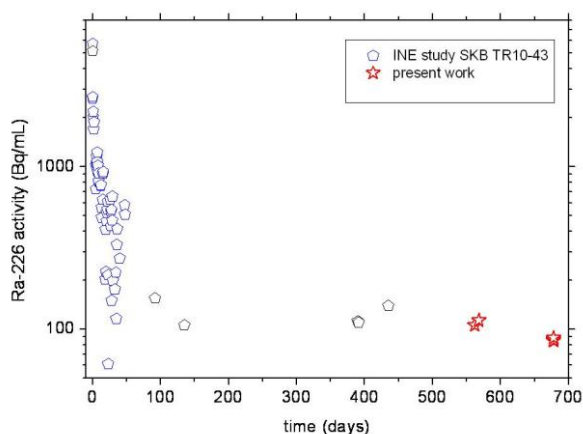


Fig. 9: Aqueous $^{226}\text{Ra}^{2+}$ concentration in Bq/mL while in contact with barite as function of time.

Based on the steady state $^{226}\text{Ra}^{2+}$ molalities of $\leq 1 \cdot 10^{-8} \text{ mol} \cdot (\text{kg H}_2\text{O})^{-1}$, the stoichiometry of the $\text{Ra}_x\text{Ba}_{1-x}\text{SO}_4$ solid solution was calculated. Assuming a regular solid solution, the uptake of $^{226}\text{Ra}^{2+}$ by barite was controlled by the solubility product of the end members – barite and $\text{RaSO}_4(\text{s})$ – as well as the Guggenheim interaction parameter, a_0 , for the $\text{Ra}_x\text{Ba}_{1-x}\text{SO}_4$ solid solution. Taking into account $a_0 = 1.5$, the lowest Guggenheim parameter derived by Curti et al. [19], a $^{226}\text{Ra}^{2+}$ molality of $1.5 \cdot 10^{-8} \text{ mol} \cdot (\text{kg H}_2\text{O})^{-1}$ in contact with $\text{Ra}_{0.000182}\text{Ba}_{0.999818}\text{SO}_4$ was computed.

In cooperation with INE, Rosenberg et al. [20] investigated (radio)barite coprecipitation under different ionic strength conditions by evaporating the fresh concentrate of a desalination plant. During evaporation the ionic strength increased from 0.7 mol kg^{-1} up to halite saturation and gypsum and barite precipitation commenced within few days. They determined a concentration-based apparent partition coefficient of $K'_{D,\text{barite}} = 1.04 \pm 0.01$, which differs from the equilibrium $K'_{D,\text{barite}}$ for diluted solutions due to kinetic and ionic strength effects. From the experimental results a Guggenheim parameter of $a_0 \sim 0.1$

was derived, which corresponds to a relative strong incorporation of Ra^{2+} into the solid in the co-precipitation experiments compared to results of $^{226}\text{Ra}^{2+}$ / barite (re)precipitation experiments.

References

- [1] M. Schmidt, T. Stumpf, C. Walther, H. Geckeis, T. Fanghänel, Dalton Transactions, (33), 6645-6650 (2009).
- [2] A. Abdelouas, J.-L. Crovisier, W. Lutze, B. Grambow, J.-C. Dran, R. Müller, Journal of Nuclear Materials, 240, (2), 100-111 (1997).
- [3] K. A. Carrado, P. Thiyagarajan, K. Song, Clay Minerals, 32, (1), 29-40 (1997).
- [4] T. Nagai, T. Hattori, T. Yamanaka, American Mineralogist, 85, (5-6), 760-764 (2000).
- [5] R. D. Shannon, Acta Crystallographica Section A, 32, (SEP1), 751-767 (1976).
- [6] W. Seidl, J. Brey, Zeitschrift Für Kristallographie, 220, (2-3), 169-176 (2005).
- [7] S. S. Jiang, J. R. Guo, S. Jiang, C. S. Li, A. Z. Cui, M. He, S. Y. Wu, S. L. Li, Nuclear Instruments & Methods in Physics Research Section B-Beam Interactions with Materials and Atoms, 123, (1-4), 405-409 (1997).
- [8] A. Olin, B. Nörling, E. Osadchii, L.-O. Öhman, E. Rosen, Chemical Thermodynamics of Selenium. OECD Nuclear Energy Agency (NEA): Vol. 7 (2005).
- [9] G. Aurelio, A. Fernandez-Martinez, G. J. Cuellar, G. Roman-Ross, I. Alliot, L. Charlet, Chemical Geology, 270, (1-4), 249-256 (2010).
- [10] L. W. Cheng, P. F. Lyman, N. C. Sturchio, M. J. Bedzyk, Surface Science, 382, (1-3), L690-L695 (1997).
- [11] C. E. Cowan, J. M. Zachara, C. T. Resch, Geochimica et Cosmochimica Acta, 54, (8), 2223-2234 (1990).
- [12] G. Montes-Hernandez, G. Sarret, R. Hellmann, N. Menguy, D. Testemale, L. Charlet, F. Renard, Chemical Geology 290, (3-4), 109-120 (2011).
- [13] X. K. Wang, X. P. Liu, Applied Radiation and Isotopes, 62, (1), 1-9 (2005).
- [14] D. L. Parkhurst, C. A. J. Appelo, User's guide to Phreeqc (Version 2); US Geological Survey: Denver, p 326 (1999).
- [15] M. L. Schlegel, A. Manceau, D. Chateigner, L. Charlet, Journal of Colloid and Interface Science, 215, (1), 140-158 (1999).
- [16] U. Berner, E. Curti, Radium solubilities from SF/HLW wastes using solid solution and

co-precipitation models.; Internal Report TM-44-02-04; Paul Scherrer Institut Villigen, Switzerland (2002).

[17] F. Grandia, J. Merino, J. Bruno, Assessment of the radium-barium co-precipitation and its potential influence on the solubility of Ra in the near-field. SKB TR-08-07; TR-08-07; Svensk Kärnbränslehantering AB: Stockholm (2008).

[18] D. Bosbach, M. Böttle, V. Metz, Experimental study on Ra^{2+} uptake by barite ($BaSO_4$). Kinetics of solid solution formation via $BaSO_4$ dissolution and $Ra(x)Ba(1-x)SO_4$ (re)precipitation. SKB TR-10-43. ; TR-10-43; Svensk Kärnbränslehantering AB: Stockholm, p 111 (2010).

[19] E. Curti, K. Fujiwara, K. Iijima, J. Tits, C. Cuesta, A. Kitamura, M. A. Glaus, W. Müller, *Geochimica et Cosmochimica Acta*, 74, 3553-3570 (2010).

[20] Y. O. Rosenberg, V. Metz, Y. Oren, Y. Volkman, J. Ganor, *Geochimica et Cosmochimica Acta*, 75, 5403-5422 (2011).

6. Applied studies: Radionuclide retention in the multi-barrier system

Long-term safety of a nuclear waste disposal depends on the multi-barrier system which consists of technical and geo-technical barriers such as the waste forms, canisters, backfill and sealing of the mined openings as well as on the natural barrier function of the host rock. A series of applied studies on subsystems of the multi-barrier system are performed, which cover a variety of components with specific characteristics and properties. The investigations and quantifications of their respective retention functions require specific approaches, methods, analytical techniques and models. Achievements presented in this chapter cover the mobilization of radionuclides from spent nuclear fuel and consecutive their immobilization by iron corrosion products, Raman spectroscopy of highly radioactive VEK-glass samples, and the preparation of the new 7th FP project FIRST-Nuclides, dealing with the fraction of radionuclides rapidly released from spent nuclear fuel. Application of basic results on disposal safety is shown, such as a study on actinide retention in cemented waste forms, and the contributions to the “Preliminary Safety Analysis Gorleben (vSG)” project and the national database project “THEREDA”. Furthermore, the results of investigations on the impact of colloids on the radionuclide migration are presented, as well as numerical modelling of fluid flow and solute transport in a shear zone at the Grimsel test site for tracer tests 09-01 and 10-01.

6.1 Key processes affecting corrosion of nuclear waste forms

E. Bohnert, C. Bube, N. Finck, E. González-Robles Corrales, B. Kienzler, A. Loida, V. Metz, V. Montoya, N. Müller, D. Schild, E. Soballa*

*Amphos21, Barcelona

Mobilization and immobilization of radionuclides from spent nuclear fuel

Introduction

The radionuclide release from spent nuclear fuel (SNF) in the aqueous phase is highly dependent on oxidative dissolution of the fuel matrix. The capacity of corroded canister iron phases to retain radionuclides was under investigation within the European collaborative project “ReCosy”. The stable corrosion product of steel under reducing disposal conditions is magnetite. By means of a long-term SNF corrosion experiment, it was intended to investigate the retention of radionuclides by magnetite which may provide for a driving force for SNF dissolution. To study the effect of magnetite on the overall corrosion behaviour of SNF in NaCl solution an experiment with a cladded SNF pellet and magnetite rich Fe(II,III) oxide (denoted as “K14Mt”) was performed over almost 10 years. After the final sampling of the gas phase and the solution, special attention was directed on the properties of the altered solid materials (SNF, magnetite). Hitherto results on radionuclide release in solution and gas phase and first solid phase characterizations are published in the INE annual report 2009 [1]. During the experiment a carbon contamination of the magnetite rich powder was released as CO₂. In parallel to a continuous increase of CO₂ in the gas phase (reaching 0.8 vol% in the final sample), aqueous radionuclide concentrations increased steadily. Even after almost 10 years,

radionuclide concentrations (e.g. $\sim 1 \cdot 10^{-4}$ mol/L uranium) did not reach a steady state level.

In the present study we characterize the Fe(II,III) oxide powder prior to and after the experiment “K14Mt”. Additionally, the distribution of released radionuclides between the magnetite rich Fe oxide, the container wall and the aqueous phase was determined.

Spent nuclear fuel corrosion experiment

The corrosion experiment was performed using a pellet sized SNF segment with a burn-up of 50 MWd/kg U and a linear power rate of 260 W/cm. The initial mass of the 10 mm long cladded segment was 6.6 grams. In contact with the SNF sample was 9.016 g of “Iron(II,III) oxide, Puratronic 99.997%” powder, purchased from Alfa Aesar (Fe₃O₄ #012962). In a glass vessel with Ar atmosphere, the SNF and Fe(II,III) oxide were immersed in 5 mol/L NaCl with an initial volume of 200 mL. The leachant was replaced entirely by fresh solution for four times within the first 65 days, in order to reduce considerably the concentration of Cs for analytical reasons. Besides Cs, other labile radionuclides, such as fission gases and iodine were released from the gap and grain boundaries to some extent and removed from the solution during this washing procedure. Afterwards the experiment was continued for 3562 days in a “static phase” without replacing the solution. Aliquots of the gas phase and the solution were sampled at 78, 215, 349, 771, 1895 and 3562 days after start of the static phase. The general experimental methodology and analytic procedures are described in [2]

and [3]. After termination of the experiment, a small amount of the Fe(II,III) oxide was recovered and analyzed using Raman spectroscopy, SEM/EDX, XPS, XRD, digestion in HCl and consecutive radiochemical analyses.

Results and discussion

A comparison of Raman spectroscopy, SEM/EDX and XRD (Fig. 1) analyses of non-reacted Fe(II,III) oxide with the respective analyses of Fe(II,III) powder recovered from experiment "K14Mt" show no significant differences. According to these analyses, the non-reacted and the recovered Fe(II,III) oxides contain magnetite ($\text{Fe}_3\text{O}_4(\text{s})$), hematite ($\alpha\text{-Fe}_2\text{O}_3(\text{s})$) and traces of maghemite ($\gamma\text{-Fe}_2\text{O}_3(\text{s})$) with a ratio of $\text{Fe}_3\text{O}_4(\text{s}) / \text{Fe}_2\text{O}_3(\text{s}) = 6$.

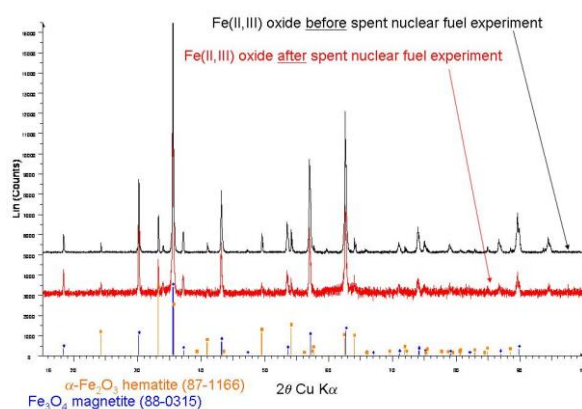


Fig.1: Diffractograms of a non-reacted aliquot of Fe(II,III) oxide and an aliquot recovered from SNF corrosion experiment "K14Mt".

XPS analyses of non-reacted and recovered Fe(II,III) oxide aliquots demonstrate that the surfaces of the powder grains are covered (partly) with $\text{Fe}_2\text{O}_3(\text{s})$ and carbon containing impurities. In addition to Fe(III) oxide and carbon, the powder recovered from the "K14Mt" experiment contains minor contributions of Si (1.3 ± 0.2 at.%, released from the glass vessel), U(VI) (0.9 ± 0.2 at.%, released from the SNF sample) and traces of Zr (≤ 0.2 at.%).

In order to quantify the total amount of carbon containing impurities, non-reacted Fe(II,III) oxide was completely digested and the production of $\text{CO}_2(\text{g})$ analyzed. Within a 250 mL autoclave an amount of 5 g non-reacted Fe(II,III) oxide powder was immersed in 30 mL HCl (30% ultrapure) under pure Ar atmosphere. An aliquot of the gas phase was sampled after 74 days and replaced by Ar. After additional 31 days a gas aliquot was sampled again. The gas aliquots were

analyzed by mass spectrometry. The results are shown in Table 1.

Table 1: Composition of the gas phase after immersion of 5 g Fe(II,III) oxide (Alfa Aesar Puratronic 99.997%) in 30 mL HCl.

	1 st Interval 74 d Percentage	2 nd Interval 31 d Percentage
Ar	33.011	26.343
CO ₂	0.106	0.082
H ₂	66.803	73.504
N ₂	0.076	0.069
O ₂	0.004	0.002
Total	100.000	100.000

After the end of both reaction intervals the Fe(II,III) oxide was found to be completely dissolved. Due to corrosion of the Fe(II,III) oxide, up to 66.8 and 73.5 vol.% H₂ was formed in the consecutive gas samples. In parallel, the fraction of Ar decreased to 33 and 26.3 vol.%, respectively. The percentage of CO₂ was found to be 0.106 vol. % after 74 d and 0.082 vol.% after 31 days, respectively. With regard to the measured N₂ contamination of 0.08 vol.% (air ingress over valves and fittings) the possible CO₂ concentration by air should not exceed $\sim 3 \cdot 10^{-5}$ vol.%. Even in the case of a complete exchange of the Ar atmosphere by air, the maximum possible amount of CO₂ would be about 0.03 vol. %, only. The total carbon content in the fresh Fe(II,III) oxide is too low, to be characterized with SEM-EDX, Raman spectroscopy or XRD. It is suggested that during the "K14Mt" experiment, the carbon impurities reacted continuously to CO₂ as consequence of radiolytic processes.

An amount of 230 mg Fe(II,III) oxide recovered from the SNF corrosion experiment was dissolved in 30% HCl to determine the amount of radionuclides retained by the magnetite rich powder. Radionuclides, retained onto the vessel wall, were determined by acid stripping (5 M HNO₃). The radiochemical analyses show that the total releases of the fission products Cs, Sr and Tc in the static state of experiment "K14Mt" (amounts in solution as well as amount retained onto vessel wall and Fe(II,III) oxide) are $1.5 \cdot 10^{-6}$ moles, $3.0 \cdot 10^{-7}$ moles and $1.5 \cdot 10^{-7}$ moles. In the following discussion we neglect the amount of radionuclides, which was retained by vessel wall and Fe(II,III) oxide during the washing procedure prior to the static state. Between 95% and 99% of Cs, Sr and Tc were found in the aqueous phase. A total U release of $5.1 \cdot 10^{-5}$ moles was measured,

whereof 70% was found upon the Fe(II,III) oxide. Am release of 3.56×10^{-8} moles was found whereof 95% was found upon the Fe(II,III) oxide. The Pu release was measured to be 2.3×10^{-8} moles with 90% re-immobilized upon the Fe(II,III) oxide. The retention of radionuclides upon the glass vessel wall did not play a significant role except for plutonium. Figure 2 shows the distribution of released radionuclides between the aqueous phase, the glass vessel wall and the Fe(II,III) oxide.

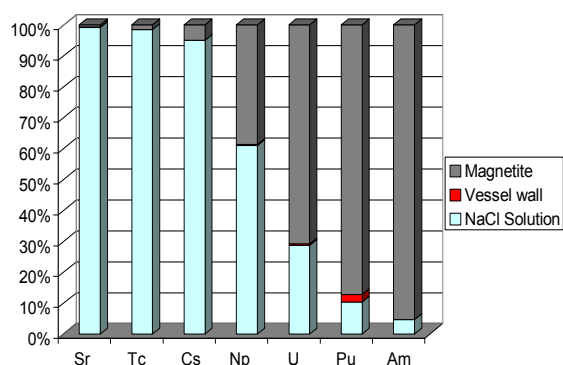


Fig.2: Distribution of radionuclides between the aqueous phase, the magnetite and the glass vessel wall in terms of percentage

At the end of experiment “K14Mt” the aqueous uranium concentration was measured to be $\sim 1 \cdot 10^{-4}$ mol/L at $\text{pH}_{\text{exp}} = 6.00$ (corresponding to $-\log(m_{\text{H}^+}) = 6.95$). This U concentration is about 2 orders of magnitude above the meta-schoepite ($\text{UO}_3 \cdot 2\text{H}_2\text{O}(\text{cr})$) solubility in carbonate-free 5 mol/L NaCl solution [4]. It is known for diluted NaCl solution that $(\text{UO}_2)_2\text{CO}_3(\text{OH})_3^-$ dominates the U speciation between $6 \leq \text{pH}_m \leq 7$ in presence of a CO_2 partial pressure as high as in experiment “K14Mt”. The carbonate complexation of U(VI) causes an increase in the concentration of dissolved U. Unfortunately, a Pitzer model for calculation of the U(VI)- CO_3 -Cl-Na system is not available, presently, and the actual U solubility cannot be calculated for the presence of carbonate in the concentrated NaCl system.

In order to estimate the potential extent of radionuclide sorption onto Fe(II,III) oxide, we calculate distribution coefficients of Cs, Sr, Tc, Np, Am, Pu and U (Table 2).

The total U release from SNF cladded segment was 5.1×10^{-5} moles. Using the dissolved U(VI) concentration, a distribution coefficient between the re-immobilized and mobile uranium of 41.3 mL/g was calculated. To relate this value to U(VI) sorption onto Fe(II,III) oxide we take, for example, the study of Missana et al. [5], in which a K_d of 4 ml/g for U(VI) onto

colloidal magnetite was determined in diluted solution under anoxic conditions.

Table 2: Calculated distribution coefficients of radionuclides upon Fe(II,III) oxide after 3562 days corrosion of SNF in 5 mol/L NaCl solution.

Nuclide	Distribution coefficient (mL/g)	Nuclide	Distribution coefficient (mL/g)
Cs	0.9	Np	10.5
Sr	0.1	Am	344.5
Tc	0.2	Pu	140.4
		U	41.3

Concluding remarks

In the long term SNF corrosion experiment with Fe(II,III) oxide, the initially pure Ar atmosphere was continuously altered due to the radiolytic production of hydrogen and oxygen, as well as due to the release from CO_2 from the Fe(II,III) oxide. The relevant carbon-containing phase in the Fe(II,III) oxide could not be identified unambiguously due to the detection limits of the applied methods (SEM/EDX, Raman spectroscopy, XRD)

Under the anoxic conditions of the SNF corrosion experiment, the dissolution of the $\text{UO}_2(\text{s})$ matrix is expected to be enhanced by the presence of CO_3^{2-} . In experiment “K14Mt” the effect of carbonate complexation on the actinides and Tc is superposed by retention on the Fe phases.

Considerable amounts of radionuclides were retained upon the Fe(II,III) oxide. With respect to Am, Pu, U and Np about 95, 87, 71, and 39 % of the released amounts were found to be re-immobilized upon the $\text{Fe}_2\text{O}_3(\text{s})$ coating of the Fe(II,III) oxide powder. In order to decide whether sorption or precipitation processes account for the U retention, a Pitzer model for calculation of the U(VI)- CO_3 -Cl-Na system is required.

The long-term SNF corrosion experiment aimed initially to correlate a reductive radionuclide trapping onto magnetite with the SNF dissolution rate. The results show that it is not possible attributing the retention to reductive processes unambiguously. Other processes such as sorption or surface precipitation affect the retention. Furthermore, the high CO_2 concentration changed the system under investigation completely.

Acknowledgment

The research leading to these results has received funding from the European Atomic Energy Community's Seventh Framework Programme (FP7/2007-2011) under grant agreements No. 212287 (RECOZY).

Examination of the VEK-glass samples by Raman spectroscopy

Introduction

For HLW, the waste form "glass" represents the primary barrier within a disposal system. Vitrified waste forms can be of a wide variety of compositions, including silicate glasses, borosilicate glasses and phosphate glasses [6]. At INE, the vitrification of liquid HLW in a borosilicate matrix by a directly heated ceramic melter was developed and applied. In 2010, the VEK vitrification process for the liquid high-level waste was finished. During the vitrification process, VEK was required to save retain samples. From this rarely available material, some small samples were prepared and transferred into the INE lab [7] where an investigation program was initiated.

In principle, radionuclides and other constituents are evenly dispersed throughout the glass matrix. Precipitates of noble metal and, in some cases, crystalline oxides enriched in radionuclides may be present [8].

Experimental

The complete description of the samples as well as the transportation from Verglasungseinrichtung Karlsruhe (VEK) to INE is explained in the INE 2010 Annual Report [2]. Two of these fragments, VEK-23-1 with a weight of (0.089 ± 0.001) g and VEK-57-2 with a weight of (0.026 ± 0.001) g were selected to be characterised with Raman spectroscopy, see Fig. 3.

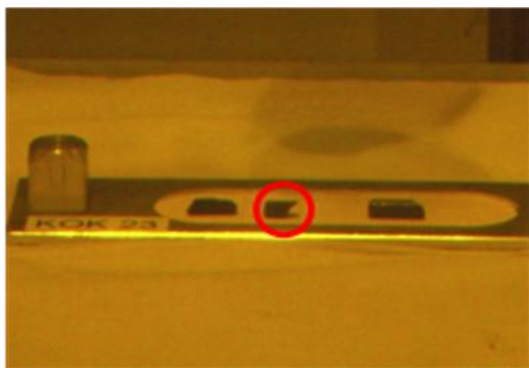


Fig. 3: Picture showing the fragments of the canister iron mould number 23, the red circle indicates the fragment selected.

To interpret the Raman spectra of the HLW glass samples, an inactively simulated glass sample was also analysed by Raman spectroscopy and compared to the results of the radioactive samples.

A SENTERRA Raman microscope spectrometer (Bruker Optics GmbH, Ettlingen, Germany) equipped with an UNILAB probe (785 nm) was used. The probe is mounted in a shielded cell, while the laser and the Raman spectrometer are installed outside the cell connected by a fiber-optic signal transmission line. The laser power output was 100 mW. The maximal power was used for the measurements. Due to attenuation of the laser light and the Raman signal by the fiber-optics, only about 1/10 of the signal intensity was achieved compared to direct measurement using the Raman microscope.

The inactive glass fragment was analysed by the Raman microscope spectrometer. A 532 nm CW diode pumped solid state laser, maximal laser output power 20 mW, and a 785 nm CW diode laser, maximal laser power output 100 mW were used at circular polarisation.

Results and discussion

The first Raman spectra were acquired from inactive glass at excitation wavelengths, 532 and 785 nm, see Fig. 4. For laser wavelength of 785 nm, it was possible to observe a peak at 1400 cm^{-1} ; in the contrary, when the laser light of 532 nm was used several peaks were observed but no one of them was similar to the peak observed with the laser of 785 nm. Hence, the peaks are due to fluorescence but they did not constitute Raman signals.

The Raman spectra recorded at 785 nm excitation did not show significant difference between the VEK glass fragment and the inactive glass fragment. A peak at 1400 cm^{-1} is observed, this peak does not correspond to a Raman line and is caused by fluorescence of the trivalent elements as Nd, or La incorporated in the glass matrix, see Fig. 5. Differences at low wavenumbers between the inactive and the VEK glass originating by different optics of the probe and the microscope (Fig. 6).

Discussion and conclusions

The glass samples emitted high fluorescence intensities at laser irradiation with 785 nm. Therefore, the examination of the different glass fragments by Raman spectroscopy did not reveal significant differences and did not allow any conclusion about phase separations or presence of precipitates in the glass. In order to investigate the effect of the radionuclides in the glass matrix, further

studies using different analytical techniques such as XPS or XRD will be carried out.

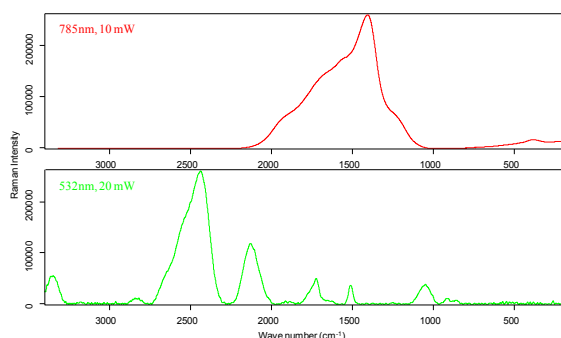


Fig. 4: Raman spectra of the inactive sample using a laser of 785 nm at 10 mW (red spectra), and using a laser of 532 nm at 5 mW (green spectra).

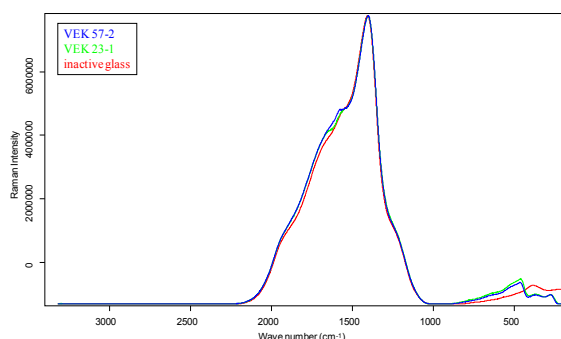


Fig. 5: Comparison of Raman spectra of the VEK 57-2 (blue line), VEK 23-1 (green line) and inactive glass (red line) fragments using a laser of 785 nm.

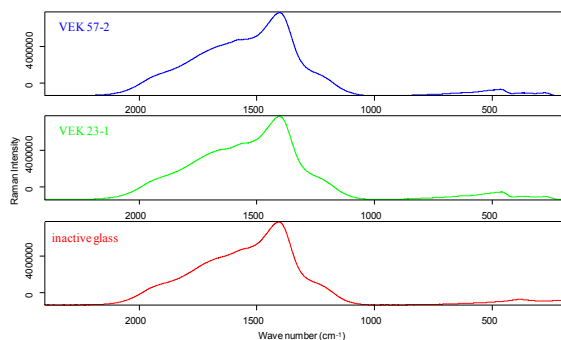


Fig. 6: Raman spectra of the VEK 57-2 (blue line), VEK 23-1 (green line) and inactive glass (red line) fragments using a laser of 785 nm.

Collaborative Project “FIRST-Nuclides”

In the Vision Report and the Strategic Research Agenda of the “Implementing Geological Disposal – Technology Platform”, a key topic deals with “waste forms and their behaviour”. On this background, the EURATOM FP7 Collaborative Project “Fast / Instant Release of Safety Relevant Radionuclides from Spent Nuclear Fuel (CP FIRST-Nuclides)” was applied, negotiated and

finally granted. KIT-INE is the coordinator of the CP.

CP FIRST-Nuclides deals with understanding the behaviour of high burn-up spent uranium oxide (UO₂) fuels in geological repositories. This waste type represents the source for the release of radionuclides after loss of the disposed canister integrity. For safety analysis, the time-dependent release of radionuclides from spent high burn-up UO₂ fuel is required. The first release consists of radionuclides (1) in gaseous form, and (2) those radionuclides showing a high solubility in groundwater.

With respect to the fast / instant release of radionuclides (RN) from spent nuclear fuel elements under deep underground repository conditions, a series of questions are still open. Consequently, FIRST-Nuclides aims on the determination of the “instant release fraction (IRF)” values of iodine, chlorine, carbon and selenium that are still largely unknown. The elements I, C, Cl and Se tend to form anionic species. Such anions are hardly chemically retained in the repository barrier system. The speciation of some radionuclides, in particular ¹⁴C, will be investigated; ¹⁴C may be present as carbide in the spent fuel and may form mobile hydrophilic organic species.

The CP is organized in six workpackages (WP). WP 1: “Samples and tools” deals with the selection, characterization and preparation of materials and set-up of tools. It is essential to the project that typical and sufficiently well characterized spent fuel is used for the experiments. WP 2 covers “Gas release and rim and grain boundary diffusion” and WP 3 investigates “Dissolution based release”. These investigations include the determination of the chemical form of released radionuclides, fission gases, ¹³⁵Cs, ¹²⁹I, ¹⁴C compounds, ⁷⁹Se, ⁹⁹Tc and ¹²⁰Sn. WP 4 “Modelling” deals with modelling of migration/retention processes of fission products in the spent fuel structure. The modelling work within FIRST-Nuclides will help to clarify which geometric scales dominate the fast/instant release. Special attention is attributed to model the fission product migration along the grain boundaries, the effects of fractures in the pellets and of holes/fractures in the cladding. WP 5 is responsible for the knowledge management, the state-of-the-art report, the general reporting, keeping the documentation up-date, and all dissemination and training measures.

The project is implemented by a consortium with ten partners (AEKI/MTA, AMPHOS21, CNRS, CTM, FZ Juelich, JRC-ITU, KIT, PSI, SCK/CEN and STUDEVIK). The Coordination Team consists of KIT and AMPHOS21 which are responsible for project management,

knowledge management, documentation, dissemination and training. Workpackage leaders head the individual workpackages. Several organisations from France, USA (2) and UK contribute without any funding by the project. A group of implementation and regulatory oriented organizations are participating as an "End-User Group". This group ensures that end-user interests are reflected in the project work, and reviews the project work and scientific-technical outcome.

The project starts January 1, 2012 and has a duration of three years.

References

- [1] H. Geckeis, T. Stumpf, (Eds.) Annual Report 2009, KIT Scientific Reports 7559, pp. 43 - 44 (2010).
- [2] B. Grambow, A. Loida, P. Dressler, et al. Wissenschaftliche Berichte, FZKA 5702, März 1996.
- [3] A. Loida, B. Kienzler, H. Geckeis, Mat. Res. Soc. Symp. Proc. Vol.757, pp. 433-439 (2003).
- [4] M. Altmaier, V. Neck, et al. (2006). 12th Int.Symp. on Solubility Phenomena and Related Equilibrium Processes (ISSP 2006), TU Bergakademie Freiberg, July 23-28, 2006.
- [5] T. Missana, M. Garcia- Guthierres, V. Fernandez, *Geochimica et Cosmochimica Acta*, Vol. 67, No 14, 2543-2550 (2002).
- [6] W. Lutze: in 'Radioactive waste forms for the future', Amsterdam, Elsevier Science. (1988).
- [7] H. Geckeis, T. Stumpf, Annual Report 2010 Institute for Nuclear Waste Disposal. Karlsruhe, KIT Scientific Reports 7600 (2010).
- [8] R. C. Ewing, W. J. Webert, F. W. Jr. Clinard, Radiation effects in nuclear waste forms for high level radioactive waste. *Progress in Nuclear Energy*, vol. 29, no. 2, pp 63-121 (1995).

6.2 Safety analyses on the basis of waste form performance, kinetics, thermodynamics and sorption

M. Altmaier, E. Bohnert, C. Bube, B. Kienzler, V. Metz, M. Plaschke, D. Schild, M. Schlieker and E. Soballa.

Actinide retention in cemented waste forms

Introduction

Cementitious waste matrices of low- and intermediate level wastes provide for significant radionuclide retention. Depending on the composition of potentially contacting solutions, alteration of the cementitious solids occurs together with the formation of secondary phases. The present work focuses on the long-term interaction of cemented waste product simulates in MgCl_2 -rich solutions and uranium retention in this system. Long-term experiments with full-scale cemented waste products in chloride-rich solutions have been conducted at the former Asse II salt mine for more than 20 years (see Fig. 1). In addition, alteration of hydrated cement paste in MgCl_2 -rich solutions is studied in laboratory-scale



Fig. 1: Full-scale experiments conducted at the former Asse II rock salt mine.

batch experiments to determine the compositions of equilibrated solutions and solids over a larger range of solid to brine ratio.

Experimental approach

Full-scale cemented waste simulates have been produced in the 1980s using OPC PZ45F (i.e. CEM I 42,5R) with a water / cement ratio of 0.5 and a load of 11 wt.-% process chemicals, e.g. NaNO_3 (9 wt.-%), Na-citrate, Na-tartrate, $\text{Na}_2\text{HPO}_4 \cdot 12\text{H}_2\text{O}$ and Na-oxalate. The cemented waste simulates studied in this work had a mass of 336 kg and were doped with 1.017 kg $(\text{NH}_4)_2\text{U}_2\text{O}_7$. After complete hydration, they were immersed in 400 L steel canisters filled with 135 L MgCl_2 -rich brine (Q-brine). The initial composition of the leachant in

$\text{mol}(\text{kg H}_2\text{O})^{-1}$ was Mg^{2+} : 4.1, Ca^{2+} : 0.0001, Na^+ : 0.4, K^+ : 0.7, Cl^- : 8.7 and SO_4^{2-} : 0.3 [1].

Hardened cement paste for the laboratory batch experiments was produced from OPC PZ35F (i.e. CEM I 32,5 R) with a water / cement ratio of 0.4. After a two months hydration period, the samples were milled and exposed to Q-brine applying solid to brine ratios between 0.025 and 1.0 g mL^{-1} [2].

Solution composition and pH were monitored regularly up to 1327 days in the laboratory and more than 20 years in case of the full-scale cemented waste simulates. Different analytical methods, e.g. SEM-EDX, XRD, XRF and Raman μ -spectrometry were used for solid phase analyses after termination of the experiments.

Modeling

“The Geochemist’s workbench” (GWB) code was used for thermodynamic equilibrium calculations. Due to the high ionic strength of the systems, calculations were based on the Pitzer approach for activity corrections. The database is mainly based on data of Reardon for the cementitious system and data from the NEA-TDB and Neck&Altmaier et al. Details on the approaches, codes and thermodynamic data can be found in [3].

Results and discussion

Cement corrosion

Within the first 11.5 years, a continuous alteration of the brine composition has been observed. The initial MgCl_2 -rich solution with a near-neutral pH changed to a CaCl_2 - NaCl -rich solution with pH_m ($-\log m\text{H}^+$) values close to 12. After 13 to 21 years, changes of solution composition and pH_m values became very low. Thermodynamic equilibrium calculations both for the laboratory and the full-scale experiments compare well to the steady-state concentrations after equilibration within 100-1000 days (Fig. 2). The experimental results compare well to the results of. Solution compositions at a solid to brine ratio of 1.0 g mL^{-1} appears to be close to the solution compositions at the higher solid to brine ratio of the cemented waste products ($\sim 2.5 \text{ g mL}^{-1}$).

Solid phase analyses of the cementitious phases with XRD reveal a complete conversion of the primary clinker and cement hydration phases to secondary phases. An

increase in Mg, K, Na and Cl is observed in the solid samples together with a decrease of Ca and Si.

Uranium retention

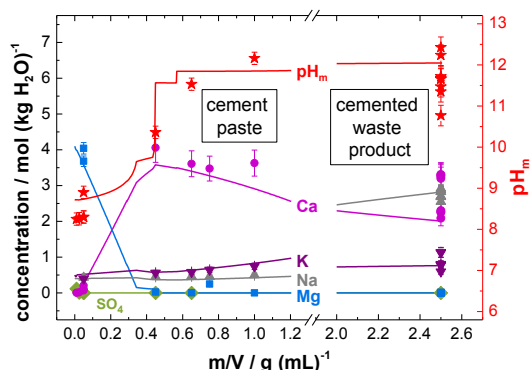


Fig. 2: Experimental steady-state solution composition (symbols) and corresponding calculated equilibrium concentrations (lines) as a function of solid to brine ratio.

Parallel to the pH_m increase, U concentrations are observed to increase from values of $5 \cdot 10^{-8}$ - $2 \cdot 10^{-9}$ mol (kg H_2O) $^{-1}$ after 8-10 years to values between $1 \cdot 10^{-7}$ and $3 \cdot 10^{-6}$ mol (kg H_2O) $^{-1}$ after more than 13 years. Over the last sampling campaigns (after 13 to 21 years), U concentrations seem to remain constant. Some of the experiments were stopped and solid phase samples were prepared for analysis. Using SEM-EDX, aggregates of 5 to 100 μm size were detected that contain up to 10 atom% U. These U-bearing solids were then analyzed by means of Raman μ -spectrometry. Spectra of U-rich aggregates (>20 μm) found at different locations within the solid show considerable similarities (see Fig. 3).

Taking into account the evolution of solution composition in the full-scale experiments, U solubilities were calculated considering relevant U(VI) phases. Since experimental Si

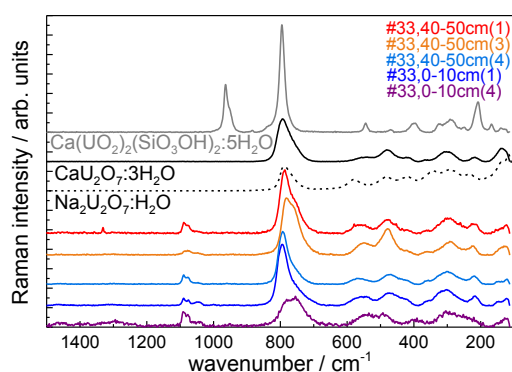


Fig. 3: Raman spectra of uranium-rich aggregates recorded at 785 nm wavelength. Spectra of uranophane (sample obtained from N. Macé, PSI), Ca- and Na-diuranate reference samples are shown for comparison.

concentrations were below the detection limit (i.e. 10^{-3} mol (kg H_2O) $^{-1}$), U concentration for equilibrium with uranophane could only be calculated for a lower and an upper limit of expected Si concentrations. For Si between $5 \cdot 10^{-6}$ to $1 \cdot 10^{-3}$ mol (kg H_2O) $^{-1}$, U concentrations with uranophane as solubility-limiting phase would be in the range of the experimentally determined values. U concentrations calculated for equilibrium with Ca- and Na-diuranates are in agreement with the experimental results as well (see Fig. 4). In equilibrium with becquerelite, metaschoepite or soddyite, calculated U concentrations were more than one order of magnitude higher than the measured ones.

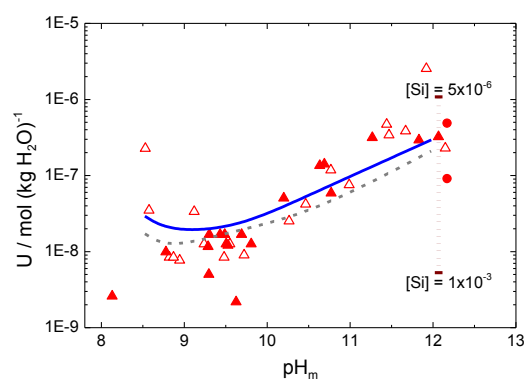


Fig. 4: Red triangles mark concentrations of dissolved U in full-scale experiments as a function of pH_m measured over 4 to 21 years [4]. Lines are calculated for equilibrium with Ca-diuranate (blue), Na-diuranate (grey dotted) and uranophane (brown dotted) for Si concentration range.

Discussion and conclusions

Results from solution composition and solid phase analyses indicate that steady-state conditions are achieved after 13 years in the full-scale experiments and within 3 years in the laboratory experiments with powdered hydrated cement. U-bearing hotspots of several μm diameter are detected by SEM-EDX and Raman μ -spectrometry. It is concluded that retention of U is caused by solubility phenomena rather than sorption. There are hints of XRD measurements on the presence of uranophane [4]. Raman μ -spectrometric spectra indicate that encountered large U-rich phases consist of Ca- or Na-diuranates. Thermodynamic equilibrium calculations support the presence of either Ca- / Na-diuranates or uranophane. It is suggested that local equilibria lead to the formation of two (or more) U(VI) phases in the corroded monoliths [3,4].

Acknowledgements

We gratefully acknowledge N. Macé (PSI) for providing a uranophane reference sample. The research leading to these results has been financially supported in part from the German Federal Office for Radiation Protection (BfS) within the projects “Analyse der Eigenschaften von simulierten, zementierten 1:1 Gebinden und ihres Phasenbestandes nach 20 Jahren Auslaugung in Salzlösungen” and “Studie zur Abschätzung der standortspezifischen Pu- und Am-Rückhaltung (Schachanlage Asse II)”.

Radionuclide Source Term in the scope of the “Preliminary Safety Analysis Gorleben (vSG)” Project

On behalf of the German Federal Ministry for the Environment (BMU) a preliminary safety analysis regarding the possible use of the salt dome ‘Gorleben’ as a repository for high-level waste (HLW) is performed. Within the framework of the vSG project, all available information on the salt dome and the results of exploration activities are summarized. The project is coordinated by GRS and is supported by a number of institutions. The main goals are (i) to develop a clearly documented statement, whether the Gorleben site can comply with the new safety requirements for the disposal of heat-generating waste, (ii) to identify the future needs for research and investigation and (iii) to establish a concept for permanent waste disposal. Therefore, the project is focused on long-term safety. The expected outcome of the preliminary safety analysis will provide a transparent prognosis whether the site is suited for safe final disposal at all, and if so, under which conditions.

INE contributes to this project by the formulation of a source term for radionuclide release from high-level waste glass, spent nuclear fuel, and compacted hulls and end pieces of fuel elements (CSD-C waste). The specific objectives of the source term study are

- to document the present scientific knowledge on the behaviour of heat-generating waste under saline conditions,
- to describe the relevant geochemical conditions and radionuclide mobilization / retention processes in the near field of the waste products,
- to provide data for a preliminary source term with respect to a scenario, which takes into account the presence of NaCl or MgCl₂ rich solutions in the near field.

Following topics are covered by the survey and update: Kinetics and temperature effects of

HLW glass dissolution, instant / rapid release from spent nuclear fuel as well as kinetics of UO₂/MOX matrix dissolution, and the hydrogen inhibition effect on spent nuclear fuel matrix dissolution. Boundary conditions are derived for the considered evolution scenario and the expected geochemical conditions such as pH and redox conditions are analyzed.

The source term is based on kinetic and thermodynamic mobilization / retention processes and on the influence of temperature. Maximum expected concentrations of the radionuclides Am, Th, U, Np, Pu, Tc, Zr, Se and rare earth elements are derived for the simplified evolution scenario. This scenario does not include the presence of carbonate. Elevated temperature effects are not treated explicitly. The concentrations to be used for the source term are provided for 5 M NaCl solution at pH_m 6 and 9 and for 4.5 M MgCl₂ solution for the same pH_m values. The concentrations are reported for following redox states: Am and Pu in the trivalent state, tetravalent Th, U, Pu, Zr, and Tc, pentavalent Np and Pu and hexavalent U. Tc(VII) concentration is not limited under these conditions.

Except sorption on canister materials and canister corrosion products, radionuclide retention by sorption processes is of minor importance for the present backfill concept. Due to simplifications in the definition of the scenario and geochemical boundary conditions, the radionuclide source term has explicitly a preliminary and orienting character. A list of required specifications with respect to the design, layout and closure concept of the disposal and of research on geochemical processes, mechanisms and data is elaborated.

References

- [1] B. Kienzler, P. Vejmělka, H.J. Herbert, H. Meyer, C. Althenhein-Haese, Nucl. Technol., 129(1):101 (2000).
- [2] V. Metz, E. Bohnert, B. Kienzler, K. Garbev, A. Bauer, K. Bender, C. Bube, S. Hilpp, S. Moisei-Rabung, J. Lützenkirchen, M. Plaschke, M. Schlieker, D. Schild, E. Soballa, C. Walschburger, Pu- und Am-Rückhaltung (Schachanlage Asse II), Abschlussbericht (2011).
- [3] C. Bube, V. Metz, D. Schild, M. Lagos, E. Bohnert, K. Garbev, M. Altmaier, B. Kienzler, NUWCEM 2011 Conference proceedings, Avignon, France (2011).
- [4] B. Kienzler, V. Metz, B. Brendebach, N. Finck, M. Plaschke, T. Rabung, J. Rothe, D. Schild, Radiochimica Acta 98(9-11):675 (2010).

6.3 Colloid impact on radionuclide (RN) migration

N. Banik, M. Bouby, J. Brendlé¹, G. Darbha², C. Fischer², H. Geckeis, R. Götz, W. Hauser, S. Heck, P. Höss, F. Huber, C. M. Marquardt, T. Schäfer, D. Schild, J. Rothe, L. Truche³

¹Lab. Mat. Mineraux, UMR CNRS 7016, Univ. Haute Alsace, 68093 Mulhouse, France ; ²University of Göttingen Goldschmidt Str. 3, 37077 Göttingen, Germany, , ³G2R/UMR/CNRS, Univ. Henri Poincaré, 54500 Nancy, France

Introduction

The influence of colloidal/nano-scale phases on the radionuclide (RNs) solubility and migration behaviour is still one of the uncertainties of the repository safety assessment. In our work, we aim 1) to identify the presence and the formation of relevant colloids in repository specific areas, 2) to determine their stability as a function of geochemical parameters, 3) to elucidate the thermodynamics and kinetics of the colloid interaction with radionuclides, 4) to perform laboratory and field experiments to quantify the colloid mobility and their interaction with surface. The final goal is to state on the relevance of the nanoparticles (NPs) / colloids for the radionuclides migration in natural geochemical conditions.

This year, in this chapter, we report on the progress concerning a- the colloid characterization in natural ground waters, b- the interaction of tetravalent neptunium (Np^{IV}) with fulvic acids (FAs), c- the reversibility kinetic of the radionuclide sorption onto synthetic Zn-/Ni-doped-montmorillonite colloids, d- the impact of mineral aggregate surface topography and Eu(III) concentration on colloid retention.

Colloid detection in natural ground waters

Analysis and characterization of colloids as a function of groundwater chemistry provides information on their relevance under these specific conditions, more precisely in the far-field of a repository. The ground waters under investigations are from the Gorleben site (Northern German Plain, Lower Saxony) which is currently under exploration for its suitability for a nuclear waste repository [1]. The peculiarity of the overlying complex aquifer system is a high content of dissolved organic matter due to microbial turn-over of Brown coal (lignite) intercalations [2]. Such a colloidal system gives insight in the (macro)molecules or NPs which might be present after long periods of time and how they interact with the dissolved inorganic elements in presence. The two ground water samples were analyzed by Asymmetrical Flow Field-Flow Fractionation (AsFFFF) coupled to an UV-Vis spectrophotometer and an ICP-MS. The

results are similar for both samples (GoHy-2227 and GoHy-532) and evidence colloidal matter heterogeneity (see exemplary Figure 1). Alkaline earth elements are mainly found as ionic species. Rare earth elements (REE) and actinides (An) are distributed in two main fractions: heavier REE and U are located in majority in the colloidal fraction < 4 nm corresponding to the size range of the organic matter (as confirmed by the UV-Vis. Fractogram recorded at 225 nm but not shown in Figure 1), while lighter REE and Th are found in (in)organic colloids of sizes between 4-18 nm. This demonstrates the homogeneity of the aquifer system and/or possible migration pathway as the two ground water samples originated from the same site but at a distance of 2 kms from one to each other. The isolation of the different size fraction for better characterization is now in progress.

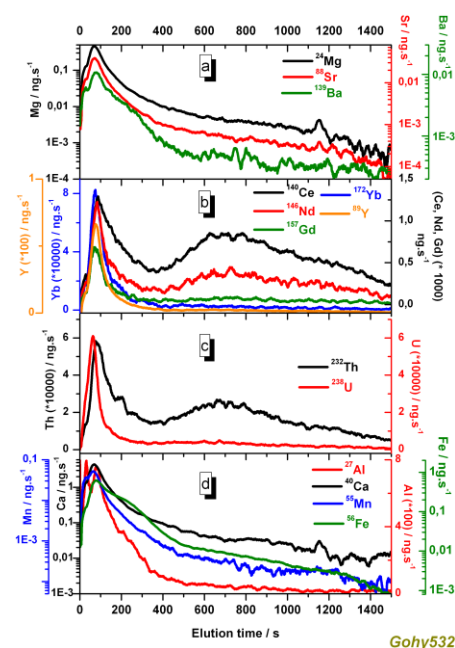


Fig. 1: ICP-MS fractograms obtained by injection of ground water sample from the Gorleben site, borehole-GoHy-532, (smoothed data).

Interaction of tetravalent neptunium (Np^{IV}) with fulvic acids (FAs)

The mechanism of tetravalent actinide complexation with humic or fulvic acids (HA or FA) is not clarified, due to various experimental difficulties (*i.e* eigen-colloid formation, strong sorption, redox reactions...). A recent review

emphasizes the need of additional experiments to get new data on the tetravalent actinides complexation by HA or FA [3]. We have thus complemented our previous studies on the Np(IV) fulvate complexation. Our goal is to elucidate the complexation mechanism by minimising eigen-colloid generation of Np(IV). Three approaches have been selected to prepare the Np(IV) fulvate complex. *Preparation I:* Np(IV) is prepared in strong acidic solution ($\text{pH} < 1$) by electrolytic reduction of Np(V). Aliquots of this solution are then mixed with a FA solution to form the Np(IV) fulvate complex (preparation I). *Preparation II:* Trivalent Np is mixed with FA solutions and then slowly and oxidised simply by the presence of oxygen impurities in the glove box atmosphere. *Preparation III:* A pentavalent Np fulvate complex is prepared at pH 9. Then the Np(V) is reduced by dithionate. All solutions are characterised by UV-Vis, X-ray photoelectron spectroscopy (XPS) and EXAFS. The Np(IV) concentration varies in the range 10^{-5} to 10^{-4} M, the FA acid concentration varies between 30 to 500 mg/L, the pH of the solutions lies between 1 and 4.5 and the ionic strength is fixed at 0.1 M by NaCl. All experiments are performed in a Ar- glove box. UV-Vis, XPS, and EXAFS show that only tetravalent Np occurred in all samples. Even at pH as low as 3 all Np(IV) is complexed at given FA concentrations. From the UV-Vis spectra at least two Np(IV) fulvate species can be identified with absorption band maxima at about 968 and 975 nm, respectively. The absorption band present initially at 968 nm at pH 1 disappears for increasing pH, whereas the band at 975 nm becomes dominant at pH 3. Seemingly, only one main Np(IV) species occurs at pH 3 irrespective of the preparation method. This is confirmed by XPS, where binding energies of the Np $4f_{5/2}$ and $4f_{7/2}$ electrons and the corresponding satellite peaks are comparable at pH 3. The same finding is obtained by XANES. All spectra are very similar irrespective of the preparation and the final pH value of 1.0 or 3.0 (Figure 2). EXAFS data show two O shells, one at Np-O distances of 2.20-2.24 Å corresponding to a bonding between Np and hydroxyl ions, and another one with Np-O distances at 2.40-2.44 Å. The latter is the average distance between coordinating water molecules and carboxyl groups. However, some samples showed only one average Np-O distance of 2.32 – 2.38 Å, which cannot be explained with respect to the preparation method at the moment. No Np-Np interaction could be found in any sample. Hence, formation of a colloidal or solid Np(IV)-oxyhydroxide coated by FA can be ruled out or is below the detection limit of the spectroscopic methods used.

To minimise the effects of mixed complexes on the thermodynamic complexation constant calculation, only the data showing two well separated peaks in the absorption spectra have been chosen for the evaluation. In the pH range 1 – 1.5, only one Np(IV) fulvate complex between Np^{4+} and the carboxylic groups of the FA (FA-COOH) is assumed. Unfortunately, the hydrolysed species of the Np(IV) ($\text{Np}(\text{OH})^{3+}$, $\text{Np}(\text{OH})_2^{2+}$, $\text{Np}(\text{OH})_3^+$, and $\text{Np}(\text{OH})_4(\text{aq})$) cannot be differentiated by absorption spectroscopy. The total uncomplexed tetravalent Np(IV), including all hydrolysed species, can be measured.

The degree of deprotonation (α_{H}) can be measured by direct acid-base titration but not lower than $\sim \text{pH} 3.5$. α_{H} values at pH 1 and 1.5 are extrapolated and estimated to be 1% and 8%, respectively. Another way to consider the pH effect on the FA is to introduce the loading capacity (LC). It corresponds to the maximum Np concentration that can be bound at a certain pH value, which means here at pH 1 and 1.5. Fitting of the data yields in LC equals to $(7 \pm 1)\%$ and $(17 \pm 1)\%$ at pH 1 and 1.5 respectively.

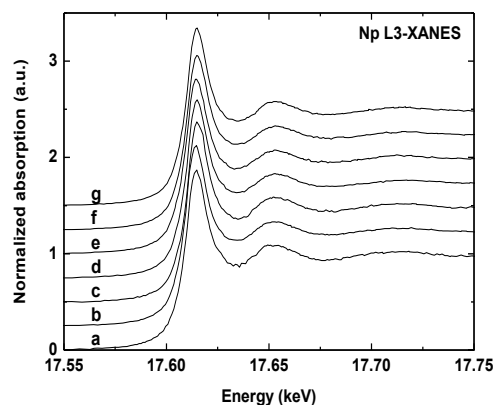


Fig. 2: XANES of Np(IV) fulvate samples prepared in various ways (a, b: preparation (II); c, d: preparation (I); e, f, g: preparation (III)). Spectra b, d, g: pH 1.0; Spectra a, c, f: pH 3.0; Spectra e: pH 4.5.

Considering one (α_{H}) or the other (LC) parameters to account for the pH dependence, complexation constant $\log\beta$ was calculated: $\log\beta(\alpha_{\text{H}}) = 7.0 \pm 0.5$ and 7.5 ± 0.4 ; $\log\beta(\text{LC}) = 6.9 \pm 0.2$ and 7.7 ± 0.2 , at pH 1 and 1.5 respectively. Although α_{H} and LC are different, the $\log\beta$ s obtained at the same pH value are very similar. The deprotonation effect is thus not significant. The $\log\beta$ values obtained can be considered as first approximations, keeping in mind that the complexation constant is pH dependent for the tetravalent neptunium.

Zn-/Ni- montmorillonite colloids as bentonite colloids homologues: a comparative RN sorption reversibility kinetics study.

The determination of FEBEX bentonite colloid mobility/recovery in previous studies [6-8] based on the structural Al of the clay reveal analytical uncertainties and thus differences between radionuclides desorption rates calculated from laboratory batch or column experiments. In situ experiments performed in the Grimsel Test Site (GTS Switzerland) (Möri et al., 2003) in the frame of the Colloid Formation and Migration (CFM) project plans to emplace a compacted bentonite source and determine the bentonite erosion rates under near-natural flow conditions. To univocally differentiate between the natural background colloid concentration and the eroded bentonite an irreversible labelling of the bentonite colloid source placed in a granite fracture would greatly improve their detection.

Synthetic montmorillonite containing structurally bound Zn and Ni in its octahedral layer is available [9]. It is thought to use an admixture to label the FEBEX bentonite. Actually, Zn and Ni are good candidates to determine more accurately the colloid concentration as the ICP-MS sensitivity is ten times higher for Zn than for Al. Furthermore, Zn and Ni background concentrations are very low in the Grimsel ground water (GGW). In the present study, the colloid are first separated and characterized by AsFIFFF-ICP-MS. Then, they are used to perform radionuclide reversibility kinetic experiments similar to those already published [6]. The aim is to compare the results obtained with the natural versus the synthetic clay colloids to decide if the latter can be used as homologues of the natural ones.

The size distribution of the colloids mobilized from the synthetic-doped montmorillonite is similar to the one obtained from the natural FEBEX. Fig.3 shows the evolution of the Al, Ni and Zn concentrations both for ultra-centrifuged (UC) and not ultra-centrifuged samples. No colloidal attachment occurs over 3500h (~ 5 months) for both types of montmorillonite colloids on fracture filling material from Grimsel. Similar results were obtained for the FEBEX bentonite colloids [6]. Figure 4 shows the evolution of the Tc(VII)-99, U(VI)-233 and Np(V)-237 concentrations in presence of labelled colloids and fracture filling material (FFM). The U-233 concentration is almost constant with only a slight decrease over 3500 h. This might be due to a slow sorption kinetic as a reduction of U(VI) to U(IV) is not likely on the basis of the redox potentials

(Eh) measured and thermodynamic calculations.

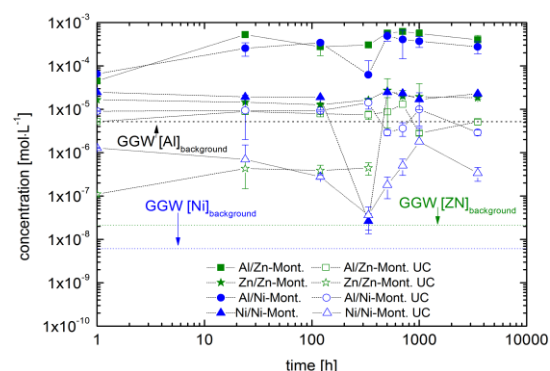


Fig. 3: Al, Zn and Ni concentrations evolution for both UC and not-UC samples.

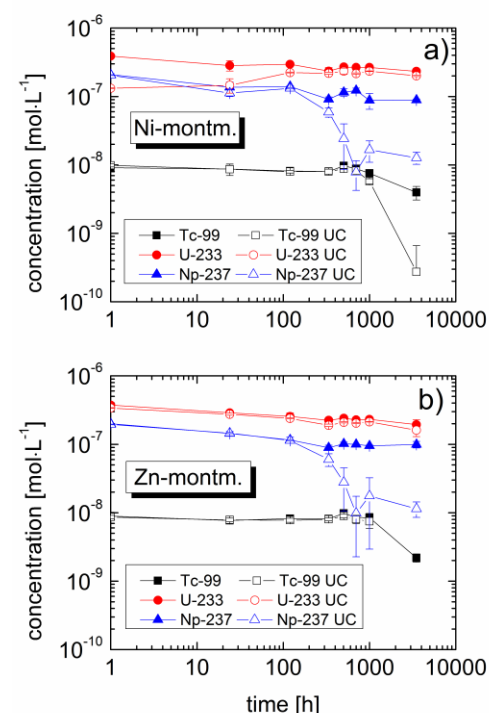


Fig. 4: Tc, U and Np concentrations evolution for both UC and not-UC samples. a) Ni-montmorillonite. b) Zn-montmorillonite.

Results obtained for Np-237 differ from those of U-233. The Np-237 concentration remaining after UC decreases clearly after ~300 h in both batch series. According to the experimental Eh-pH conditions, the initial Np(V) is probably reduced into Np(IV). Thus, Np(IV) may be present as Np(IV) colloids ("eigencolloids") or may be attached to the montmorillonite colloids, which explains the concentration decrease after UC. Unfortunately, based on the data available so far one cannot differentiate which of the two explanations holds. Nevertheless, the Np does not sorb on the FFM since its concentration in the not-UC batch samples remains constant, which is a clear difference compared to the FEBEX data presented in [6].

The Tc-99 behaves similarly to the Np-237. No reduction to Tc(IV) is observable which is in line with the measured redox potentials. After ~1000 h, differences in the concentration for UC and not-UC samples are detectable and explained as for the Np-237. According to the experimental Eh-pH conditions, a reduction of pertechnetate to the tetravalent Tc-99 is feasible.

Results for the trivalent (Am(III)-243) and the tetravalent radionuclides (Th(IV)-232 and Pu(IV)-242) are shown in Figure 5. The results obtained after UC show clearly lower concentrations. This demonstrates a radionuclide colloidal association, either as surface complex or maybe in form of sorbed eigencolloids. In more details, 96% and 98% of the Th-232 are bound to the Ni- and Zn-colloids, respectively, whereas ~70-81% of the Pu-242 and ~80% of the Am-243 is centrifuged of as colloidal phase in good agreement with results obtained on natural FEBEX clay colloids [6].

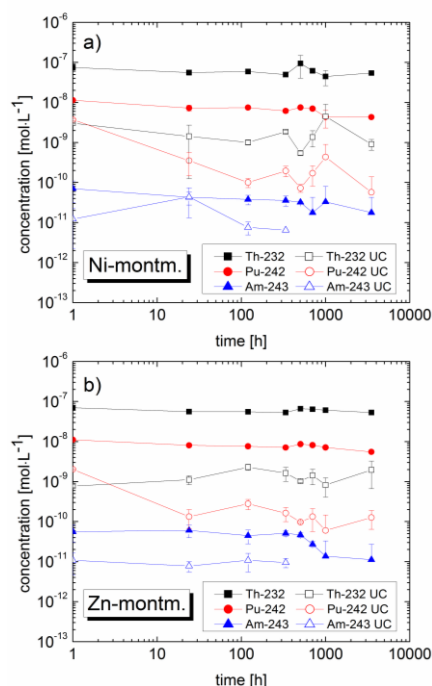


Fig.5: Th, Pu and Am concentrations evolution for both UC and not-UC samples. a) Ni-montmorillonite. b) Zn-montmorillonite.

Nevertheless, no clear radionuclide sorption reversibility is observed over 3500 h in contrast to [6], except for Am(III)-243 sorbed onto the Zn-montmorillonite colloids. This can be explained by the difference of the specific surface area of the synthetic Ni- and Zn-doted colloids with ~130 m²/g being a factor of 4 times higher than the specific surface area of the natural FEBEX colloids with ~33 m²/g. Based on the conceptual model that the driving force for the radionuclide- colloid desorption

process/kinetics and subsequent sorption to the FFM is the excess in surface area offered by the FFM [6] the observed slower kinetics of reversibility may be simply related to the different colloid/FFM surface area ratio.

In conclusion, the synthetic Ni- and Zn-montmorillonite colloids behave similar to the natural FEBEX bentonite colloids used in previous studies but possess higher specific surface areas, which in turn influences the radionuclide desorption kinetics. Further experiments are necessary to examine in more detail this point. Nonetheless, the synthetic structural labelled montmorillonite colloids appear suitable as a homologue for the natural FEBEX bentonite colloids circumventing the high uncertainties in the previous Al ICP-MS analysis.

Impact of mineral aggregate surface topography and Eu(III) concentration on colloid retention.

In many natural processes, the deposition of colloids is explained inter alia by the chemical and charge heterogeneity of the surfaces, the presence of impurities. However, under unfavorable conditions, where repulsive forces between mineral surfaces and particles prevail, the roughness becomes a more important factor which has to be quantitatively implemented in simulations. This study emphasizes the role of surface topography and Eu(III) concentration on colloid retention under unfavorable conditions.

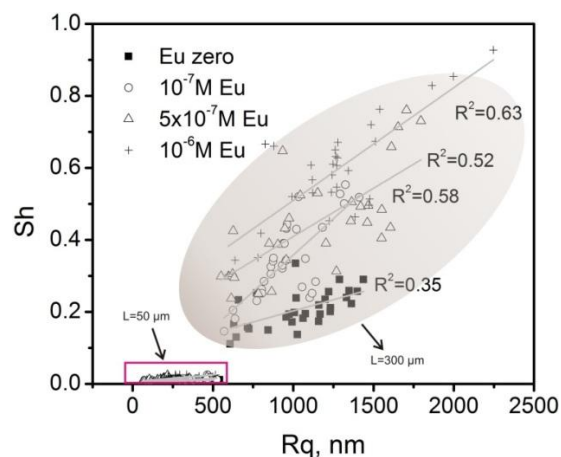


Fig .6: Deposition of polystyrene colloids on Grimsel granodiorite surface as a function of surface roughness Rq. Lower Rq (box) values were obtained by extracting the sub data sets of Scan length L = 50 μm from the L = 300 μm (encircled) scanned data. For comparison, Sherwood number (Sh) values reported for L=50 μm are normalized to the scan length L=300 μm.

A colloidal suspension (synthetic carboxylated polystyrene particles, $\phi = 1000 \pm 25$ nm,

$48 \cdot 10^6$ particles/mL, $\text{NaCl} = 10^{-3}$ M) is exposed to granodiorite surface (surface roughness: $R_q = 1100 \pm 300$ nm) in a circular open-channel fluid cell (velocity = $4.7 \cdot 10^{-7}$ m/s) for 1 h.

The results demonstrate (see Figure 6) an enhancement of colloid deposition in the presence of Eu(III) and a significant influence of roughness. Vertical Scanning Interferometry (VSI) along with Scanning Probe Image Processing (SPIP) is applied to characterize the surface topography and to quantify the colloids. At all Eu(III) concentrations, the heterogeneous high density colloid deposition on granodiorite surface was due to the grain aggregates and grain boundaries. The colloid deposition is affected by pore volume when Eu(III) is below 5×10^{-7} M. At 10^{-6} M the chemical nature controls colloid deposition rather than surface parameters.

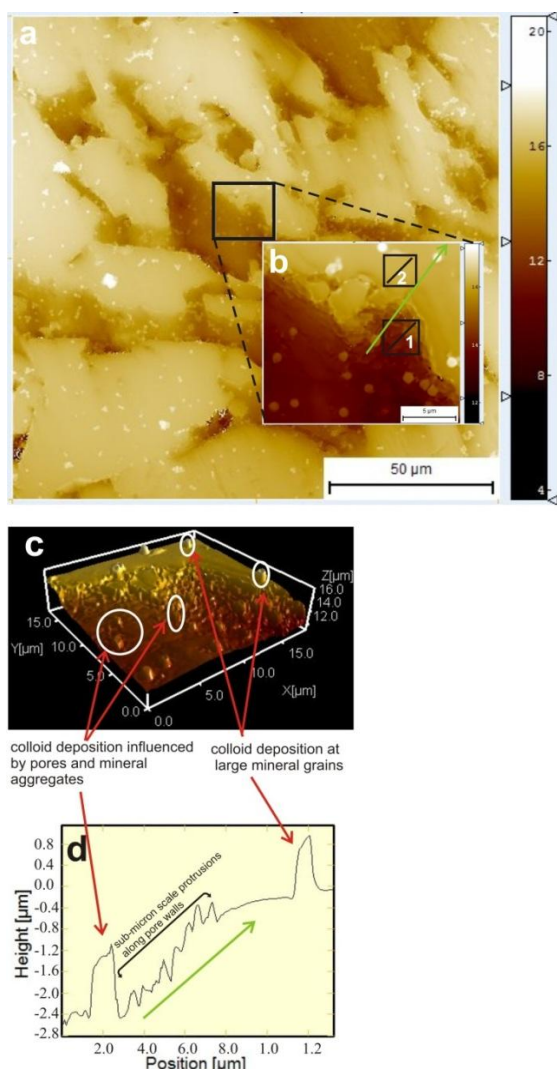


Fig. 7: (a) Topographic map of rough granodiorite surface with sorbed colloids; (b) close-up section (highlighted in (a)) showing preferred particle deposition at the walls of half-pores; (c) three-dimensional view of (b) depicting the particle deposition at walls of half-pores, (d) height profile (see location in (b), green line) showing sub-micron scaled protrusions along pore walls .

The collision efficiency of the colloids is proportional to the intergranular porosity (half-pores) of the mineral surface. Moreover, the complete topographical information (inter- and intragranular porosities) can be included at scan lengths $L=300$ μm to a larger extent than at $L=50$ μm. The colloid deposition is more efficient at the pore walls (see Figures 7a, 7b and 7c). These pore spaces/cavities are identified as favorable patches for interaction. A lower colloid deposition is observed at single and large feldspar or quartz grains. The micron-scale surface roughness from surface height deviation in sub-micron range (Figure 7d) plays an important role to reduce the effective contact area of colloids during adhesion. These protrusions (0.16 ± 0.08 μm) which are 4 to 6 times smaller in comparison to the diameter of the colloids diminish the electrostatic repulsion with the surface and thus attractive van der Waals forces become a significant contributor to the interaction when the colloid is approaching the surface.

The influence of surface fluctuations along with locally attractive regions on the surface due to positively charged patches (resulting from the Eu(III) adsorption) have a pronounced effect resulting in frequent surface contacts [10]. The total interaction energy is significantly attenuated with an increase in the ratio of particle size to asperity size [11]. This agrees with our study where the colloid sorption lies in asperities with smaller dimensions (density = 2.6 ± 0.55 μm⁻¹, size = 0.55 ± 0.18 μm, height = 0.41 ± 0.06 μm) rather than asperities with large dimensions (density = 1.2 ± 0.62 μm⁻¹, size = 1.41 ± 0.35 μm, height = 0.63 ± 0.22 μm). The absence of such protrusions on large feldspar and quartz grains leads to an enhanced applied torque (drag force) over adhesion force. This explains less colloidal retention onto their surfaces.

References

- [1] <http://www.grs.de/> Vorläufige – Sicherheitsanalyse – Gorleben – VSG.
- [2] G. Buckau, R. Artinger, P. Fritz, S. Geyer, J.I. Kim, M. Wolf. App. Geochem. 15, 171–179 (2000).
- [3] P.E. Reiller, N.D.M. Evans, G. Szabo. Radiochim. Acta, 96, 345-358 (2008).
- [4] C.M. Marquardt, J.I. Kim, V. Pirlet, V., Book of Abstracts, Actinides-2001 Conference, 140 (2001).
- [5] V. Pirlet, PhD thesis, University of Liege, Liege (2003).
- [6] F. Huber, P. Kunze, H. Geckeis, T. Schäfer. Appl. Geochem., 26, 2226-2237 (2011).

[7] T. Missana, U. Alonso, M. Garcia-Gutierrez, M. Mingarro. *Appl. Geochem.*, 23, 1484-1497 (2008).

[8] A. Möri, W. R. Alexander, H. Geckeis, W. Hauser, T. Schäfer, J. Eikenberg, T. Fierz, C. Degueldre, T. Missana, *Colloids Surf. A*, 217, 33-47 (2003).

[9] M. Reinholdt, J. Miehè-Brendlé, L. Delmotte, M.H. Tuilier, R. Le Dred, R. Cortès, A.M. Flank. *Eur. Journ. Inorg. Chem.*, 2001, 2831-2841 (2001).

[10] J.M. Davis, R.D. Duffadar. *J Coll. Int. Sci*, 326, 18-27 (2008).

[11] X.F. Huang, S. Bhattacharjee, E.M.V. Hoek. *Langmuir*, 26, 2528-2537 (2010).

6.4 Numerical simulation and database

M. Altmaier, C. Bube, X. Gaona, C.M. Marquardt, A. Pudewills

Simulation of the CFM experiment tracer tests 09-01 and 10-01

Introduction

The crystalline rock is nearly impermeable and the groundwater flows predominantly through discrete features as fractures or shear zones filled with porous material. Such features provide the primary pathway for the migration of radionuclides from an underground repository to the biosphere. In order to predict the movement of radionuclides, the processes involved must be understood and quantified. For this purpose, laboratory tests, field experiments and adequate numerical models are needed.

The Colloid Formation and Migration (CFM) project aims to investigate and quantify the impact of colloids on the transport of waste-derived radionuclides in a water-conducting fracture over repository relevant spatial and temporal conditions. The in situ experiment is located in the Grimsel underground laboratory in Switzerland [1].

In the reporting time the focus was to analyze two tracer tests, performed in a dipole at the CFM experimental site. The objectives of these numerical analyses are to calibrate the model and determine its effective parameters. It was assumed that (1) the groundwater flow and the solute transport take place in fractures filled with fault gouges, and (2) the shear zone at the test location is plane which allows a two dimensional approach for the model geometry. The mathematical model is based on the Darcy's law for groundwater flow and the advection-dispersion equations for solute transport with a linear sorption in the fracture material. However, the model represents a planar confined porous media with a constant porosity and an anisotropic permeability. The analyses were performed with the ADINA-F finite element code [2].

Numerical modeling

The layout of the two tests is shown in Fig.1. The distance between injection and extraction borehole is about 6.08 m and both tests were performed in recirculation flow rate of 45-50ml/min to provide a comparison with the transport conditions similar to those when a bentonite source will be emplaced. The tests parameters are listed in the table below. The detailed description is provided in the experimental report [3].

A comparison of the numerical results and test data is presented as breakthrough curves at the extraction hole (see Fig. 2).

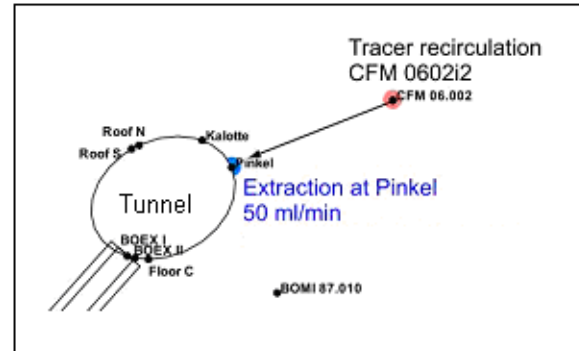


Fig.1: Layout of tracer test 09-01 and 10-01. The figure shows the position of the injection and extraction boreholes in the plane of the shear zone

	Test 09-01 Uranine	Test 10-01 Uranine
Initial concentration [ppm]	50	5
Injected tracer volume [ml]	100	1000
Extraction flow rate [ml/min]	~48	~48

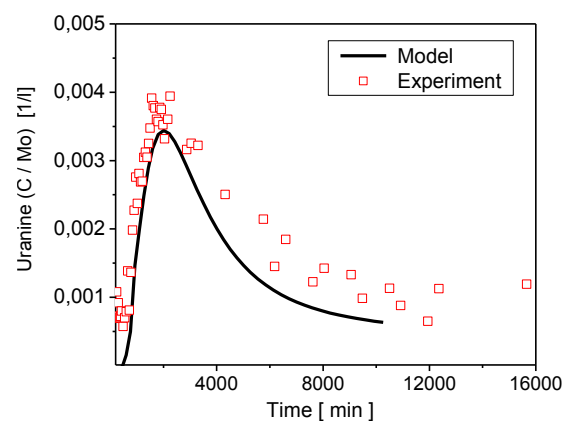


Fig. 2: Comparison of measured and calculated breakthrough curves for uranine tracer test 10-01 (Presentation on linear scale).

The overall agreement of model results and experimental data is reasonable. However, the comparison of calculation results in the tailing part shows some deviations. The long tailing seems to be induced by progressive release of

the tracer late in the injection interval due to the fluid recirculation process.

Fig. 4 shows the migration and dispersion of the uranium tracer between the injection and extraction boreholes in the plane of the shear zone for several time steps (18, 32 and 118 hours).

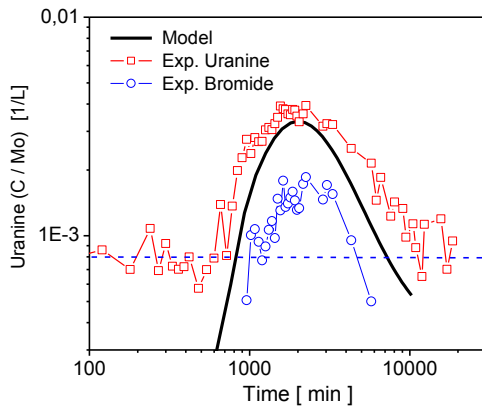


Fig.3: Calculation and experimental breakthrough curves for uranine and bromide.

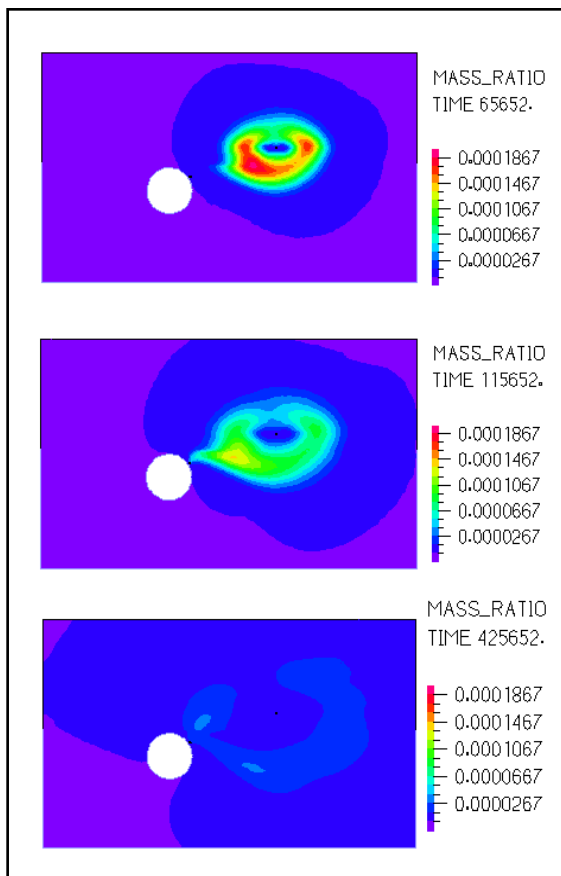


Fig. 4: Distribution of the uranine concentration after different times (The time is given in seconds).

Conclusions

The field data and modelling results provide a fairly consistent picture of the flow and transport characteristics in the shear zone at the location of the CFM experiments.

The 2D model considers uniform but anisotropic permeability and constant porosity in different zones. Therefore, the estimated flow and transport parameters must be considered as an approximation of the real structure which indicates heterogeneities in the distribution of hydraulic conductivity.

The hydraulic and transport properties obtained from this calibration work on the new tracer tests show a preferential pathway for fluid migration.

The application of relatively low velocity at the injection/extraction boreholes seems to induce a long residence time in the shear zone; the dispersive/diffusive processes become dominant.

In the next project step, further work is required to explore how the uncertainties on parameter estimation and the subsequent predictions at lower hydraulic gradients are affected by the choice of the present conceptual model. However, the tests with homologue radionuclides will be simulated using the transport parameters obtained by fitting the uranine tests.

THEREDA project

In order to establish a thermodynamic reference database, the THEREDA project was initiated with the goal of providing consistent and reliable thermodynamic data for all repository host rock formations (salt, clay, granite) under discussion in Germany. Presently, 5 institutions participate in the project.*

Web Interface for data input

One of the main tasks was testing of the user interface for data input into the THEREDA database. The interface developed by LINEAS, Braunschweig consists of different modules, such as main page, input for phases, phase constituents, thermodynamic data and interaction parameters. The interface is also designed for processing queries on the data in the database (see Fig. 5). Several control functions are implemented in the web interface to ensure data consistency, identify gaps in the data and to produce error messages for the editor, e.g. missing entry in a mandatory field, entry incompatible with previous entries.

Benchmark calculations

To guaranty correctness and consistency of the data in THEREDA and the generated output files, several benchmark calculations have been done for the first two data releases, which are available on the THEREDA homepage. An intercomparison has been performed between the results of several codes in order to demonstrate the successful operation of the specific parameter files for each geochemical code and illustrate the results produced with the THEREDA thermodynamic data selections.

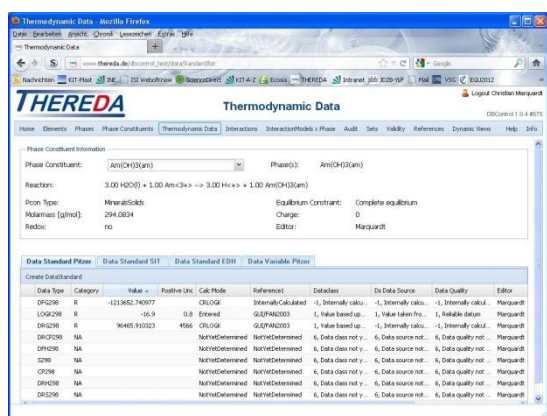


Fig. 5: Screenshot of the THEREDA input interface for Thermodynamic Data.

The first release comprises the carbonate-free oceanic salt system (Na, K, Mg, Ca, Cl, SO₄, H and H₂O(l)). The second release includes the trivalent actinides Am and Cm (+ Nd) in NaCl, MgCl₂ and CaCl₂ solutions (Na, Mg, Ca, Cl - Am(III), Nd(III), Cm(III) - H₂O). Parameter files can be generated directly from the database via export programs for ChemApp, Geochemist's Workbench (GWB), Phreeqc and EQ3/6. The benchmark calculations with Phreeqc and EQ3/6 as well as the main editorial work for the second release have been done at INE. The selected test systems were Am (III), Cm (III), Nd (III) in NaCl solutions and Am (III), Cm (III), Nd (III) in MgCl₂ and CaCl₂ solutions, both at 298.15 K.

The results generated by different geochemical codes were compared and validated against experimental data [4]. The calculated values were identical within numerical inaccuracies and the code specific parameter files proved to work correctly (cf. Fig. 6). The experimental data could be described well within the experimental error. The Benchmark documents can be found on the THEREDA homepage after registration (www.thereda.de).

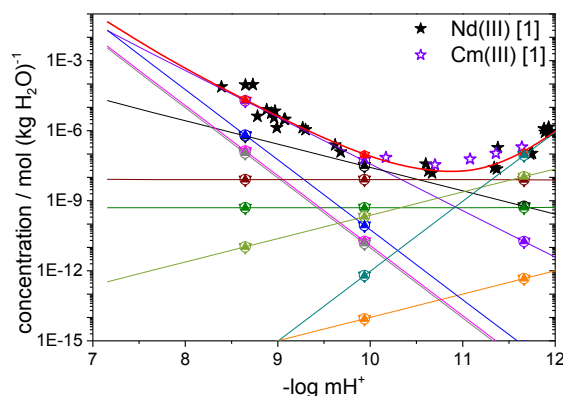


Fig. 6: Typical THEREDA benchmark case: Solubility and speciation of Am(OH)₃(am) in 3.86m CaCl₂ solution compared to experimental data [1].

*The four institutions beside KIT-INE within the THEREDA project and the institutional representatives are:

- IRE-HZDR, Dresden (D): F. Bok, V. Brendler, A. Richter
- GRS, Braunschweig (D): H. Moog, A. Muñoz, T. Schrage
- TU-BAF, Freiberg (D): D. Sukhanov, W. Voigt
- AFC, Baden (CH): S. Wilhelm

References

- [1] I. Blechschmidt et al., Arbeitsbericht NAB 06-361, Nagra, Wettingen, Switzerland (2006).
- [2] R Adina & D Inc., Report ARD 01-9, Watertown, MA, USA (2010).
- [3] NAGRA, Aktennotiz AN/07-XXX, Tracer Tests 09-01 and 10-01 Draft 16-03-10.doc.
- [4] V. Neck, M. Altmaier, T. Rabung, J. Lützenkirchen, T. Fanghänel, Pure Appl. Chem. 81:1555 (2009).

7 Separation of long-lived minor actinides

B. Beele, A. Bremer, C. Carpentier*, A. Geist, U. Müllich, D. Magnusson, P.J. Panak, C. Ruff

*Chimie Paristech

Background

Separation of transuranium elements from irradiated nuclear fuel may provide potential advantages over long term storage of once through spent fuel [1]. Several separation processes are being considered in Europe which involve the PUREX process to remove uranium and plutonium, then routing the raffinate through a minor actinide and lanthanide co-extraction process (DIAMEX) followed by An(III)/Ln(III) separation (SANEX).

Work at INE regards hydrometallurgical (i.e., based on chemical liquid-liquid extraction) actinide separation, with a focus on the separation of trivalent americium and curium from the chemically similar lanthanides.

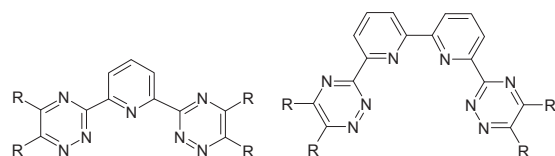


Fig. 1: BTP and BTBP.

This separation is possible using *N*-donor extracting agents such as alkylated bis-triazinylpyridines (BTP, Fig. 1 left) [2, 3] and alkylated bis-triazinylbipyridines (BTBP, Fig. 1 right) [4, 5]. These extract trivalent actinides with excellent selectivity over lanthanides (usually expressed as the separation factor for Am(III) over Eu(III), $SF_{Am(III)/Eu(III)}$, which is in the range of 100–300 for BTP and BTBP).

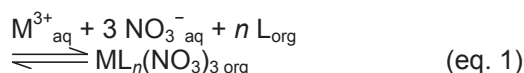
Nevertheless, these extracting agents require further optimisation towards a possible industrial application. To support this development, we continuously perform fundamental studies aimed at understanding selectivity and performance of such compounds.

As an alternative to the PUREX-DIAMEX-SANEX concept, so-called GANEX processes are under development in the European Collaborative Project ACSEPT [6]: after bulk uranium separation, all transuranium elements (TRU = Np, Pu, Am, Cm) are co-separated into one product solution. In collaboration with several laboratories involved in ACSEPT, we are working on the development of chemical separation systems useful for a GANEX process.

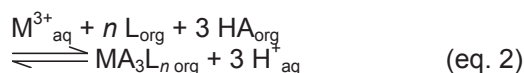
N-Donor Ligand Comparative Study

Introduction

Over the recent two decades a vast number of (mostly tridentate) *N*-donor ligands have been synthesized and tested for selective extraction or complexation of trivalent actinides [7]. Only few of them exhibit sufficient selectivity for trivalent actinides over lanthanides. And even less are able to extract trivalent actinides from nitric acid solutions of relevant concentrations (≥ 0.5 mol/L HNO_3). And finally, only two classes of ligands — BTP and BTBP — directly extract trivalent actinide nitrates from nitric acid according to equation 1 (*L* = *N*-donor ligand):



Other *N*-donor ligands require a lipophilic anion such as carboxylates; equation 2 (*A* = carboxylate anion):



To further complicate the matter, the reasons for insufficient performance is not always understood; in some cases it was reasoned that the compound tested simply was not lipophilic enough to work as an extracting agent. But would it be worth synthesizing a more lipophilic version?

To shed light on these issues we determined stability constants for the complexation of Cm(III) with several tridentate *N*-donor ligands having similar structures, using TRLFS. These were compared to distribution data from liquid-liquid extraction experiments.

Ligands studied

The ligands studied were: a BTP (2,6-di(5,6-dipropyl-1,2,4-triazin-3-yl)pyridine, Fig. 1 left, $R = n-C_3H_7$), a *hemi*-BTP (6-(5,6-dipentyl-1,2,4-triazin-3-yl)-2,2'-bipyridine, Fig. 2 left, $R = n-C_5H_{11}$), a BPP (2,6-bis-(5-(2,2-dimethylpropyl)-1*H*-pyrazol-3-yl)pyridine, Fig. 2 right, $R = 2,2$ -dimethylpropyl), a BDP (2,6-di(6-ethylpyridazin-3-yl)pyridine, Fig. 3 left) and a BTtP (2,6-di(6-propyl-1,2,4,5-tetrazin-3-yl)pyridine, Fig. 3 right, $R = n-C_3H_7$).

With these ligands, liquid-liquid distribution data for Am(III) and Eu(III) were determined by extraction experiments (or taken from the literature). The complexation of Cm(III) (which behaves similar to Am(III)) was studied by TRLFS, titrating solutions of Cm(III) in wa-

ter/alcohol with solutions of the ligands and recording the laser-induced fluorescence emission spectra at varied ligand concentrations.

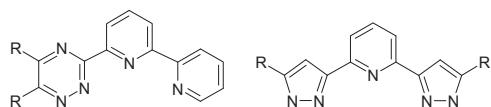


Fig. 2: *hemi-BTP* (left) and *BPP* (right).

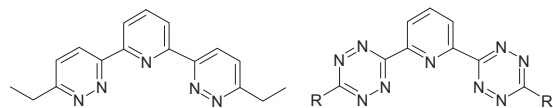


Fig. 3: *BDP* (left) and *BTtP* (right).

Results

BTP

BTP is known to extract both Am(III) and Cm(III) nitrates with high selectivity over Ln(III) ($SF_{Am(III)/Eu(III)} \approx 150$) from nitric acid (0.5–2 mol/L) by solvation of metal nitrates according to equation 1 [2, 8]:

Also, Cm(III) is strongly complexed by BTP, forming a 1:3 complex, $[Cm(BTP)_3]^{3+}$ in solution. The respective stability constant in H₂O/methanol (1:1) determined by TRLFS is $\log \beta = 14.4$ [9]. The 1:3 complex identified by TRLFS is identical to the one formed in extraction experiments [10]; the metal ion is exclusively coordinated by three BTP ligands; the nitrate anions required for charge compensation do not coordinate to the metal ion.

BPP

Similar to BTP, BPP extracts Am(III) with high selectivity over Ln(III) ($SF_{Am(III)/Eu(III)} \approx 100$) from nitric acid (≤ 1 mol/L). In contrast to BTP, it does not extract metal nitrates but only the more lipophilic carboxylates according to equation 2 [11].

TRLFS investigations revealed that BPP forms strong complexes with Cm(III); the stability constant of the 1:3 complex, $[Cm(BPP)_3]^{3+}$ in methanol is $\log \beta = 14.8$ [12].

Furthermore, the complex relevant to extraction conditions (i.e. in the presence of a carboxylic acid) was identified by TRLFS to be the 1:3 complex, $[Cm(BPP)_3]^{3+}$, too. The carboxylate anions required for charge compensation are not present in the first coordination sphere.

hemi-BTP

hemi-BTP was developed as an intermediate between BTP and BTBP, removing one triazinyl ring from BTBP (or substituting one of BTP's triazinyl with pyridyl) [13]. This modification severely impacted the extraction properties; *hemi-BTP* extracts Am(III) (as carboxy-

late; eq. 2) only from weakly acidic solutions (pH > 1.5) [13, 14]. Also, the selectivity for trivalent actinides vs. lanthanides ($SF_{Am(III)/Eu(III)} \approx 30$) is lower than with BTP or BPP.

The complexation of Cm(III) by *hemi-BTP* in H₂O/2-propanol (1:1) has extremely slow kinetics. E.g., with 0.16 mmol/L *hemi-BTP*, equilibrium is attained only after > 300 h.

Nevertheless, the stability constant of the 1:3 complex, $[Cm(hemi-BTP)_3]^{3+}$ in H₂O/2-propanol (1:1) was determined to $\log \beta = 12.1$ [14].

As had been done with BDP, the *hemi-BTP* complex relevant to extraction was identified by TRLFS. In contrast to BPP, a 1:2 complex $[Cm(hemi-BTP)_2A]^{2+}$ forms with *hemi-BTP*, with one carboxylate coordinated to the metal ion.

BDP

BDP was initially tested as a selective extracting agent for trivalent actinides in the framework of the European EUROPART project in 2005. It did not show useable extraction properties. Nevertheless, we resumed studying it from a more fundamental point of view: In what way does removing the *N* atom in 4-position affect the extraction and complexing properties?

After synthesis, BDP was tested for extraction of Am(III) and Eu(III) from HNO₃. BDP does not extract metal nitrates (eq. 1). Carboxylates (eq. 2) are slightly extracted; however, extraction of Am(III) (i.e., Am(III) distribution ratios $D_{Am(III)} > 1$) would occur only at pH > 2 (see Fig. 4) and with moderate selectivity ($SF_{Am(III)/Eu(III)} < 10$).

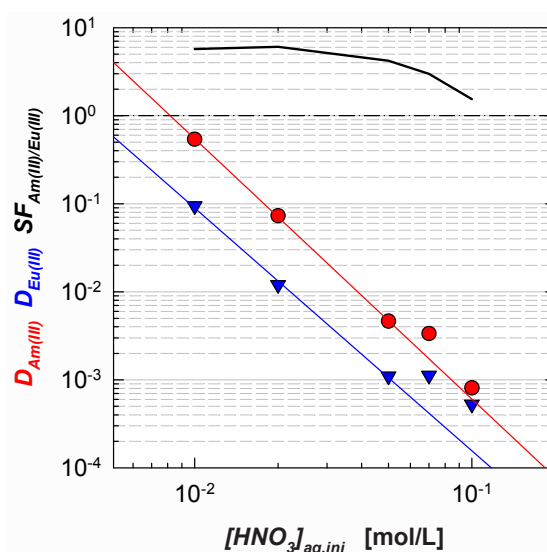


Fig. 4: Extraction of Am(III) and Eu(III) by BDP. Organic phase, 3.2 mmol/L BDP + 0.5 mol/L 2-bromodecanoic acid in kerosene. Aqueous phase, ²⁴¹Am(III) + ¹⁵²Eu(III) (1 kBq/mL each) in HNO₃.

Results from the TRLFS titration of Cm(III) with BDP in H₂O/2-propanol (1:1) are shown in Fig. 5. Successive formation of the 1:1, 1:2 and 1:3 complexes with emission maxima at 599.8 nm, 608.5 nm and 614.2 nm is observed upon addition of BDP. The 1:3 complex, [Cm(BDP)₃]³⁺ becomes dominant only with > 10 mmol/L BDP. This reflects in its rather low complex stability constant of log β = 7.6.

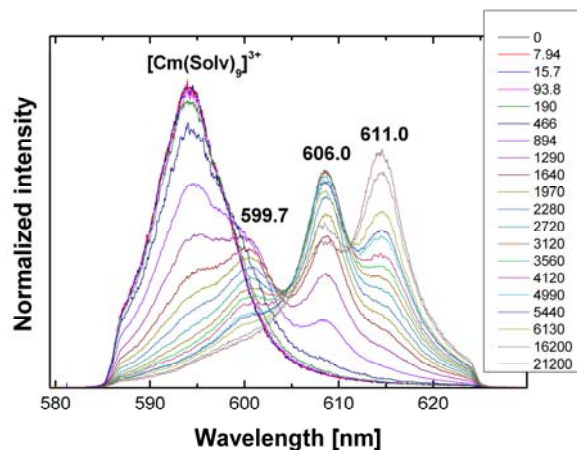


Fig. 5: Fluorescence emission spectra of the titration of Cm(III) with BDP in H₂O/2-propanol (1:1). [Cm(III)]_{ini} = 2 · 10⁻⁷ mol/L.

BTtP

This molecule is another variation to the BTP scheme: Going from three to two *N* atoms in the lateral rings had a negative impact. Would increasing the number of *N* atoms to four help?

A batch was synthesized and tested for Am(III) and Eu(III) extraction. Results are similar to those for BDP: no extraction of metal nitrates, slightly better extraction of Am(III) carboxylate at low acidity (pH ≥ 2), see Fig. 6. The selectivity is $SF_{Am(III)/Eu(III)} \approx 10$.

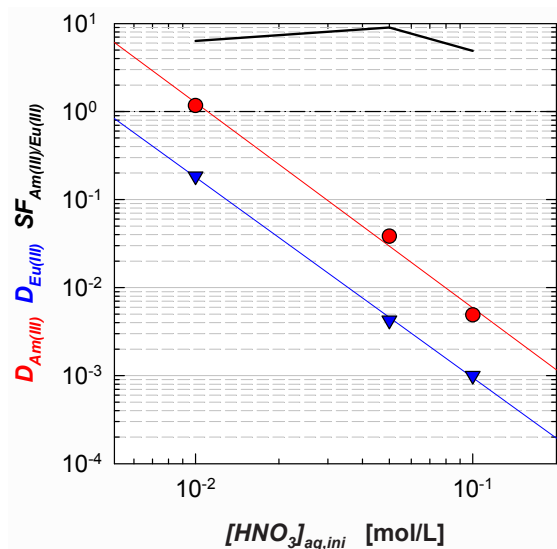


Fig. 6: Extraction of Am(III) and Eu(III) by BTtP. Organic phase, 6.5 mmol/L BTtP + 0.5 mol/L 2-bromodecanoic acid in kerosene. Aqueous phase, ²⁴¹Am(III) + ¹⁵²Eu(III) (1 kBq/mL each) in HNO₃.

The complexation of Cm(III) by BTtP was studied by TRLFS titration, see Fig. 7. Successive formation of the 1:1, 1:2 and 1:3 complexes with emission maxima at 599.7 nm, 606.0 nm and 611.0 nm is observed upon addition of BTtP. The 1:3 complex, [Cm(BTtP)₃]³⁺ becomes dominant at > 1 mmol/L BTtP. The stability constant of the 1:3 complex has a value of log β = 9.9.

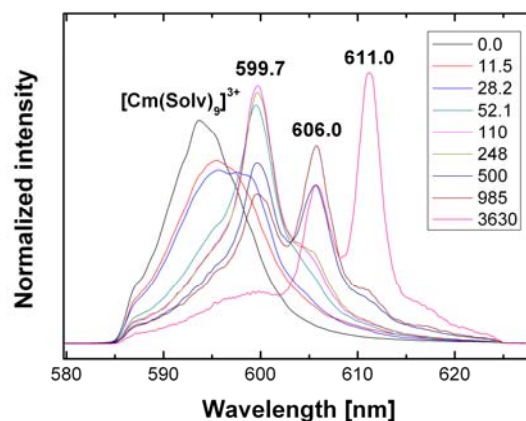


Fig. 7: Fluorescence emission spectra of the titration of Cm(III) with BTtP in H₂O/2-propanol (1:1). [Cm(III)]_{ini} = 2 · 10⁻⁷ mol/L.

Discussion

Despite the structural similarity of the ligands studied, they show vastly different extraction behaviour. Only BTP and BPP are capable of extracting Am(III) from nitric acid. They also exhibit rather high Cm(III) complex stability. *hemi*-BTP, BDP and BTtP have lower complex stabilities; they extract Am(III) only from slightly acidic solutions. The data in Table 1 show a qualitative link between extraction performance and complex stability: ligands having rather low complex stabilities are weak extracting agents. This implies that these ligands' weak extracting performance is not (exclusively) a consequence of too low hydrophobicity; more lipophilic derivatives are not expected to show better properties.

	BTP	BPP	<i>h</i> BTP	BDP	BTtP
[HNO ₃]	≈ 1	≤ 1	pH > 1.5	pH > 2	pH ≥ 2
SF	≈ 150	100	≈ 30	< 10	≈ 10
log β	14.4	14.8	12.1	7.6	9.9

Table 1. Comparison of extraction and complexation data for the *N*-donor ligands studied. "[HNO₃]" represents the nitric acid concentration (or pH) from which extraction of Am(III) is possible. SF is the Am(III)/Eu(III) selectivity. log β are the stability constants for the Cm(III) 1:3 complexes.

The ligands also have quite different selectivity in extraction experiments: separation factors are $SF_{Am(III)/Eu(III)} \geq 100$ for BTP and BPP; ≈ 30 for *hemi*-BTP and ≤ 10 for BDP and BTtP.

These differences may originate from differences in the extracted complexes' first coordination sphere: In the case of BTP and BPP, the metal ion is coordinated by three *N*-donor ligands; high selectivity is achieved. With *hemi*-BTP, the metal ion is coordinated by two *N*-donor ligands and one (unselective) carboxylate; selectivity is intermediate. The present data do not allow an identification of the complexes formed with BDP or BTtP under conditions relevant to extraction. Nevertheless, more than one *N*-donor ligand may be displaced by carboxylate due to the even weaker complexation. This could be an explanation for the low selectivity.

Conclusions

Varying *N*-donor ligands' lateral heterocycles has a tremendous effect on complexation and extraction properties. Obviously the extraction performance of *N*-donor extracting agents is governed by their complexation strength for trivalent actinides. The lipophilicity of the ligands may be of lesser importance.

Also, there is an indication that the *composition* of the extracted complexes' first coordination sphere (and not so much the *N*-donor ligand *itself*) is driving selectivity: the more completely the central metal ion is coordinated by *N*-donor ligands, the higher the selectivity.

Further investigations are required to support these statements.

GANEX process

Introduction

To avoid pure Pu product streams (as is the case with the PUREX process), alternative processes are being developed that are capable of handling all the transuranium elements (TRU = Np, Pu, Am, Cm) in one stream throughout the process. This requires a solvent capable of extracting all TRU and being able to cope with high Pu loading (up to 50 g/L). Furthermore, all TRU must be selectively back-extracted from the loaded solvent in one section.

The GANEX process (Group ActiNide EXtraction) was developed by the French CEA for the homogenous recycling of actinides. After the selective extraction of uranium(VI) from the fuel dissolution solution in the 1st cycle, TRU are co-separated in the 2nd cycle [15]. The 2nd cycle solvent is composed of a neutral extracting agent (DMDOHEMA) and an acidic one (HDEHP, di(2-ethylhexyl)phosphoric acid), which may complicate the solvent regeneration. Additionally, HEDTA is used for stripping

TRU, which works only in a narrow pH region, requiring a buffer.

In the framework of the European ACSEPT project an alternative GANEX 2nd cycle has been developed in collaboration with NNL-UK, FZJ, JRC-ITU and CEA. The first step involved developing a solvent capable of co-extracting TRU at relevant concentrations. The next step was to develop a system for co-stripping the TRU into one product solution. This could be achieved by combining SO₃-Ph-BTP (2,6-bis(5,6-di(sulphophenyl)-1,2,4-triazin-3-yl)pyridine, Fig. 8 top) and AHA (acetohydroxamic acid, Fig. 8 bottom).

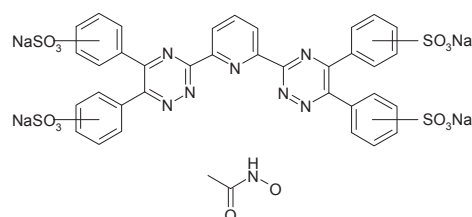


Fig. 8: SO₃-Ph-BTP (top) and AHA (bottom).

Solvent formulation

Initially developed in Japan [16], the tridentate ligand TODGA (*N,N,N',N'*-tetraoctyl diglycolamide, Fig. 9 left) efficiently extracts actinides(III, IV, VI). In kerosene diluents, TODGA is prone to 3rd phase formation. Additives such as TBP [17], 1-octanol [18] and amines [19] can serve to suppress 3rd phase formation but none of these allows for sufficiently high Pu(IV) loading.

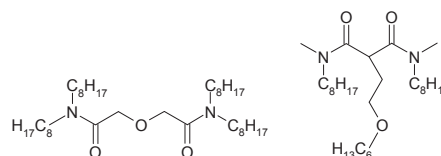


Fig. 9: TODGA (left) and DMDOHEMA (right).

Following extensive testing at the National Nuclear Laboratory (NNL) in the UK, a solvent composed of 0.2 mol/L TODGA + 0.5 mol/L DMDOHEMA (Fig. 9 right) in Exxsol D80 (a kerosene) was selected; it can handle initial aqueous Pu(IV) concentrations of up to 40 g/L in 3 mol/L HNO₃ [20].

TRU + Ln(III) co-extraction

Data for the extraction of Pu(IV), Am(III) and Ln(III) from HNO₃ are shown in Fig. 10 as a function of [HNO₃]. Similar to TODGA alone, the TODGA + DMDOHEMA solvent co-extracts An(III) and Ln(III) with high distribution ratios. Lighter Ln(III) are less extracted than heavier ones. Pu(IV) and Am(III) are extracted with distribution ratios similar to Nd(III), Sm(III).

In summary, all TRU are well extracted into the TODGA + DMDOHEMA solvent at acidities

relevant to a GANEX 2nd cycle process, i.e., 3–4 mol/L HNO₃ [20].

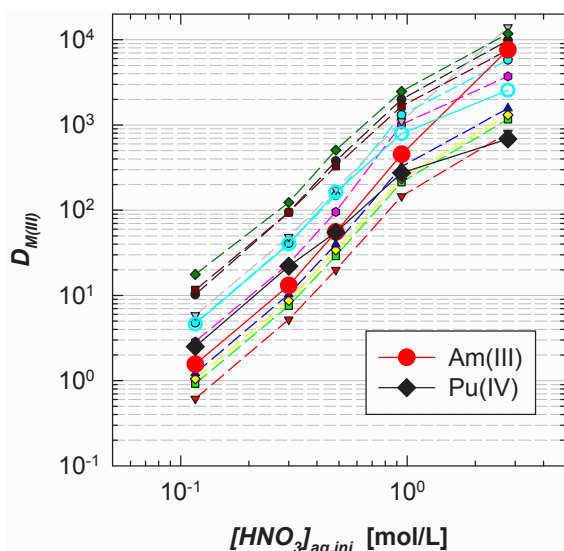


Fig. 10: Pu(IV) + Am(III) + Ln(III) extraction, distribution ratios as a function of [HNO₃]. Organic phase, 0.2 mol/L TODGA + 0.5 mol/L DMDOHEMA in Exxsol D80. Aqueous phase, ²⁴²Pu(IV) + ²⁴¹Am(III) + ¹⁵²Eu(III) + Ln(III) in HNO₃.

TRU stripping

The initially adopted strategy for the selective TRU back-extraction involves using a solution containing a hydrophilic 2,6-bis(1,2,4-triazin-3-yl)pyridine (BTP) [21] and acetohydroxamic acid (AHA) [22] in nitric acid. The former strips Am(III) and Cm(III), while the latter strips Pu(IV) and Np. Lanthanides are kept in the organic phase by a sufficiently high nitric acid concentration; no salting out or buffering agents are required.

TRU stripping with SO₃-Ph-BTP

Tests analogous to those reported in [21] show that SO₃-Ph-BTP can be used for stripping Am(III) + Cm(III) from the TODGA + DMDOHEMA solvent, while Ln(III) are kept in the aqueous phase by a sufficiently high HNO₃ concentration of approx. 0.5 mol/L. Am(III) and Cm(III) have distribution ratios which are almost identical. Am(III) and Ln(III) distribution ratios for similar experimental conditions are presented below in Fig. 11.

Fig. 11 shows data for the separation of TRU from Ln(III) at varied HNO₃ concentration. SO₃-Ph-BTP suppresses the extraction of Pu(IV), Am(III) and Cm(III) (Cm(III) data not shown as the distribution ratios are identical to those of Am(III)). The results indicate that an efficient separation of TRU from Ln(III) is viable for the range of [HNO₃] 0.3–0.7 mol/L.

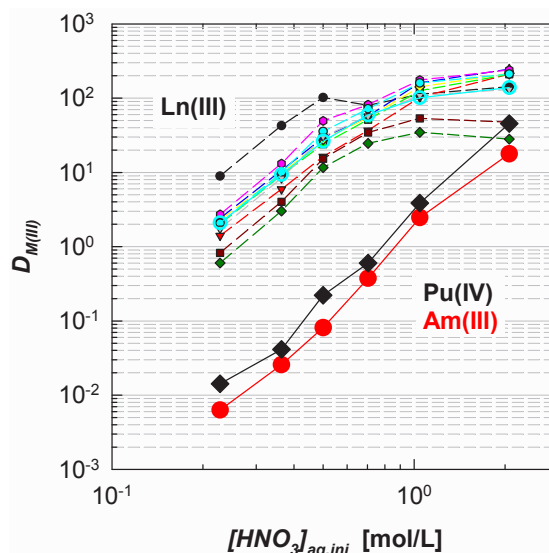


Fig. 11: TRU stripping by SO₃-Ph-BTP, distribution ratios as a function of [HNO₃]. Organic, 0.2 mol/L TODGA + 0.5 mol/L DMDOHEMA in Exxsol D80. Aqueous, ²⁴²Pu(IV) + ²⁴¹Am(III) + ¹⁵²Eu(III) + Ln(III) + 20 mmol/L SO₃-Ph-BTP in HNO₃.

TRU stripping with SO₃-Ph-BTP + AHA

Tests performed at NNL-UK showed that AHA efficiently strips Np + Pu from a loaded GANEX solvent. Using a mixture of 20 mmol/L SO₃-Ph-BTP + AHA (0–3 mol/L) for suppressing TRU extraction is shown in Fig. 12. Adding AHA has only a slight effect on Pu(IV) distribution ratios; obviously SO₃-Ph-BTP is a stronger complexing agent for Pu(IV) than is AHA.

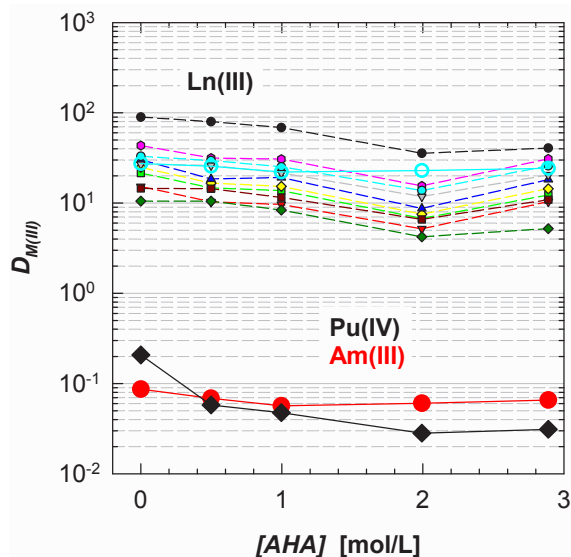


Fig. 12: TRU stripping by SO₃-Ph-BTP + AHA, distribution ratios as a function of [AHA]. Organic, 0.2 mol/L TODGA + 0.5 mol/L DMDOHEMA in Exxsol D80. Aqueous, ²⁴²Pu(IV) + ²⁴¹Am(III) + ¹⁵²Eu(III) + Ln(III) + 20 mmol/L SO₃-Ph-BTP + AHA in 0.5 mol/L HNO₃.

Conclusions

A promising GANEX 2nd cycle solvent system consisting of 0.2 mol/L TODGA + 0.5 mol/L DMDOHEMA in Exxsol D80 was developed at NNL-UK, extracting up to 40 g/L Pu(IV) without precipitation or 3rd phase formation.

Since lanthanides(III) are co-extracted by this solvent system, a selective TRU stripping system had to be developed. Initially it was planned to use a solution containing AHA (to strip Pu(IV) + Np) and SO₃-Ph-BTP (to strip Am(III) and Cm(III)) in HNO₃ (to keep lanthanides(III) in the organic phase). Since AHA does not efficiently strip Pu(IV) + Np at HNO₃ concentrations sufficient to keep lanthanides(III) from also being stripped by SO₃-Ph-BTP, a different TRU stripping strategy is currently being developed:

A surplus of SO₃-Ph-BTP could be used to strip Pu(IV), Am(III) and Cm(III). Np stripping will be achieved by reduction to Np(IV) using AHA. Np(IV) is expected to be stripped by SO₃-Ph-BTP similarly to Pu(IV).

These tests will lead to the development of a GANEX 2nd cycle flow-sheet to be tested on a surrogate feed solution containing approx. 10 g/L Pu(IV). The ultimate goal is a hot counter-current test to be performed at JRC-ITU with a genuine spent fuel feed solution.

Acknowledgement

Financial support for this research was provided by the European Commission (project ACSEPT, Contract № FP7-CP-2007-211 267), by the German Federal Ministry of Education and Research (BMBF; contract numbers 02NUK012A and 02NUK012D) and the Baden-Württemberg Stiftung gGmbH, Energie Baden-Württemberg (EnBW-Stiftung).

References

- [1] M. Salvatores, G. Palmiotti, Prog. Part. Nucl. Phys., 66, 144–166 (2011).
- [2] Z. Kolarik, U. Müllich, F. Gassner, Solvent Extr. Ion Exch., 17, 1155–1170 (1999).
- [3] S. Trumm, A. Geist, P.J. Panak, T. Fanghänel, Solvent Extr. Ion Exch., 29, 213–229 (2011).
- [4] M.J. Hudson, M.G.B. Drew, M.R.S. Foreman, C. Hill, N. Huet, C. Madic, T.G.A. Youngs, J. Chem. Soc. Dalton Trans., 1675–1685 (2003).
- [5] A. Geist, C. Hill, G. Modolo, M.R.S. Foreman, M. Weigl, K. Gompper, M.J. Hudson, C. Madic, Solvent Extr. Ion Exch., 24, 463–483 (2006).

[6] ACSEPT, www.acsept.org

[7] Z. Kolarik, Chem. Rev., 108, 4208–4252 (2008).

[8] M. Steppert, C. Walther, A. Geist, Th. Fanghänel, New J. Chem., 33, 2437–2442 (2009).

[9] S. Trumm, P.J. Panak, A. Geist, Th. Fanghänel, Eur. J. Inorg. Chem., 3022–3028 (2010).

[10] M.A. Denecke, A. Rossberg, P.J. Panak, M. Weigl, B. Schimmelpfennig, A. Geist, Inorg. Chem., 44, 8418–8425 (2005).

[11] A. Geist, U. Müllich, A. Wilden, S. Gülland, G. Modolo, Proc. 19th Internat. Solvent Extraction Conf. (ISEC 2011), Santiago, Chile, 3.–7.10.2011.

[12] A. Bremer, C.M. Ruff, D. Girnt, U. Müllich, J. Rothe, P.W. Roesky, P.J. Panak, A. Karpov, T.J.J. Müller, M.A. Denecke, A. Geist, submitted.

[13] M.G.B. Drew, M.R.S. Foreman, A. Geist, M.J. Hudson, F. Marken, V. Norman, M. Weigl, Polyhedron, 25, 888–900 (2006).

[14] A. Bremer, A. Geist, P.J. Panak, submitted.

[15] M. Miguiditchian, H. Roussel, L. Chareyre, P. Baron, D. Espinoux, J-N. Calor, C. Viallesoubranne, B. Lorrain, M. Masson, Proc. GLOBAL 2009, Paris, France, 6–11 September 2009.

[16] Y. Sasaki, S. Tachimori, Solvent Extr. Ion Exch., 20, 21–34 (2002).

[17] G. Modolo, H. Asp, C. Schreinemachers, H. Vijgen, Solvent Extr. Ion Exch., 25, 703–721 (2007).

[18] A. Geist, G. Modolo, Proc. Internat. Conf. GLOBAL 2009, Paris, France, 6–11 September 2009.

[19] S. Tachimori, Y. Sasaki, S. Suzuki, Solvent Extr. Ion Exch., 20, 687–699 (2002).

[20] K. Bell, C. Carpentier, M. Carrott, A. Geist, C. Gregson, X. Hérès, D. Magnusson, R. Malmbeck, G. Modolo, U. Müllich, M. Sypula, R. Taylor, A. Wilden, To be presented at the Nuclear Fuel Cycle Conference, Manchester, UK, 23–25 April 2012.

[21] A. Geist, U. Müllich, D. Magnusson, P. Kaden, G. Modolo, A. Wilden, T. Zevaco, Solvent Extr. Ion Exch. 2012, 30 (accepted).

[22] M.J. Carrott, O.D. Fox, C.J. Maher, C. Mason, R.J. Taylor, S.I. Sinkov, G.R. Choppin, Solvent Extr. Ion Exch., 25, 723–745 (2007).

8. Vitrification of high-level radioactive liquid waste

The world-wide favored way of conditioning of highly radioactive waste solutions of final disposal is their immobilization in borosilicate glass by a melting process. Those processes have been under industrial application since the late seventies of the last century. The process of a liquid-fed ceramic-lined waste glass melter has been developed at KIT in the scope of several national and international projects. Among these also two plants (PAMELA plant at Mol/Belgium, VEK plant at Karlsruhe/Germany) equipped with KIT technology were operated under radioactive routine conditions. A third radioactive application of the technology will take place in China within the next years.

8.1 VEK Project

H. Braun, W. Grünwald, K. Hardock, J. Knobloch, K. Meyer, G. Roth, A. Salimi, W. Tobie, S. Weisenburger, U. Weiler, K.-H. Weiß

Fourteen years after its establishment the mission of the VEK project has been fulfilled by end of 2010. The VEK project has been founded to immobilize approx. 60 m³ of high-level liquid waste (HLLW) with a total radioactive inventory of 7.7E+17 Bq in the VEK vitrification plant. This task had been fulfilled by hot operation from September 2009 until October 2010 [1,2]. As a very last step of this project, the produced 140 glass canisters contained in five Castor casks had been shipped by train to the Zwischenlager Nord (ZLN) near Lubmin for interim storage. Start of decommissioning/dismantling of VEK is planned from 2013 on.

8.2 VPC Project

The VPC project has been founded to construct an HLLW vitrification plant in the Sichuan province of China on the basis of the technology developed by KIT-INE. Official start of the project had been December 1st, 2009. In 2010 the main part of the project was dedicated to elaboration of the basic design of the vitrification plant and the intermediate storage building to be used for waste glass canisters. The first edition of basic design documentation (BDD) had been delivered in September 2010. A second revised BDD edition was delivered in December 2010.

Detailed Design (DD)

As the second phase after the Basic Design, the Detailed Design Documentation has to be created. The DD includes the elaboration of drawings, data sheets and diverse lists for each part of a component as well as its 3D arrangement. The purpose of the DD is to deliver a set of detailed information to a potential manufacturer as basis for calculation of an offer price as well as a basis for the subsequent manufacturing procedure. All DD documents have to be checked by an

independent quality assurance step before release to the manufacturer. The QA procedure follows a well-defined control sequence. KIT-INE's responsibility for the detail design comprehends the following core process components:

Glass melter

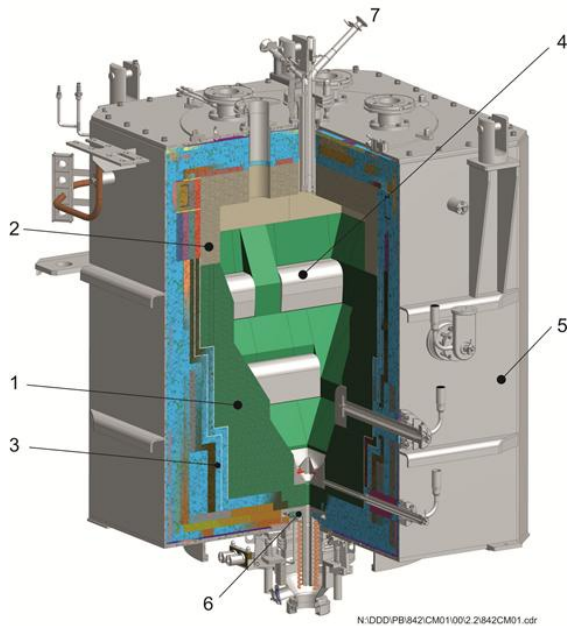
The glass melter (Fig. 1) is the key component of the vitrification process. The VPC melter is designed as a noble metals-compatible melting system [3] with the following main features:

Table 1: Main features of the VPC melter

Parameter	Data
HLLW throughput	65 l/h
Glass production rate	41 kg/h
Glass pool surface	1.52 m ²
Glass melt inventory	2000 kg
Pouring batch	400 kg
Power electrodes	6
Weight (empty)	27 metric tons
Dimensions (LxWxH)	2.1x2.1x2.7 m

The glass melter is composed of 19 subcomponent groups. As the most important parts they include the melt tank refractory, the plenum ceramics, the power electrodes, the bottom electrode, the stainless steel containment, the bottom drain housing, the HLLW and glass frit feeding pipe, the off-gas pipe, a thermowell for monitoring process temperatures and the glass level detection system as well as two air bubblers.

The DD of the refractories, of the power electrodes, of the bottom electrode and of the stainless steel box are completed, those of others are still in progress. Partly, major subcomponents like the power electrodes made of INCONEL 690, are already in the manufacturing step. Still in 2012 brickwork of the melter will be completed.



- | | |
|----------------------------------|------------------------|
| 1. Ceramic refractory glass tank | 5. Stainless steel box |
| 2. Ceramic refractory plenum | 6. Bottom drain |
| 3. Thermal insulation | 7. Melter feeding tube |
| 4. Power electrodes | |

Fig. 1: Simplified scheme of the VPC waste glass melter

Other process components

Besides the melter as the main component there are other components contained inside the V2 melter cell which are subject to detail design of KIT-INE. These are the HLLW feeding vessel including the feeding airlift, the dust scrubber and the condenser as the first two components of the off-gas line. Also belonging to the V2 cell equipment are the remote connectors of the HLLW feeding line and of the glass frit line. From these components the feeding vessel and the condenser have reached a final stage of detail design. The design of the dust scrubber has to undergo a new design procedure as the arrangement and number of the valve plates inside the column have changed compared to those used by VEK. Moreover, the operating conditions are quite different from that of VEK. As described below the off-gas volume flow rate is drastically increased which strongly affects the operating conditions of the valve plates column. The final design of the dust scrubber will be completed early 2012 after testing by a transparent model.

Offgas pipe of the glass melter

The improvement of the technique for periodic cleaning of the offgas pipe of the melter required considerable R+D effort to overcome problems which were associated with the present cleaning technique using air blasters. By this technique pressure air waves are generated in the offgas pipe by air blasters to

remove deposited material from the inner wall of the offgas pipe.

The principle of the new cleaning technique is based on periodic water flooding of the vertical section of the pipe. This section is designed as a film cooler and schematically illustrated in Fig. 2. Water flooding, using two phase flow properties is described in reference [4]. The film cooler consists of a slit pipe, an inner pipe and an outer pipe. The slit pipe is formed by annular ring elements and of an end slit. Compressed air is continuously supplied to the slit pipe (Air flow I) and flows through the slits into the offgas along the inner surface of the annular ring elements, forming a laminar air film along the wall. This minimizes depositing of airborne materials from offgas. A second air stream (Air flow II) flows exclusively through the end slit. For cleaning of deposited material water is periodically added to the air stream through the end slit or supplied separately (e.g. every 1 to 2 days about 20 l).

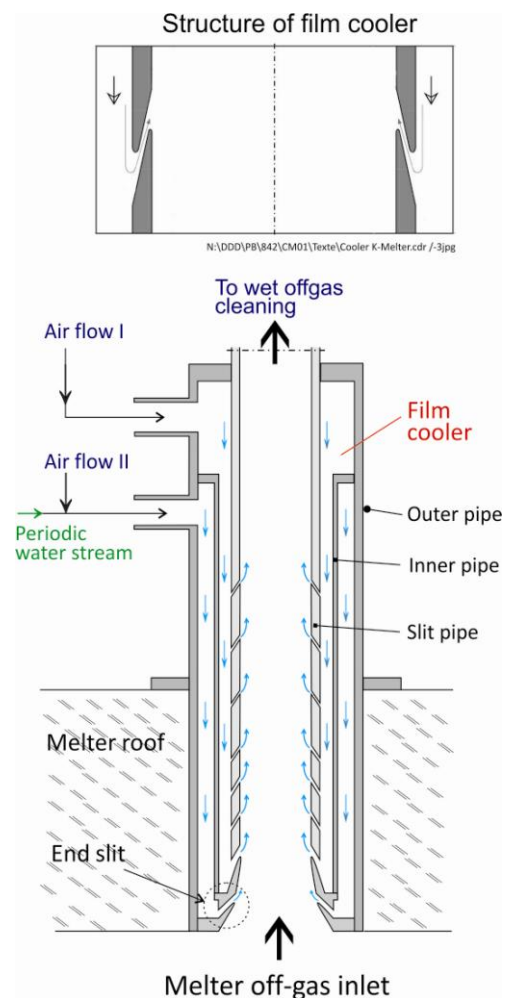


Fig. 2: Scheme of film cooler based offgas pipe and cleaning by water flooding technique.

If the offgas velocity is sufficiently high the interfacial shear of the offgas on the water film becomes dominant over gravity. The water then flows as a film upwards along the inner wall of the film cooler, and removes the deposits. In 2011, a physical model has been constructed and operated to get the basic understanding of the function and to collect relevant data. The experimental arrangement is shown in Fig. 3. Furthermore, a first basic

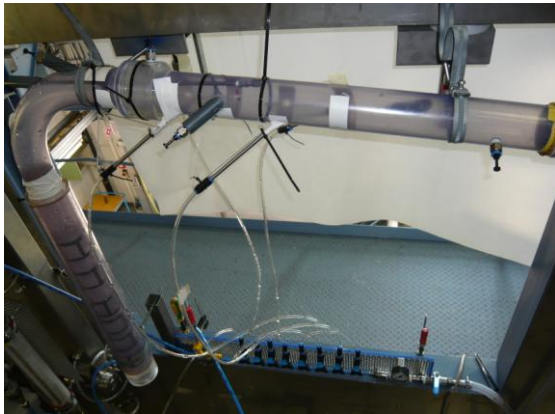


Fig. 3: Physical model of the new offgas pipe

design of the new offgas pipe has been performed and optimized. Detail design and manufacturing of the offgas pipe will be performed in 2012 and manufacturing in the first half of 2013.

Investigation of high temperature corrosion of glass canister material

Due to experiences made with difficult decontamination of waste glass canisters using supersonic velocity technique in a 1M HNO₃ bath, R+D effort has been made to get information about the surface structure of canister material after exposition to 700, 900 and 1100°C for 8 hour. Motivation was to look at possibilities to enhance the effectiveness of the decontamination process. A lab-scale furnace has been used and the experiments conducted by the equipment shown in Fig. 4 under environments of argon and air. Small pieces of 15x15x3 mm of the canister material under investigation (1.4833) were placed within an Al₂O₃ tube which in turn was put into an oven as shown in Fig. 4. Afterwards, the corroded surfaces of the samples were investigated by the analytical department of KIT-INE using SEM and EDX technique. Fig. 5 shows a typical image of the surface of a sample which had been exposed to 900°C for 8 hours in air along with an analysis of the surface made by EDX.

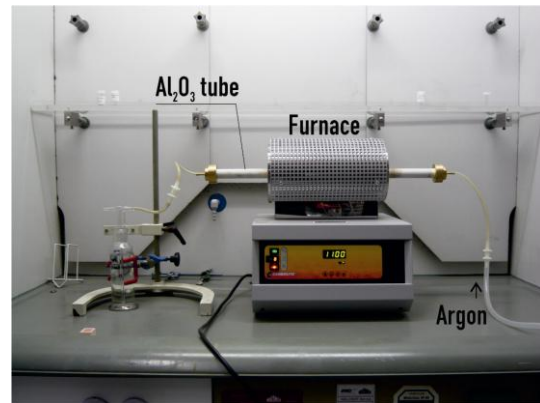


Fig. 4: Experimental arrangement for investigation of high temperature corrosion of canister material.

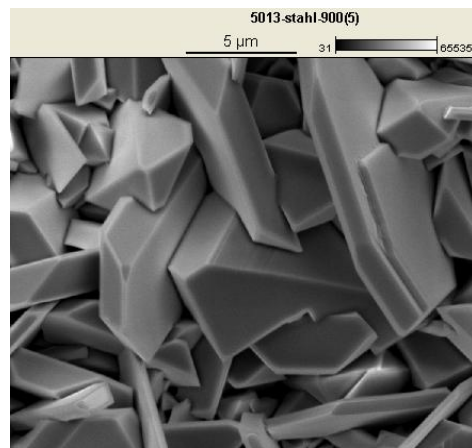


Fig. 5: SEM image and local EDX analysis of a sample exposed to 900°C (in air) for 8 hours.

Compared to samples exposed to the same temperature in argon atmosphere, no final conclusions can be drawn yet and further experiments are intended. Nevertheless from the many measurements of SEM/EDX of 6 samples it appears that the applied inert atmosphere by argon is of limited protection effect only.

Outlook

Major activities in the coming year are dedicated to the finalization of the KIT-INE's DD of all melter subcomponents, and of the other process components as well as the remote equipment placed in the V2 cell. Parallel to this work, the manufacturing of the melter parts will be carried out. By mid of 2012 the melter assembly will be started in the area of INE's prototype test facility (PVA). The assembly time is estimated to be about 10 months. Another important step will be performed by testing the RFD pumps that are used for transfer of HLLW in the receipt area. These tests will be carried out using the equipment of the PVA facility.

References

- [1] W. Grünewald, G. Roth, W. Tobie, J. Fleisch, F.J. Schmitz, W. Weishaupt, "Hot Operation Performance of the German Vitrification Plant VEK", GLOBAL 2011, Makuhari, Japan, Dec. 11-16, 2011 Paper No. 392619.
- [2] W. Grünewald, M. Plaschke, G. Roth, W. Tobie, K.H. Weiß, S. Weisenburger, A. Stollenwerk, A., Eissler, "Process Control and Glass Product Quality Assessment Applied in the VEK Plant", GLOBAL 2011 Makuhari, Japan, Dec. 11-16, 2011, Paper No. 392621.
- [3] W. Grünewald, G. Roth, W. Tobie, S. Weisenburger, K.H. Weiß, "Application of Advanced Large-Scale Ceramic Melter Technology for HLLW Vitrification", GLOBAL 2011, Makuhari, Japan, Dec. 11-16, 2011 Paper No. 392622.
- [4] G. F. Hewitt, "Handbook of multiphase systems" (Ed. G. Hetsori), Hemisphere Publishing Corporation, New York, Part Fluiding and Flow reversal, pp 2-44 (1982).

9 Development of actinide speciation methods

Activities concerning developments of instrumentation and techniques available for actinide speciation continue to be a significant thematically cross-cutting activity at INE. A number of notable new developments have been achieved over this past year:

The capabilities at the INE-Beamline have been improved by extending the license for working with radioactivity to include the fissile isotopes ^{235}U and ^{239}Pu and by construction and commissioning an improved design for the single analyzer crystal high-resolution X-ray emission spectrometer. The foundation for future pioneering speciation studies using synchrotron radiation have been laid down in initial activities for construction of a new experimental station at ANKA, the CAT-ACT-Beamline.

Examples of fundamental laser-based investigations in 2011 include, studies to assess parameters affecting emission lifetimes and determination of an empirical relation to determine the number of coordinating N-donor ligands in Eu-complexes, and implementation of a LIBD data processing mode to extend online measurements to several hours.

Further development activities include first results of plutonium speciation studies using the high resolution sector-field ICP-MS instrument, NMR investigations of a Am(III)-BTP_3 solution complex (see 2011 Highlights) and plane wave DFT with periodic boundary conditions (PBC) studies of ions sorbed onto corundum.

In contrast to annual reports in the past, this 2011 report does not contain a separate chapter of XPS and electron microscopy activities. This is because two brand new instruments have been delivered and commissioned (an environmental FEI Quanta 650 FEG SEM in June 2011) or is still under commissioning (a new XPS PHI VersaProbe delivered in October 2011). Please look forward to reports of exciting results from these versatile modern instruments in 2012!

9.1. R&D projects conducted at the INE-Beamline for Actinide Research at ANKA and at external SR sources

K. Dardenne, M. A. Denecke, T. Prüßmann, J. Rothe, T. Vitova

Introduction

The INE-Beamline for actinide research at the synchrotron radiation source ANKA, situated on KIT's North Campus, offers dedicated instrumentation for X-ray spectroscopic characterization of actinide samples and other radioactive materials [1]. R&D work at the beamline focuses on various aspects of nuclear waste disposal within INE's mission to provide the scientific basis for assessing long-term safety of a future high level nuclear waste repository. The INE-Beamline is accessible for the German and international actinide and radiochemistry community through the ANKA proposal system [2]. Additionally, the beamline is a "pooled facility" within the European Union Integrated Infrastructure Initiative ACTINET-i3 [3], thereby making its unique experimental and analytical equipment available to scientists from Europe for joint research projects. The modular INE-Beamline design offers sufficient flexibility to adapt sample environments and detection systems to many specific scientific questions. The beamline staff continually adapts and extends the pool of analytical methods to match user needs. Besides offering user support and conducting own research projects at ANKA, INE scientists perform various experiments at external SR sources

offering capabilities not - or not yet - available at KIT.

INE-Beamline user operation in 2011

In 2011 a total of 29 INE in-house and external projects were hosted at the INE-Beamline. The time share available for INE internal research amounted to ~35% of all available shifts (42 days). 10 days were spent for maintenance and development. The majority of beamtime shifts in 2012 was given for external projects with (45 days) and without (12 days) ARC (ANKA Review Committee) ranking. INE projects at the beamline generally cover a broad range of topics related to safe disposal of high level radioactive waste (HAW) and alternative disposal strategies, e.g., the reduction of HAW radiotoxicity. Many of these studies are presented in more detail elsewhere in this annual report or the ANKA 2010/2011 User Report [4]. In-house projects in 2011 included studies of the effect of Keggin-ions (GaAl_{12}) on the interfacial behaviour of gibbsite, structural investigations of molybdate phases in nuclear waste glass simulates, investigations of Eu incorporation into phosphate minerals, XAFS studies of Se and Rb sorption species on calcite surfaces, polarized XAFS investigations of Y and Eu

incorporation into layered hydroxides, Np(VI) / Pu(VI) precipitate formation at high pH and salinity, U L3 μ -XAFS and μ -XRF investigation of U phases formed during salt brine cement corrosion, U(VI) / Pu(VI) polymerization in aqueous solution or studies of Pu(V), Np(V) and Tc(VII) sorption and redox speciation on Opalinus clay and Callovo-Oxfordian fracture filling material.

General user research projects receive beamtime following ARC evaluation (biannually - at least 30% of all available shifts) or through direct cooperation with KIT-INE. In 2011 scientists from the 17 German and European research institutions listed below conducted experiments at the INE-Beamline:

- JRC-Institute for Transuranium Elements, Karlsruhe, EU
- Institut für Kernchemie, Universität Mainz, Germany
- Physics and Astronomy Department, Uppsala University, Sweden (*)
- Institut für Anorganische Chemie, Universität Erlangen, Germany
- KIT Institut für Nanotechnologie, Karlsruhe, Germany
- KIT Institut für Mikrostrukturtechnik, Karlsruhe, Germany
- KIT Institut für Mineralogie und Geochemie, Karlsruhe, Germany
- Chemistry Department, Radiochemistry Division, Lomonosov Moscow State University, Russia
- Institut für Geowissenschaften, Universität Jena, Germany
- Institut de Chimie Separative de Marcoule, CEA Marcoule, France (*)
- Laboratoire Subatech, Ecole des Mines de Nantes, France
- Department of Materials, Imperial College, London, Great Britain (*)
- Department of Chemistry, Helsinki University, Finland
- Institut für Energie- und Klimaforschung 6, Forschungszentrum Jülich, Germany
- Universität Bonn, Physikalisches Institut (PI-Bonn)

(*) in the framework of an ACTINET-i3 Joint Research Project

As in previous years, a significant percentage of in-house and ARC beamtime was used by PhD students to perform experiments in the framework of their theses (a total of 13 projects corresponding to more than 30% of all available shifts).

INE-Beamline license extension

ANKA holds a license to handle non-fissile radioactive isotopes with activities up to $1E+6$ times the isotope specific European exemption limit in the experimental hutch of the INE-Beamline. Beamtime projects employing radioactive materials are supervised by INE radiation safety officers supported by KIT-KSM radiation safety technicians. In December 2011 the original license issued in 2005 was extended upon user request to include the fissile isotopes ^{235}U and ^{239}Pu . Total masses up to 200 mg for each isotope are now allowed for experiments at the beamline. Initial XAFS measurements including ^{239}Pu shipped to INE from CEA Cadarache within an approved ACTINET-i3 joint research project are scheduled for March 2012.

ANKA CAT-ACT project

To strengthen KIT's international leadership in actinide research and rapidly expanding expertise in catalysis, a top-notch hard X-ray beamline at ANKA for CATalysis and ACTinide research is currently being designed and will be constructed and operated with emphasis on X-ray spectroscopy techniques, including 'flux hungry' photon-in / photon-out techniques (cf. the following section on the development of HRXES). The CAT-ACT beamline will help serve growing needs to establish additional capabilities for high flux / high energy spectroscopy measurements at ANKA, complementing the existing, strongly overbooked XAS endstations. The CAT-ACT beamline will comprise two alternately operated experimental stations at a superconducting insertion device (high-field wiggler) in a 1m short straight section next to the INE-Beamline (Fig. 1). The beamline will be jointly funded and operated by KIT-ITCP (Institute for Technical and Polymer Chemistry, South Campus) for catalysis experiments and KIT-INE for actinide research. The CAT-ACT wiggler source provides a spectrum extending into the hard X-ray regime up to 60 keV, thus giving access to actinide L1- and lanthanide K-edges. At the same time, the photon flux increase by about two orders of magnitude compared to ANKA bending magnet radiation will improve HRXES studies requiring high photon flux, as well as increase the spectroscopic sensitivity for dilute sample systems, e.g., for far field studies or radionuclides in environmental, i.e., 'natural' samples.

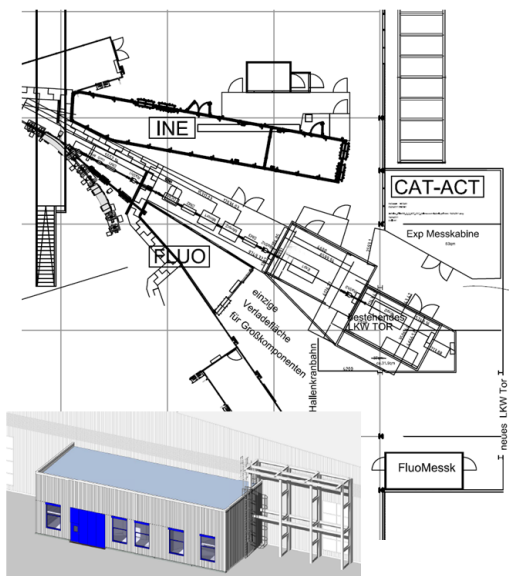


Fig. 1: ANKA floor plan section showing a draft layout of the future CAT-ACT beamline next to the INE-Beamline. The inset depicts a 3D visualization of the annex to building 348 accommodating the new installations.

The CAT-ACT project officially commenced in April 2011. The necessary extension of the ANKA hall to accommodate the CAT experimental hutch and CAT-ACT control cabin began in October 2011. The superconducting wiggler was ordered from Butker Institute (Novosibirsk, Russia) in November 2011. Currently the design concept for the CAT-ACT optic section is being reviewed. In 2012 core components for the multi-(analyzer)crystal HRXES spectrometer (cf. next section), which will be the heart of the ACT experimental infrastructure, will be assembled and tested at the INE-Beamline.

High-resolution X-ray emission spectroscopy (HRXES)

In 2011 an improved modification of the single analyzer crystal HRXES spectrometer based on an original NIST (National Institute of Standards) design [5] was manufactured and successfully tested at the INE-Beamline. The modified spectrometer extends the maximum Bragg angle (θ) limit from 45° to 70° . The higher θ allows recording XANES spectra with enhanced energy resolution while minimizing crystal-detector distances and thereby reducing time required for data sets with sufficiently high signal-to-noise ratio.

In Fig. 2 the conventional Pu M5-XANES white line (WL) obtained from a 100 nm PuO_2 film is compared to high-energy resolution XANES

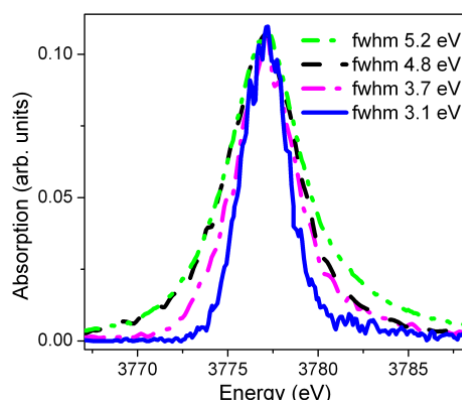


Fig. 2: Conventional fluorescence mode Pu M5-XANES (fwhm 5.2 eV) obtained for a 100 nm PuO_2 film; HR-XANES at 0.5 m crystal-detector distance (D), $\theta=36.3^\circ$ (fwhm 4.8 eV); $D= 1$ m, $\theta=36.3^\circ$ (fwhm 3.7 eV); and at 0.5 m crystal-detector distance, $\theta=68.2^\circ$ (fwhm 3.1 eV).

(HR-XANES) data recorded with the HRXES spectrometer at different distances between detector and Ge(220) analyzer crystal and different θ . The Pu M5-HR-XANES recorded at 0.5 m crystal-detector distance with at $\theta=68.2^\circ$ Bragg angle exhibits the smallest WL width (fwhm 3.1 eV) compared to the other spectra. (conventional fwhm 5.2 eV; $\theta=36.3^\circ$, 0.5 m fwhm 4.8 eV; $\theta=36.3^\circ$, 1 m fwhm 3.7 eV). This observation clearly demonstrates the improved energy resolution by measuring at higher θ .

In 2011 the potential of the HR-XANES technique to study electronic and coordination structures of actinides (An) was further explored in experiments using the multi-analyzer crystal spectrometer at the ID26 experimental station, ESRF (European Synchrotron Radiation Facility) in Grenoble, France. Two uranium minerals, autunite and schroeckingerite, were used to compare the structural sensitivity of HR-XANES spectra at the U M4 and L3 edges. Autunite and schroeckingerite possess tetragonal (P4/nmm) and triclinic (P -1) crystal structures, respectively. In both mineral phases U(VI)O_2^{2+} dioxo cations are coordinated solely by O atoms in the equatorial plane; second coordination neighbours are P atoms (autunite) or C atoms (schroeckingerite). In Fig. 3 the autunite and schroeckingerite U L3-HR-XANES spectra (a) are compared to their conventional fluorescence XANES spectra (b). All HR-XANES spectral features are sharper than in the conventional XANES and an additional pre-edge feature is resolved. The U M4-HR-XANES for these minerals also exhibits significantly improved energy resolution (Fig. 3c); the distinct fine structure is not visible in

conventional fluorescence mode spectra (not shown). Surprisingly, only subtle differences between the mineral phases are observed in their U M4-HR-XANES spectra such as the energy shift of feature D (enlarged in Fig. 3c inset). In contrast, the different U coordination environments in these mineral structures are clearly reflected in distinct variations of the U L3- HR-XANES features, e.g., different pre-edge and WL intensities and different post-edge (EXAFS) resonances (Fig. 3a). Note that these differences are not as pronounced in their conventional spectra (Fig. 3b).

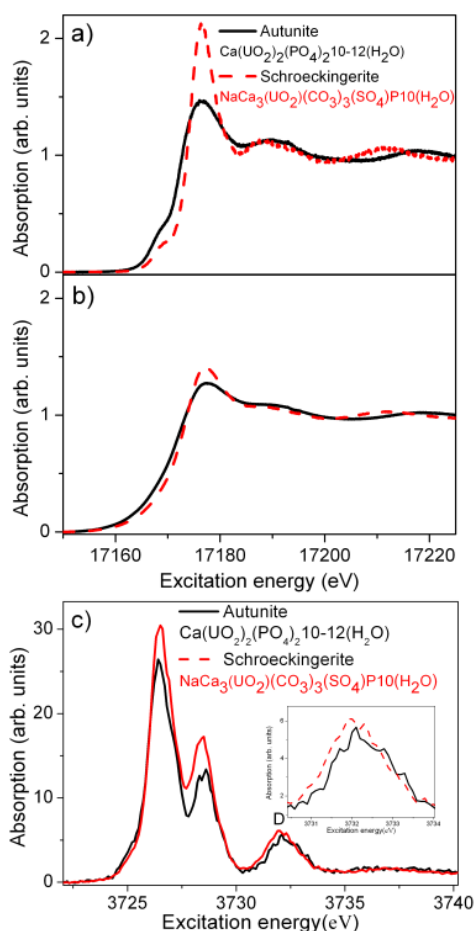


Fig. 3: HR (a) and conventional (b) U L3-edge XANES and HR U M4-edge XANES spectra (c) for the natural U minerals autunite and schroekingerite.

The An M4,5-edges are of special interest as they directly probe unoccupied An 5f electronic state densities ($3d \rightarrow 5f$ transitions) and potentially can reveal subtle bonding differences such as metal-to-ligand charge donation. M4-XANES is expected to be especially useful for An speciation, since the reduced core-hole life-time broadening at the M4-edge compared to the L3-edge theoretically sharpens spectral features, thereby facilitating detection of minority valence species in oxidation state mixtures.

However, these initial results on these minerals indicate that the An L3 edge might be more sensitive to changes in coordination environment [6].

Acknowledgement

Cooperation with W. Mexner and T. Spangenberg (ISS IT-group) for hardware and software implementation at the INE-Beamline, is gratefully acknowledged. Many thanks to H. Blank (PI-Bonn), A. Neumann, V. Krepper, J. Thomas and G. Christill (INE) for invaluable technical support.

References

- [1] K. Dardenne et al., Journal of Physics: Conference Series 190, 012037 (2009).
- [2] http://ankaweb.fzk.de/website.php?page=userinfo_main
- [3] <http://www.actinet-i3.eu>
- [4] Report of User Experiments at ANKA 2010/2011, KIT-ISS.
- [5] T. Vitova et al., IOP Conf. Ser.: Materials Science and Engineering 9, 012053 (2010).
- [6] T. Vitova et al., Experimental Report, ESRF Annual Report (2011).

9.2 Laser spectroscopy

S. Büchner, A. Chagneau, A. Chai, R. Götz, A. Geist, W. Hauser, P. Hoess, R. Klenze, J. Laber, P. Lindqvist-Reis, P.J. Panak, U. Müllich, C.M. Ruff, T. Schäfer, M. Steppert and C. Walther

Introduction

Time-resolved laser fluorescence spectroscopy (TRLFS) is a powerful tool for characterization and quantification of luminescent lanthanide and actinide ions in solution and solids. The TRLFS spectra of trivalent europium, Eu(III), for instance, provide information about the number of species, their concentration, symmetries, and vibrational states. In the following, TRLFS results from investigations on two different systems Eu(III) are presented. In the first contribution, the TRLFS results on crystalline trihydroxides doped with Eu(III) in $M(\text{OH})_3$ ($M = \text{La}, \text{Gd}, \text{Y}$) are presented. The aim is to elucidate the hydrolysis reaction and especially the quench-rate of Eu(III) in various matrices. The relationship between quench-rate and hydration number (Horrocks' equation [1]) was recalibrated recently for Eu(III) in various environments. However, such information is not known for inorganic hydroxides [2]. The second example involves TRLFS investigations of Eu(III) complexed with neutral N-donors (e.g., BTP) are excited by direct excitation in the wavelength range from 578 to 582 nm. The $^5\text{D}_0 \rightarrow ^7\text{F}_0$ transitions of various $\text{Eu}(\text{BTP})_n$ -complexes ($n=1,2,3$) are recorded, yielding important structural information.

In addition, results from Laser-induced Breakdown Detection (LIBD) studies as a highly sensitive determination of the homogeneous nucleation of celestine and strontianite in aqueous solution by colloid detection to retrieve the critical saturation index.

TRLFS studies of luminescent Eu^{3+} ions in $M(\text{OH})_3$ ($M = \text{La}, \text{Gd}, \text{Y}$)

Trivalent Eu-doped amorphous La, Gd and Y hydroxides were precipitated from the corresponding rare-earth chloride, nitrate, or perchlorate solutions by adding sodium hydroxide. The precipitates were washed with water, dispersed in aqueous sodium hydroxide solution, transferred to autoclaves and reacted at 200 °C for 3 days. The resulting pastes were washed with water and then dried in an oven at 100 °C. Powder XRD showed that the obtained $M(\text{OH})_3$ solids were well-crystalline and single-phase. Although the particles were all needle-shaped, their particle size varied greatly; the average size of the $\text{La}(\text{OH})_3$ particles was

about 30×1000 nm, that of $\text{Y}(\text{OH})_3$ considerable larger (Fig. 1).

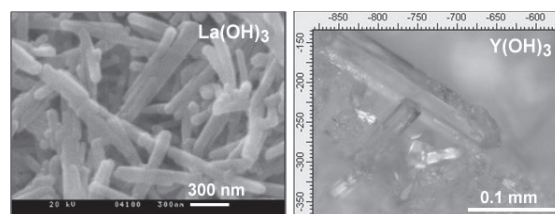


Fig. 1: SEM (left) and optical light microscope (right) pictures of $\text{La}(\text{OH})_3$ and $\text{Y}(\text{OH})_3$. TRLFS was performed on Eu-doped (1% Eu).

TRLFS was performed on the prepared Eu-doped (1% Eu) in $M(\text{OH})_3$ at 300 and 20 K. Fig. 2 shows the low-temperature Eu^{3+} emission spectra. While the spectra of the Gd and Y hosts are virtually identical, indicating very similar local structure at the Eu^{3+} sites, the $^5\text{D}_0 \rightarrow ^7\text{F}_2$ transition intensity is slightly stronger in the La host. This may be explained by the smaller particle size and therefore a larger surface, containing Eu^{3+} ions with different local structure compared to those in the bulk. The fact that the $^5\text{D}_0 \rightarrow ^7\text{F}_0$ transition has zero intensity, $^5\text{D}_0 \rightarrow ^7\text{F}_1$ is strong and two-fold split, and $^5\text{D}_0 \rightarrow ^7\text{F}_2$ is weak and not split, is indeed characteristic for Eu^{3+} in D_{3h} symmetry.

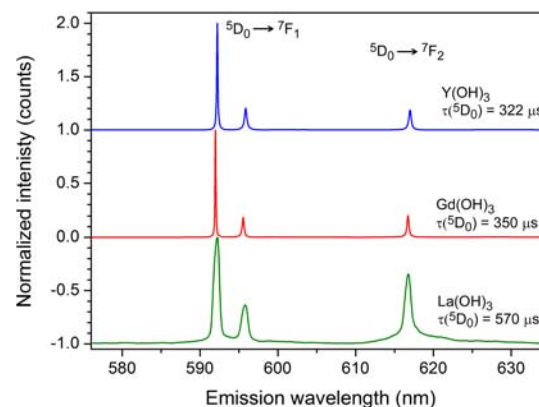


Fig. 2: Emission spectra of 1% $\text{Eu}(\text{III})$ in $\text{Gd}(\text{OH})_3$, $\text{Y}(\text{OH})_3$ and $\text{La}(\text{OH})_3$ at 20 K. $\lambda(\text{ex}) = 395$ nm.

Although emission spectra of the Gd and Y hosts are nearly undistinguishable, their emission lifetimes are quite different. The observed lifetimes at 300 K were 263, 285 and 310 μs ($\pm 3 \mu\text{s}$), for $M = \text{Y}, \text{Gd},$ and La , respectively; at 20 K the corresponding lifetimes were found to be significantly longer, 322, 350, and 570 μs (see Fig. 3). The reason for the increase of the emission lifetime with decreasing temperature may be due to fewer accessible pathways of non-radiative decay at

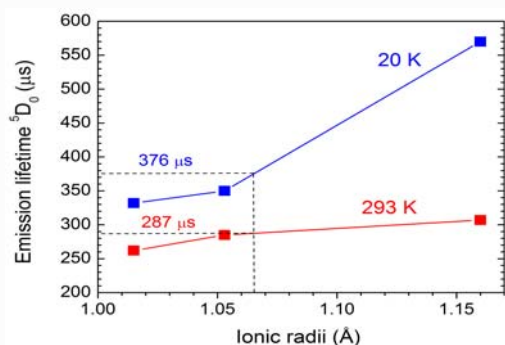


Fig. 3: Emission lifetimes of Eu^{3+} doped in $\text{Y}(\text{OH})_3$, $\text{Gd}(\text{OH})_3$ and $\text{La}(\text{OH})_3$ at 293 and 20 K vs. the ionic radii of the host trivalent metal ions.

low temperature. The measured $\text{Eu}(\text{III})$ emission lifetime correlates with the size of the host unit cell, i.e. with the host metal ionic radii.

Deconvolution of $\text{Eu}(\text{III})$ ${}^7\text{F}_0$ - ${}^5\text{D}_0$ spectra interacting with neutral N-donors (BTP)

TRLFS is a well known and versatile tool to determine the coordination structure of both organic and inorganic $\text{Eu}(\text{III})$ complexes in solution and solids [3]. Important structural information are derived by detection of the first excited state lifetime and the subsequent calculation of the remaining water molecules bound in the inner-sphere using an empirical equation [1].

However, difficulties occur particularly for complexes with energy transfer processes between coordinated ligand and metal cation and for mixtures of different $\text{Eu}(\text{III})$ species, which require multi-exponential fitting procedures. The former represents a fundamental problem because, due to the additional energy relaxation path, a quantitative lifetime evaluation to determine the number of coordinating molecules fails. Energy transfer phenomena often appear in metal-organic systems containing aromatic ligands [4].

A way to bypass this difficulty is to correlate the $\text{Eu}(\text{III})$ ${}^7\text{F}_0$ - ${}^5\text{D}_0$ transition shift with the total ligand coordination number, as an alternate method to predict the complex structure. Choppin and Wu were able to derive an empirical equation based on 40 organic $\text{Eu}(\text{III})$ complexes using this strategy [5]. While this approach gives good results for mono- and multi-dentate O-donor ligands, the coordination numbers of N-heteroaromatic ligands are significantly overestimated.

The tridentate and water-soluble ligand of the Bis-triazinylpyridine-type Aq-BTP [6] (see Fig. 4) shows strong energy transfer processes when coordinated to $\text{Eu}(\text{III})$. Aq-BTP can be

used as aqueous complexing agent for the selective back extraction of actinides (An) from organic phases loaded with both trivalent An and lanthanides (Ln) in the so-called innovative SANEX process [7]. In the following we present results of investigations of the $\text{Eu}(\text{III})$ ${}^7\text{F}_0$ - ${}^5\text{D}_0$ transition shift in complexes of aq-BTP [8].

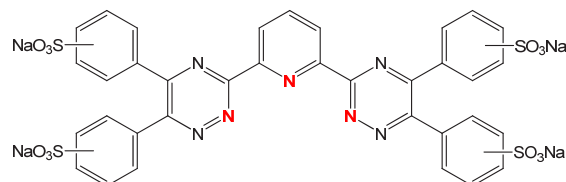


Fig. 4: Molecular structure of aq-BTP (coordinating N-atoms are marked red)

Results and Discussion

High resolution ${}^7\text{F}_0$ - ${}^5\text{D}_0$ excitation spectra of 0.02 mM $\text{Eu}(\text{III})$ were recorded at pH 3.0 with aq-BTP concentrations of 0.15 mM and 2.5 mM (Fig. 5).

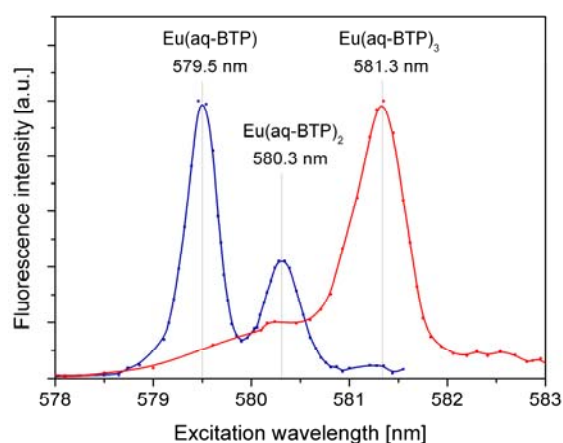


Fig. 5: ${}^7\text{F}_0$ - ${}^5\text{D}_0$ excitation spectra of 0.02 mM $\text{Eu}(\text{III})$ with $[\text{aq-BTP}] = 0.15$ mM (blue line) and 2.5 mM (red line) at pH 3.0

Under these conditions, three sharp excitation bands at 579.5 nm, 580.3 nm, and 581.3 nm are observed, corresponding to complex $[\text{Eu}(\text{H}_2\text{O})_{9-3n}(\text{aq-BTP})_n]$ ($n=1,2,3$) species. In comparison to the fully hydrated $\text{Eu}(\text{III})$ aquo ion, which exhibits a ${}^7\text{F}_0$ - ${}^5\text{D}_0$ transition frequency of 17.276 cm^{-1} (578.8 nm), the three $\text{Eu}(\text{III})$ -aq-BTP complexes show a red-shift in frequency with increasing number of coordinating aq-BTP ligands. This shift can be explained by the nephelauxetic effect typically known for transition metal complexes [9].

The observed shift $\Delta\nu$ of the ${}^7\text{F}_0$ - ${}^5\text{D}_0$ transition frequency is plotted as a function of the total ligand coordination number in Fig. 6. The value of $\Delta\nu$ is correlated with the total ligand

coordination number in a linear fashion. Linear regression yields the following empirical equation:

$$CN_L = 0.122 \cdot \Delta\nu + 0.293 \quad (1)$$

with $R^2 = 0.996$. According to equation (1), the solution coordination structure of Eu(III) complexes coordinated with N-heteroaromatic ligands can easily be estimated by measuring the ${}^7F_0-{}^5D_0$ transition frequency from excitation or emission spectra.

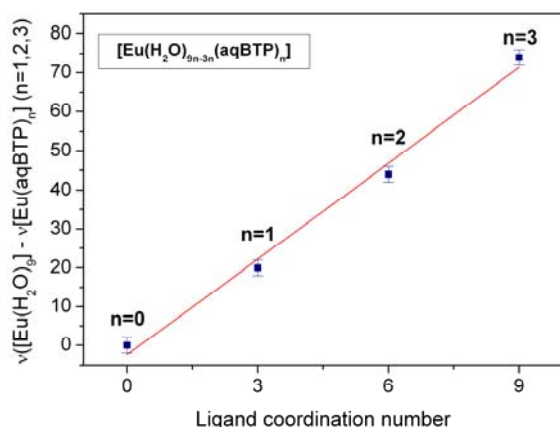


Fig. 6: Correlation of the ${}^7F_0-{}^5D_0$ transition frequency shift of the $[\text{Eu}(\text{H}_2\text{O})_{9-3n}(\text{aq-BTP})_n]$ ($n=0-3$) complexes and the total ligand coordination number

Several Eu(III) complexes with different heteroaromatic N-donor ligands were analyzed to validate the empirical correlation in (1) (Table 1). The difference between ligand coordination number determined experimentally and calculated using (1) of ~ 0.3 is very good, which confirms the applicability of this new correlation.

Table 1: ${}^7F_0-{}^5D_0$ transition frequency shift and experimental and calculated ligand donor numbers for several Eu(III)-N-donor ligand complexes

Eu(III) complex	$\Delta\nu$ [cm^{-1}]	CN_L exp	CN_L calc	ΔCN_L
[Eu(aq-BTP)]	19.8	3	2.7	0.3
[Eu(aq-BTP) ₂]	44.1	6	5.7	0.3
[Eu(aq-BTP) ₃]	73.8	9	9.3	0.3
[Eu(nPr-BTP) ₂]	49.4	6	6.3	0.3
[Eu(nPr-BTP) ₃]	70.2	9	8.9	0.1
[Eu(C5-BTBP) ₂]*	64.3	8-9	8.1	-
[Eu(^t Bu-C2-BTBP) ₂]*	64.3	8-9	8.1	-
[Eu(CyMe ₄ -BTBP) ₂]*	61.3	8-9	7.8	-

*taken from [10], structure is suggested to be $[\text{Eu}(\text{R-BTBP})_2(\text{NO}_3)_x]$ with $x = 0-1$

An extended 2d-optical LIBD for the online detection of mineral (celestite and strontianite) precipitation

The main objective of the present investigation is to test newly made modifications of the Laser Induced Breakdown Detection (LIBD) set-up for application to determine precisely the induction time and critical saturation index (SI_{crit}) for celestite (SrSO_4) and strontianite (SrCO_3) nucleation. The induction time and SI_{crit} are the time and the level of supersaturation required for formation of the first nuclei. As the precipitation under homogeneous nucleation starts with colloid formation, LIBD method offers a highly sensitive detection system, advantageous over classical chemical analyses, allowing determination of these parameters with high precision.

LIBD set-up

The data processing of the mobile 2d-optical LIBD for colloid quantification has been modified for the precipitation kinetics investigations of celestite and strontianite. The allowable online measurement period was extended to several hours using a differential mode of determination of varying colloid content with time. In this mode the Nd:YAG-laser is pulsed with 15 Hz for thermal stability, while the breakdown image detection and data storage on a server drive is performed with only 5 Hz. This is done to avoid loss of data due to the speed limitations of the storage drive. Additionally, the amount of data is significantly reduced to the benefit of overall detection time. Test measurements indicate that in this mode 900,000 breakdown images can be stored for subsequent evaluation. With an integral breakdown probability of $<100\%$ a detection time of more than 50 h is now possible.

Experimental protocol

A stock solution of $1 \times 10^{-2} \text{ mol L}^{-1}$ $\text{SrCl}_2(\text{aq})$ was prepared in a 1L plastic bottle and pumped through the LIBD detection cell at a constant pump rate of 1.5 mL min^{-1} . After acquisition of a background measurement (giving basically the nucleation surface from impurities), an aliquot of $\text{Na}_2\text{SO}_4(\text{aq})$ or $\text{Na}_2\text{CO}_3(\text{aq})$ at 0.3 mol L^{-1} was added to the solution, in order to reach the desired supersaturation. The solution was stirred during the entire time of the measurement (5 to 8 hours).

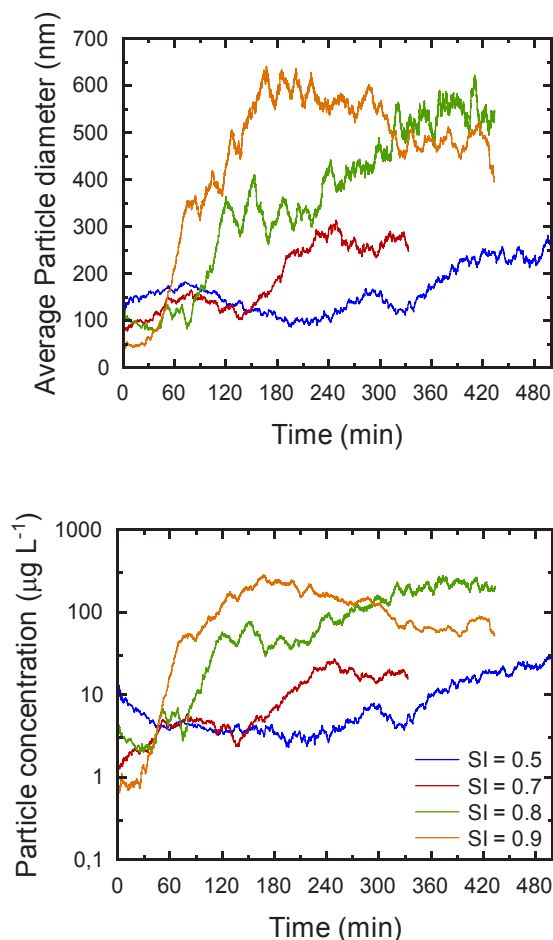


Fig. 7: Precipitation of celestite (SrSO_4) measured as particle formation observed with the new LIBD set-up at various values of SI.

Results and discussion

Nucleation is a relatively slow process. Induction times, when detected as concentration changes in time with chemical analyses, are usually on the order of several hours (e.g., around 18 hours for strontianite, Bucca et al. [11]). However, when detected by LIBD, nucleation induction times are only a few hours (Fig. 7). The modified LIBD set-up allows one to follow the evolution of nucleation with time, and to accurately compare results for various saturation indices (SI). From initial measurements, a clear relation between SI, induction time, particle concentration, and average particle size was observed.

These results obtained with the modified LIBD set-up are promising and clearly can be used to derive the SI dependent induction time of homogeneous nucleation (Fig. 8). This method will be used for detailed investigations of the formation kinetics of celestite and strontianite in the coming year, including studies of the role of pH for strontianite precipitation and tests of the “equality range” theory.

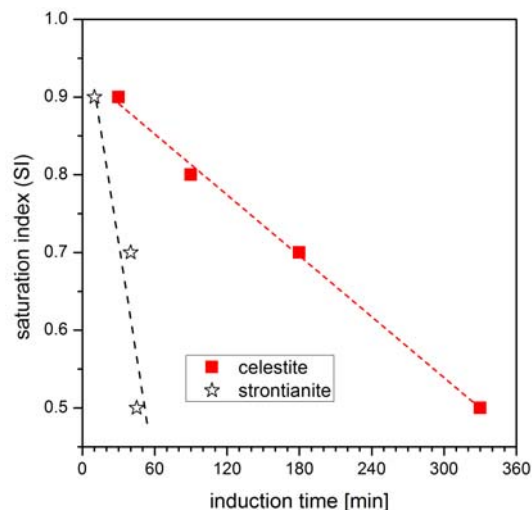


Fig. 8: Saturation index dependent induction time before the onset of celestite or strontianite colloid formation based on the LIBD measurements.

References

- [1] W. D. Horrocks, D. R. Sudnick, *J. Am. Chem. Soc.*; 101 (2), 334-340 (1979).
- [2] R.M. Supkowski, D. W. Horrocks, *Inorg. Chim. Acta*, 340, 44 (2002).
- [3] J.-C.G. Bünzli, G. R. Choppin (Eds.) *Lanthanide probes in life, chemical and earth science*, Elsevier, Amsterdam (1989).
- [4] P. J. Panak, R. Klenze, H. Wimmer, J. I. Kim, *J. Alloys Compd.*; 225 (1-2), 261-266 (1995).
- [5] G. R. Choppin, Z. M. Wang, *Inorg. Chem.*; 36, 249-252 (1997).
- [6] Traister, G. L.; Schilt, A. A.; *Anal. Chem.*; 48 (8), 1216-1220 (1976)
- [7] A. Geist, U. Müllich, D. Magnusson, P. Kaden, G. Modolo, A. Wilden, T. Zevaco, *Solvent Extr. Ion Exch.* 30 (2012) (accepted).
- [8] C. M. Ruff, U. Müllich, A. Geist, P.J. Panak, *Int. J. Nucl. Power*, 56 (8/9), 489-491 (2011).
- [9] C. E. Schäffer, C. K. Jorgensen, *J. Inorg. Nucl. Chem.*, 8, 143-148 (1958).
- [10] M. Steppert, I. Cisarova, T. Fanghänel, A. Geist, P. Lindqvist-Reis, P.J. Panak, P. Stepnicka, S. Trumm, C. Walther, *Inorg. Chem.* 51 (1), 591-600 (2012).
- [11] M. Bucca M. Dietzel, J. Tang, A. Leis, S.J. Köhler, *Nucleation and crystallization of otavite, witherite, calcite, strontianite, hydrozincite and hydrocerussite by CO₂ membrane diffusion technique*. *Chemical Geology*, 266, 143-156 (2009).

9.3 Mass spectrometry methods

N. L., Banik, H., Geckeis, F., Geyer, C. H., Graser, M., Lagos, C. M., Marquardt, C., Walschburger

Introduction

Speciation has a strong impact on the mobility of radionuclides potentially released from different radioactive waste forms (ceramics, glass, spent fuel, etc) in a nuclear waste repository and is therefore subject to intensive study. Especially the redox-state is an essential property which determines the solubility in groundwater, as well as the sorption behaviour on mineral phases. Both aspects are of key interest in the assessment of the retention potential of nuclear waste repositories.

In addition to different spectroscopic techniques (TLRFS, EXAFS, etc.), modern Sector Field-ICP-MS (Element XR of Thermo Fisher Scientific, Bremen) is now available at KIT-INE. Transuranium elements with nearly zero background can be detected, even at concentrations as low as $\sim 10^{-15}$ mol/L (sub-ppq level), depending on the sample introduction system [1]. So far we have calculated a DL (detection limit) of ~ 60 ppq or 10^{-14} mol/L for U using a concentric glass nebulizer (with 1 mL/min uptake rate) fitted to a cyclonic spray-chamber. The DL for U is of course expected to be higher than the DLs of transuranium elements because of higher background.

ICP-MS combined with species selective tools like CE (capillary electrophoresis) or chromatographic techniques (in so-called hyphenated techniques) have been already successfully applied for speciation studies on actinides [2,3]. Because of the excellent sensitivity of CE-ICP-MS and the advantage of analyzing small sample volumes (nL range) we choose this method for speciation studies of actinides.

The CE-ICP-MS system at INE

Our capillary electrophoresis instrument (Beckman P/ACE™ MDQ, Fullerton, USA) and the Element XR (adapted to a glove box) are both located in the INE radioactive laboratories. We use a specially designed sample introduction system for CE-ICP-MS work consisting of a Mira Mist CE parallel path nebulizer (Burgener Research Inc.) with low uptake rates (typically below $10 \mu\text{L}/\text{min}$) fitted to a low volume glass spray-chamber (Fig. 1).

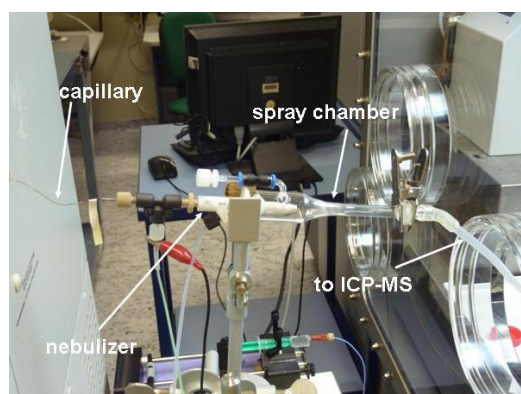


Fig. 1: CE-ICP-MS coupling of capillary, nebulizer, and spray-chamber.

Determination of actinide redox species in aqueous solutions

Before studying experimental solutions or natural samples we have investigated a series of elements with different valence states (Lu(III), Th(IV), Np(V), U(VI)), in order to evaluate DLs in bare fused silica capillaries ($50 \mu\text{m}$ ID) and to optimize the different physical parameters (nebulizer uptake rate, position of the capillary, Ar flow-rate of the sample gas, separation voltage, etc.) to ensure a high sensitivity of our CE-ICP-MS system. We used 1M HAc (acetic acid) as a background electrolyte (BE). These four elements serve as homologues for different Pu redox states, which were subsequently studied. These results are presented further below.

The calibration graphs of our homologue series indicate that Np(V) has almost no background and can be detected down to $\sim 3 \times 10^{-12}$ mol/L (Fig. 2 B). The other elements have DLs in the range of $\sim 10^{-10}$ mol/L; the calibration curve for uranyl, as an example, is depicted in Fig. 2 A. The DL for Np(V) falls within the range of values (10^{-10} to 10^{-12} mol/L) published in the literature for transuranium elements [2,3]. The DL calculated for Np(V) also agrees with estimates derived from our previous measurements of Np redox species in supernatant solutions from sorption experiments [4]. To further improve the efficiency and selectivity of our CE-measurements, we also adopted a new separation method.

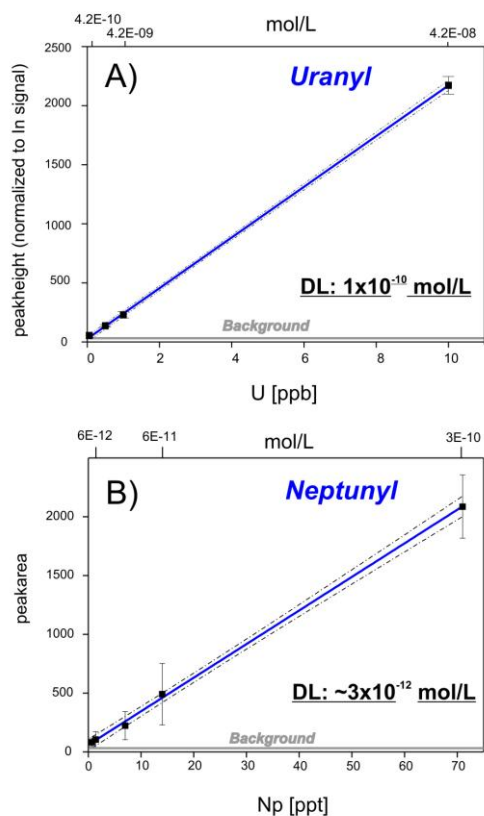


Fig. 2: CE-ICP-MS calibrations of A) uranyl (peak height normalized to the In signal in the HNO_3 makeup solution) and B) neptunyl. The DL for U(VI) is about 1×10^{-10} mol/L, that for Np about 2 orders of magnitude lower ($\sim 10^{-12}$ mol/L). Separations were performed at 30 kV using 1 M HAc as the background electrolyte. All solutions were injected hydrodynamically.

The new approach is based on a technique which is called NACE (non-aqueous capillary electrophoresis), using electrolyte solutions which are mainly composed of organic solvents [e.g., 5]. NACE is a promising method because it yields lower currents at higher ionic strengths and therefore lower joule heating, which allows the use of capillaries with larger diameters and injection of larger sample volumes. We tested a BE consisting of MeOH (methanol), 1M HAc and 50 mM imidazole and injected the sample (10^{-10} mol/L Lu in the BE 500-fold diluted with MeOH; see Fig. 3). This procedure is essentially an isotachophoretic separation, where a larger volume sample zone (sample injection: 120 s at 0.8 psi) is focused into a narrow zone. In this case the estimated DL is $\sim 1.3 \times 10^{-11}$ mol/L, which is an order of magnitude lower than the DL that was achieved in CE separations using 1 M HAc. Further efforts to refine this method are planned for the near future, which should also provide a higher separation resolution because of lower electroosmotic flow. This can be beneficial for the separation of species such as

Pu(V) and Pu(VI), which show similar mobilities.

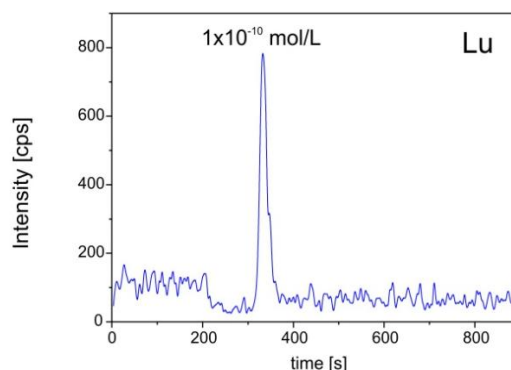


Fig. 3: Electropherogram (20 kV and 0.6 psi) of 10^{-10} mol/L Lu diluted 500-fold with MeOH. BE = 1 M HAc and 50 mM imidazole in MeOH. Hydrodynamic injection (120 s at 0.8 psi).

Pu redox states in aqueous solutions

A fresh solution of 3×10^{-8} mol/L $^{242}\text{Pu(VI)}$ in 0.1 M HClO_4 was prepared in an inert gas box and shortly after that introduced into our CE system by electrokinetic injection (20 s at 2 kV), in order to avoid any oxidation bias which could be potentially produced by hydrodynamic injection. Unfortunately the CE instrument at INE uses air as a pressure medium in the hydrodynamic mode. We are planning to modify our system so that Ar can be used in the future. The electropherogram obtained (Fig. 4 A) shows two peaks with separation times that closely match those of Pu(V) and Pu(VI) published by Kuczewski et al [6]. Three more replicate measurements were carried out over the following 2.5 h with the same sample. The last two were conducted with hydrodynamic injection. During the hydrodynamic injections the relative amounts of Pu(V) and Pu(VI) changed and the amount of Pu(VI) appeared to increase relative to Pu(V). This could be explained by increasing amounts of O_2 introduced in the system. Two additional small peaks also appear in the electropherograms (Fig. 4 B), which can be attributed to Pu(III) and Pu(IV). This demonstrates that our analytical procedure is capable of separating and detecting different Pu redox species. It is important to note that the CE measurements should be carried out with freshly prepared samples, i.e. immediately analyzed after removal from an inert gas box, in order to avoid changes in Pu redox state.

We also analyzed an artificial clay porewater solution with 0.1 M NaCl and 3×10^{-7} mol/L $^{242}\text{Pu(V)}$ that was aged for 18 months in an inert gas atmosphere. The pH of the sample

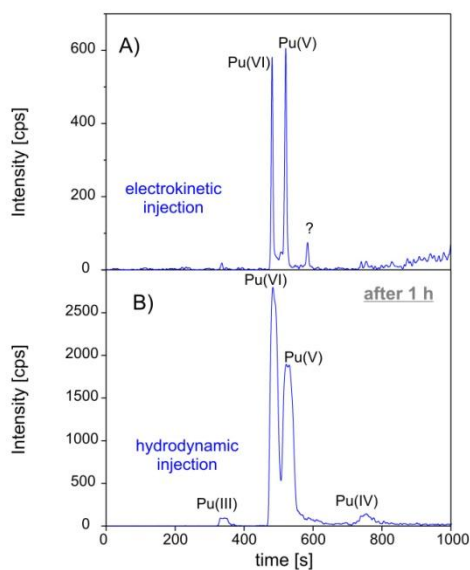


Fig. 4: Electropherograms (30 kV and 0.4 psi) of an initially 3×10^{-8} mol/L $^{242}\text{Pu(VI)}$ solution in 0.1 M HClO_4 . A) Measured directly after removal from an inert gas box (sample was electrokinetically injected (20 s at 2 kV). The small peak to the right of the Pu(V) is probably an artifact. B) Hydrodynamic injection (10 s at 0.8 psi) of the same sample after 1 h. Next to Pu(V) and Pu(VI) peaks, small peaks of Pu(III) and Pu(IV) appear.

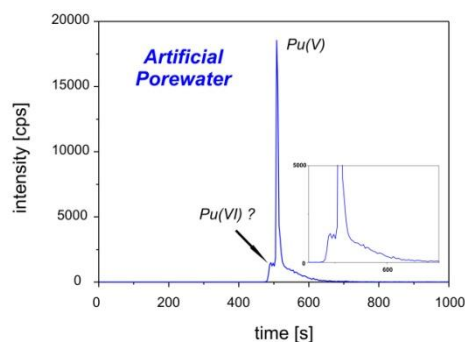


Fig. 5: Electropherogram (30 kV and 0.4 psi) of Pu in artificial clay porewater, 0.5 M NaCl, 3×10^{-7} mol/L $^{242}\text{Pu(V)}$. Contact time was 18 months in an inert gas atmosphere.

solution was 7.2. The electropherogram is shown in Fig. 5. Apart from Pu(V), a small shoulder on the Pu(V) peak is also observed, likely indicating the presence of Pu(VI) in the sample. It is quite remarkable that after 18 months Pu remains mostly in the pentavalent state, with only minor reaction to the hexavalent state.

References

- [1] J. S. Becker and H.-J. Dietze, J. of Anal. At. Spec. 14, 1493 (1999).
- [2] S. Topin, J. Aupiais, N. Baglan, T. Vercouter, P. Vitorge, and P. Moisy, Anal. Chem. 81, 5354 (2009).
- [3] C. Ambard, A. Delorme, N. Baglan, J. Aupiais, F. Pointurier and C. Madic, Radiochim. Acta 93, 665 (2005).
- [4] N. L. Banik, S. Büchner, M. Fuss, F. Geyer, M. Lagos, C.M. Marquardt, J. Rothe, T. Sasaki, M. Steppert and C. Walther, INE Annual report, (2010).
- [5] C.-H. Tsai, C.-C. Tsai, J.-T. Li and C.-H. Lin, J. of Chromatography A 1068, 115 (2005).
- [6] B. Kuczewski, C. M. Marquardt, A. Seibert, H. Geckeis, J. V. Kratz and N. Trautmann, Anal. Chem. 75, 6769 (2003).

9.4 NMR spectroscopy – first results of actinide-N-donor complexes

P. Kaden, Ch. Adam, B. Schimmelpfennig, P.J. Panak, A. Geist, M.A. Denecke

Introduction

Nuclear Magnetic Resonance spectroscopy (NMR) has only in recent years become available as a speciation method in nuclear chemistry. Applied to radioactive samples, NMR provides insight into the configuration, constitution and conformation of organic and inorganic compounds in solution. This information is relevant for the safety assessment of a nuclear repository and for partitioning strategies. Additionally, the facile access to important dynamic information for molecules in solution by probing magnetic relaxation and diffusion behavior is a key feature of NMR spectroscopy.

One of the most sensible sensors in NMR spectroscopy is the chemical shift, which can be measured with an accuracy of down to $1/10^7$ of the applied magnetic field. Nuclei with a non-zero magnetic moment sense the strong static external magnetic field in the spectrometer and align their molecular magnetic moments parallel or antiparallel to the magnetic field lines. The relative orientation leads to subsequent amplification or damping of the magnetic field sensed by the observed nuclei, influencing their resonance frequency, translating to an associated NMR chemical shift. Since the strength of the observed effect is directly proportional to the electron density around the nucleus, chemical shift measurements offer an easy access to the electron density distribution in a molecule.

However, the chemical shift is influenced additionally by paramagnetic nuclei. Nuclei with spin quantum numbers larger than $\frac{1}{2}$ are known to have a quadrupole moment. This moment leads to accelerated relaxation of the experimentally induced magnetization and thus to a broadening of signals from all nuclei near the quadrupolar nucleus. Additionally, paramagnetic metal ions with unpaired electron spins induce additional shifts (KNIGHT shifts, δ^{para})^[1,2] which are caused by the magnetic anisotropy of the metal ion. These add to the diamagnetic chemical shift (δ^{dia}) in the surrounding ligand nuclei. In addition to these two contributions to chemical shift, counter ions associated with metal cation complexes also make a small contribution (δ^{anion}):

$$\delta^{obs} = \delta^{dia} + \delta^{para} + \delta^{anion} . \quad (1)$$

We have recently initiated an extensive comparative study of differences in chemical shift between lanthanide (Ln) and actinide (An) complexes and separation of the individual factors contributing to δ^{obs} . Both Ln and An ions show paramagnetic properties to a variable extent and our NMR studies focusing on the paramagnetism of the compounds is a sensitive and versatile spectroscopic method for understanding differences in their complex behavior on a molecular level.

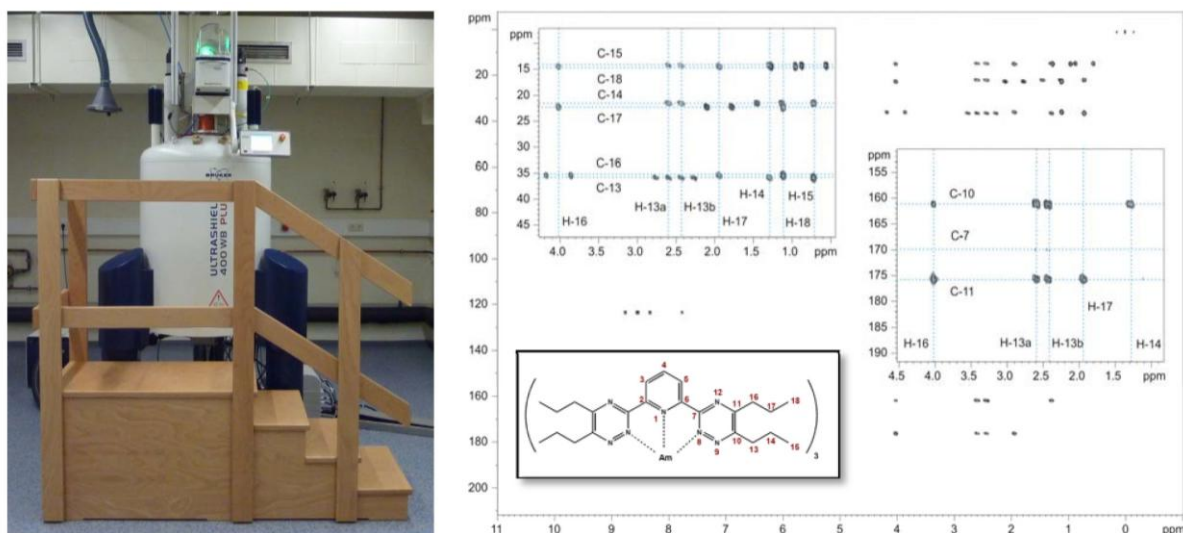


Fig. 1: left: The NMR spectrometer in the controlled area. right: the fully assigned $2D^1H,^{13}C$ -HMBC spectrum of $Am(BTP)_3(NO_3)_3$, showing resonances indicative of a diamagnetic 1:3 complex.

Paramagnetism and NMR spectroscopy

Referencing the chemical shift of a paramagnetic complex to the shift of an isostructural diamagnetic complex with the same counter ion cancels the other addends in (1), leaving the paramagnetic shift in the complexes for comparison.^[3,4] The paramagnetic chemical shift contribution in metal organic complexes affords direct access to the nature of metal-ligand interactions in the complexes.^[4] Two major contributions to KNIGHT shifts exist: a) the *FERMI contact contribution* (FCS), which results from electron transfer *via* covalent bonds and b) the *pseudo contact contribution* (PCS), which is a dipolar interaction term.^[2] The FCS can be described as a multiplication of the spin expectation value of the paramagnetic center and the hyperfine coupling constant. The PCS consists of geometrical factors, which are tabulated for Ln, and the second rank ligand field parameter that characterizes the magnitude of metal-ligand interaction. In complexes with high axial symmetry a number of methods are known to separate FCS and PCS contributions. One method utilizes the different temperature dependencies of FCS and PCS by application of variable temperature NMR.^[5]

NMR research on paramagnetic Ln complexes has been conducted extensively, especially in medicinal chemistry with the objective of synthesizing contrast agents for MRI purposes. All relevant parameters have been tabulated and are available in literature.^[6] In contrast, data for An compounds is nearly non-existent. This is of course due to extensive safety measures required in order to perform NMR spectroscopy on actinide samples in millimolar solution concentrations.

Experimental

Ongoing in-house research on Ln and An complexes of N-donor ligands aims to elucidate differences in their coordination which might explain the observed differences in separation behavior. Due to KNIGHT shift and relaxation enhancement, paramagnetic metal ions are challenging for measurement and assignment of NMR spectra, regardless of the observed nucleus. To achieve sufficient signal-to-noise ratios that allow measurement of the smallest couplings under fast relaxation, development of new measurement strategies and advanced pulse programs are necessary.

Only solubility limits the concentration of solutions in NMR studies of the Ln solution complexes. A concentration of 10 mM Ln ions in 600 μ L solution proved to be feasible. For investigations of An complexes, the maximal activity is the limiting factor; the 7 mM solution concentration for Am(III) nitrate used in the

complexation step already exhibits 11 MBq alpha activity. The complexes studied with NMR described below are prepared as follows. Solutions of ligand in methanol / water mixtures are added in stoichiometric amounts for formation of the 1:3 complex to the dry metal nitrate.

DFT calculations are performed with the Program package Turbomole utilizing basis sets of TZVP-quality and small-core pseudo potentials of Stuttgart type on Ln and An centers.^[9]

Results

The first An complex of the BTP ligand type has been studied with NMR at KIT-INE with Am(III) as metal ion. Americium is expected to be fairly diamagnetic, as the atomic ground state is diamagnetic and the first excited ground state has a bandgap of approximately 3100 cm^{-1} .^[7] NMR results show an approximate diamagnetic behavior for signals in ^1H and ^{13}C spectra that closely resemble those in the analogous diamagnetic Lu(III) complex. Variable NMR temperature measurements reveal only minor T dependency,^[8] supporting the notion of a diamagnetic ground state in Am(III). However, in the ^{15}N dimension a dramatic change for the directly coordinating nitrogen atom of the pyridine ring is observed (Fig. 2). Under the assumption of a purely diamagnetic ground state, this nitrogen atom senses an electron density one would expect for electron rich amines. This electron density is restricted directly to the coordinating pyridine nitrogen and does not propagate over the conjugate aromatic ring system, as the neighboring carbon atoms show no significant additional chemical shift.

In Ln complexes with BTP ligands small contributions to the chemical shift due to changes in the charge compensating anions are known. This led to the assumption that those anions, which are expected to be located on the C_2 axes perpendicular to the C_3 axis of the molecule (overall D_3 symmetry) cause a polarization of the $m = \pm 3$ *f*-orbitals ($m =$ magnetic quantum number) of the metal ion. This leads to a change in metal-ligand bond length, influencing the electron density sensed by NMR measurements of nuclei in the ligands.

If this were the reason for the dramatic change of electron density on the coordinating pyridine nitrogen atoms in the Am-BTP complexes, one would expect that changing the anion would influence the electron density at this nitrogen. However, NMR experiments conducted on BTP complexes with Am(III) nitrate and chloride show no differences in ^{15}N chemical shifts. This result clearly shows that there is no elec-

tronic interaction between the aromatic system of the ligand and anion molecular orbitals.

Studying the temperature dependence of the chemical shift of paramagnetic metal organic complexes can be used to verify the nature of the metal-ligand interaction, i.e. characterize the degree of covalency or dipolar character in bonding. Diamagnetic complexes only show minor changes of the chemical shift with temperature (due to small distance changes or freezing of rotational barriers between two conformations). In variable temperature experiments of the Am(III) BTP complexes, the coordinating pyridine nitrogen is observed to exhibit a strong temperature dependency (several hundred Hz), whereas the chemical shifts for the non-coordinating nitrogen atoms in the triazine moiety show little. In ^1H and ^{13}C experiments there is only a minor shift for both types of nitrogen atoms. This indicates that there is an electron transfer between the metal and the ligands of a yet unknown nature. Theoretical DFT calculations of Ln and An BTP complexes suggest that the electron density on the coordinating nitrogen atoms in actinide complexes is larger than that for the complexes of Ln.^[9] Further in-depth studies of this phenomenon are underway.

EURACT-NMR

In recent years substantial investment has been made to realize the joint effort of JRC-ITU and KIT-INE to establish the "Actinide NMR Centre of Excellence". Two NMR spectrometers at INE and JRC-ITU (both Bruker

Avance III 400 MHz) have been commissioned and nuclearized for work on radioactive samples. The FP7 funded EURACT-NMR project has been established, in order to provide access for European scientists to these modern instruments and associated laboratory infrastructure. User access is provided through application, which is peer-reviewed by an expert scientific advisory committee.^[10]

Following the first call for proposals in May 2011, six groups from France, Belgium and the UK were awarded access to the facilities and allotted time to use the spectrometers to conduct their projects. Research projects focus on characterization of nuclear materials, including exotic actinide superconductors, oxide nuclear fuels, waste forms and complexes related to separation chemistry. At KIT-INE the emphasis within the EURACT-NMR project is placed on separation chemistry and related topics, as well as on fundamental research on actinide behavior in solution. Collaborations with groups from Manchester (UK) and Liège (Belgium) have already been established and work commences in 2012.

Acknowledgements:

This work is supported by the German Federal Ministry of Education and Research (BMBF) under contract numbers 02NUK012A and 02NUK012D.

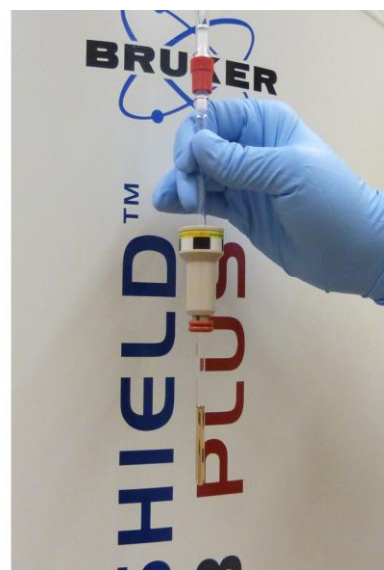
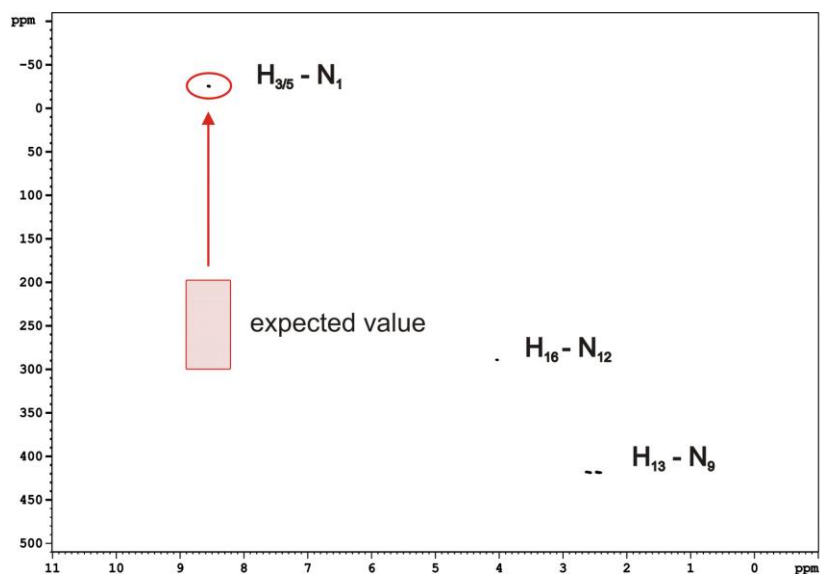


Fig. 2: left: Fully assigned ^1H , ^{15}N -HMQC showing three of four possible ^{15}N resonances. The missing resonance is not accessible by magnetization transfer via J-couplings. The expected value range for pyridine nitrogen is indicated. The exceptional ^{15}N chemical shift is the first significant difference in coordination/electronic structure measured for 1:3 BTP complexes of An(III) and Ln(III). right: the Am(III) NMR sample in a J. Young tube in front of the magnet prior to measurement.

References

- [1] W. D. Knight, *Phys Rev* **1949**, *76*, 1259-1260 (1949).
- [2] R. von Ammon, R. D. Fischer, *Angewandte Chemie* **1972**, *84*, 737-755 (1972).
- [3] S. Di Pietro, S. L. Piano, L. Di Bari, *Coordin Chem Rev*, *255*, 2810-2820 (2011).
- [4] A. G. Martynov, Y. G. Gorbunova, A. Y. Tsivadze, *Dalton Transactions*, *40*, 7165-7171 (2011).
- [5] B. Bleaney, *Journal of Magnetic Resonance (1969)*, *8*, 91-100 (1972).
- [6] G. Pintacuda, M. John, X.-C. Su, G. Otting, *Accounts of Chemical Research*, *40*, 206-212 (2007).
- [7] W.T. Carnall and H.M. Crosswhite, *A.N.L. Report*, 84-90 (1984).
- [8] J. F. Desreux, C. N. Reilley, *Journal of the American Chemical Society*, *98*, 2105-2109 (1976).
- [9] a) P. A. M. Dirac, *Proc. R. Soc. London, Ser. A* 1929, *123*, 714-733; b) J. C. Slater, *Phys. Rev.* 1951, *81*, 385-390; c) S. H. Vosko, L. Wilk, M. Nusair, *Can. J. Phys.* 1980, *58*, 1200-1211; d) J. P. Perdew, *Phys. Rev. B* 1986, *33*, 8822-8824; e) A. D. Becke, *Phys. Rev. A* 1988, *38*, 3098-3100; f) K. Eichkorn, O. Treutler, H. Öhm, M. Häser, R. Ahlrichs, *Chem. Phys. Lett.* 1995, *242*, 283-290; Erratum: K. Eichkorn, O. Treutler, H. Öhm, M. Häser, R. Ahlrichs, *Chem. Phys. Lett.* 1995, *242*, 652; g) K. Eichkorn, F. Weigend, O. Treutler, R. Ahlrichs, *Theor. Chim. Acta* 1997, *97*, 119-124; h) TURBOMOLE V6.0, TURBOMOLE GmbH Karlsruhe,; <http://www.turbomole.com>. 2009.
- [10] more information about the EURACT-NMR program and application forms can be found on <http://www.euract-nmr.eu>

9.5 Computational chemistry

B. Schimmelpfennig, R. Polly, M. Trumm, T. Rabung, F. Heberling, Th. Stumpf

Introduction

Since its introduction into the research portfolio at INE, computational chemistry has been used as a predicting and supporting tool in various different research areas such as studying chemical and physical properties of mineral surfaces, extraction chemistry, studies of oxo-hydroxo systems ranging in size from small solution species to nano-particles and other aspects of actinide solution behavior.

Describing actinide elements by means of quantum theory is non-trivial. The main obstacles are not the important relativistic effects but rather the complicated couplings in the open 5f-shell, which require a balanced description of electron-electron correlation beyond the mean-field approach. We routinely apply Density Functional Theory (DFT), but try to assess the accuracy of this approach by comparing results with high-quality wave-function-based ab initio methods such as Møller Plesset perturbation theory (MP2) and Coupled Cluster Singles Doubles with triple corrections (CCSD(T)). Where good agreement with experimental data is found, we are able to provide important additional information such as structural parameters or reaction energies, which are experimentally not accessible.

There is a wide range of computational tools available at INE, including ab initio methods and DFT, which treat the electrons explicitly, more approximate classical Monte Carlo (MC) simulations and Molecular Dynamics (MD) based on classical mechanics. The main results applying these tools to specific research activities at INE over the past year are described in the following.

Theoretical study of sorption and incorporation of trivalent lanthanides and actinides at mineral surfaces

The sorption and incorporation of metal ions at mineral surfaces is an important process which leads to the retention/retardation of radionuclides such as actinide ions and fission products. Accordingly, reliable long-term prediction of actinide migration in geological formations requires understanding of the adsorption/desorption and incorporation mechanisms at a molecular level. Hence, this issue is of crucial importance for long term safety assessment of nuclear waste disposal.

Sorption of La^{3+} , Eu^{3+} and Cm^{3+} at the corundum (001)/water interface

We have previously studied the structure of inner-sphere trivalent actinide and lanthanide ion complexes at the corundum (001) [1,2] and (110) surfaces [3,4] using the cluster model ansatz and orbital based methods of theoretical chemistry with success. This work helped improve understanding of sorption processes at the corundum (001) and (110) surfaces.

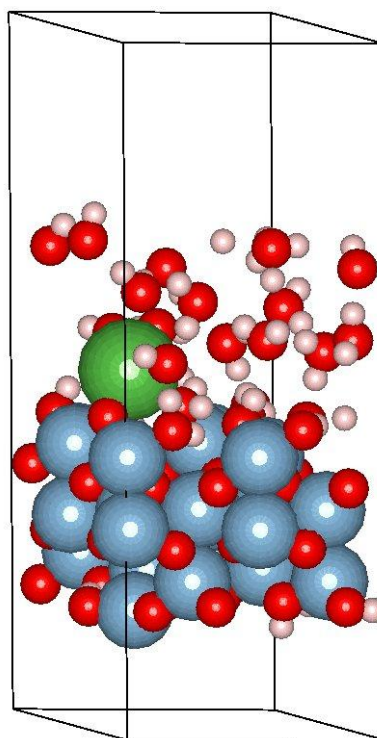


Fig. 1: Unit cell in the study of the inner sphere complexes of trivalent actinide and lanthanide ions at the corundum (001)/water interface. Blue spheres: aluminum, red spheres: oxygen, white spheres: hydrogen, green sphere: metal ion.

To augment these studies, we began investigations of the same systems using plane wave DFT with periodic boundary conditions (PBC), as implemented in the Vienna ab initio simulation package (VASP). This allows us to improve on theoretical information from the cluster calculations and refine understanding of the sorption of trivalent lanthanides and actinides from a different point of view.

Both strategies, cluster calculations and calculations using PBC, have their advantages and disadvantages. Cluster calculations suffer from boundary and cluster size effects but allow application of all standard ab initio methods such as MP2 and CCSD(T). Calculations using PBC formally allow a

correct theoretical description of solids and mineral surfaces but are restricted to DFT only.

At the corundum (001) surface we studied inner-sphere complexes as a function of the degree of deprotonation of the aluminol groups at the surface (see Fig. 1). We used a four layer (O-Al-O) slab with all dangling bonds of the oxygens saturated with hydrogen atoms as the corundum surface model. Three protons from the oxygen atoms were removed at the bottom of the cluster (slab), in order to have a neutral unit cell. One, two or three protons were removed from the surface located directly below the metal ion in the studies of the inner-sphere surface complexes. These protons were in turn added to the bottom of the cluster, where the three oxygen atoms were initially deprotonated to ensure a neutral unit cell. This surface model was completed by the metal ion with six ligating water molecules in the first coordination shell and seven additional water molecules representing interfacial water.

We determined the most likely structure of the inner sphere complex and found in agreement with our earlier study [2] that only one aluminol group located directly below the sorbed ion at the surface is deprotonated. Metal ion – oxygen bond lengths were also determined. We obtained an average value of 233 pm for the metal ion – surface oxygen bond length and 278 pm for the metal ion – water oxygen bond length. Using the cluster model, we found 267 and 261 pm for these distances, respectively. Thus the different approaches yield significantly different inner-sphere complex structures.

Future studies employing the cluster model ansatz and high level ab initio methods along with DFT calculations using PBC will be performed, which will give us a better understanding of the systematic errors associated with different theoretical approaches for metal ion – oxygen bond length determinations in these systems.

The DFT calculations employing PBC were carried out with the plane wave DFT program VASP.

Interaction of selenite with the hydrated calcite (104) surface

Se-79 is a fission product of U-235 with a long radioactive half-life of 1.1×10^6 years. Selenite (SeO_3^{2-}) and selenate (SeO_4^{2-}) as anions interact only weakly with common mineral surfaces. Therefore they have been identified as crucial fission product species for long term safety of disposed nuclear waste.

We initially studied the calcite (104)/water interface (Fig. 2). Different surface models with varying slab thicknesses were investigated, to ensure a sound theoretical description.

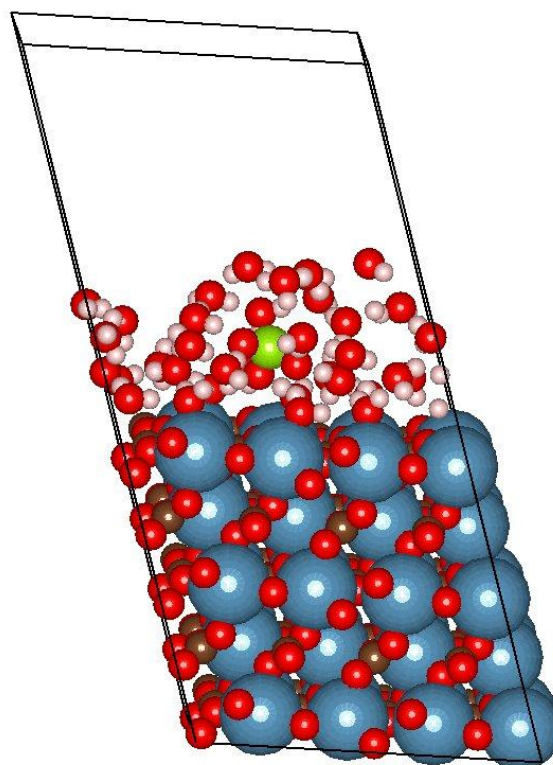


Fig. 2: Unit cell of the study of outer sphere complexes of selenite the hydrated calcite (104) surface. Blue spheres: calcium, red spheres: oxygen, white spheres: hydrogen, green sphere: selenium.

We found two water layers above the surface, with the water molecules sitting on top of either the Ca^{2+} ions or the CO_3^{2-} groups. The average distances of these two water layers to the surface were found to be 242 and 317 pm, which is in a very good agreement with experimental values of 235 and 324 pm [5], respectively.

We then used this calcite (104)/water interface model system to further study surface sorbed and incorporated selenite species. We studied outer sphere complexes of selenite and found the metal atom located 490 pm above the surface with nine water molecules in the first coordination shell. The average Se-O bonds of selenite were observed to be 173 pm. This is only marginally different from the Se-O bond length in the gas phase case or with the case including one hydration shell of water, 176 pm. The average distance between water molecule oxygen atoms and selenium was 393 pm. Incorporation of selenite into the first layer of the calcite surface was investigated (Fig. 3), with selenite ions replacing carbonate ions. Incorporation is another retention mechanism potentially hindering transport of radionuclides in ground water. Selenite has no planar structure, as the carbonate ion has, and hence the Se atom added to the layer is found protruding more towards the surface, compared to the C atom positions.

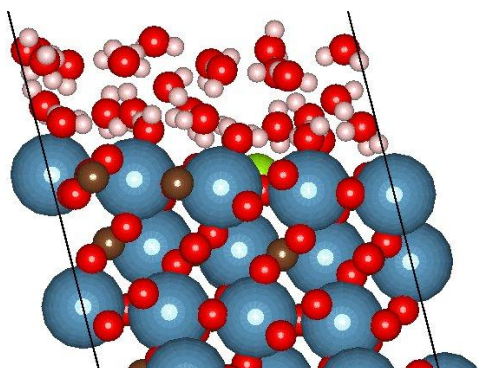


Fig. 3: Incorporation of selenite into the calcite (104) surface. Blue spheres: calcium, red spheres: oxygen, brown spheres: carbon, white spheres: hydrogen, green sphere: selenium.

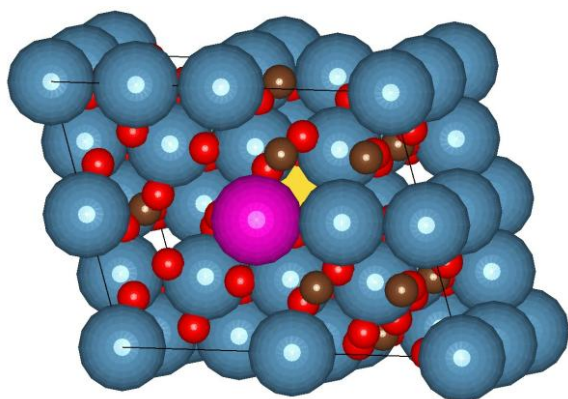


Fig. 4: Incorporation of trivalent lanthanide and actinide ions into the calcite structure. Two Ca^{2+} ions are replaced by one $\text{Ln}^{3+}/\text{An}^{3+}$ and one Na^+ . Blue spheres: calcium, red spheres: oxygen, brown spheres: carbon, yellow sphere: sodium, pink sphere: trivalent lanthanide or actinide ion.

These calculations were carried out with the plane wave DFT program VASP.

Incorporation of La^{3+} , Eu^{3+} and Cm^{3+} into calcite

We also studied the incorporation of La^{3+} , Eu^{3+} and Cm^{3+} into calcite by replacing two calcium ions Ca^{2+} by one trivalent lanthanide or actinide ion and one sodium atom to achieve charge neutrality. The resulting structures were optimized with DFT employing PBC (Fig. 4). The most likely relative position of the substituting ions were determined, along with the stability of the resulting structure. We found that the shape of the unit cell hardly changed in the incorporation model (replacing two Ca^{2+} ions by one $\text{Ln}^{3+}/\text{An}^{3+}$ and one Na^+). The observed changes of unit vectors of the unit cell are only around 0.1%.

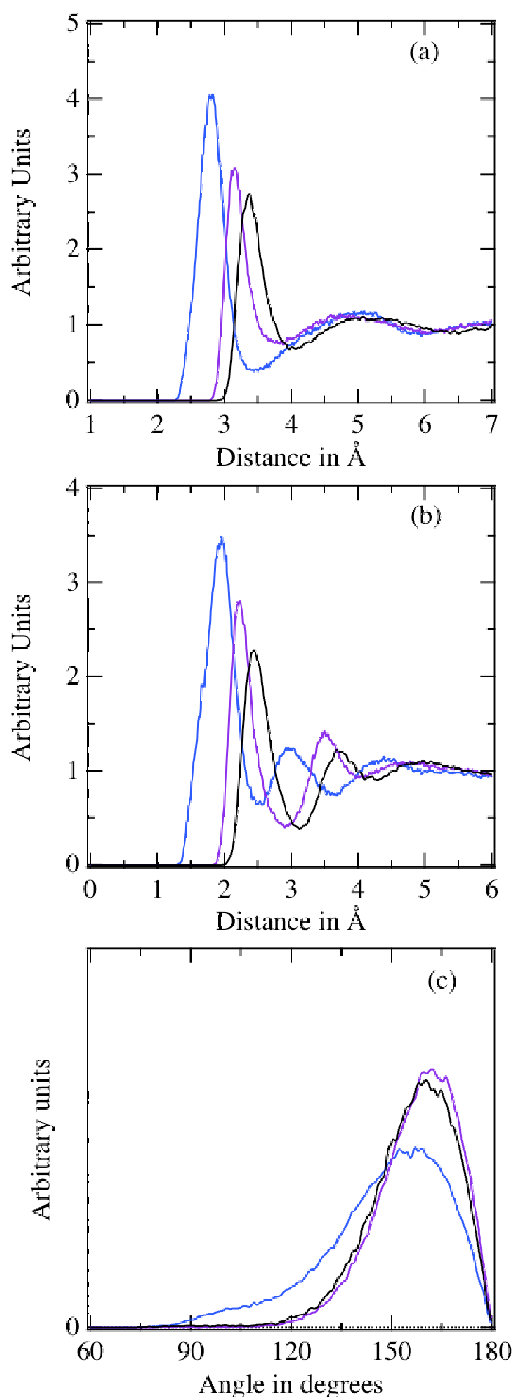


Fig. 5: Radial distribution functions corresponding to the anion/water-oxygen (a) and the anion/water-hydrogen (b) distances, as well as the $\text{X} \dots \text{H-O}$ angular distribution function (c). The blue, violet, and black lines refer to F^- , Cl^- and Br^- , respectively.

Molecular Dynamics for actinide complexes in aqueous solution

Detailed understanding of actinide complexes in solution, including dynamic processes, has been a key-topic of the theoretical work in the past year. In close international collaboration with groups in France (Lille and CEA-Saclay), we have developed a new ansatz to parameterize the actinide – water interaction

potential, including non-additive charge-transfer terms. These force fields are implemented in the POLARIS MD-software package. A wide range of data, which is directly comparable to experiment, can be extracted from the trajectories, including

- coordination numbers,
- structural parameters,
- Gibbs Free energies,
- exchange rates and mechanisms,
- activation volumina,
- thermo-dynamic properties and
- diffusion coefficients.

EXAFS spectra can be simulated from the structural parameters and coordination numbers by interfacing to the FEFF software [6]; Debye-Waller factors can be extracted from the statistical average over the MD sampling period. An overview of the technical work can be found in the doctoral thesis of Michael Trumm [7].

In our investigations, major focus was put on the description of anions, esp. the halides in solution [8], as they are possible counter ions in the environment. Structures for halide-water complexes were optimized at the MP2-level using basis sets of aug-cc-pVTZ quality and used as reference data. Energies were obtained, where computationally feasible, at the CCSD(T) level. Radial and angular distribution functions were obtained (Fig. 5), which allow detailed comparison of F^- , Cl^- and Br^- . The number of water molecules in the first coordination sphere was found to vary over a large range, with the distribution becoming broader for the heavier halides (Fig 6).

Quantification of the mean residence time of a water molecule in the first coordination shell was also obtained from the trajectories and are of interest, as this is sensitive to barriers for exchange processes. Fig. 7 graphically depicts how the bond length time correlation function is used for this purpose. We obtained 28.1, 11.8, and 10.4 ps for F^- , Cl^- and Br^- , respectively, which is fully in line with published literature [9].

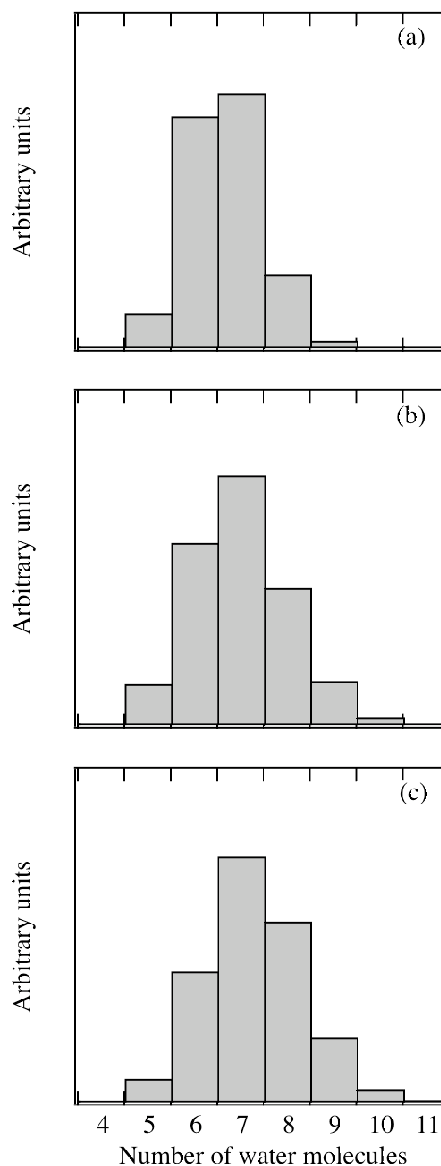


Fig. 6: Relative abundance of the anion hydrated clusters in liquid water. (a) : F^- , (b) : Cl^- and (c) Br^- :

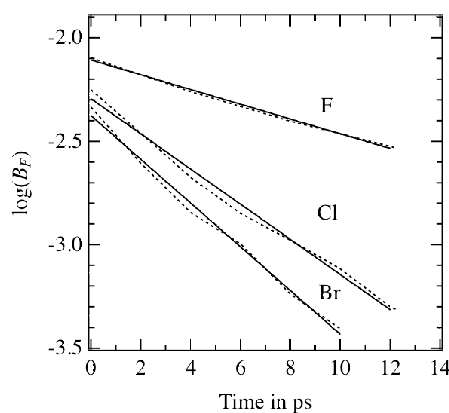


Fig. 7: Logarithm of the bond length time correlation function B_F versus time. The slope is reciprocal to the mean residence time.

References

- [1] R. Polly, B. Schimmelpfennig, M. Flörsheimer, K. Kruse, A. AbDelMonem, R. Klenze, G. Rauhut and T. Fanghänel, *J. Chem. Phys.* 130(6), 064702 (2009).
- [2] R. Polly, B. Schimmelpfennig, T. Rabung, M. Flörsheimer, R. Klenze and H. Geckeis, *Radiochim. Acta* 98, 627 (2010).
- [3] R. Polly, B. Schimmelpfennig, M. Flörsheimer, R. Klenze and H. Geckeis, in preparation.
- [4] R. Polly, B. Schimmelpfennig, T. Rabung, M. Flörsheimer, T. Rabung, T. Kupcik, R. Klenze and H. Geckeis, in preparation.
- [5] F. Heberling, T. P. Trainor, J. Lützenkirchen, P. Eng, M. A. Denecke, D. Bosbach, *JCIS* 354, 843 (2011).
- [6] J. J. Rehr, R. C. Albers, *Rev. Mod. Phys.* 72, 621 (2000).
- [7] „Molekulardynamische und quantenchemische Rechnungen an wässrigen Actinidkomplexen“, M. Trumm, Doktorarbeit, Naturwissenschaftlich-Mathematische Fakultät, Ruprecht-Karls Universität Heidelberg (2011).
- [8] M. Trumm, Y. O. Guerrero Martínez, F. Réal, M. Masella, V. Vallet, and B. Schimmelpfennig, *J. Chem. Phys.* 136, 044509 (2012).
- [9] S. Koneshan, J. C. Rasaiah, R. M. Lynden-Bell, S. H. Lee, *J. Phys. Chem. B* 102, 211 (2004).

10. Radiation protection research

B. Breustedt, P. Panak, F. Becker, A. Benzler, C. Blunck, B. Heide, W. Klein, D. Leone, O. Marzocchi, S. Poelz, G. Zhang

Introduction

Radiation Protection Research at INE is focusing on assessing radiation exposures by estimation of doses either from external radiation fields or from intakes of radionuclides. Besides measurements, the modeling and simulation of radiation fields and their interaction with tissues of the human body or detectors measuring the field are the techniques applied in the work of the group. Basic vision of the work is to provide techniques and models for an individualized dosimetry, which goes beyond the current approach of applying reference models in the dose assessments. The exposed individual with his or her anatomical and physiological properties as well as the radiation fields – properly characterized – are taken into account in an individualized dosimetry. In 2011 we focused on three main topics

- Dosimetry in external radiation fields
- Dosimetry after intakes of radionuclides
- Modeling and Simulation of Radiation Protection Scenarios

The ASF group is collaborating with national and international partners in several research projects funded by BmBF (e.g. Projects “Strahlung und Umwelt” in Competence Alliance Radiation Research KVSF) or EC (e.g. Project “BOOSTER” in FP7Sec). Our group is also engaged in the European Radiation Dosimetry Group (EURADOS e.V., <http://www.eurados.org>). In different working groups EURADOS promotes and develops research and European Collaboration in radiation dosimetry. INE-ASF is actively participating in the working groups:

- WG6 computational dosimetry,
- WG7 internal dosimetry and
- WG12 European Medical ALARA Network.

Selected results from the 2011 work of the radiation protection research group at INE are reported in this chapter.

Dosimetry in external radiation fields

Simulation supported dosimetry is a main topic of the external dosimetry at KIT. This approach is mainly employed for cases where measurements are difficult or not feasible. This includes the performance of Albedo dosimeters in a

radiation field of an interim storage facility: Monte Carlo simulations yield the spectra and the dose rate distributions [2].

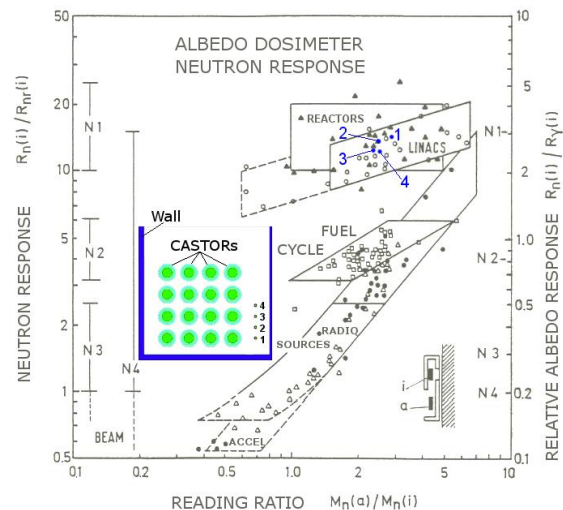


Fig. 1: Classification of the response of an Albedo dosimeter for four different neutron field positions – see numbers 1 to 4 in the interim storage model [1]

Based on the simulation results, classifications could be made without complex series of measurements. For a representative radiation field in an interim storage facility, 16 CASTORs and 4 dosimeter positions have been considered. The four simulation results together with the application ranges for Albedo dosimeters in different neutron fields are shown in Fig. 1. The simulation results show that the calibration factor N1 for reactors and linacs fits to the neutron field of the investigated interim storage facility.

Simulation of Track detectors

Similarly, the response in a Cf-252 neutron radiation field for a Makrofol track detector was investigated. Such detectors can detect fast neutrons by recording neutron-induced heavy recoils. Based on our investigation [3], the response of track detectors to fast neutrons is dependent on the angle of incident neutrons. The angular dependence of neutron dosimeter extremely affects the accuracy of dose measurements. Therefore the geometry of track detector based neutron dosimeters needs to be well designed to reduce the angular dependence. In this work different shapes, such as tetrahedron, pyramid and cube, have been tested. These shapes, as displayed in Fig. 2, fulfill also the constraint of easy manufacturing.

As a result, the tetrahedron dosimeter shows a flatter angular response than the others.

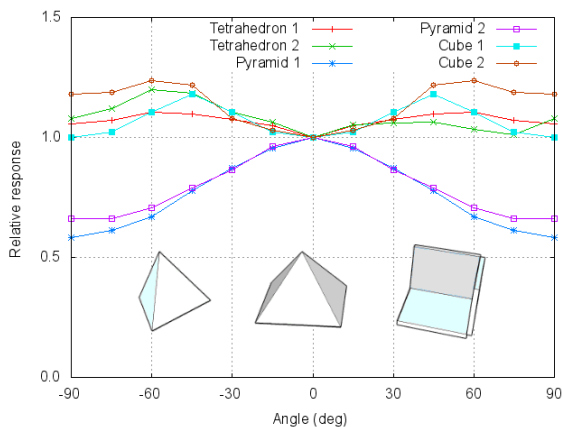


Fig. 2: Angular response of different dosimeters.

Dosimetry for handling of Beta emitters

Simulations are also important to assess the handling of open radionuclides as for example in nuclear medicine. Mixed beta and photon radiation fields of high local dose rate can occur, in particular near the source. Large local inhomogeneous distributed skin doses are hard to quantify by measurements. Over the last few years a method was developed to model such handling scenarios based on the information of images taken by a multi camera system. Subsequent simulations with a Monte-Carlo code like MCNPX reveals the corresponding information for radiation protection purpose. With the code radiation exposure scenarios can be modeled geometrically and simulated with radiation transport calculations. With this method the radiation fields and the potentially occurring partial body dose can be analyzed in detail.

The method was tested for the first time in the clinic of nuclear medicine of the St. Vincentius-Kliniken gAG Karlsruhe. Examples for simulations of local distribution of doses $H_P(0.07)$ and corresponding dose rates across the hand e.g. during the injection of Y-90 during a nuclear medicine therapy application are displayed in figures 3 and 4.

It is promising that the method can become a useful tool for analyzing operation procedures with respect of radiation protection assessments without the need of disturbing and complex measurements.

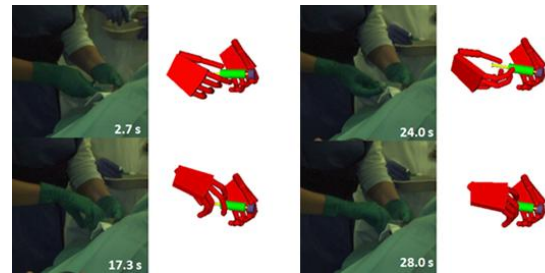


Fig. 3: Four different snapshots of an Y-90 injection procedure together with the geometrical model for the simulation.

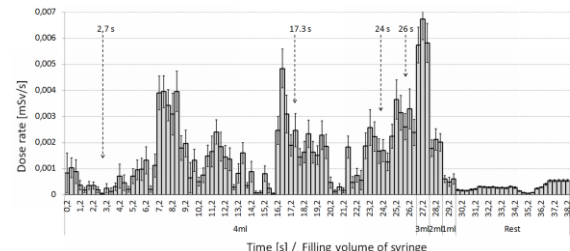


Fig. 4: Dose rate $dH_P(0.07)/dt$ at distal phalange of the middle finger at the outer side of the right hand against the time of handling for the therapy application (190 MBq Y-90). The corresponding exposure scenarios for the moments at 2.7 s, 17.3 s, 24 s, 26 s are shown in figure 3.

Dosimetry after intakes of radionuclides

If radionuclides are incorporated they follow the metabolic processes foreseen for the according element or chemical analogues. The result is a distribution inside the body with accumulation in selected organs (e.g. in the thyroid for isotopes of iodine) and the following excretion via feces or urine. The radiation dose deposited following the decay inside the body cannot be measured directly, because it is delivered over long periods of time and a dosimeter cannot be placed inside the body. Thus the only way to assess the dose due to an intake of radionuclides is the monitoring of activities (either directly inside the body – in-vivo, or indirectly by measuring excreted activities – in-vitro) followed by a modeling of the biokinetic behavior of the nuclide.

In-vivo monitoring

The installation of the newly developed whole and partial body counter [4] in the in-vivo monitoring laboratory at KSM was finished in the end of 2010. Figure 5 shows the final setup in a whole body configuration with four HPGe-detectors.

In 2011 tests, the fine tuning of the setup and calibration measurements were the main task. Accurate modeling of the detectors was performed, including a determination of the dead

layer thicknesses of the individual detectors [5].

Some routine measurements with measurable activities were repeated with the new counter for validation purposes. The results of all validation measurements were in good agreement. After the incidents in Fukushima, the in-vivo monitoring laboratory was counting several persons returning from Japan.



Fig. 5: The in-vivo counter at KSM-IVM in a whole body counting geometry

This provided another opportunity to validate the “new” counter by comparing the measurements with the “old” body counter with NaI(Tl) detectors. Only two of the approx. 30 persons measured in the lab, were slightly contaminated. The results for the highest contamination are given in Table 1 below. As expected only fission products were identified. A dosimetric evaluation was done using the conversion factors provided by the Federal Office for Radiation Protection (BfS), which gave an effective dose of 0.1mSv, i.e. ~5% of the natural dose in Germany.

Tab. 1: Measured activities in a Person returning from Japan 6 days after the Fukushima incident

Nuclide	Activity [Bq]
I-131	725 +- 58
I-132	80 +- 16
Te-132	163 +- 40
Cs-134	50 +- 12
Cs-137	75 +-11

The results of the measurements are promising; the minimum detectable activities and the efficiency factors estimated by the simulations are confirmed by the measurements. As soon as the software development for the automated use of the counter is finished, the new machine will be included in the quality management system of the in-vivo monitoring laboratory and routine use will be started.

Biokinetic modeling

Models describing the biokinetic behavior are usually applying compartmental formalism. The structures of a model depict the relevant parts of the human body involved in the radionuclides metabolism, while the parameters (transfer coefficients) describe the velocities of the processes. Models describing the biokinetic behavior for a reference person are published by the International Commission on Radiological Protection. The parameter values are selected to describe an average behavior, uncertainties of the values are usually not provided. However it's reasonable that the biokinetic processes of an (healthy) individual will follow the same structure than the reference person, while the velocities of the single processes depicted by the transfer coefficients might be different from the reference. Using distributions of parameter values instead of fixed values the uncertainty of the models can be studied using a Monte Carlo Approach. The techniques developed in ASF [6] were applied to several models of plutonium biokinetics before. In 2011 a quality assurance with the results of the group in the Helmholtzzentrum München has been performed and the INE method was applied to a new model on Zirconium biokinetics based on real measurement data [7]. As can be seen on the following figure 6 the observed results can be reproduced assuming an overall parameter variation with a cv-value of 20%.

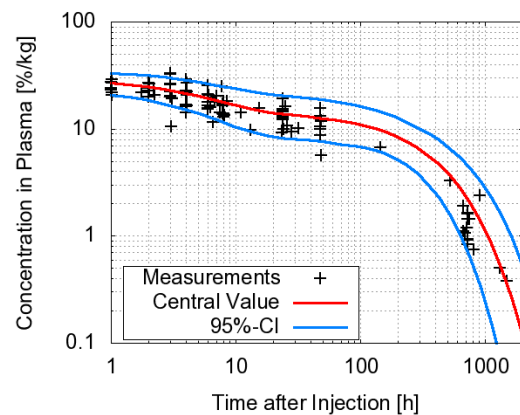


Fig. 6: Estimation of a confidence interval for the concentration of Zr in Plasma.

The studies on uncertainties will continue within the framework of EURADOS Working group 7.

The second topic investigated by the biokinetic modeling group is the development of a model describing the effect of decorporation therapy with DTPA [8]. In 2011 data from an Am-241 inhalation case of the United States Uranium and Transuranium Registries (USTUR) have been compiled and a first analysis of the initial incorporation scenario was begun. The main problem in analyzing this case is that the intake was detected in a routine test in the 1960's with no information about possible incidents with acute intakes are available. As a first step for defining an intake scenario several possible patterns of intake - based on the original information available in USTUR's files - have been calculated and compared to the few pre-therapy data points available. A mix of some acute intake events seems to be more plausible than a constant chronic intake over the working period.

Modeling and Simulation of radiation protection scenarios

In order to perform Monte Carlo simulations of radiation protection scenarios these need to be modeled, e.g. the geometry and the properties of the relevant material need to be defined. Software supporting this process has been developed and several different scenarios from the fields of internal and external dosimetry were modeled and simulated in 2011.

Model of detectors and their validation

The already existing models of the HPGe detectors operating in the body counter [4] are being optimized via systematic comparisons between measurements and simulations. An agreement within 5% was the goal and has been reached for two of the four detectors. The models of the other two detectors will be optimized in 2012.

A similar work has been carried out within the Working Group 6 of EURADOS. The action concerning the intercomparison of Monte Carlo lung counting [9] planned also a comparison between simulation and measurements performed in the partial body counter of CIEMAT in Madrid (Spain). A scenario maximizing the efficiency was set up using a Livermore phantom and measurements using two uranium-contaminated lungs have been performed (figure 7). Model of the four detectors and the voxel model of the Livermore phantom were provided from the organizers of the intercomparison. Simulations with MCNPX were run in the same configuration as the measure-

ments and comparisons have been carried out. Loading separately the two lungs and looking individually at the four detectors, in some cases (each lung is measured from one of the four detectors) an agreement between measurements and simulations up to some per-cent have been observed.

The cases showing discrepancies have been justified with a bad relative positioning detector-phantom or with a bad model of the detectors. Further studies, with the collaboration of the in-vivo monitoring laboratory at KSM are planned.

Voxel2MCNP

To support and improve the processes concerned with numerical efficiency calibration, e.g. phantom management, detector positioning, calculation of anthropometric parameters and generation of input files for Monte Carlo simulations, an abstract model was created to describe nearly all aspects involved in this field. This model was implemented as the kernel of the software tool *Voxel2MCNP* [10].



Fig. 7: Measurement setup of the Livermore phantom performed in CIEMAT.

As an ongoing effort, several plugins are being developed to extend its functionalities to other areas like external radiation fields and dose assessment with biokinetic models. Another example is the calculation of dose conversion factors for internal and external dosimetry scenarios. Using published values in [11], the method for calculating dose conversion factors has been successfully validated [12].

Anatomic features and efficiencies

Two studies to quantify the influence of anatomic features on (numerical) efficiency calibration were conducted using *Voxel2MCNP*.

First, six phantoms implementing the ICRP reference man and woman [13] were com-

pared for lung and liver counting scenarios [14]. Detectors were positioned semi-automatically to improve reproducibility. A visual comparison shows large variations in anatomy resulting in different lung and liver shapes and positions. This is also visible in the computed counting efficiencies.

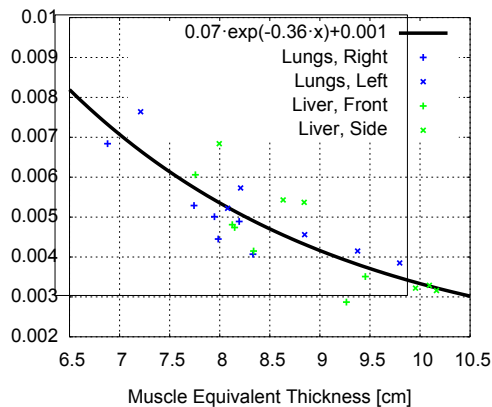


Fig. 8: Calculated counting efficiencies for different detector positions with corresponding effective wall thicknesses for all six phantoms.

To explain these variations several anthropometric parameters were computed. Among those, the effective (chest) wall thicknesses at the different detector positions show a good correlation with individual counting efficiency (Figure 8), but cannot explain all observed variations.

Second, a phantom with respiratory motion was reconstructed from medical 4D CT imaging data [15]. Two lung counting setups were created: the breathing phantom and the phantom fixed at maximum inhalation. A comparison of counting efficiencies shows an underestimation of about 1.5% using the fixed phantom (Figure 8), which results in a slight overestimation of incorporated activity. The error of the interactive segmentation was estimated to be at least 5.8%, which is the relative standard deviation of the segmented bone volume over all time frames of the 4D CT data.

References

[1] G. Zhang, Monte Carlo Simulation of Mixed Neutron-Gamma Radiation Fields and Dosimetry Devices, PhD Dissertation, Karlsruhe Institute of Technology (2011).
 [2] F. Becker, R. Fritschek, G. Zhang, S. Prys, Numerische Simulation von Strahlenfeldern in einem Zwischenlager für Brennelemente, Institut für Strahlenforschung, Jahresbericht (2009).

[3] G. Zhang, F. Becker, M. Urban, Y. Xuan, M. Fürstner, S. Mayer, Radiation Measurements, 46, 405-408 (2011).

[4] O. Marzocchi, Design and Setup of a New HPGe Detector Based Body Counter Capable of Detecting Also Low Energy Emitters, PhD Dissertation, Università di Bologna (2011).

[5] A. Elanique, O. Marzocchi, D. Leone, L. Hegenbart, B. Breustedt, L. Oufni, Applied Radiation and Isotopes, 70(3), 538-542 (2012).

[6] W. Klein, B. Breustedt, M. Urban, Health Physics, 99(4), 577-580 (2010).

[7] M. Greiter, Study of the biokinetics of zirconium isotopes in humans and its relevance to internal dosimetry. PhD Dissertation, TU München (2008).

[8] B. Breustedt, E. Blanchardon, P. Berard, P. Fritsch, A. Giussani, M.A. Lopez, A. Luciani, D. Nosske, J. Piechowski, J. Schimmelpfeng, A-L. Seandour. Health Physics, 99(4), 547-552 (2010).

[9] D. Broggio et al. Submitted to Radiation Measurements (2011).

[10] L. Hegenbart, S. Pölz, A. Benzler, M. Urban, Health Physics, 102(2), 221-229 (2012).

[11] Annals of the ICRP, 39 (2009).

[12] A. Häußler, Routinetaugliche numerische Ermittlung von Dosis-Umrechnungsfaktoren mit Voxelmodellen, Bachelorarbeit, Duale Hochschule Baden-Württemberg, Karlsruhe, (2011).

[13] Annals of the ICRP, 32(3-4).

[14] S. Pölz, The 3rd International Workshop on Computational Phantoms for Radiation Protection, Imaging and Radiotherapy, Beijing, China, August 8-9 (2011).

[15] T. Schneider, Auswirkung der Atembewegung auf die Zähleffizienz von in vivo Messsystemen bei Lungenteilmessungen. Bachelorarbeit, Duale Hochschule Baden-Württemberg Karlsruhe.

11 Publications

Papers in books and peer reviewed journals

ADEKOLA, F.; FEDOROFF, M.; GECKEIS, H.; KUPCIK, T.; LEFEVRE, G.; LÜTZENKIRCHEN, J.; PLASCHKE, M.; PREOCANIN, T.; RABUNG, T.; SCHILD, D.

Characterization of acid-base properties of two gibbsite samples in the context of literature results.

Journal of Colloid and Interface Science, 354 (2011) 306-317.

BECKER, F.; BLUNCK, CH.

Investigation of radiation exposure of medical staff: Measurements supported by simulations with an articulated hand phantom

Radiation Measurements, 46 (2011) 1299-1302.

BELLONI, F., HIMBERT, J., MARZOCCHI, O., ROMANELLO, V.

Investigating incorporation and distribution of radionuclides in trinitite Journal of Environmental Radioactivity, 102 (9) (2011) 852-862.

BLUNCK, CH., BECKER, F., URBAN M.

Simulation of beta radiator handling procedures in nuclear medicine by means of a movable hand phantom

Radiation Prot Dosimetry, 144 (2011) 497-500.

BOURG, S.; HILL, C.; CARAVACA, C.; RHODES, C.; EKBERG, C.; TAYLOR, R.; GEIST, A.; MODOLO, G.; CASSAYRE, L.; MALMBECK, R.; HARRISON, M.; DE ANGELIS, G.; ESPARTERO, A.G.; BOUVET, S.; OUVRIER, N.

ACSEPT—Partitioning technologies and actinide science: Towards pilot facilities in Europe.

Nuclear Engineering and Design, 241 (2011) 3427– 3435.

BOUBY, M., GECKEIS, H.

Characterization of Colloid-Borne Actinides by Flow Field Flow Fractionation (FIFFF) Multidetector Analysis (MDA)

in KALMYKOV, S., DENECKE, M.A. (EDS.)

Actinide Nanoparticle Research, Springer Verlag Heidelberg, (2011) 105-136.

BOUBY, M; GECKEIS, H; LUTZENKIRCHEN, J; MIHAI, S.; SCHAEFER, T.

Interaction of bentonite colloids with Cs, Eu, Th and U in presence of humic acid: A flow field-flow fractionation study

Geochimica Cosmochimica Acta, 75 (2011) 3866-3880.

BREUSTEDT B., MOHR U., BIEGARD N., CORDES G.

Quality management system and accreditation of the in-vivo monitoring laboratory at Karlsruhe Institute of Technology

Radiation Prot Dosimetry, 144 (2011) 95-97.

CHRISTIANSEN, B.C.; GECKEIS, H.; MARQUARDT, C.M.; BAUER, A.; RÖMER, J.; WISS, T.; SCHILD, D.; STIPP, S.L.S.

Neptunyl (NpO_2^+) interaction with green rust, $\text{GR}_{\text{Na},\text{SO}_4}$

Geochim. Cosmochim. Acta, 75 (2011) 1216-1226.

CLARET, F.; TOURNASSAT, C.; CROUZET, C.; GAUCHER, E.C.; SCHÄFER, T.; BRAIBANT, G.; GUYONNET, D.

Metal speciation in landfill leachates with a focus on the influence of organic matter.

Waste Management, 31(9-10) (2011) 2036-2045.

DENECKE, M.A., DE NOLF, W., RACK, A., TUCOULOU, T., VITTOVA, T., FALKENBERG, G., ABOLHASSANI, S., CLOETENS, P., KIENZLER, B.

Speciation of Actinides in Granite Subjected to Tracer Studies.

in KALMYKOV, S., DENECKE, M.A. (EDS.)

Actinide Nanoparticle Research, Springer Verlag Heidelberg, (2011) 413–436.

DILLMANN, I.; COQUARD, L.; DOMINGO-PARDO, C.; KÄPPELER, F.; MARGANIEC, J.; UBERSEDER, E.; GIESEN, U.; HEISKE, A.; FEINBERG, G.; HENTSCHEL, D.; HILPP, S.; LEISTE, H.; RAUSCHER, T.; THIELEMANN, F.K.

Cross sections for proton-induced reactions on Pd isotopes at energies relevant for the g process.

Physical Review C, 84 (2011) 015802/1-11.

GECKEIS, H., RABUNG, T., SCHÄFER, T.

Actinide Nanoparticle Interaction: Generation, Stability and Mobility

in KALMYKOV, S., DENECKE, M.A. (EDS.)

Actinide Nanoparticle Research, Springer Verlag Heidelberg, (2011) 1–30.

HARTMANN, E.; BRENDEBACH, B.; POLLY, R.; GECKEIS, H.; STUMPF, T.

Characterization and quantification of Sm(III)/ and Cm(III)/clay mineral outer-sphere species by TRLFS in D₂O and EXAFS studies.

Journal of Colloid and Interface Science, 353 (2011) 562-568.

HEBERLING, F.; TRAINOR, T. P.; LÜTZENKIRCHEN, J.; ENG, P.; DENECKE, M.A.; BOSBACH, D.

Structure and reactivity of the calcite(104) – water interface

Journal of Colloid and Interface Science, 354 (2011) 843-857.

HEBERLING, F.; SCHEINOST, A.C.; BOSBACH, D.

Formation of a ternary neptunyl(V) bicarbonato inner-sphere complex inhibits calcite growth rate,

Journal of Contaminant Hydrology, 124 (2011) 50-56.

HEGENBART L., BREUSTEDT B.,

A New Position Recording System for the Partial Body Counter at KIT

Radiation Prot Dosimetry, 144 (2011) 389-392.

JORDAN, N.; FOERSTENDORF, H.; WEIß, S.; HEIM, K.; SCHILD, D.; BRENDLER, V.

Sorption of selenium(VI) onto anatase: Macroscopic and microscopic characterization.

Geochim. Cosmochim. Acta, 75 (2011) 1519-1530.

KALLAY, K., PREOCANIN, T., KOVACEVIC, D., LÜTZENKIRCHEN, J., VILLALOBOS, M.

Thermodynamics of the Reactions at Solid/Liquid Interfaces.

Croatia Chemica Acta, 84 (2011) 1-10.

KALMYKOV, S., DENECKE, M.A. (EDS.)

Actinide Nanoparticle Research Springer Verlag Heidelberg, (2011).

KELM, M., METZ, V., BOHNERT, E., JANATA, E., BUBE, C.

Interaction of hydrogen with radiolysis products in NaCl solutions – comparing pulse radiolysis experiments with simulations.

Radiation Physics and Chemistry, 80 (2011) 426-43.

KIRSCH, R., FELLHAUER, D., ALTMAIER, M., NECK, V., ROSSBERG, A., FANGHÄNEL, TH., CHARLET, L., SCHEINOST, A.C.

Oxidation State and Local Structure of Plutonium Reacted with Magnetite, Mackinawite, and Chukanovite.

Environ. Sci. Technol., 45 (17) (2011) 7267–7274.

KÖNIG, S.; MÜNKER, C.; HOHL, S.; PAULICK, H.; BARTH, A.R.; LAGOS, M.; PFÄNDER, J.; BÜCHL, A.

The Earth's tungsten budget during mantle melting and crust formation.

Geochimica et Cosmochimica Acta, 75 (2011) 2119-2136.

- LEONE D., BREUSTEDT B.
Simulation of phoswich detectors using MCNPX and EGSnrc
Radiation Prot Dosimetry, 144 (2011) 402-406.
- LÜTZENKIRCHEN, J., VAN MALE, J., LEERMAKERS, F., SJÖBERG, S.
Comparison of Various Models to Describe the Charge-pH Dependence of Poly(acrylic acid)
J. Chem. Eng. Data, 56 (2011) 1602- 1612.
- LOPEZ M.A., BLANCHARDON E., BREUSTEDT B., BROGGIO D., CASTELLANI C.M., FRANCK D.,
GIUSSANI A., HURTGEN C., JAMES A.C., KRAMER G.H., MARSH J.W., NOBKE D., OEH U.,
SCHIMMELPFENG J., VRBA T.
EURADOS coordinated action on research, quality assurance and training of internal dose
assessments
Radiation Prot Dosimetry, 144 (2011) 349-352.
- MAGNANI, N.; APOSTOLIDIS C.; MORGENSTERN; A.; ET AL.
Magnetic Memory Effect in a Transuranic Mononuclear Complex
Angewandte Chemie International Edition, 50 (7) (2011) 1696-1698.
- MANDALIEV, P., STUMPF, T., TITS, J., DAEHN, R., WALTHER, C., WIELAND, E.
TRLFS and EXAFS study on the Eu(III) uptake by 11 Å tobermorite
Geochim. Cosmochim. Acta, 75 (2011) 2017-2029.
- MARZOCCHI O., BREUSTEDT B.
Theoretical assessment of whole body counting uncertainties using numerical phantoms of varying
sizes and sexes
Radiation Prot Dosimetry, 144 (2011) 339-343.
- MARZOCCHI, O., BREUSTEDT, B., MOSTACCI, D., URBAN, M
Comparison of stretched and sitting configurations for partial-body measurements.
Applied Radiation and Isotopes, 69 (8) (2011) 1156-1158.
- METZ, V., ROSENBERG, Y.O., BOSBACH, D., BÖTTLE, M., GANOR, J.
Formation of (Ba,Ra)SO₄ solid solutions – results from barite (re)precipitation and coprecipitation
experiments. In B. Merkel, M. Schipek (eds.), The New Uranium Mining Boom – Challenges and
Lessons learned. Springer, Heidelberg, (2011) 635-642.
- NOSSKE D., BLANCHARDON E., BOLCH W.E., BREUSTEDT B., ECKERMAN K.F., GIUSSANI J.D.,
HARRISON, J.D., KLEIN W., LEGGETT R.W., LOPEZ M.A., LUCIANI A., ZANKL M.
New developments in internal dosimetry models.
Radiation Prot Dosimetry, 144 (2011) 314-320.
- PLASCHKE, M., ROTHE, J., DENECKE, M.A.
Synchrotron Based X-Ray Spectromicroscopy of Organic Nanoparticles Complexing Actinides
in KALMYKOV, S., DENECKE, M.A. (EDS.)
Actinide Nanoparticle Research, Springer Verlag Heidelberg, (2011) 161–186.
- ROSENBERG, Y. O., METZ, V., GANOR, J.
Co-precipitation of radium in high ionic strength systems: 1. Thermodynamic properties of the Na-Ra-
Cl-SO₄-H₂O system - Estimating Pitzer parameters for RaCl₂.
Geochimica et Cosmochimica Acta, 75 (2011) 5389-5402.
- ROSENBERG, Y. O., METZ, V., OREN, Y., VOLKMAN, Y., GANOR, J.
Co-precipitation of radium in high ionic strength systems: 2. Kinetic
and ionic strength effects.
Geochimica et Cosmochimica Acta, 75 (2011) 5403-5422.
- RUFF, C.M.; MÜLLICH, U.; GEIST, A.; PANAK, P.J.
A novel path in partitioning: Water-soluble BTP ligands for the innovative
SANEX process.
ATW - International Journal for Nuclear Power, 56 (2011) 489-491.

- SCHIMMELPFENNIG, B.
From Molecules to Nanoparticles: A Computational Chemist's Point of View.
in KALMYKOV, S., DENECKE, M.A. (EDS.)
Actinide Nanoparticle Research, Springer Verlag Heidelberg, (2011) 187–194.
- SEIBERT, A., STUMPF, S., GOUDER, T. SCHILD, D., DENECKE, M.A.
Actinide Thin Films as Surface Models
in KALMYKOV, S., DENECKE, M.A. (EDS.)
Actinide Nanoparticle Research, Springer Verlag Heidelberg, (2011) 275-314.
- TRUMM, S.; GEIST, A.; PANAK, P.J.; FANGHÄNEL, T.
An improved hydrolytically-stable bis-triazinyl-pyridine (BTP) for selective actinide extraction.
Solvent Extraction and Ion Exchange, 29 (2011) 1532-2262.
- TRUMM, S., LIESER, G., PANAK, P. J.
Luminescence study on the solvation of Cm(III) in binary aqueous solvent mixtures, Radiochim. Acta, 99 (2011) 783-790.
- TRUMM, S.; WIPFF, G.; GEIST, A.; PANAK, P.J.; FANGHÄNEL, T.
Optimising BTP ligands by tuning their basicity.
Radiochim. Acta, 99 (2011) 13–16.
- WALLEZ, G.; BREGIROUX, D.; POPA, K.; RAISON, P.E.; APSOTOLIDIS, C.; LINDQVIST-REIS, P.; KONINGS, R.J.M.; POPA, A.F.
BaAnIV(PO₄)₂ (AnIV = Th, Np) - A new family of layered double phosphates.
European Journal of Inorganic Chemistry, (2011) 110-115.
- WALTER, M.; SOMERS, J.; BOUËXIÈRE, D.; ROTHE, J.
Local structure in solid solutions of stabilised zirconia with actinide dioxides (UO₂, NpO₂).
Journal of Solid State Chemistry, 184 (2011) 911–914.
- WALTHER, C.
Actinide Nanoparticle Characterization by Mass Spectrometry in KALMYKOV, S., DENECKE, M.A. (EDS.)
Actinide Nanoparticle Research, Springer Verlag Heidelberg, (2011) 137-160.
- ZHANG G., BECKER F., URBAN M., XUAN Y.
Simulating Makrofol as a detector for neutron-induced recoils
Radiation Prot Dosimetry, 144 (2011) 218-221.
- ZHANG, G.; BECKER, F.; URBAN, M.; XUAN, Y.; FÜRSTNER, M.; MAYER, S.
Simulating the angular response of Makrofol as a detector for neutron induced recoils
Radiation Measurements, 46 (2011) 405-408.

Proceedings of workshops and conferences

ADAM, C., GEIST, A., PANAK, P. J., DENECKE, M. A., KADEN, P.,
A comparative NMR study of complexes of trivalent actinides and lanthanides with partitioning relevant N-donor ligands,
EUROMAR 2011 und 33. Fachgruppentagung der Fachgruppe Magnetische Resonanz der GDCh,
Frankfurt, 21.-25.08.2011.

ALTMAIER, M. BRENDLER, V., BUBE, C., MARQUARDT, C.M., MOOG, H.C., RICHTER, A.,
SCHARGE, T., VOIGT, W., WILHELM, S., THEREDA – Thermodynamic Reference Database,
Summary of Final Report, GRS – 265, Gesellschaft für Anlagen- und Reaktorsicherheit (GRS) mbH,
March 2011.

ALTMAIER, M., BISCHOFER, B., BOSBACH, D., BRENDLER, V., CURTIUS, H., GECKEIS, H.,
HERBERT, H.-J., JORDAN, N.
V E S P A – Verbundprojekt zur Untersuchung des Verhaltens langlebiger Spalt- und
Aktivierungsprodukte im Nahfeld eines nuklearen Endlagers.
GDCh Wissenschaftsforum Chemie 2011, Bremen (Germany), September 04-07, 2011. CD of
Abstracts, Abstract No. 696.

ALTMAIER, M., BUCKAU, G., DURO, L., GRIVE, M., MONTOYA, V., KIENZLER, B.
The Euratom FP7 Collaborative Project RECOSEY
13th International Conference on the Chemistry and Migration Behaviour of Actinides and Fission
Products in the Geosphere (MIGRATION), Beijing (China), September 18-23, 2011. Book of Abstracts,
181-182.

ALTMAIER, M., GAONA, X., FELLHAUER, D., BUCKAU, G.
Results and Recommendations from the RECOSEY Intercomparison Exercise
on Redox Determination Methods.
GDCh Wissenschaftsforum Chemie 2011, Bremen (Germany), September 04-07, 2011. CD of
Abstracts, Abstract No. 100.

ALTMAIER, M., GAONA, X., FELLHAUER, D., BUCKAU, G.
RECOSEY Intercomparison Exercise on Redox Determination Methods – Final Report on Main
Conclusions and Recommendations.
13th International Conference on the Chemistry and Migration Behaviour of Actinides and Fission
Products in the Geosphere (MIGRATION), Beijing (China), September 18-23, 2011. Book of Abstracts,
182-183.

APOSTOLIDIS, C.; WALTER, O.; BRUCHERTSEIFER, F.; MÜLLICH, U.; MORGENSTERN, A.
BTP, an important and interesting ligand, not only in the extraction chemistry
of lanthanides and actinides.
24. Tage der Seltenen Erden (Terrae Rarae 2011), Karlsruhe, 12.-14. Oktober 2011
Book of Abstracts O5.

BANIK, N. L.; MARQUARDT, C. M.; SCHILD, D.; ROTHE, J.; LUETZENKIRCHEN, J.; SCHÄFER, T.
Sorption and redox behavior of neptunium on Opalinus clay and Callovo–Oxfordian argillite.
Goldschmidt, 14.-19. August, 2011, Prague, Czech Republic. Mineralogical Magazine 75(3), 478.
(2011).

BANIK, N. L.; MARQUARDT, C. M.; SCHILD, D.; ROTHE, J.; SCHÄFER, T.
Sorption and redox behaviour of radionuclides in natural clay rock
ANKA Experimental Report, Annual Report 2011.

BANIK, N. L.; MARQUARDT, C. M.; SCHILD, D.; ROTHE, J.; SCHÄFER, T.; GECKEIS, H.
Sorption and redox behavior of neptunium, plutonium and technetium in natural clay rock. Migration,
18.-23. September, 2011, Beijing, China. Book of Abstracts, 226.

BANIK, N. L.; MARQUARDT, C. M.; SCHILD, D.; ROTHE, J.; SCHÄFER, T.; Geckeis, H.
Sorption and redox behavior of radionuclides in natural clay rock. 3rd ANKA & KNMF Users' Meeting,
13.-14. October, 2011, Karlsruhe-Neureut, Germany. Book of Abstracts.

BANIK, N. L.; MARQUARDT, C. M.; SCHILD, D.; ROTHE, J.; SCHÄFER, T.
Sorption and redox behaviour of radionuclides in natural clay rock. 3rd Annual Workshop Proceedings, 7th EC FP - Recosy CP, 21.– 24. March 2011, Balaruc-les-Bains, France, KIT Scientific Report 7603.

BANIK, N. L.; MARQUARDT, C. M.; SCHILD, D.; ROTHE, J.; SCHÄFER, T.
Sorption and Redox Behaviour of Radionuclides in Natural Clay Rock. Reports of user experiments at ANKA .2009/2010. 105-107.

BANIK, N. L.; WALZ, S.; MARQUARDT, C. M.; PANAK, P.; SKERENCAK, A.
Complexation studies of Np(V)-Lactate at elevated temperature. HiTAC , 9th November, 2011 Karlsruhe, Germany. Book of Abstracts.

BACH, D.; SCHILD, D.; CHRISTIANSEN, B.C.; GECKEIS, H.
TEM study of neptunyl ion (NpO_2^+) - green rust interaction.
Proceedings of Microscopy Conference MC 2011, Kiel (Germany), August 28 - September 2, 2011, ISBN 978-3-00-033910-3, 2011, Contribution M6-P618.

BEELE, B.; MÜLLICH, U.; GEIST, A.; PANAK, P.J.
A TRLFS study on the complexation of CmIII with 2,6-bis(6-ethyl-1,2-diazine-3-yl)pyridine (Et-BDP) and 2,6-bis(5,6-dipropyl-1,2,4-triazin-3-yl)pyridine (nPr-BTP).
Jahrestagung Kerntechnik, Berlin, 17.-19.Mai 2011 Darmstadt : GLOBIT GmbH, CD-ROM.

BLUNCK, CH.; BECKER, F.; URBAN, M.
MCNPX Modellierung mit Hilfe eines Multikamerasystems.
Jahrestagung Kerntechnik, Berlin, 17.-19.Mai 2011
Darmstadt : GLOBIT GmbH, 2011, CD-ROM.

BOURG, S.; HILL, C.; CARAVACA, C.; RHODES, C.; EKBERG, C.; TAYLOR, R.; GEIST, A. ;
MODOLO, G.; CASSAYRE, L.; MALMBECK, R.; HARRISON, M.; DE ANGELIS, G.; ESPARTERO, A.;
BOUVET, S.; OUVRIER, N.
Partitioning technologies and actinide science: towards pilot facilities in Europe (ACSEPT project).
FISA 2009 : 7th European Commission Conf.on Euratom Research and Training in Reactor Systems, Praha, CZ, June 22-24, 2009
Conf.Proc.S.269-285, Luxembourg : Publications Office of the European Union, 2010
EUR-24048 EN.

BOURG, S.; BOUVET, S.; CARAVACA, C.; CASSAYRE, L.; DE ANGELIS, G.; EKBERG, C.;
ESPARTERO, A.G.; GEIST, A.; GUILBAUD, P.; HARRISON, M.; KLAASSEN, F.; MALMBECK, R.;
MODOLO, G.; OUVRIER, N.; RHODES, C.; TAYLOR, R.
ACSEPT – the current European project on actinide recycling.
Proceedings of GLOBAL 2011 Makuhari, Japan, Dec. 11–16, 2011, Paper No. 355757.

BUBE, C., ALTMAIER, M., METZ, V., SCHILD, D., KIENZLER, B.,
Thermodynamics of long-term metastable magnesium (chloro) hydroxo carbonates at 25°C.
Goldschmidt 2011, Prague, Czech Republic.
Mineralogical Magazine 75(3), 591 (2011).

BUBE, C., METZ, V., KIENZLER, B., BOHNERT, E., SCHILD, D., DARDENNE, K., ROTHE, J.
Interactions of U(VI) with cement alteration products in brines
NUWCEM 2011, 1st International Symposium on Cement-based Materials for Nuclear Wastes, Avignon, October 11-14.
Avignon (France), 2011, Book of Abstracts, 0319.

BUBE, C., METZ, V., SCHILD, D., LAGOS, M., BOHNERT, E., GARBEV, K., ALTMAIER, M.,
KIENZLER, B.
Interactions of U(VI) with cement alteration products in highly saline solutions

NUWCEM 2011, 1st International Symposium on Cement-based Materials for Nuclear Wastes, Avignon, October 11-14.
Avignon (France), 2011, Conference Proceedings CD-ROM Paris :Societe Francaise d'Energie Nucleaire (SFEN), 2011.

BREUSTEDT, B.; BLANCHARDON, E.; CASTELLANI C.; GIUSSANI, A.; LI W.; MARSH J.; NOSSKE D.; OEH U.; LOPEZ M.

Doses due to other excretion pathways in biokinetic models.

56th Annual Meeting of the Health Physics Society, West Palm Beach, Fla., June 26-30, 2011

Abstract in: Health Physics, 101(2011) Suppl., 36 (Abstract).

BREUSTEDT B.

Quantities and Units

External Dosimetry

Internal Dosimetry

In: Pilot Modules in Radiation Protection according to the ERPTS Training Scheme

KIT, Karlsruhe, 14.03.-30.03.2011.

FINCK, N.; DARDENNE, K.,

Americium co-precipitation with the smectite hectorite: powder and polarized EXAFS Actinide XAS, SPring-8, Japan, March 02nd – 04th 2011

Book of abstract, O-23.

FINCK, N.; DARDENNE, K.

Am(III) coprecipitation with and adsorption to hectorite: powder and polarized XAS insights

ANKA Experimental Report, Annual Report 2011.

FINCK, N.; DARDENNE, K. BOSBACH, D.

Selenide retention by mackinawite: a multi-edge XAS approach.

Goldschmidt 2011, August 14 – 19, Prague, Czech Republic.

Mineralogical Magazine 75(3), 846.

FLEISCH, J., GRÜNEWALD, W., ROTH, G., SCHMITZ, F.-J., TOBIE, W., WEISHAUPT, M.

Successful Hot Operation of the German Vitrification Plant VEK – Results and Experiences, WM 2011-Conference, Paper 11277, February 27 - March 3, 2011, Phoenix, AZ.

FLEISCH, J.; SCHMITZ, F.J.; WEISHAUPT, M.; ROTH, G.; GRÜNEWALD, W.; TOBIE, W.

Verglasung des HAWC der WAK - eine Erfolgsgeschichte.

Jahrestagung Kerntechnik, Berlin, 17.-19.Mai 2011

Darmstadt : GLOBIT GmbH, 2011, CD-ROM.

GAONA, X., TITS, J., DARDENNE, K., WIELAND, E., ALTMAIER, M.

XAFS investigations of Np(V/VI) redox speciation in hyperalkaline TMA-OH solutions

ReCosy 3rd annual workshop (S&T contribution), Balaruc les Bains, France, March 21-24, 2011.

GECKEIS, H.

Research on geochemical aspects of nuclear waste disposal.

US-German Workshop on Salt Repository Research, Design and Operation, Canton,

Miss., May 25-27, 2010

KIT-Scientific Reports, KIT-SR 7569 (2011) 412-446.

GECKEIS, H.; KIENZLER, B.; GOMPPER, K.

Endlagerung von hochradioaktiven Abfällen. Internationaler Forschungsstand und Perspektiven.

Frühjahrstagung DPG, Arbeitskreis Energie, Dresden, 13.-18.März 2011

Verhandlungen der Deutschen Physikalischen Gesellschaft, R.6, B.46(2011) AKE 3.1

GEIST, A.; MÜLLICH, U.; MODOLO, G.; WILDEN, A.
Actinide(III)/lanthanide(III) separation via selective aqueous complexation of actinides(III) in nitric acid.
19th International Solvent Extraction Conference (ISEC2011), Santiago, Chile, 3.–7.10.2011 CD-ROM.

GEIST, A.; MÜLLICH, U.; WILDEN, A.; GÜLLAND, S.; MODOLO, G.
C5-BPP—a new highly selective extractant for the separation of trivalent actinides from lanthanides.
19th International Solvent Extraction Conference (ISEC2011), Santiago, Chile, 3.–7.10.2011 CD-ROM.

GRÜNEWALD, W., PLASCHKE, M., ROTH, G., TOBIE, W., WEISS, K.H., WEISENBURGER, S., STOLLENWERK, A., EISSLER, A.
Process Control and Glass Product Quality Assessment Applied in the VEK Plant,
Proceedings of GLOBAL 2011 Makuhari, Japan, Dec. 11-16, 2011 Paper No. 392621.

GRÜNEWALD, W., ROTH, G., TOBIE, W., FLEISCH, J., SCHMITZ, F.J., WEISHAUPT, W.
Hot Operation Performance of the German Vitrification Plant VEK, Proceedings of GLOBAL 2011 Makuhari, Japan, Dec. 11-16, 2011 Paper No. 392619.

GRÜNEWALD, W., ROTH, G., TOBIE, W., WEISENBURGER, S., WEISS, K.H.
Application of Advanced Large-Scale Ceramic Melter Technology for HLLW Vitrification, Proceedings of GLOBAL 2011 Makuhari, Japan, Dec. 11-16, 2011 Paper No. 392622.

HANNIG, C.; SCHILD, D.; DIRSCHKA, M.; LÄNGE, K.; RAPP, B. E.
PTFE-like / PDMS hybrids: synthesis of photocurable, highly chemically resistant polymers and their applications in microfluidics.
15th International Conference on Miniaturized Systems for Chemistry and Life Sciences (MicroTAS), Seattle, Washington, USA, October 2-6, 2011, "The Proceedings of the TAS 2011", (2011), 1146-1148.

HUITTINEN, N.; RABUNG, TH.; LEHTO, J.; GECKEIS, H.
The role of dissolved silicon on Curium speciation in alkaline kaolinite suspensions
13th International Conference on the Chemistry and Migration Behaviour of Actinides and Fission Products in the Geosphere, Beijing, China, 18-23 September 2011, book of abstract, 239.

KADEN, P., ADAM, C., SCHIMMELPFENNIG, B., GEIST, A., PANAK, P. J., DENECKE, M. A.
Comparative NMR study of partitioning-relevant complexes with trivalent actinides and lanthanides to elucidate the origin of their selectivity,
GDCh- Wissenschaftsforum Chemie 2011, Bremen, 04.-07.09.2011.

KOBAYASHI, T.; BACH, D.; ALTMAIER, M.; SASAKI, T.; MORIYAMA, H.
Effect of Temperature on the Solubility and Solid Phase of Zirconium Hydroxide.
13th International Conference on the Chemistry and Migration Behaviour of Actinides and Fission Products in the Geosphere (MIGRATION 2011), Beijing (China), September 18-23, 2011, Abstract Book, 54-55.

KOBAYASHI, T., GAONA, X., FELLHAUER, D., ALTMAIER, M.,
Systematic Evaluation of Tc(VII)/Tc(IV) Redox Processes in 0.1 M NaCl Solutions.
ReCosy 3rd annual workshop (S&T contribution), Balaruc les Bains, France, March 21-24, 2011.

KULIK D.; LÜTZENKIRCHEN J.
Consistent Treatment of Entropy, Enthalpy and Volume Effects of Multi-Dentate Adsorption Reactions,
Goldschmidt 2011, Prag, 14.-19. August, 2011, Book of Abstracts.

KUPCIK, T., HUITTINEN, N.; RABUNG, TH.; LÜTZENKIRCHEN, J.; GECKEIS, H.; FANGHÄNEL, TH.
Interaction of trivalent metal ions with aluminium(hydr)oxides
13th International Conference on the Chemistry and Migration Behaviour of Actinides and Fission Products in the Geosphere, Beijing, China, 18-23 September 2011, book of abstract, 62.

KUPCIK, T., HUITTINEN, N., RABUNG, T., LÜTZENKIRCHEN, J., GECKEIS, H., FANGHÄNEL, TH.
Aluminium(hydr)oxide als Modellminerale zur Untersuchung der Metallionensorption an der Mineral-
Wasser-Grenzfläche.

GDCh Wissenschaftsforum Chemie 2011, Bremen (Germany), September 04-07, 2011, Book of
Abstracts.

KUTZER, A.; VITOVA, T.; DENECKE, M: A.; ROTH, G.; GECKEIS, H.

Mo K-edge XAS study of Mo-rich model nuclear waste glass

ANKA Experimental Report, Annual Report 2011.

LI, B.; DARDENNE, K.; VITOVA, T.; ROTHE, J.; FOERSTENDORF, N.; RAFF, J.

P and S k-edge XANES investigation of U(VI) complexes with several organic model compounds

ANKA Experimental Report, Annual Report 2011.

LINDQVIST-REIS, P., KLENZE, R. STEPERT, M., FUSS, M., WALTHER, C, LÜTZENKIRCHEN, J.,
GECKEIS, H.

Europium(III) and Curium(III) Hydrolysis Species in Solids and in Solution Studied by Time-Resolved
Laser Fluorescence Spectroscopy (TRLFS)

26th Rare Earth Research Conference, June 19-23, 2011, Santa Fe, USA, Book of Abstracts, 130-
131.

LINDQVIST-REIS, P., KLENZE, R., SCHIMMELPFENNIG, B.

Spectroscopic Evidence of Ion-Association in Aqueous Ln^{3+} and An^{3+} Perchlorate Solutions at Low
Water Activity

ABC-Salt Workshop '11, Karlsruhe, November 7-8, 2011. Book of Abstracts.

LINDQVIST-REIS, P., KLENZE, R., FANGHÄNEL, TH.

Octa- and Nonahydrated Cm(III) in Aqueous Solution from 20 to 200 °C

HiTAC Workshop '11, Karlsruhe, November 9, 2011. Book of Abstracts.

LOIDA, A., METZ, V., BOHNERT, E., KIENZLER, B., MÜLLER, N., SCHILD, D, SOBALLA, E.

Trapping of Radionuclides/Actinides in the Canister Corrosion Product Magnetite. ReCosy 3rd annual
workshop (S&T contribution), Balaruc les Bains, France, March 21-24, 2011.

LOIDA, A., GENS, R., METZ, V., LEMMENS, K., CACHOIR, C., MENNECART, T., KIENZLER, B.

Corrosion Behaviour of Spent Nuclear Fuel in High pH Solutions – Effect of Hydrogen

XXXV International Symposium Scientific Basis for Nuclear Waste Management, MRS 2011, October
2-7, 2011, Buenos Aires, Argentina

Book of Abstracts 51.

LÖBLE, M.; VITOVA, T.; BRENDENBACH, B.; ROTHE, J.; DARDENNE, K.; DENECKE, M: A.;
BREHER, F.

New insights in electronic properties of f-element coordination compounds

ANKA Experimental Report, Annual Report 2011.

MAGNUSSON, D.; GEIST, A.; WILDEN, A.; MODOLO, G.; MALMBECK, R.

Computer code development for flow-sheet design and modeling with verification towards a novel
partitioning Process.

Proceedings of GLOBAL 2011

Makuhari, Japan, Dec. 11–16, 2011 Paper No. 355757.

MARQUARDT, C.M., BANIK, N.L., SCHILD, D., ROTHE, J., GECKEIS, H., Interaction of tetravalent
Neptunium with fulvic acid, Migration'11, 13th International Conference on the Migration of Actinides
and Fission Products in the Geosphere, September 18 – 23, 2011, Beijing, China, Conference
Abstracts 2011, 202.

MARZOCCHI, O.

Design and Setup of a New HPGe Detector Based Body Counter Capable of Detecting Also Low
Energy Photon Emitters.

PhD Thesis published on the website of the University of Bologna:

<http://amsdottorato.cib.unibo.it/3929/>

METZ, V., BUBE, C., BOHNERT, E., SCHLIEKER, M., KIENZLER, B.
Am(III) retention by cement corrosion products under highly saline conditions.
21st Annual VM Goldschmidt Conference, Prague, Czechia, August 2011, Mineralogical Magazine, 75, 1458 (2011).

PEKOV, I. V., CHUKANOV, N. V., FILINCHUK, Y. E., ZADOV, A. E., KONONKOVA, N. N.,
EPANCHINTSEV, S. G., KADEN, P., KUTZER, A., GÖTTLICHER, J.,
(2011) Kasatkinite, IMA 2011-045.
CNMNC Newsletter No. 10, October 2011, 2559; Mineralogical Magazine, 75, 2549-2561.

PAYNE, T., LÜTZENKIRCHEN, J.
Theoretical and experimental basis of thermodynamic sorption models,
NEA/RWQ/NSC/TDB4(2011)3, 45-46.

PETROV, V.G., KALMYKOV, S.N., ALTMAIER, M.
Solubility and phase transformations of Np(V) hydroxide in solutions with different ionic strengths.
Moscow State University Chemistry Bulletin. 2011, 66(2), 107-115.

PETROV, V. G.; ROTHE, J.; DARDENNE, K.; GAONA, X.; FELLHAUER, D.; KALMYKOV, S. N.;
ALTMAIER, M.
Solid phase transformation of Np(V) hydroxide in NaCl solutions
ANKA Experimental Report, Annual Report 2011.

PLASCHKE, M; ROTHE, J; DENECKE, M.A.; GECKEIS, H.
STXM / NEXAFS study of Fe(III) induced humic acid aggregates at different pH
11th International Conference on the Biogeochemistry of Trace Elements (ICOBTE), July 3-7, 2011,
Florence, Italy, Abstract CD-ROM.

PUDEWILLS, A.
Evaluation and improvement of the THM modelling capabilities for rock salt
repositories.
Papadrakakis, M. [Hrsg.] Computational Methods for Coupled Problems in Science and Engineering
IV :
Proc.of the Internat.Conf., Kos, GR, June 20-22, 2011
CD-ROM Barcelona : CIMNE, 2011.

RABUNG, TH.; MONTOYA, V.; MOLINERO, J.
CROCK: Crystalline Rock Retention Processes,
A 7th Framework Programme Collaborative Project (2011-2013)
13th International Conference on the Chemistry and Migration Behaviour of Actinides and Fission
Products in the Geosphere, Beijing, China, 18-23 September 2011, book of abstract, 186.

ROSENBERG, Y.O., METZ, V., GANOR, J.
The co-precipitation of Ra in a large scale evaporitic system.
21st Annual VM Goldschmidt Conference, Prague, Czechia, August 2011 Mineralogical Magazine, 75,
1754 (2011).

ROTHMEIER, M.; PETROV, V.; RABUNG, T.; LÜTZENKIRCHEN, J.; FINCKN.; ALTMAIER, M.
Surface charging of (oxyhydr)oxide minerals to high ionic strength
ABC Salt, Workshop, 7.-8.11.2011, Karlsruhe, Book of Abstracts.

RUFF, C.M.; MÜLLICH, U.; GEIST, A.; PANAK, P.J.
A novel path in partitioning: Water-soluble BTP ligands for the innovative
SANEX process.
Jahrestagung Kerntechnik, Berlin, 17.-19.Mai 2011
Darmstadt : GLOBIT GmbH, 2011 CD-ROM.

RUFF, C.M.; MÜLLICH, U.; GEIST, A.; PANAK, P.J.
A novel path in partitioning: water-soluble BTP ligands for the innovative SANEX process.
atw 2011, 56 (8-9), 489-491.

- SCHEPPERLE, J.; FINCK, N.; VITOVA, T.
Probing Eu(III) adsorbed to Fe-containing clay mineral : an application for high-resolution X-ray emission spectroscopy
ANKA Experimental Report, Annual Report 2011.
- SCHNURR, A.; PETROV, V.; RABUNG, TH.; LÜTZENKIRCHEN, J.; GECKEIS, H.
Trivalent metal ion sorption under saline conditions
13th International Conference on the Chemistry and Migration Behaviour of Actinides and Fission Products in the Geosphere, Beijing, China, 18-23 September 2011, book of abstract, S. 246
- STEPPERT, M.; BATUK, O.; KALMYKOV, S.; ROTHE, J.; WALTHER, C.
Polymerisation processes in Pu(V) chloride solutions
ANKA Experimental Report, Annual Report 2011.
- STEPPERT, M., TRUMM, S., LINDQVIST-REIS, P., GEIST, A., WALTHER, C., PANAK P., FANGHÄNEL, TH.
"Direct detection of nitrate coordination in Eu-BTBP complexes", GDCh Wissenschaftsforum Chemie 2011, Bremen, Germany, 04.-07.09.2011, CD-ROM.
- STEPPERT, M., WALTHER, C.
"Comparison of U(VI) and Pu(VI) hydrolysis products by means of electrospray ionization mass spectrometry", 13th International Conference on the Chemistry and Migration Behaviour of Actinides and Fission Products in the Geosphere, Migration 2011, Beijing, China, 18.-23.09.2011, Abstract Book, 69-70.
- SYPULA, M.; WILDEN, A.; MODOLO, G.; GEIST, A.
Innovative SANEX process for actinide(III) separation from PUREX raffinate using TODGA-based solvents.
19th International Solvent Extraction Conference (ISEC2011), Santiago, Chile, 3.–7.10.2011 CD-ROM.
- TITS, J., GAONA, X., LAUBE, A., WIELAND, E.
Influence of oxidation state on the Neptunium sorption by cementitious materials
ReCosy 3rd annual workshop (S&T contribution), Balaruc les Bains, France, March 21-24, 2011.
- TITS, J., GAONA, X., MACÉ, N., KULIK, D., STUMPF, T., WALTHER, C., WIELAND, E.
Immobilisation of Uranium(VI) in cementitious materials: evidence for structural incorporation in calcium-silicate-hydrates and solid solution formation
Proceedings of the 10th International Congress on Applied Mineralogy (ICAM), Trondheim, Norway, August 1-5, 2011.
- VITOVA, T.; BUTORIN, S. M.; SEIBERT, A.; ROTHE, J.; DARDENNE, K.; VEGELIUS, J.; CACIUFFO, R.; DENECKE, M. A.
High-resolution X-ray absorption spectroscopy study of plutonium dioxide in contact with water
ANKA Experimental Report, Annual Report 2011.
- VITOVA, T.; HUBER, F.; ROTHE, J.; DARDENNE, K.; SCHÄFER, T.
Interaction of uranium(VI) with synthetic magnetite nanoparticles
ANKA Experimental Report, Annual Report 2011.
- VITOVA, T.; DENECKE M.A.; GEIST, A.; LÖBLE, M.; ROTHE, J.; CACIUFFO, R.; GECKEIS, H.
Actinide speciation with high-resolution X-ray absorption and inelastic X-ray scattering spectroscopy
GDCh Wissenschaftsforum Chemie 2011, Bremen (Germany), September 04-07, 2011, Book of Abstracts 29.
- VITOVA, T.; DENECKE M.A.; LÖBLE, M.; PRÜßMANN, T.; ROTHE, J.;
High-resolution X-ray absorption spectroscopy as an advanced tool for structural studies of lanthanide complexes
XXIV. Tage der Seltenen Erden (Terrae Rarae 2011), Karlsruhe, 12.–14.10.2011
Book of Abstracts.

VITOVA, T.; KVASHNINA, K.O.; DENECKE, M.A.; CACIUFFO, R.; HUBER, F.; ROTHE, J.; SCHÄFER, T.; BUTORIN, S.M.; GECKEIS, H.;
The potential of high-resolution X-ray emission spectroscopy and non resonant inelastic X-ray scattering for advanced studies of actinide-materials
AnXAS 2011: 6th Workshop on Speciation Techniques and Facilities for Radioactive Materials at Synchrotron Light Sources and other Quantum Beam Sources, Harima Science Garden City, Hyogo, Japan, March 2-4, 2011. Book of Abstracts.

WALTHER, C.; STEPPERT, M.; BÜCHNER, S.; FUSS, M.; GEIST, A.; GECKEIS, H.
Massenspektrometrie in der Nuklearen Entsorgung.
Frühjahrstagung DPG, Fachverband Massenspektrometrie, Dresden, 13.-18.März 2011, Verhandlungen der Deutschen Physikalischen Gesellschaft, R.6, B.46 (2011) MS 5.6.

WEISER, M.; RABUNG, TH.; GECKEIS, H.
Influence of Organic Buffer Materials on Trivalent Metal Ion Speciation
13th International Conference on the Chemistry and Migration Behaviour of Actinides and Fission Products in the Geosphere, Beijing, China, 18-23 September 2011, book of abstract, 62.

WERSIN, P.; LÜTZENKIRCHEN, J.
The influence of temperature on sorption: A preliminary assessment for Uranium(VI) sorption to bentonite
HITAC, Workshop, 9.11.2011, Karlsruhe, Book of Abstracts.

WIELAND, E., DÄHN, R., GAONA, X., MACÉ, N., TITS, J.
Micro- and macroscopic investigations on actinide binding to cementitious materials and implications for the safe disposal of radioactive waste
Proceedings of the NUWCEM 2011, 1st International Symposium on Cement-based Materials for Nuclear Wastes, Avignon, France, October 11-14, 2011.

WILDEN, A.; SYPULA, M.; MODOLO, G.; GEIST, A.
Direct actinide(III) separation from PUREX raffinate using a BTBP/TODGA solvent.
19th International Solvent Extraction Conference (ISEC2011), Santiago, Chile, 3.-7.10.2011 CD-ROM.

ZHANG, G.; BECKER, F.; URBAN, M.
MCNP surface source and CASTOR simulations.
Jahrestagung Kerntechnik, Berlin, 17.-19.Mai 2011, Darmstadt : GLOBIT GmbH, 2011, CD-ROM.

Reports

ALTMAYER, M.; GAONA, X.; FELLHAUER, D.; BUCKAU, G.
Intercomparison of redox determination methods on designed and near-natural aqueous systems. FP 7 EURATOM collaborative project 'Redox phenomena controlling systems'.
KIT Scientific Reports 7572.

ALTMAYER, M., KIENZLER, B., DURO, L., GRIVE, M., MONTOYA, V., (EDS),
3rd Annual Workshop Proceedings of the Collaborative Project "Redox Phenomena Controlling Systems" (7th EC FP CP RECOSY).
KIT Scientific Reports 7603.

BUCKAU, G.; KIENZLER, B.; DURO, L.; GRIVE, M.; MONTOYA, V.
2nd Annual Workshop Proceedings of the Collaborative Project 'Redox Phenomena Controlling Systems' (7th EC FP CP RECOSY).
KIT Scientific Reports 7557.

KUTZER, A.; VITOVA, T.; CALIEBE, W.; DENECKE, M.A.
Eu L2 edge high-resolution X-ray absorption spectroscopy study of Eu doped borosilicate glasses
HASYLAB Experimental Report, Annual Report 2011.

PUDEWILLS, A.

Coupled processes in salt host-rock repositories.

THERESA : Coupled Thermal-Hydrological-Mechanical-Chemical Processes for Application in Repository Safety Assessment
Final Report of Work Package 3, Deliverable D9, European Commission.

PUDEWILLS, A.

Numerische Simulation zum mechanischen Langzeitverhalten eines realen Untertagebauwerks im Steinsalz.

BMBF - Verbundprojekt 02C1597, Einzelbericht zum Teilprojekt 3.
KIT Scientific Reports 7579.

VITOVA, T.; BUTORIN, S. M.; SEIBERT, A.; ROTHE, J.; DARDENNE, K.; VEGELIUS, J.; CACIUFFO, R.; DENECKE, M. A.

High-resolution X-ray absorption spectroscopy study of plutonium dioxide in contact with water
ANKA Experimental Report, Annual Report 2011.

VITOVA, T.; HUBER, F.; ROTHE, J.; DARDENNE, K.; SCHÄFER, T.

Interaction of uranium(VI) with synthetic magnetite nanoparticles
ANKA Experimental Report, Annual Report 2011.

VITOVA, T.; ROTHE, J.; DENECKE M.A.; SCHÄFER, T; HUBER, F.; NICOLAS F.; GÖTTLICHER J.; KVASHNINA K..

High energy resolution X-ray absorption valence state and electronic structure investigation of uranyl magnetite nanoparticles
ESRF Experimental Report, Annual Report 2011.

Internal reports

LOIDA, A., MÜLLER, N., SCHILD, D., SOBALLA, E., KIENZLER, B.,
Investigation of the Corrosion Behaviour of Irradiated Spent Fuel
in High pH Solutions – Effect of H₂ overpressure
ONDRAF/NIRAS project, Phase 2009 - 2010

Patents

BECKER, F.

Detektor zur Messung der Richtungs-Äquivalentdosis (2011). Deutsches Patent- und Markenamt:
Gebrauchsmuster 202010017004.4 Anmelder: Berthold Technologies GmbH & Co KG und KIT (Dr. Frank Becker, INE-ASF).

GEIST, A., MÜLLICH, U., ZEVACO, T.

Wasserlösliche Bis-triazinyl-pyridine, -bipyridine und -terpyridine, deren Synthese und Anwendung.
EP 2 377 861 A1 (19.10.2011).

TRUMM, S., GEIST, A., PANAK, P.J. FANGHÄNEL, TH.

Verbesserte Bis(triazin)pyridin-Derivate und Verfahren zu deren Herstellung.
EP 2 377 859 A1 (19.10.2011).

Presentations

Invited oral presentations

BACH, D.

TEM Investigations of Green Rust ($\text{GR}_{\text{Na},\text{SO}_4}$) Interacted with Neptunyl Ion (NpO_2^+).
3rd ANKA/KNMF Joint Users' Meeting, Karlsruhe (Germany), October 13 - 14, 2011.

BOUBY, M., GECKEIS, H.

Caractérisation de colloïdes d'origine naturelle ou synthétique dans le contexte du stockage des déchets radioactifs.

Séminaire LHyGeS, Ecole et Observatoire des Sciences de la Terre, Strasbourg (France), 18 February 2011.

BREUSTEDT, B.

Biokinetic modeling of DTPA decorporation therapy – The EURADOS approach
Seminar of LRRRI Lovelace Respiratory Research Institute
Albuquerque, NM. July 8th 2011.

BREUSTEDT, B.

Biokineticische Modellierung der Dekorporationstherapie mit DTPA
Medizinphysiker Konferenz (274. Sitzung) gleichzeitig Treffen der Regionalsektion
Nordrhein/Ruhrgebiet der DGMP, Köln, 5.12.2011.

DENECKE, M. A.

X-ray absorption spectroscopy in nuclear waste disposal. Advanced EXAFS Data Analysis workshop
2011, Ghent, B, 12.-14. January 2011.

DENECKE, M.A.,

Synchrotron-based X-ray methods in nuclear waste disposal. Glenn T. Seaborg Center, Lawrence
Berkeley National Laboratory, 27. June 2011.

DENECKE, M. A.

3D chemical information in clays using synchrotron techniques
NEA Clay Club Workshop „Clays under Nano- to Microscopic resolution“, Karlsruhe, 6. – 8. September
2011.

DENECKE, M. A.

ACTINET i3 Pooled Facilities
J-ACTINET Meeting, Tokyo, Japan, 1.-2. September 2011.

DENECKE, M. A.

Geochemistry of the actinide elements
J-ACTINET Summer School, Tokyo, Japan, 29.-31. August 2011.

DENECKE, M.A., BANIK, N., GEIST, A., LOEBLE, M. PANAK, P.J., PLASCHKE, M., ROTHE, J.,
SCHIMMELPFENNIG, B., VITOVA, T.

Characterization of actinide/lanthanide complexes with natural and tailored organic ligands by means
of X-ray spectroscopy combined with quantum chemistry methods
26th Rare Earth Research Conference (RERC11), June 19-23, 2011, Santa Fe, NM
Section “Actinide Theory and Chemistry”.

DENECKE, M.A., GEIST, A., KADEN, P., PANAK, P., SCHILD, D., SCHIMMELPFENNIG, B.,
STEPPERT, M., VITOVA, T., WALTHER, C.

Multi-Method Approach Towards Understanding Actinide/Lanthanide Separation in Liquid-Liquid
Extraction With N-Donor Ligands. Actinide XAS 2011 – 6th Workshop on Speciation, Techniques, and
Facilities for
Radioactive Materials at Synchrotron Light Sources Spring-8, Japan; 2. – 4. March 2011.

GECKEIS, H.

Nuklearchemische Aspekte der Endlagerung hochradioaktiver Abfälle.
Entsorgungsstrategien für radioaktive Abfälle; Vortragsreihe im Institut für Endlagerforschung, TU
Clausthal, 12.01.2011

GECKEIS, H.

Actinide behaviour in the geosphere - Still research needed?
First ACTINET I3 Plenary Meeting, February 1-3, 2011, CEA Marcoule.

GECKEIS, H.

Nukleare Entsorgung – Lösungsvorschläge aus der Chemie
Wissenschaftler im Dialog mit der Politik, mit Verbänden und Medien; Umbau des Energiesystems;
Beiträge der Chemie; GDCH; Chemie und Energie; 24. Februar, 2011, Berlin.

GECKEIS, H.; KIENZLER, B.; GOMPPER, K.

Endlagerung von hochradioaktiven Abfällen. Internationaler Forschungsstand und
Perspektiven.

Frühjahrstagung DPG, Arbeitskreis Energie, Dresden, 13.-18.März 2011.

GECKEIS, H.

„Nukleares Recycling“ – Option für die sichere Entsorgung hochradioaktiver Abfälle?
Institut für Radiochemie, HZDR, Dresden, 29.April, 2011.

GECKEIS, H.

Streitpunkt Kernenergie: Das Problem der Nuklearen Entsorgung
und Lösungsvorschläge aus der Chemie
GDCH Jungchemikerforum, Uni Stuttgart, 05. Mai 2011.

GECKEIS, H.

Nuklearchemische Grundlagenforschung: Baustein für eine sichere Entsorgung
radioaktiver Abfälle
Jahrestagung Kerntechnik 2011, KTG, Berlin, 17.05.-19.05.2011.

GECKEIS, H.

Streitpunkt Kernenergie: Das Problem der Nuklearen Entsorgung
und Lösungsvorschläge aus der Chemie
GDCH Jungchemikerforum, Uni Hamburg, 05. Juli 2011.

GECKEIS, H.,

Nukleares Recycling – sichere Entsorgungsoption für hochradioaktive Abfälle?
Energie: Neue Entwicklungen aus der Chemie, Jahrestagung AG Chemie und Energie (AG Chemie
und Energie),
GDCH Wissenschaftsforum, Bremen, 4.-7. September, 2011.

GECKEIS, H.; KIENZLER, B.; GOMPPER, K.

Endlagerung von hochradioaktiven Abfällen. Internationaler Forschungsstand und
Perspektiven.

Frühjahrstagung DPG, Arbeitskreis Energie, Dresden, 13.-18.März 2011.

GEIST, A.

Kinetic limitations for separation processes.
6th European Practical Summer School of Separation and Analytical Chemistry,
Marcoule, Frankreich, 17.–22.7.2011.

LOIDA, A., KIENZLER, B.

Investigation of the Corrosion Behavior of Irradiated Spent Fuel in High pH Solutions
- Effect of H₂ -
Seminar at ONDRRAF-NIRAS, Bruxelles, (B) Oct 24-25, 2011.

LOIDA, A.,
Untersuchungen zum Korrosionsverhalten von hoch abgebranntem UO₂ Kernbrennstoff in endlagerrelevanten Wässern. Seminarvortrag bei FZJ-IEK6, Jülich, 24. November 2011.

MARZOCCHI, O.
Design and Setup of a New HPGe Detector Based Body Counter Capable of Detecting Also Low Energy Photon Emitters.
PhD final defense, University of Bologna, Italy, 13 June 2011.

PANAK, P. J.
Spectroscopic Speciation of Actinides, Summer School on Actinide Science and Applications, ITU, Karlsruhe, Germany, June, 14-17th, 2011.

STUMPF, T.
Nuclear waste disposal: Facts and perspectives
ITU summer school of actinide science and applications 2011, Karlsruhe, Germany.

WALTHER, C.; STEPERT, M.; BÜCHNER, S.; FUSS, M.; GEIST, A.; GECKEIS, H.
Massenspektrometrie in der Nuklearen Entsorgung.
Frühjahrstagung DPG, Fachverband Massenspektrometrie, Dresden, 13.-18.März 2011.

Presentations at conferences and workshops

ALTMAIER, M., BISCHOFER, B., BOSBACH, D., BRENDLER, V., CURTIUS, H., GECKEIS, H., HERBERT, H.-J., JORDAN, N.
V E S P A – Verbundprojekt zur Untersuchung des Verhaltens langlebiger Spalt- und Aktivierungsprodukte im Nahfeld eines nuklearen Endlagers.
GDCh Wissenschaftsforum Chemie 2011, Bremen (Germany), September 04-07, 2011.

ALTMAIER, M., BUCKAU, G., DURO, L., GRIVE, M., MONTOYA, V., DELOS, A.
The FP7 Collaborative Project ReCosy.
ICEM'11 (The 14th International Conference on Environmental Remediation and Radioactive Waste Management), 25-29.09-2011, Reims, France.

ALTMAIER, M., BUCKAU, G., DURO, L., GRIVE, M., MONTOYA, V., KIENZLER, B.
The Euratom FP7 Collaborative Project RECOSY
13th International Conference on the Chemistry and Migration Behaviour of Actinides and Fission Products in the Geosphere (MIGRATION), Beijing (China), September 18-23, 2011.

ALTMAIER, M., GAONA, X., FELLHAUER, D., BUCKAU, G.
Results and Recommendations from the RECOSY Intercomparison Exercise on Redox Determination Methods.
GDCh Wissenschaftsforum Chemie 2011, Bremen (Germany), September 04-07, 2011.

ALTMAIER, M., GAONA, X., FELLHAUER, D., BUCKAU, G.
RECOSY Intercomparison Exercise on Redox Determination Methods – Final Report on Main Conclusions and Recommendations.
13th International Conference on the Chemistry and Migration Behaviour of Actinides and Fission Products in the Geosphere (MIGRATION), Beijing (China), September 18-23, 2011.

ALTMAIER, M., GAONA, X., FELLHAUER, D., BUCKAU, G.
Final Report on ReCosy ICE on redox determination methods.
ReCosy 3rd annual workshop (S&T contribution), Balaruc les Bains, France, March 21-24, 2011.

APOSTOLIDIS, C.; WALTER, O.; BRUCHERTSEIFER, F.; MÜLLICH, U.; MORGENSTERN, A.
BTP, an important and interesting ligand, not only in the extraction chemistry of lanthanides and actinides.
XXIV. Tage der Seltenen Erden (Terrae Rarae 2011), Karlsruhe, 12.-14.10.2011.

BACH, D.; SCHILD, D.; CHRISTIANSEN, B.C.; GECKEIS, H.
TEM study of neptunyl ion (NpO_2^+) - green rust interaction.
Microscopy Conference MC 2011, Kiel (Germany), August 28 - September 2, 2011.

BANIK, N. L.; MARQUARDT, C. M.; SCHILD, D.; ROTHE, J.; SCHÄFER, T.
Sorption and redox behaviour of radionuclides in natural clay rock. 3rd Annual Workshop, 7th EC FP - Recosy CP, 21.-24. March 2011, Balaruc-les-Bains, France.

BANIK, N. L.; MARQUARDT, C. M.; SCHILD, D.; ROTHE, J.; LUETZENKIRCHEN, J.; SCHÄFER, T.
Sorption and redox behavior of neptunium on Opalinus clay and Callovo-Oxfordian argillite.
Goldschmidt, 14.-19. August, 2011, Prague, Czech Republic.

BANIK, N. L.; MARQUARDT, C. M.; SCHILD, D.; ROTHE, J.; SCHÄFER, T.; Geckeis, H.
Sorption and redox behavior of neptunium, plutonium and technetium in natural clay rock, Migration, 18.-23. September, 2011, Beijing, China.

BANIK, N. L.; MARQUARDT, C. M.; SCHILD, D.; ROTHE, J.; SCHÄFER, T.; Geckeis, H.
Sorption and redox behavior of radionuclides in natural clay rock. 3rd ANKA & KNMF Users' Meeting, 13.-14. October, 2011, Karlsruhe, Germany.

BANIK, N. L.; WALZ, S.; MARQUARDT, C. M.; PANAK, P.; SKERENCAK, A.
Complexation studies of Np(V)-Lactate at elevated temperature. HiTAC, 9th November, 2011
Karlsruhe, Germany.

BARIÉ R.-E.; BECKER, F.
Investigation of radiation exposure of medical personnel in SIRT
International Workshop ORAMED 2011, Barcelona, 20.-22. Januar 2011.

BECKER, F.
Bericht vom Programm- und Organisationskomitee FS-2012
74. AKD-Sitzung in Braunschweig 4.- 5. April 2011.

BECKER, F.
Jahrestagung des FS im Jahr 2012: der FS und seine Arbeitskreise am KIT Karlsruhe - Thema der 77.
AKD-Sitzung und des Plenarbeitrags
75. AKD-Sitzung in München 7.- 8. November 2011.

BECKER, F.
Status Report EURADOS WG 12 - SG1: CT-Fluoroscopy staff dosimetry
EURADOS Annual Meeting, Prag 7.-11. Februar 2011.

BECKER, F.
Meeting Report EURADOS WG 12 - SG1: CT-Fluoroscopy staff dosimetry
EURADOS WG12: European Medical ALARA Network, Meeting, IFJ, Krakow, 29.-30. September
2011.

BECKER, F.
New Tools to Improve Radiation Protection of Medical Staff
ITN-Presentation, Lisbon, 17. November 2011.

BEELE, B.; MÜLLICH, U.; GEIST, A.; PANAK, P.J.
A TRLFS study on the complexation of Cm(III) with 2,6-bis(6-ethyl-1,2-diazine-3-yl)pyridine (Et-BDP) and 2,6-bis(5,6-dipropyl-1,2,4-triazin-3-yl)pyridine (nPr-BTP).
Jahrestagung Kerntechnik, Berlin, 17.-19. Mai 2011.

BEELE, B.; MÜLLICH, U.; GEIST, A.; PANAK, P. J.
A TRLFS Study on complexation of Cm(III) with N donor ligands
GDCh Wissenschaftsforum 2011, Bremen, September 4 – 7, 2011.

BLUNCK, CH.; BECKER, F.

Investigation of radiation exposure of medical staff: Measurements supported by simulations with an articulated hand phantom

International Workshop ORAMED 2011, Barcelona, 20.-22. Januar 2011.

BLUNCK, CH.; BECKER, F.; URBAN, M.

MCNPX Modellierung mit Hilfe eines Multikamerasystems.

Jahrestagung Kerntechnik, Berlin, 17.-19.Mai 2011.

BOUBY, M; FINCK, N.; DARDENNE, K.; GECKEIS, H.

Flow-Field Flow Fractionation coupled to sensitive detection techniques: a way to get insight into the radionuclides interaction with colloidal systems.

Frontiers in Environmental Geoscience, 21-23 June 2011 Aberystwyth (United Kingdom).

BOUBY, M.; FINCK, N.; TRUCHE, L.; BRENDLÉ, J.; SCHÄFER, T., GECKEIS, H.

Characterization of colloids extracted from two synthetic clay materials by Flow Field-Flow Fractionation (FFFF) coupled to ICP-MS.

NEA Clay Club Workshop, "Clays under Nano- to Microscopic resolution", 6-8 September 2011, Karlsruhe (Germany).

BOUBY, M.; GECKEIS, H.; BUCKAU, G.

Humic acid agglomeration study as a function of ionic strength and metal ion loading

ABC-SALT II, Actinides Brine Chemistry, 7-8 November 2011, Karlsruhe (Germany).

BOURG, S.; BOUVET, S.; CARAVACA, C.; CASSAYRE, L.; DE ANGELIS, G.; EKBERG, C.;

ESPARTERO, A.G.; GEIST, A.; GUILBAUD, P.; HARRISON, M.; KLAASSEN, F.; MALMBECK, R.;

MODOLO, G.; OUVRIER, N.; RHODES, C.; TAYLOR, R.

ACSEPT – the current European project on actinide recycling.

GLOBAL 2011 Makuhari, Japan, Dec. 11–16, 2011.

BUBE, C.; ALTMAIER, M.; METZ, V.; NECK, V.; SCHILD, D.; KIENZLER, B.

Thermodynamics of long-term metastable magnesium (chloro) hydroxo carbonates at 25°C.

International workshop on Actinide Brine Chemistry in a Salt-Based Repository - ABC-Salt (II), 7.-8.

November 2011, Karlsruhe.

BUBE, C., ALTMAIER, M., METZ, V., SCHILD, D., KIENZLER, B.,

Thermodynamics of long-term metastable magnesium (chloro) hydroxo carbonates at 25°C.

Goldschmidt 2011, Prague, Czech Republic.

BUBE, C.; METZ, V.; SCHILD, D.; LAGOS, M.; BOHNERT, E.; GARBEV, K.; ALTMAIER, M.;

KIENZLER, B.

Interactions of U(VI) with cement alteration products in highly saline solutions.

1st Internat.Symp.on Cement-based Materials for Nuclear Wastes (NUWCEM 2011),

Avignon, F, October 11-14, 2011.

BREMER, A.; GEIST, A.; PANAK, P. J.

Complexation of Cm(III) with C5-hemi-BTP studied by TRLFS

GDCh Wissenschaftsforum 2011, Bremen, September 4 – 7, 2011.

BREUSTEDT, B.; BLANCHARDON, E.; CASTELLANI C.; GIUSSANI, A.; LI W.; MARSH J.; NOSSKE D.; OEH U.; LOPEZ M.

Doses due to other excretion pathways in biokinetic models.

56th Annual Meeting of the Health Physics Society, West Palm Beach, Fla., June

26-30, 2011.

BREUSTEDT B.

Quantities and Units, External Dosimetry, Internal Dosimetry

Pilot Modules in Radiation Protection according to the ERPTS Training Scheme

KIT, Karlsruhe, 14.03.-30.03.2011.

BREUSTEDT, B.

Normen für Ganz- und Teilkörperzähler – DIN VDE 0493-200 und DIN EN 61582 (VDE 0493-2-3).
77. Sitzung des Arbeitskreis Inkorporationsüberwachung (AKI) des deutsch Schweizerischen
Fachverbandes für Strahlenschutz e.V. Hannover 13./14.10. 2011.

BREUSTEDT, B.

USTUR Case 0846 – Studying Chelation Therapy after Am-241 Inhalation
EURADOS WG 7: Internal Dosimetry Ghent, 14.-16.09.2011.

DARDENNE, K.; DENECKE, M. A. ; ROTHE, J.; VITOVA, T.; GECKEIS, H.
The INE Beamline for actinide science at ANKA

Frontiers in Environmental Geoscience 2011, Aberystwyth June 21-24, 2011.

DURO, L, GRIVÉ, M., COLÀS, E., GAONA, X., RICHARD, L.

TDB for elevated temperature conditions using entropy estimations.

HiTAC - High Temperature Aqueous Chemistry, Karlsruhe (Germany), November 9, 2011.

FELLHAUER, D., ALTMAIER, M., NECK, V., RUNKE, J., FANGHÄNEL, TH.

Solubility and speciation of Np(IV), Np(V) and Np(VI) in CaCl₂ solutions (pHc 8–12).

GDCh Wissenschaftsforum Chemie 2011, Bremen (Germany), September 04–07, 2011.

FELLHAUER, D., ALTMAIER, M., NECK, V., RUNKE, J., GAONA, X., FANGHÄNEL, TH.

Speciation and solubility of Np(V) and Np(VI) in alkaline CaCl₂ solutions.

13th International Conference on the Chemistry and Migration Behaviour of Actinides and Fission
Products in the Geosphere (MIGRATION), Beijing (China), September 18-23, 2011.

FELLHAUER, D., ALTMAIER, M., NECK, V., RUNKE, J., LÜTZENKIRCHEN, J., GAONA, X.,
FANGHÄNEL, TH.

Solubility and speciation of Np in dilute to concentrated CaCl₂ solutions under different redox
conditions.

ABC-Salt II workshop "Actinide Brine Chemistry in a Salt-Based Repository", Karlsruhe (Germany),
November 7-8, 2011.

FELLHAUER, D., KIRSCH, R., ALTMAIER, M., NECK, V., SCHEINOST, A.C., CHARLET, L., WISS,
T., FANGHÄNEL, TH.

Thermodynamic evaluation of Pu redox processes in homogeneous solutions and heterogeneous Fe
mineral suspensions.

13th International Conference on the Chemistry and Migration Behaviour of Actinides and Fission
Products in the Geosphere (MIGRATION), Beijing (China), September 18-23, 2011.

FINCK, N.; DARDENNE, K.

Americium co-precipitation with the smectite hectorite: powder and polarized EXAFS insights.

Actinide XAS 2011, March 02 – 04, Spring-8, Japan.

FINCK, N.; DARDENNE, K.

Trivalent cations retention upon brucite precipitation.

ABC-Salt Workshop (II), November 07 – 08, Karlsruhe, Germany.

FINCK, N.; DARDENNE, K.

Y(III) binding to the smectite hectorite.

NEA Clay Club Workshop "Clays under nano- to microscopic resolution", September 06 – 08,
Karlsruhe, Germany.

FINCK, N.; DARDENNE, K.

Americium coprecipitation with the smectite hectorite: powder and polarized EXAFS insights.

3rd ANKA / KNMF Joint Users Meeting, October 13 – 14, Neureut, Germany.

FINCK, N.; DARDENNE, K. BOSBACH, D.

Selenide retention by mackinawite: a multi-edge XAS approach.

Goldschmidt 2011, August 14 – 19, Prague, Czech Republic.

FLEISCH, J., GRÜNEWALD, W., ROTH, G., SCHMITZ, F.-J., TOBIE, W., WEISHAUPT, M.
Successful Hot Operation of the German Vitrification Plant VEK – Results and Experiences, WM 2011-
Conference, February 27 - March 3, 2011, Phoenix, AZ.

FLEISCH, J.; SCHMITZ, F.J.; WEISHAUPT, M.; ROTH, G.; GRÜNEWALD, W.; TOBIE, W.
Verglasung des HAWC der WAK - eine Erfolgsgeschichte.
Jahrestagung Kerntechnik, Berlin, 17.-19. Mai 2011.

GAONA, X., DÄHN, R., TITS, J., SCHEINOST, A.C., WIELAND, E.
Uptake of Np(IV) by C-S-H phases and cement: an EXAFS study.
ReCosy 3rd annual workshop, Balaruc les Bains (France), March 21-24, 2011.

GAONA, X., FELLHAUER, D., DARDENNE, K., ROTHE, J., ALTMAIER, M.
Redox chemistry of Np(V/VI) under hyperalkaline conditions: aqueous speciation, solubility and
chemical analogies with Pu.
ABC-Salt II workshop "Actinide Brine Chemistry in a Salt-Based Repository", Karlsruhe (Germany),
November 7-8, 2011.

GAONA, X., GRIVÉ, M., TAMAYO, A., SKERENCAK, A., ALTMAIER, M., DURO, L.
Assessing temperature effects: methods for the estimation of S°_m for aqueous actinide species and
applicability of the van't Hoff expression.
HiTAC - High Temperature Aqueous Chemistry, Karlsruhe (Germany), November 9, 2011.

GAONA, X., GRIVÉ, M., TAMAYO, A., SKERENCAK, A., ALTMAIER, M., DURO, L.
Temperature effects: empirical approach for the estimation of S°_m for aqueous actinide species –
comparison with experimental data.
13th International Conference on the Chemistry and Migration Behaviour of Actinides and Fission
Products in the Geosphere (MIGRATION), Beijing (China), September 18-23, 2011.

GAONA, X., NECK, V., ALTMAIER, M.
Formation and equilibrium conditions of An(III,IV,V,VI)-eigencolloids in dilute to concentrated NaCl,
CaCl₂ and MgCl₂ solutions.
ABC-Salt II workshop "Actinide Brine Chemistry in a Salt-Based Repository", Karlsruhe (Germany),
November 7-8, 2011.

GAONA, X., NECK, V., ALTMAIER, M.
An(III,IV,V,VI)-eigencolloids in aqueous solid-liquid systems: assessment of formation and equilibrium
conditions.
13th International Conference on the Chemistry and Migration Behaviour of Actinides and Fission
Products in the Geosphere (MIGRATION), Beijing (China), September 18-23, 2011.

GAONA, X., TITS, J., DÄHN, R., DARDENNE, K., FELLHAUER, D., WIELAND, E., ALTMAIER, M.
Redox chemistry of Np(V/VI) under hyperalkaline conditions: sorption on cementitious materials,
aqueous speciation and solid phase formation.
13th International Conference on the Chemistry and Migration Behaviour of Actinides and Fission
Products in the Geosphere (MIGRATION), Beijing (China), September 18-23, 2011.

GAONA, X., TITS, J., FELLHAUER, D., DARDENNE, K., WIELAND, E., ALTMAIER, M.
Redox chemistry of Np(V/VI) in alkaline conditions: aqueous speciation and solubility.
ReCosy 3rd annual workshop, Balaruc les Bains (France), March 21-24, 2011.

GAONA, X., TITS, J., WIELAND, E., FELLHAUER, D., DARDENNE, K., ROTHE, J., ALTMAIER, M.
Redox chemistry and thermodynamics of Np(V/VI) in hyperalkaline systems.
3rd ANKA / KNMF Joint Users Meeting, Karlsruhe (Germany), October 13-14, 2011.

GEIST, A.; MÜLLICH, U.
Hydrophile BTP zur selektiven Komplexierung von Actiniden.
Jahrestreffen der ProcessNet-Fachausschüsse Extraktion, Fluidverfahrenstechnik,
Mehrphasenströmungen und Phytoextrakte – Produkte und Prozesse.
Fulda, 3.–4. März 2011.

GEIST, A.; MÜLLICH, U.; MODOLO, G.; WILDEN, A.
Actinide(III)/lanthanide(III) separation via selective aqueous complexation of actinides (III) in nitric acid.
19th Internat.Solvent Extraction Conf. (ISEC 2011), Santiago de Chile, RCH, October 3-7, 2011.

GEIST, A.; MÜLLICH, U.; WILDEN, A.; GÜLLAND, S.; MODOLO, G.
C5-BPP - a new highly selective extractant for the separation of trivalent actinides from lanthanides.
19th Internat.Solvent Extraction Conf. (ISEC 2011), Santiago de Chile, RCH, October 3-7, 2011.

GRÜNEWALD, W., PLASCHKE, M., ROTH, G., TOBIE, W., WEISS, K.H., WEISENBURGER, S., STOLLENWERK, A., EISSLER, A.,
Process Control and Glass Product Quality Assessment Applied in the VEK Plant, GLOBAL 2011 Makuhari, Japan, Dec. 11-16, 2011.

GRÜNEWALD, W., ROTH, G., TOBIE, W., FLEISCH, J., SCHMITZ, F.J., WEISHAUPT, W.
Hot Operation Performance of the German Vitrification Plant VEK, GLOBAL 2011 Makuhari, Japan, Dec. 11-16, 2011.

GRÜNEWALD, W., ROTH, G., TOBIE, W., WEISENBURGER, S., WEISS, K.H.
Application of Advanced Large-Scale Ceramic Melter Technology for HLLW Vitrification, GLOBAL 2011 Makuhari, Japan, Dec. 11-16, 2011.

HEBERLING, F., HECK, S., ROTHE, J.
The calcite – water interface and its interactions with selenium IV and VI
Goldschmidt Conference 2011, 14.08. – 19.08.2011, in Prag, Czech Republic.

HUITTINEN, N.; RABUNG, TH.; LEHTO, J.; GECKEIS, H.
The role of dissolved silicon on Curium speciation in alkaline kaolinite suspensions
13th International Conference on the Chemistry and Migration Behaviour of Actinides and Fission Products in the Geosphere, Beijing, China, 18-23 September 2011.

HINZ, K., ALTMAIER, M., RABUNG, TH., GECKEIS, H.
Complexation of Nd(III)/Cm(III) with borate in dilute to concentrated alkaline NaCl and CaCl₂ solutions.
ABC-Salt II workshop "Actinide Brine Chemistry in a Salt-Based Repository", Karlsruhe (Germany), November 7-8, 2011.

KIENZLER, B., LOIDA, E.
Trapping of Radionuclides/Actinides in the Canister Corrosion Product Magnetite. ReCosy 3rd annual workshop (S&T contribution), Balaruc les Bains, France, March 21-24, 2011.

KIRSCH, R., FELLHAUER, D., ALTMAIER, M., ROSSBERG, A., FANGHÄNEL, TH., CHARLET, L., SCHEINOST, A.C.
Plutonium redox reactions with iron oxides under anoxic conditions.
Goldschmidt 2011, Prague (Czech Republic), August 14-19, 2011.

KIRSCH, R., FELLHAUER, D., ALTMAIER, M., ROSSBERG, A., FANGHÄNEL, TH., CHARLET, L., SCHEINOST, A.C.
XANES and EXAFS analysis of oxidation state and local structure of plutonium reacted with iron oxides under anoxic conditions.
13th International Conference on the Chemistry and Migration Behaviour of Actinides and Fission Products in the Geosphere (MIGRATION), Beijing (China), September 18-23, 2011.

KOBAYASHI, T.; BACH, D.; ALTMAIER, M.; SASAKI, T.; MORIYAMA, H.
Effect of Temperature on the Solubility and Solid Phase of Zirconium Hydroxide.
13th International Conference on the Chemistry and Migration Behaviour of Actinides and Fission Products in the Geosphere (MIGRATION 2011), Beijing (China), September 18-23, 2011

KOBAYASHI, T., BACH, D., ALTMAIER, M., SASAKI, T., MORIYAMA, H.,
Temperature Effect on Solubility and Solid Phase of Zr(IV) Hydroxide.
HiTAC - High Temperature Aqueous Chemistry, Karlsruhe (Germany), November 9, 2011.

KOBAYASHI, T., GAONA, X., FELLHAUER, D., ALTMAIER, M.
Redox Behaviour of the Tc(VII)/Tc(IV) Couple in Diluted NaCl Solution in Various Reducing Systems.
7th International Symposium on Technetium and Rhenium – Science and Utilization, Moscow, Russia,
jul. 4-8, 2011.

KOBAYASHI, T., GAONA, X., FELLHAUER, D., ALTMAIER, M.,
Redox Behaviour of the Tc(VII)/Tc(IV) Couple in Various Reducing Systems and the Solubility of
Tc(IV) Hydroxide.
13th International Conference on the Chemistry and Migration Behaviour of Actinides and Fission
Products in the Geosphere (MIGRATION), Beijing (China), September 18-23, 2011.

KOBAYASHI, T., YALCINTAS, E., ALTMAIER, M.,
Solubility of $TcO_2(s) \cdot xH_2O$ in dilute to concentrated NaCl, $CaCl_2$, and $BaCl_2$ solutions.
ABC-Salt II workshop "Actinide Brine Chemistry in a Salt-Based Repository", Karlsruhe (Germany),
November 7-8, 2011.

KULIK D.; LÜTZENKIRCHEN J.
Consistent Treatment of Entropy, Enthalpy and Volume Effects of Multi-Dentate Adsorption Reactions,
Goldschmidt 2011, Prag, 14.-19. August, 2011.

KUPCIK, T., HUITTINEN, N.; RABUNG, TH.; LÜTZENKIRCHEN, J.; GECKEIS, H.; FANGHÄNEL, TH.
Interaction of trivalent metal ions with aluminium(hydr)oxides
13th International Conference on the Chemistry and Migration Behaviour of Actinides and Fission
Products in the Geosphere, Beijing, China, 18-23 September 2011.

KUPCIK, T., HUITTINEN, N., RABUNG, T., LÜTZENKIRCHEN, J., GECKEIS, H., FANGHÄNEL, TH.
Aluminium(hydr)oxide als Modellminerale zur Untersuchung der Metallionensorption an der Mineral-
Wasser-Grenzfläche.
GDCh Wissenschaftsforum Chemie 2011, Bremen (Germany), September 04-07, 2011.

LINDQVIST-REIS, P., KLENZE, R. STEPPERT, M., FUSS, M., WALTHER, C, LÜTZENKIRCHEN, J.,
GECKEIS, H.
Europium(III) and Curium(III) Hydrolysis Species in Solids and in Solution Studied by Time-Resolved
Laser Fluorescence Spectroscopy (TRLFS)
26th Rare Earth Research Conference, June 19-23, 2011, Santa Fe, USA.

LINDQVIST-REIS, P., KLENZE, R., SCHIMMELPFENNIG, B.
Spectroscopic Evidence of Ion-Association in Aqueous Ln^{3+} and An^{3+} Perchlorate Solutions at Low
Water Activity
ABC-Salt Workshop '11, Karlsruhe, November 7-8, 2011.

LINDQVIST-REIS, P., KLENZE, R., FANGHÄNEL, TH.
Octa- and Nonahydrated Cm(III) in Aqueous Solution from 20 to 200 °C
HiTAC Workshop '11, Karlsruhe, November 9, 2011.

LOIDA, A., GENS, R., METZ, V., LEMMENS, K., CACHOIR, C., MENNECART, T., KIENZLER, B.
Corrosion Behaviour of Spent Nuclear Fuel in High pH Solutions – Effect of Hydrogen
XXXV International Symposium Scientific Basis for Nuclear Waste Management, MRS 2011, October
2-7, 2011, Buenos Aires, Argentina.

MAGNUSSON, D.; GEIST, A.; WILDEN, A.; MODOLO, G.; MALMBECK, R.
Computer code development for flow-sheet design and modeling with verification towards a novel
partitioning Process.
GLOBAL 2011 Makuhari, Japan, Dec. 11–16, 2011.

